School of Civil and Mechanical Engineering

Properties of Geopolymer Concrete Using Ultrafine Fly Ash and Nanosilica

Partha Sarathi Deb

This thesis is presented for the Degree of
Doctor of Philosophy
of
Curtin University

June 2018

DECLARATION

To the best of my knowledge and belief this thesis contains no material previously published by any other person except where due acknowledgement has been made.

This thesis contains no material which has been accepted for the award of any other degree or diploma in any university.

ACKNOWLEDGEMENTS

First and foremost, I take this opportunity to express my profound gratitude and deep regards to my supervisors Dr. Prabir Kumar Sarker and Dr. Salim Barbhuiya for their exemplary guidance, monitoring and constant encouragement throughout the course of the thesis. Their useful suggestions, kind supports, precious discussions and constant encouragements at various stages throughout the research work are highly appreciated.

The experimental work was carried out in the laboratories of the Faculty of Engineering at Curtin University. I am grateful to the laboratory technical staff Dr Ray Mahidasht, Mr. Ashley Hughes, Mr Luke English, Mr Craig Gwyther and Mr. Mick Ellis for the valuable information provided by them in their respective fields. I am grateful for their co-operation during the period of my laboratory work.

I take this opportunity to express my gratitude to Curtin University, Western Australia for the financial support in form of APA and Curtin scholarship. I am also grateful to acknowledge the support of Coogee Chemicals for supplying the chemicals used in this study. The use of equipment, scientific and technical assistance of the Curtin University Electron Microscope facility, which has been partially funded by the university, State and Commonwealth Governments is also gratefully acknowledged.

The help in performing the laboratory work, suggestions and discussions by my friend and well-wisher Dr. Pradip Nath at Curtin University is gratefully acknowledged.

Last but not least, I thank the Almighty, my parents Swapan kumar Deb and Minakshi rani Deb, my wife Sathi Dey and my son Iyan Sarathi Deb for their constant encouragement without which this mission would not be possible.

ABSTRACT

Utilisation of fly ash based geopolymer concrete as an alternative material of ordinary Portland cement adds sustainability to the environment by reducing greenhouse gas emission associated with the cement production. This new type of binder has brought forth the production of concrete without use of Portland cement. Moreover, to reduce the carbon footprint from cement industry, alkali-activated binders (AABs) or geopolymers have also been at the centre of research curiosity as an environmentally favourable alternative to OPC.

Low calcium fly ash (class F) has been recognised as a suitable material for geopolymers because of its favourable chemical composition and wide availability. However, the use of fly ash in geopolymer at ambient condition still have some drawbacks due to its slow setting, high porosity and subsequent slow strength development. Improvement of these properties is essential in order to increase the use of geopolymers in concrete as an alternative to energy-intensive OPC binders.

Use of finer particles such as nanosilica and ultrafine fly ash are gaining widespread attention due to the significant effect that it can have on the microstructural and mechanical development of the Portland cement-based binders. However, research on the effects of nanosilica and ultrafine fly ash on the properties of geopolymers is scarce in literature. Therefore, this study aimed to investigate the effect of nanosilica and ultrafine fly ash on the properties of fly ash geopolymers.

A class F fly ash locally available in Western Australia was used to make geopolymer concrete. Nanosilica (NS), ultrafine fly ash (UFA), ground granulated blast-furnace slag (GGBFS) and ordinary Portland cement Type I (OPC) were used as a partial replacements of fly ash in this study. The mix proportions were developed based on a constant total binder content of 400

kg/m3. The mixtures are divided into three main series as fly ash-only (FA), OPC blended fly ash (FA-PC) and GGBFS (slag) blended fly ash (FA-S). For example, in the ultrafine fly ash blended fly ash-only (FA) series, fly ash was used as the main binder with 0-15% ultrafine fly ash. In the slag blended (FA-S) series, 0-15% ultrafine fly ash was used with 15% GGBFS and 70-85% fly ash. Similarly, in the OPC blended (FA-PC) series, 0-15% ultrafine fly ash was used with 10% OPC and 75-90% fly ash. After casting, the geopolymer concrete samples were cured at ambient condition of the laboratory (15-22 oC and 60±10% relative humidity) until the test.

The setting time, flow behaviour and workability of fresh geopolymer mixtures were determined. Cylinder specimens of 100 mm in diameter and 200 mm in height were cast and used for compressive strength and sorptivity tests. Small cut samples were examined by scanning electron microscopy (SEM), nanoindentation, X-ray diffraction analyses (powder) and MIP.

Resistance to sulfuric acid was determined by the modified test method B of the ASTM C 267 standard. The geopolymer cube mortar specimens were fully immersed in 3% sulfuric acid solution at the age of 28 days for 12 weeks. For sulphate resistance tests, the test specimens were immersed in 5% sodium sulphate and magnesium sulphate solutions for various periods. Cylinder specimens of dimension 100 mm diameter and 200 mm height were used for changes in compressive strength and mass change tests, and prism specimens of 75 mm × 75 mm × 285 mm were used to test the length change for each mix.

Compressive strength of ambient-cured geopolymers was found to increase with the addition of nanosilica and ultrafine fly ash at early ages. Strength increased with the addition of nanosilica up to a dosage of 2% and then it declined with further addition. The maximum 28-day compressive strength among all the mixes was 72 MPa which was obtained for the

geopolymer paste containing 83% fly ash, 15% GGBFS and 2% nanosilica. The compressive strength of geopolymers containing 5% percentages of ultafine fly ash were between 31 MPa and 36 MPa at 7 days, and between 48 MPa and 54 MPa at 28 days.

The SEM images showed that the addition of nanosilica and ultrafine fly ash improved compactness of the reaction product. The contribution of nanosilica and ultrafine fly ash to the formation of a more compact and dense microstructure with better interlocking morphology has resulted in the increase of compressive strength. The EDX spectra showed that additional reaction products such as CSH or CASH and NASH are produced in the mixes containing OPC and GGBFS.

Sorptivity of the specimens with 2% nanosilica was less than that of the control specimen. The average mass loss of the specimens of three series decreased from 2.6% to 1.8% after 90 days of immersion in sulphuric acid. The strength loss of specimens without nanosilica ranged from 30% to 41% while that of the specimens with 2% nanosilica ranged from 9% to 11% after 90 days of immersion in sulphuric acid.

The volume fractions of hydrated aluminosilicate gel in fly ash only geopolymer increased from 70.0% to 78.9% with the addition of 2% nanosilica. The volume fractions of porous phases in fly ash-GGBFS and fly ash-OPC geopolymer with 2% nanosilica were much lower than the values in corresponding mixes without nanosilica. The changes in volume fractions of the unreacted and partially reacted phases were not significant with the addition of 2% nanosilica. In general, inclusion of nanosilica and ultrafine fly ash in fly ash based geopolymer improved the mechanical and microstructure properties and performed satisfactorily in aggressive environments when cured at ambient temperature.

List of Publications

The following publications have resulted from the work carried out for this degree.

1. Deb, P.S., Sarker, P.K., Barbhuiya, S. Effects of nanosilica on the strength development of geopolymer cured at room temperature. Construction and Building Materials, 101(2015) 675-683.

2. Deb, P.S., Sarker, P.K. Effects of ultrafine fly ash on setting, strength, and porosity of geopolymers cured at room temperature. Journal of Materials in Civil Engineering 29 (2) (2016) 06016021.

3. Deb, P.S., Sarker, P.K., Barbhuiya, S. Sorptivity and acid resistance of ambient-cured geopolymer mortars containing nanosilica. Cement and Concrete Composites, 72 (2016) 235-245.

4. Deb, P.S., Sarker, P.K., Nath, P. Drying shrinkage of slag blended fly ash geopolymer concrete cured at room temperature. Procedia Engineering, 125(2015) 594-600.

TABLE OF CONTENTS

LIST OF FIGURES

LIST OF TABLES

NOMENCLATURE

A	Cross sectional area	mm^2
B	Mass of saturated-surface-dry test sample in air	gm
C	Apparent mass of saturated test sample in water	gm
D	Diameter of the specimens	mm
f_c	Compressive strength	MPa
f'_{cr}	Required average compressive strength	MPa
f_{ct}	Indirect tensile strength	MPa
f_{cf}	Modulus of rupture	MPa
G	Mass of the aggregate plus the measure	kg
I	Absorption	mm
K	Empirical factor	-
L	Length of the specimens'	mm
L_{ds}	Drying shrinkage	microstrain
L_t	Length of the individual specimen at any specified time t	mm
L_i	Initial length of the individual specimen	mm
M	Bulk density of the aggregate	kg/m^3
M_t	The change in specimen mass in grams, at the time t	gm
M_1	Weight of the oven dried samples	gm
M_{2i}	Saturated weight after immersion	gm
M_{3b}	Weight of the sample after boiling and cooling	gm
M_{4ib}	Weight of the sample suspended in the water	gm
P	Maximum force applied	kN
P	Average compressive strength of reference cement mortar cubes	MPa (psi).
SP	Average compressive strength of slag-reference cement mortar cubes	MPa(psi)
S	Mass of saturated surface dry sample	gm
SS/SH	Sodium silicate to sodium hydroxide ratio	-
T	Mass of the measure	kg
V	Volume of the measure	m3
W/C	Water cement ratio	-
W/S	Water solid ratio	

ABBREVIATIONS

AAR	Alkali aggregate reaction
ACI	American concrete of institute
AS	Australian standard
ASR	Alkali-silica reaction
ASTM	American society for testing materials
BS	British standard
EDX	Energy-Dispersive X-ray Spectroscopy
GGBFS	Grand granular blast furnace slag
HSC	High strength concrete
HVFA	High volume fly ash
LOI	Loss of ignition
MIP	Mercury Intrusion Porosimetry
OPC	Ordinary Portland cement
PDF	Probability Density Functions
SEM	Scanning electron microscope
SSD	Saturated surface dry
VPV	Volume of permeable voids
XRD	X-ray powder diffraction
XRF	X-Ray florescence

CHAPTER 1

INTRODUCTION

1.1 Background

Development of Portland cement (PC) and its application has greatly matured in last few decades. However, the production of cement is one of the industry's most energy intensive processes second only to steel and aluminium [1]. Development of new alternatives to ordinary Portland cement based binders in the concrete industry can play a vital role in the context of sustainability and environmental issues [2]. Therefore, utilizing the by-products in the concrete industry eventually gained a lot of attention in the fields of concrete research. Different researchers [3, 4] noted that manufacturing of alkali activated binders (AAB) using the industrial waste such as fly ash produced a cementitious binder with the same advantages of OPC but at a lower cost, with a large reduction in CO_2 emissions [5, 6, 7].

According to Davidovits [8] various aluminosilicate materials can be synthesized with the alkaline solution to form an inorganic aluminosilicate polymer commonly named as a geopolymer. Previous researchers revealed that the chemical composition of geopolymer binders are similar to the analogue of zeolites or zeolitic precursors [9, 10]. Diaz et al. [11] and Yip et al. [12] noted that the final hydrated products of geopolymer binders are influenced by several factors based on chemical composition of the source materials. The polymerization process involves a substantially fast chemical reaction under alkaline conditions on Si-Al minerals, resulting in a three-dimensional polymeric chain and ring structure consisting of Si-O-Al-O bonds [13]. However, the choices of the source materials for making geopolymers depends on factors such as availability, cost, type of application, and specific demand of the

end users [14]. Previous researchers reported that fly ash based geopolymer blended with calcium reached materials, higher molarity of sodium hydroxide and curing conditions possess higher mechanical strengths with better durability properties.

Despite the fact that geopolymer mechanism was developed over a couple of decades ago and has many advantageous characteristics, it has not yet been used in concrete as extensively as Portland cement. Widespread use of ambient-cured low calcium fly-ash geopolymers is hindered due to some of its limitations such as slow setting, high porosity and subsequent slow strength development. Improvement of these properties is essential in order to increase the use of geopolymers in concrete as an alternative to energy-intensive OPC binders.

Addition of very fine materials such as nanosilica and ultrafine fly ash in OPC systems are widely investigated and it was found as an effective additive towards the mechanical, microstructural and nanostructural development. Moreover, it is widely accepted that the microstructure of hydrated paste can be enhanced with the modification of hydrated gel, unreacted particles and the pore phases. Quantitative evaluation of these parameters and establishment of their relationships with the properties of a product is critically important for development of a material. This study focused on the effects of nanosilica and ultrafine fly ash on various properties of ambient-cured low-calcium fly ash geopolymers.

1.2 Aim and objectives

Enhancement of concrete properties by the addition of fine particles has been documented well in literature. The aim of this study is to study the effects of ultrafine fly ash and nano silica on the properties of ambient-cured low-calcium fly ash geopolymers. A series of mixes including

different proportions of these fine materials were tested and the properties such as workability, strength development, microstructural development, nanoindentation and durability in aggressive environments were studied. The specific objectives are as follows:

- Development of geopolymer mixes suitable for curing in room temperature using low-calcium fly ash with or without blending with calcium reached materials and with ultrafine fly ash and nanosilica.
- Investigating the changes in setting time and workability of fresh mixes and resulting mechanical properties of hardened geopolymers due to the incorporation of ultrafine fly ash and nanosilica, and thus determine the optimum percentage of these additives.
- Assessment of the effects of ultrafine fly ash and nanosilica on long term properties of geopolymers such as shrinkage and durability in aggressive environment.
- Understand the development of different phases in microstructure by using different advanced techniques and relate them to the observed mechanical and durability properties.

1.3 Scope of study

Due to the growing concern on sustainability and environmental issues regarding concrete production with cement, alternative binders such as fly ash based geopolymer possess a great potential in the construction industry. Fly ash based geopolymer binder exhibited increased strength with the increase of activator concentration and increased curing temperature. However, the microstructure of the fly ash based geopolymer binders are porous when cured at room temperature. Additions of ultrafine fly ash and nanosilica can potentially densify the micro and nanostructures of fly ash based geopolymers.

Three different series based on fly ash only, GGBFS blended fly ash and OPC blended fly ash with the variation of 0-3% nanosilica and 0-15% ultrafine fly ash was cast in the laboratory. The setting and workability behaviours and compressive strength development of the mixes were studied. Effects of ultrafine fly ash and nanosilica on the microstructural development were studied by using scanning electron microscopy (SEM), energy dispersive X-ray spectroscopy (EDS) and X-ray diffraction (XRD) of the geopolymer specimens. Based on these results, most suitable mixes with nanosilica were selected for further study on nanomechanical and durability properties. Nanoindentation was used to determine the micromechanical properties such as hardness and elastic modulus of the different phases of the geopolymer products phases were evaluated. The interfacial transition zone (ITZ) between aggregate and geopolymer product was also investigated during the study.

1.4 Research significance

Aluminosilicate materials such as fly ash and GGBFS are well known to be the reactive with different alkaline solutions. Previous research works showed that curing at elevated temperature improved mechanical properties of geopolymer products. However, use of elevated temperature curing is mainly limited to precast members and is not be suitable for in-situ concrete constructions. Therefore, it is essential to develop geopolymer concrete mixes suitable for curing at ambient temperatures.

It was reported in literature that the controlled use of calcium bearing materials could accelerate the geopolymer reaction. Previous studies were carried out on the development of low-calcium fly ash geopolymer concrete mixes of usable setting time and workability by blending with GGBFS, OPC and hydraulic lime based [15,16]. However, there is no

comprehensive study on the use of nanosilica and ultrafine fly ash as a part of the geopolymer binders cured at ambient temperature and the effects of these ultrafine materials on development of the microstructural phases of geopolymers not yet clearly evaluated. For this reason, this study investigated the effects of the addition of 0-3% nanosilica and 0-15% ultrafine fly ash on the ambient-cured geopolymers. The main aluminosilicate source material was fly ash only or fly ash blended with a small percentage of GGBFS or OPC.

It is noteworthy that the engineering properties such as strength, shrinkage and durability of a binder are governed by the microstructure and porosity of the hydrated product. This research studied the effects of ultrafine fly ash and nanosilica on the microstructural development and the resulting engineering properties of geopolymers. The developed knowledge will make significant contribution to the mix design of geopolymers for ambient curing conditions. Thus, the results of this study will help promote in-situ casting of geopolymer concrete for sustainable concrete constructions.

1.5 Structure of this thesis

Chapter 1 presents the objectives, scopes and significance of the current study.

Chapter 2 entitled “Literature Review” focuses on providing the required background and information on the status of different geopolymer binders both in heat and ambient cured conditions.

Chapter 3 presents the mix details of fly ash geopolymer binders with nanosilica and ultrafine fly ash. Added to this, the mixing process and curing and experimental conditions are also discussed in this chapter.

Chapter 4 presents a detailed discussion on the influences of ultrafine fly ash and nanosilica in fly ash-only and GGBFS and OPC blended fly ash geopolymer paste.

Chapter 5 presents the workability, mechanical and durability properties of fly ash-only and GGBFS and OPC blended fly ash geopolymer mortars.

Chapter 6 presents the results of fly ash based geopolymer concrete with ultrafine fly ash and nanosilica.

Chapter 7 is on the nanomechanical properties the fly ash-only and GGBFS and OPC blended fly ash geopolymers. Nano indentation test results on the interfacial transition zone (ITZ) are also presented.

Chapter 8 provides the sulfate resistance properties of geopolymer concrete with ultrafine fly ash and nanosilica.

Finally, Chapter 9 presents the conclusions drawn in the course of this research and recommendations for future work.

1.6 Summary

It was shown that addition of nanosilica and ultrafine fly ash in OPC or other cementitious binders significantly enhanced the compressive strength along with its durability properties. Addition of a small percentage of nanosilica and ultrafine fly ash could be a potential way to improve the strength and durability properties of low-calcium fly ash geopolymers cured at ambient temperature. Thus, a comprehensive study is required to understand the possible beneficial effects of nanosilica and ultrafine fly ash in fly ash geopolymers cured at room temperature. This study investigated the effects of the addition of 0-3% nanosilica and 0-15%

ultrafine fly ash on the mechanical, microstructure and durability properties of fly ash-only and fly ash blended with GGBFS or OPC.

1.7 Reference

1. J. G. J. Olivier, G. Janssens-Maenhout, M. Muntean, and J. Peters. Trends in global CO_2 emissions: 2015 Report. The Hague

2. D.N. Huntzinger, and T.D. Eatmon. A life-cycle assessment of cement manufacturing: comparing traditional process with alternative technologies, J Clean Prod, 17 (7) (2009) 668–675

3. P. Duxson, G.Lukey, and J. Deventer. Physical evolution of geopolymer derived from metakaolin up to 1000 °C. Journal of Materials Science, 42(9) (2007) 3044-3054, retrieved from http:// www.springerlink.com

4. P. Duxson, J.L. Provis, G.C. Lukey, S.W. Mallicoat, W.M. Kriven, and J.S.J. Deventer. Understanding the relationship between geopolymer composition, microstructure and mechanical properties, Coll Surf A: Physicochem Eng Aspects 269(2005) 47–58.

5. B. Singh, G. Ishwarya, M. Gupta, and S.K. Bhattacharyya. Geopolymer concrete: A review of some recent developments. Construction and Building Materials, 85(15) (2015) 78-90

6. H. Rami, and O. Haddad. Production of geopolymer concrete using natural pozzolan: A parametric study. Construction and Building Materials, 114 (2016) 699-707

7. A. Islam, U. Alengaram. M. Jumaat, I.I. Bashar, and S.M. Kabir. Engineering properties and carbon footprint of ground granulated blast-furnace slag-palm oil fuel ash-based structural geopolymer concrete. Construction and Building Materials, 101 (30) (2015) 503-521

8. J. Davidovits. Geopolymer Chemistry and Application, second ed., Institut Géopolymère, Saint-Quentin: France, 2008.

9. A. Fernandez-Jimenez, and A. Palomo. Characterisation of fly ashes potential reactivity as alkaline cements, Fuel 82 (2009) 2259–2265, http://dx.doi.org/10.1016/S0016-2361 (03)00194-7

10. J.S.L. Jaarsveld, and D. Lorenzen. Factors affecting the immobilisation of metals in geopolymerised fly ash, Metall. Mater. Trans. B 29B (1998) 283–291.

11. E.I. Diaz, E.N. Allouche, and S. Eklund. Factors affecting the suitability of fly ash as source materials for geopolymers. Fuel 89 (2010) 992-996, retrieved from http:// www.sciencedirect.com

12. C.K.Yip, and J.S.J. Deventer. Microanalysis of calcium silicate hydrate gel formed within a geopolymeric binder, J. Mater. Sci. 38 (2003) 3851–3860.

13. J. Davidovits. Geopolymer Chemistry and Application, second ed., InstitutGéopolymère, Saint-Quentin: France, 2008.

14. B.V. Rangan. FLY ASH-BASED GEOPOLYMER CONCRETE", Research Report GC 4, Engineering Faculty, Curtin University of Technology, Perth, Australia, 2008

15. P. Nath, and P. K. Sarker. Effect of GGBFS on setting, workability and early strength properties of fly ash geopolymer concrete cured in ambient condition Constr. Build. Mater., 66 (2014) 163–171.

16. P. Nath, and P.K. Sarker. Use of OPC to improve setting and early strength properties of low calcium fly ash geopolymer concrete cured at room temperature." Cem. Concr. Comp., 55 (2015) 205–214.

Every reasonable effort has been made to acknowledge the owners of copyright material. I would be pleased to hear from any copyright owner who has been omitted or incorrectly acknowledged.

CHAPTER 2

Literature review

2.1 Overview

This chapter reviews the literature on different geopolymer binders both in heat and ambient cured conditions. It starts with the existing literature on the impact of OPC production on the environment, use of fly ash and slag in concrete as a replacement material, addition of nanosilica and ultrafine fly ash in cementitious binders, the background on the development of geopolymer and its chemistry and mechanism, and then focuses on materials, characterization and properties.

2.2 Environmental concerns of OPC based binder

Ordinary Portland cement (OPC) is the traditional binder for manufacturing of concrete worldwide, fulfilling a demand of over 1.5 billion tonnes annually. The cement production in china alone accounts as much as the combined production of the other top ten countries as shown in Fig. 2.1. It has been reported that the production of OPC is energy-intensive and releases a significant volume of carbon dioxide (CO_2) to the atmosphere [1]. Approximately 5% of global CO_2 emissions originate from the manufacturing of cement [2]. According to Lawrence [3], the production of 1 tonne of Portland cement produces approximately 1 tonne of CO_2 to atmosphere. Feely et al. [4] reported that the current level of carbon dioxide (CO_2) in the atmosphere is approaching 380 ppm and will dramatically increase to higher levels by the end of the century. Thus, in looking for ways to reduce the CO_2 emissions originated from the cement industry, development of alternatives to OPC based binders is necessary. By-product materials such as ground granulated blast furnace slag (GGBFS) has been shown to

release up to 80% less greenhouse gas emissions than the production of conventional Portland cement [5], and there are 80% to 90% less greenhouse gas emissions from the production of fly ash [6].

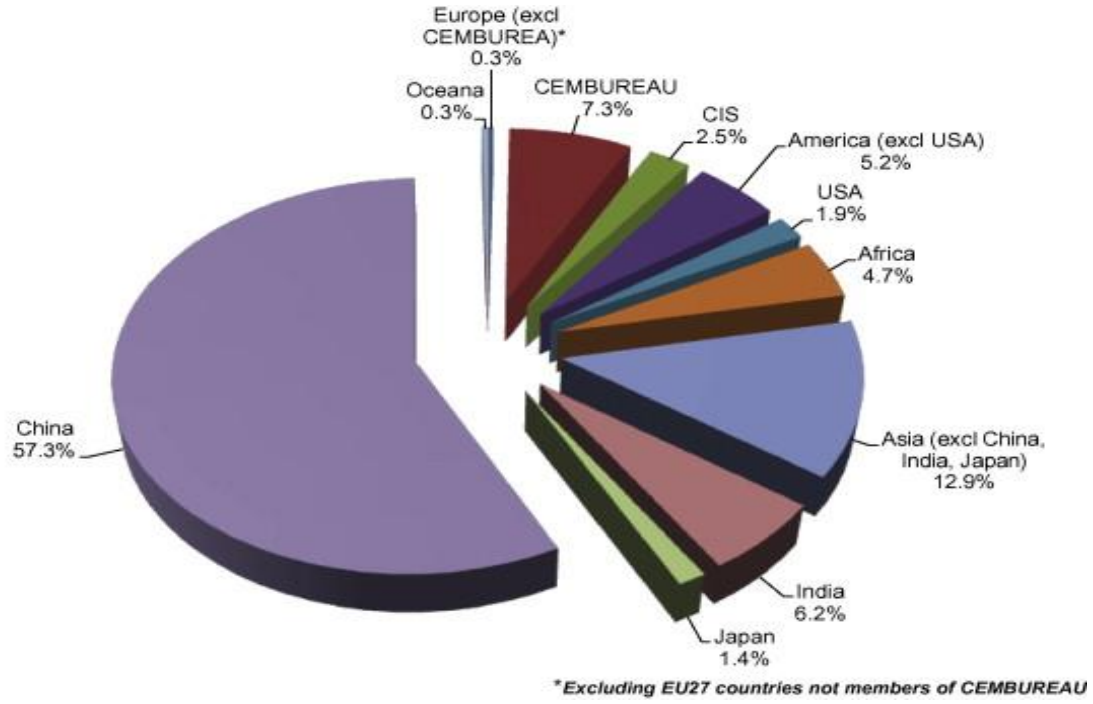

Fig.2.1 World Portland cement production today [141]

2.3 Use of fly ash and slag in concrete

Fly ash and blast furnace slag are the most common alternative binders (replacement) used in traditional cement concrete. It has been reported that a partial replacement of Portland cement with fly ash and slag offer improvements of various late–age properties of concrete. Using of fly ash in concrete has been widely reported in terms of better workability, reducing permeability and thermal behaviours [4,5]. It was observed that up to 60% of Portland cement can be replaced by fly ash in high volume fly ash (HVFA) concrete which showed excellent

mechanical properties with enhanced durability performance and proved to be more durable and resource-efficient than the OPC concrete [6]

On the other hand, it is noted that the chemical composition of slag remains relatively constant, especially compared to fly ash and found that higher replacement of slag in Portland cement eventually increased the compressive strength of concrete. Besides, use of slag in concrete has other advantages like low heat of hydration, high sulphate resistant and lower chloride ingress.

The benefits offered by the fly ash and slag coupled with the concern of environmental issues in the construction industry have led to intensive study on alkali-activated binders (AABs) or geopolymers. The new type of binder has brought forth the production of concrete without the use of Portland cement. Moreover, to reduce the carbon footprint from the cement industry, alkali-activated binders (AABs) or geopolymers have also been at the centre of research curiosity as an environmentally favourable alternative to OPC.

2.4 Brief history of alkali-activated binders (AABs) or geopolymers

Geopolymer and alkali-activation technology has been known to the cement and concrete industry for more than seven decades. The advancement of geopolymer concrete is an important step towards the production of environmentally friendly concrete. The team of Fernandez-Jimenez and Palomo from Spain, van Jaarsveld and van Deventer from Australia and Joseph Davidovits from French reported numerous studies on geopolymer technology especially focusing microstructural and morphological development of different types of alkali activated materials.

2.4.1 Environmental benefits of geopolymers binder

Development of an inorganic polymer binder for concrete, commonly named as geopolymer can play a vital role in the context of sustainability and environmental issues. Geopolymer binders can provide a comparable performance to traditional cementitious binders in a range of applications and also reduce greenhouse gas emissions [7]. The choice of the source materials for making geopolymers depends on factors such as availability, cost, type of application, and specific demand of the end users [8]. Works on the development of geopolymer binder as an alternative to traditional cement has been considerably increased in the recent years. This is because of the numerous benefits of geopolymers over traditional cement binder such as lower CO_2 emission, requirement for less processing of the raw materials [9] and development of desired strength and structural properties [10, 11, 12].

2.4.2 Geopolymerization process of alkali-activated binders

Geopolymerization is a process where a large amount of amorphous aluminosilicate phase is transformed into compact binder by hydrothermal polycondensation [13,14]. Previous researchers revealed that geopolymer binder may be viewed as an amorphous analogue of zeolites or zeolitic precursors [38, 39] that follows the same formation process as in zeolites [15,16]. Davidovits [15] used different chemical unit's terminology to address the geopolymer structure such as Si-O-Al-O (polysialate), Si-O-Al-O-Si-O (sialate-siloxo) and Si-O-Al-O-Si-O-Si-O (sialate-disiloxo).

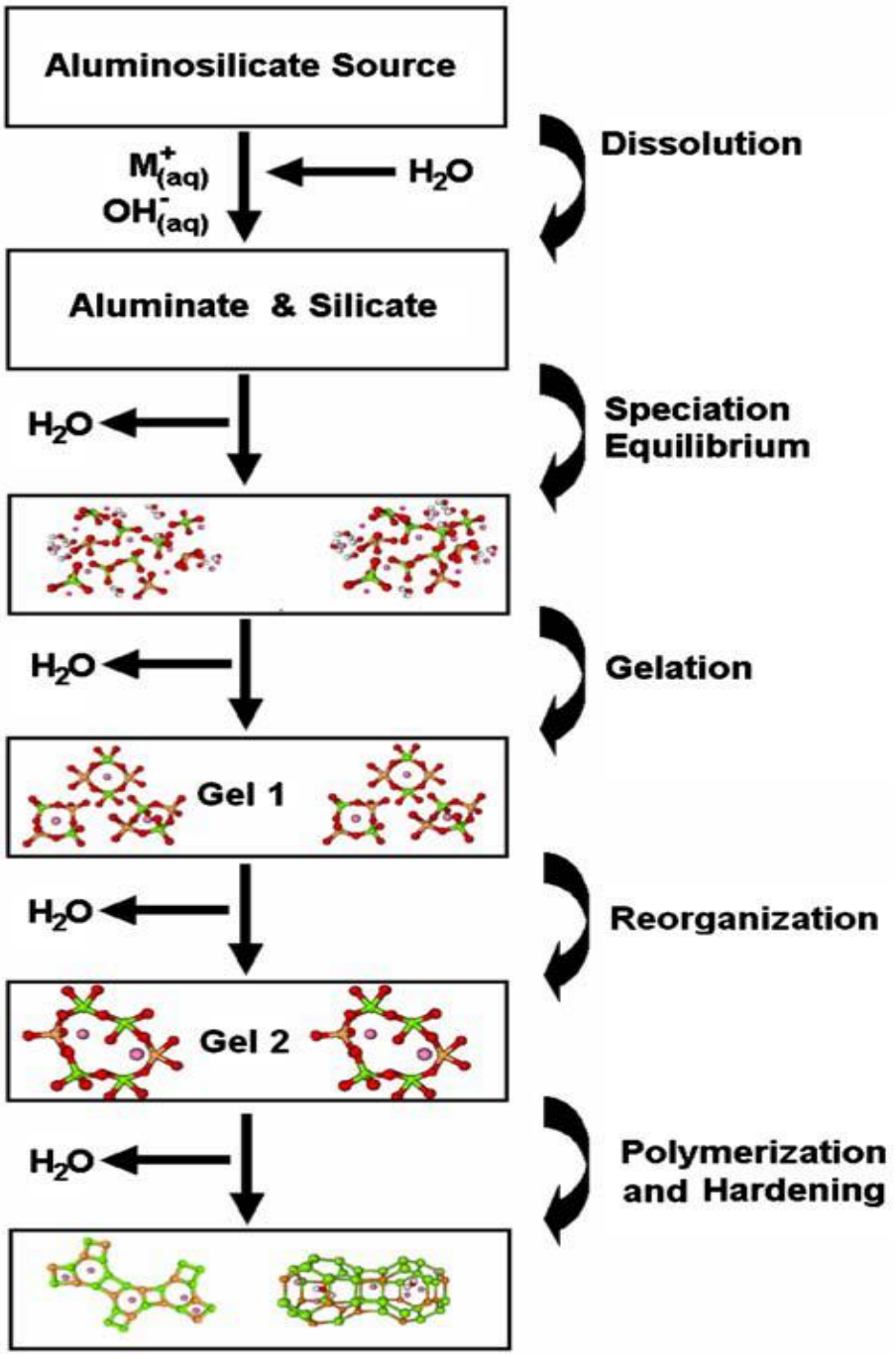

Fig. 2.2 Conceptual model for geopolymerization [49]

Duxson et al. [17] presented a conceptual model with three basic stages for geopolymirization process. As shown in Fig. 2.2, the process involves dissolution of Si and Al atoms from the source material then followed by orientation or condensation of precursor ions

into monomers and finally, setting or polycondensation of monomers into polymeric structures. In the alkaline environment, aluminosilicate materials dissolve in the solution to form free SiO_4 and AlO_4 tetrahedral units which link together through the sharing of all oxygen atoms between two tetrahedral units to yield polymeric precursors. Continuous linking of these precursors eventually forms amorphous geopolymer. With the progress of the reaction, water is gradually removed.

2.4.3 Factors affecting the geopolymers binder

Coal fly ash, calcined clay, metakaolin and blast furnace slag are some common aluminosilicate source materials used in the synthesis of geopolymers. Reaction of the source material with an alkali provides a rapid transformation to some specific structures followed by the destruction, coagulation and condensation processes [18].

The degree of geopolymerization, strength and the microstructure development of geopolymer are influenced by several factors such as particle size and chemical composition of the source material, type and concentration of the alkaline liquid and curing temperature. Most commonly used activators are alkali silicates, hydroxides, carbonates or combinations of these chemicals selected based on the chemical compositions of the source material. Finer particles are known to have greater reactivity as compared to larger particles of the same composition due to increased surface-to-volume ratio. An increase in fineness of the source materials was shown to increase compressive strength of geopolymers [19,20].

2.5. Fly ash based geopolymer

2.5.1 Fly ash as a source material

The difference of chemical contents in class C and class F fly ashes [21] leads to follow different mechanism when they are activated in a basic environment. The higher amount of cementitious component such as CaO (20%) in class C fly ash typically leads to accelerate the rate of reaction and geopolymerization process. On the other hand, in class F fly ash, low CaO (4%), a low percentage of unburnt material lower than 5%, iron (Fe2O3) content not higher than 10%, the content of reactive silica between 40–50% was observed [21]. Added to this, the percentage of particles with size lower than 45 μm between 80 and 90% was observed in class F fly ash [22, 23]. Therefore, class F fly ash is usually recommended and was used in this study.

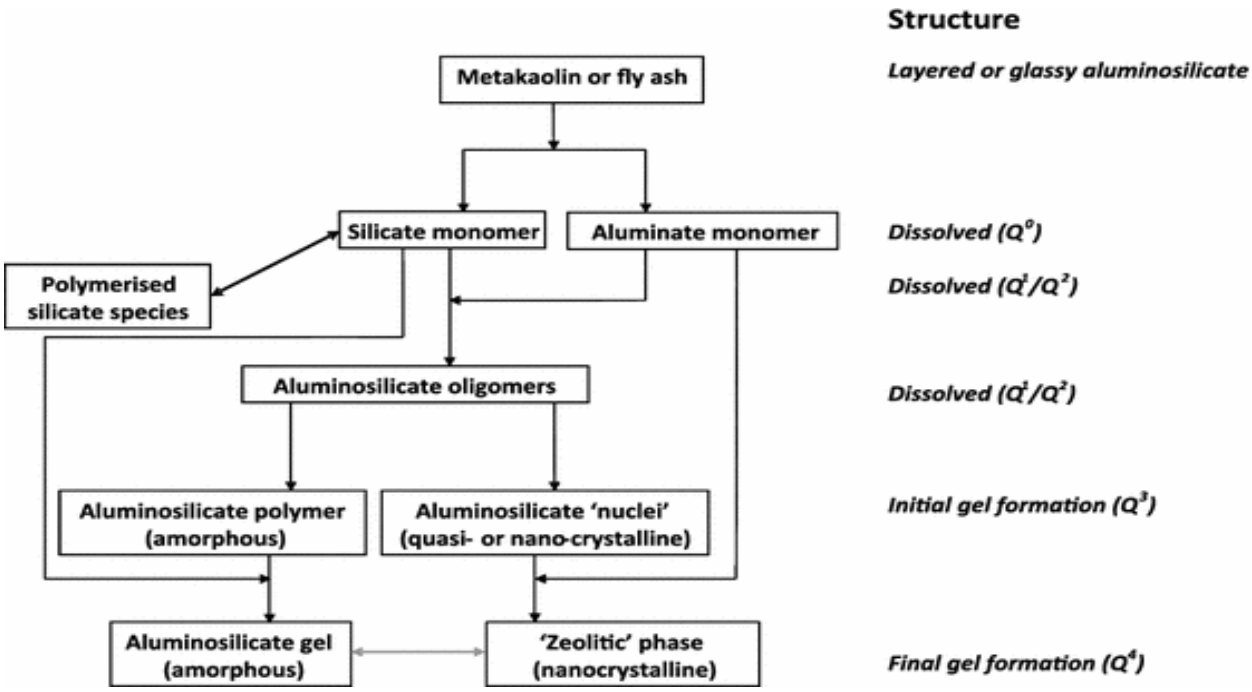

Fig. 2.3 Schematic diagram of an alkali activated low-Ca aluminosilicate source such as metakaolin or low-Ca (siliceous/Class F) fly ash [55]

2.5.2 Research on fly ash based geopolymer

The utilisation of by-product materials in particular fly ash as a geopolymer binders were investigated extensively in recent years [24,25], Previous studies reported that any materials composed of silica and aluminium such as kaolinitic clays, metakaolin, fly ashes, blast furnace slag and blended of fly ashes with slag, metakaolin, red mud, kaolin and stilbite can be alkali-activated. However, according to Rahier et al. [26], Jaarsveld et al. [27], and Hos et al. [28,60] not all the silica and aluminium of prime materials are reactive. The reactivity is linked to the material structure with higher reactivity for higher amorphous content. Moreover, particle size and chemical composition, curing condition, type and concentration of the activator also played critical roles. Divya et al., [29] observed that the activation process and degree of reaction within the fly ash based geopolymer paste is directly related to its glassy content of the ash. The process of fly ash based geopolymerization involves leaching, diffusion, condensation and hardening steps. The thermal treatment of fly ash based geopolymer materials also can change their microstructure with an increase in the amorphous phase as compared to ambient cured flay ash based geopolymer.

Provis [30] and Davidovits [31] concluded that highly alkaline media and curing temperatures are required to kick-start the geopolymerization process of class F fly-ash. However, Fernandez-Jimenez et al. [32] had divided the activation mechanisms in to two main stages; firstly, the dissolution stage where the vitreous phase of aluminosilicate glass is dissolved in alkali solution. Secondly, the polymerisation stage formed with a series of complex ionic species. Fernandez-Jimenez and Palomo **[**32] observed that the reactivity of fly ash in alkali solutions where reactive silica and alumina contents played a vital roles in the geopolymerization process. Divya and Chaudhary [33] suggest that certain synthesis limits

should be used to form strong geopolymeric products. Compositions should lay in the range of 0.2– 0.48, 3.3–4.5, 10–25 and 0.8–1.6 for M_2O/SiO_2 (M represents Na/K/metallic ions), SiO_2/Al_2O_3, H_2O/M_2O and M_2O/Al_2O_3 ratio, respectively. Most of the studies support that geopolymeric materials are prepared from alumino-silicate clay minerals and sodium silicate using restricted range of Si/Al compositions. Xu and van Deventer [34] showed that the dissolution of silicon and aluminium from various aluminosilicate minerals is slower in alkali activator of lower OH^- concentration.

There are several distinct reaction processes from initial pozzolanic activation to final microstructure development. The schematic formation of geopolymer material can be shown as described by Equations (2-2) and (2-3) [35,36]:

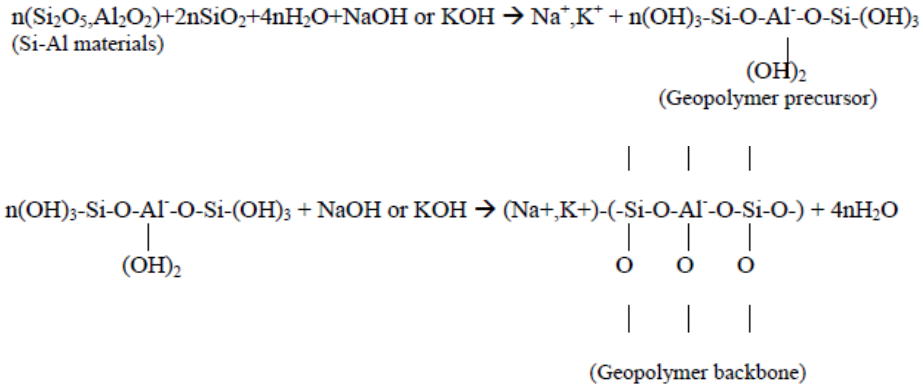

---- (2-2)

---------- (2-3)

2.5.3 Influence of calcium in Fly ash based geopolymer

Calcium content in aluminosilicate materials has a leading influence on the setting process at the initial stages of geopolymerization process. Previous research pointed out that low calcium class F Fly ash based geopolymer usually harden slowly compared to heat cured specimens [37-52]. Inclusion of an appropriate amount of calcium bearing compound such as GGBFS and OPC in fly ash geopolymer helped to overcome this drawback. It is noteworthy that the high CaO content of GGBFS and OPC resulted a very rapid setting in alkaline media which may

not be suitable to use this materials as a geopolymer binder alone. Moreover, the latent hydraulic property of GGBFS and OPC also makes these two materials as an ideal replacement of calcium bearing materials. Krivenko [53] concluded that slag and OPC based binders resulted greater reactivity and provided an extra nucleation site during the geopolymerization process.

Reactivity of calcium bearing materials such as slag and OPC in alkaline solution largely depends on its vitreous structure and its component phases [54, 55]. Yip et al. [56] observed that activation of calcium bearing materials followed a series of reactions:

$$=Si\text{-}O^{-} + R^{+} == Si\text{-}O\text{-}R$$

$$=Si\text{-}O\text{-}R + OH^{-} == Si\text{-}O\text{-}R\text{-}OH^{-}$$

$$=Si\text{-}O\text{-}R\text{-}OH^{-} + Ca^{2+} == Si\text{-}O\text{-}Ca\text{-}OH + R^{+}$$

The amount of CaO in the precursor materials was found to have a considerable effect on the resulting hardened geopolymer. Geopolymers synthesized from materials rich in calcium such as GGBFS and OPC also produce calcium silicate hydrate (CSH) gel or in the form of calcium aluminosilicate gel when activated with an alkaline solution [57, 58, 59]. Puertas et al. [60] observed a formation of CSH gel, hydrotalcite ($Mg_6Al_2CO_3$ (OH) $_{16,}$ 4H2O), pirssonite (Na_2Ca (CO_3), 2H2O) and calcite as a final hydrated product for fly ashes and blast furnace slag blended geopolymer. Tailby and MacKenzie [61] revealed no trace of CSH gel in the final hydrated matrix of OPC blended fly ash based geopolymer. Brough and Atkinson [54] studied the activation of blast furnace slag, and reported that XRD analysis shows no crystalline products Kriven [52] analyzed the heat release in alkali-activated blast furnace slag, and noticed that the hydration process was influenced by the sodium content and the silica modulus (Ms).Yip and Deventer [56] reported that calcium compound increased strength due to the

formation of Ca–Al–Si amorphous structures and observed a coexistence of geopolymeric gel and CSH.

2.5.4 Nature of hydrated geopolymer gel

Previous studies [32, 35, 36] observed sodium aluminosilicate gel as a final hydrated product of alkali activated fly ash which exhibits long- and medium-range of chain length and making it amorphous to X-ray diffraction. Brough et al. [62] and Criado et al. [63] found that no significant amount of crystalline hydration products had formed neither before nor after thermal curing at 80 ^{0}C. However, Steenbruggen and Hollman [64] observed a slight alteration of some crystalline phases such as mullite and quartz in the strong alkaline medium.

The physical and microstructural properties of the geopolymers depend primarily on the ratio of Si/Al, Na/Al and the water content [8]. Hajimohammadi et al. [65] observed analcime formation in systems with low Si availability, while faujasite development was promoted at intermediate or high Si availability. Duxson et al. [66] also observed a correlation between the developments of microstructure with the variation in Si/Al ratio. Specimens with Si/Al $\leq$1.40 exhibited a microstructure comprising large interconnected pores, loosely structured precipitates and unreacted material. Geopolymers with Si/Al ratio $\geq$1.65 are categorized by a largely homogeneous binder containing unreacted particles and some smaller isolated pores a few microns in size.

Effect of Na/Al ratio in the geopolymerization process has been studied previously by several authors [32-56]. Rowles [67]] found that compressive strength increased with increasing Na/Al molar ratios up to a specific value, above which the strength is reduced. Xu and Deventer [34] concluded that increasing sodium content leads to increasing dissolution rates of silica and aluminium in the geopolymeric systems. Fernandez-Jimenez and Palomo

[36] pointed out that the amount of OH^- ion in the alkaline solution contributes towards the dissolution step of Si^{4+} and Al^{3+} from fly ash, whilst the Na^+ ion contributes to the crystallization process. Jianbing et al. [17] found that high specific surface area of nanosilica particles constituted a highly reactive siliceous media in the alkaline environment. High reactive silica content also involves the formation of high amount of alkali aluminosilicate gel and consequently a higher mechanical strength in the resulting material [140]. Catherine et al. [68] reported that beyond maximum specific value of Na/Al ratio, further increases in NaOH content give a reduced rate of geopolymer formation.

2.5.5 Microstructure of fly ash based geopolymer

Microstructure analysis of fly ash based geopolymer has been highlighted to a microporous framework with the high amount of aluminosilicate gel in the matrix. The characterizations of the micro and nanostructures of geopolymer pastes are complex and generally consist of amorphous gels and different unreacted crystalline phases in the activated systems [69-82].

The composition and structure of this alkali aluminosilicate gel depends essentially on the size, structure and concentration of the ionic species present in the medium, as well as on the synthesis temperature on the curing time, and the pH of the mixture [42, 58, 59, 60]. The main reaction product of fly ash based geopolymer is a three-dimensional inorganic alkaline polymer denoted as a N-A-S-H (geopolymer) gel. Rodriguez et al. [83] noted that fly ash geopolymers activated with commercial sodium silicate exhibit a heterogeneous gel structure, with embedded particles of varying morphologies. Kutchko and Kim [84] reported that the microstructure of fly ash based geopolymer mostly consists of amorphous aluminosilicate, along with iron- rich spheres composed of iron oxide mixed with amorphous aluminosilicate with variations in the contents of Al, Si and Fe.

2.6 Mechanical properties of fly ash based geopolymer.

Uses of fly ash based geopolymer in various structural applications were proven by its performance as reinforced concrete beams [85, 86], columns [87] and its resistance to fire [88]. Different studies indicates an equivalent or superior structural performance of fly ash geopolymer concrete as compared to OPC concrete. While most of the previous studies of geopolyers used heat curing for setting and hardening, it is necessary to develop geopolymer mixtures suitable for curing at ambient temperature. This will widen its application beyond precast concrete and reduce the energy required in the heat-curing process.

Geopolymer cements develop through a series of several distinct reaction processes from initial pozzolanic activation to final microstructure development. Divya and Chaudhary [29] suggest that certain synthesis limits should be used to form strong geopolymeric products. Jaarsveld et al. [89] showed that the surface charge on the fly ash particle may also affect the initial setting time of a geopolymer mixture. Diaz et al. [88] found that the setting time of fly ash based geopolymers might be governed by the type of dominant glass structure in the fly ash.

The amorphous aluminosilicate content of the fly ash and its dissolution rate are also considered as the other influencing factors for strength development of geopolymers [90]. However, Xu and Deventer [34] confirm that the dissolution rate of all prime materials are not equal and could not provide enough soluble Si to start the geopolymerization. Previous studies indicate that addition of soluble silica has a significant impact on the reactivity of fly ash. Higher amount of fine particles will result in higher surface area, and therefore higher reactivity, resulting in higher compressive strength [58]. Xu and Deventer [34] observed that fineness of the fly ash plays an important role in the development of mechanical strength of the

hardened geopolymer. Criado et al. [82] found that products of higher strengths consisted of higher soluble silica content when compared the reaction of fly ash with pure NaOH and sodium silicates with moduli up to 1.27.

The roles of other factors such as molarity of NaOH, alkaline content, curing conditions, composition of binder materials [89-92] and post curing chemical treatments [60] were also investigated by other researchers. Results indicated that higher molarity with low alkaline content and elevated curing temperature at early ages enhanced the high early strength of geopolymer systems. Kumar et al. [93] showed that mechanically activated fly ash based geopolymers display higher compressive strength due to the formation of a compact microstructure. The water content in the mixture also played an important role on the properties of geopolymer binders [94]. Hardjito and Rangan [95] found that the compressive strength of geopolymer concrete decreases as the ratio of water-to-geopolymer solids increases.

Fernandez-Jimenez et al. [96] reported that Al-rich aluminosilicate gel develops relatively low mechanical strength with lower Si/Al ratio, whereas Si-rich aluminosilicate gel develops higher mechanical strength with higher Si/Al ratio. The presence of calcium compound in the source material plays a vital role because the Ca^{2+} is capable of acting as a charge-balancing cation within the geopolymeric binder [97] and forms Ca–Al–Si amorphous structures [98]. The Ca^{2+} available in blast furnace slagand OPC are able to create a coexistence of geopolymeric gel and C–S–H that leads to the increase of mechanical strength [98] of geopolymer materials. Several authors [89-92] reported higher compressive strength with slag content increase, explaining that with higher reactivity of the blast furnace slag. Yip and Deventer [36] observed a coexistence of geopolymeric and CSH gel in the final hydrated product which eventually increased the final mechanical strength. However, the major

difference between hydrated calcium silicate gel and aluminosilicate gel will be in terms of their elemental composition with calcium.

2.7 Durability properties of fly ash based geopolymer.

Concrete structures are often exposed to acidic environment such as in ground water, industrial effluents and acid rains. Therefore, acid resistance of concrete is an important property for its performance in aggressive environment. Mehta [99] observed that acid attack on a cementitious binder caused decalcification and formation of soluble products. Chindaprasirt et al. [100] noted that the high strength loss by the acid exposure of alkali activated fly ash-silica fume composites was due to the low initial strength of the mortar and the favourable dissolution of excess silica in the acid solution. However, Bakharev [60] observed better resistance of geopolymers than OPC binders in exposure to aggressive environment. Breck [101] noted that polymer structures with a Si/Al ratio of 1 are more easily attacked by the acid than more siliceous polymers. Ismail et al. [102] found that the H^+ from H_2SO_4 ionization could destroy the alumino-silicate network in geopolymer and yielded silicic acid ($Si(OH)_4$) and aluminium ions (Al^{3+}) from the gel polymer.

The evaluation of the sulfate attack in cementitious binder are generally based on changes in mechanical properties along with expansion of cementitious mortar bar in sulfate solutions. Ismail et al. [102] observed that the presence of magnesium leads to decalcification of the Ca-rich gel phases present in the blended ash/slag geopolymer system, causing degradation of the binder system and the precipitation of gypsum. Bakharev [103] noted that the most significant fluctuation of strength and microstructural changes were took place in 5% sodium sulfate and magnesium sulfate solutions. However, Bascarevic et al. [104] didn't observed any new phases due to a reaction of the geopolymeric material with sulfate ions.

The consequence of carbonation in concrete structure causes a significant reduction of its service life, especially when the structures are reinforced with steel rebar [82,83]. Mohammed et al. [105] found that macro and micro diffusivity properties of hardened concrete such as internal porosity and its pore distribution could be altered due to the longer period of CO_2 exposure. However, the diffusion of CO_2 in hardened concrete depends on a number of factors such as CO_2 concentration, porosity and moisture content of the concrete [106]. Several authors [107,108,109] had studied the effects of carbonation in alkali-activated binders and noted that carbonation mechanism in alkali activated binder might be different from the OPC based binder. According to Bernal et al. [107] different carbonate and bicarbonate phases usually generated in alkali activated binders after the prolonged CO_2 exposure.

2.8 Nanoparticles in fly ash based geopolymer

2.8.1 Brief history of nanoparticles

The field of nano-particles are rapidly maturing into fertile and interdisciplinary research areas from which new multifunctional and smart materials can be developed. Chemical stability, diverse mechanical properties and predicted extreme strength of the nano materials have placed them as fundamental materials in the rapidly growing field of nanotechnology. Application of nano-particles in different types of cementitious binders is receiving ongoing research attention in concrete technology. A relatively good understanding exists regarding the fundamental principles of these materials.

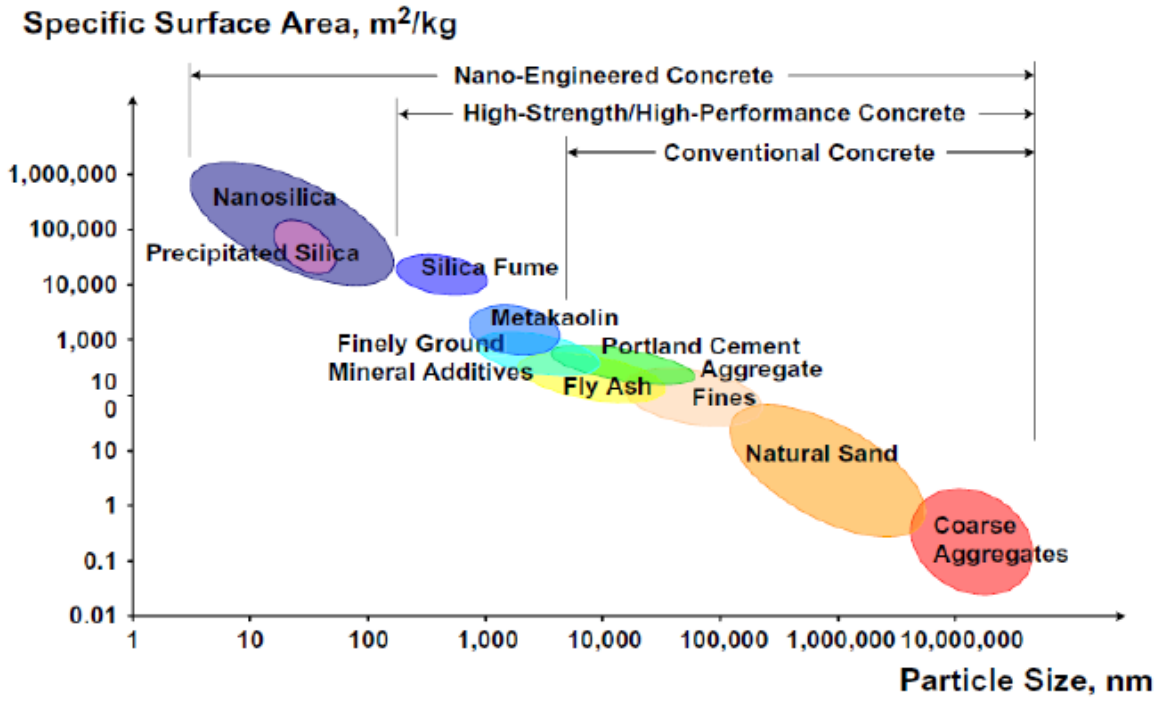

Fig. 2.4 The particle size and specific surface area scale related to concrete materials [7]

Researchers [110,111,112] pointed out that using different nanocomposites into conventional building materials can result in enhanced properties required for civil and infrastructures. Ccementations binders containing different nano particles such as nanosilica, nano aluminia, carbon nanotubes and nanoclays were utilized to improve the microstructure, rate of hydration, pore structure, strength and protective barrier in concrete. Among these nano-particles, nanosilica has been widely used in cement-based composites due to its high content of amorphous SiO_2 (more than 99 % in most products) and large specific surface area.

2.8.2 Challenges in the Preparation of Nanocomposites

It is well established that the final properties of hydrated cement composite with nanoparticles relies on the dispersion of nanoparticles. Kawashima et al. [111] reported that due to the high surface area and energy of nanoparticles the adhesion between two particles are significantly controlled by van der Waals, electrostatic and magnetic forces. Jiang et al. [112] also observed

that when nanoparticle are dispersed in solutions, their hydrodynamic size usually larger than their primary size and tend to remain as agglomerates by an electrical double layer which includes both the inner and outer layers of nuclei. However, previous studies [113,114,115] showed that nanosilica can be well dispersed in liquid media due to the hydrogen bonding between the deprotonated surface silanol groups and the water molecules lead to a formation of a water layer around the particle. Jianbing et al. [116] reported that the self-agglomeration of nanosilica in the liquid media can be reduced with the single dispersion of nanosilica by increasing the thiol-ene click reaction on the nanosilica surface. Moreover, the hydrophilic nature of silane is expected to improve the workability of the mixture and enhance the dispersion of admixtures in the matrix [117]. It has been also reported that proper dispersion of nanomaterials accelerate the hydration process of cementitious binders and increase the capillary pressure, evaporation rate, reduced early age drying shrinkage and cracked area of cementitious binders. Aileen and Wille [118] found that proper dispersion of nanoparticles can lead to improved particle packing density, a key parameter in improving the mechanical, chemical, and durability properties of the cementitious composite.

2.8.3 Mechanical and morphological properties of binders containing nano particles

Nanosilica which is produced synthetically, in the form of a water emulsion of ultrafine amorphous colloidal silica with sizes of 1‑50 nm provides more atoms on the surface of each particle due to its higher surface area. These factor eventually alter the chemical reactivity of nanosilica with enhanced mechanical and microstructure properties of various cementitious binders [119].

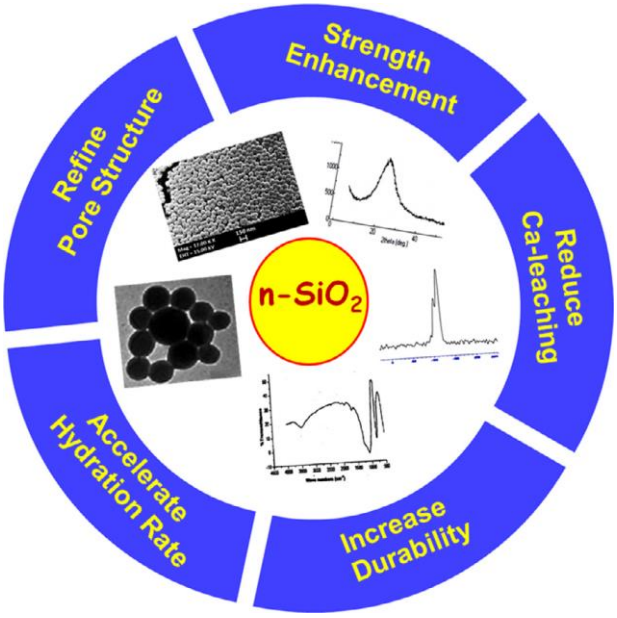

Fig. 2.5 Role of nanosilica in cementitious system [21].

It was reported by different researchers that a small percentage of nanosilica in the cementitious system can result in a considerable strength improvement with a denser microstructure. However, the performance of nanosilica in cementitious materials is dependent on its morphology, method of preparation and its uniform dispersion throughout the cementitious matrix [120,121]. Dolado et al. [122] reported that compressive strength of cementations binders increased progressively with the increase of nanosilica content within the range from 0.2% to 12% by mass of cement. Gaitero et al. [123] and Jain and Neithalath [124] reported that the use of nanosilica in the cementations binders modified the micro and nanostructure of hydrated paste with an improvement of chemical stability of hydrated paste against aggressive environment.

2.8.4 Experimental Determination of Nano-mechanical behaviours of cementitious materials.

Nanoindentation has been a novel and popular technique for measuring the mechanical properties at the surface of concrete specimens. The recorded load versus displacement curves obtained from nanoindentation experiments are widely used to find Young's modulus and the

hardness of the tested materials. This section summarizes the work done by different researchers using nanoindentation technique in an effort to determine nano-mechanical properties of cementitious materials. Oliver and Pharr [125] deduced a method to calculate the E-modulus and hardness of the indent materials based on the curvature of its unloading curve. Zeng and Chiu [126] and Zeng and Shen [127] used an empirical approach to analyse the unloading curve of the indent materials based on the finite element analysis. Constantinides et al. [128] had used grid indentation technique to calculate the E-modulus and hardness of the indent materials. Ulm et al. [129] concluded that a statistical analysis of grid indentation data provides a valuable insight of nanomechanical properties of indent materials. Oliver [125] pointed out that the elastic properties of homogeneous and heterogeneous materials such as cementitious binders can be calculated by nanoindentation techniques. Mondal and Shah [130] reported that the fundamental properties of heterogeneous materials are highly dependent on the microstructure, morphology, and distribution of each phase present at the nanoscale level. Hughes and Trtik [131] used a depth sensing nanoindentation technique to calculate the nanomechanical properties of hydrated cement phases. However, Smilauer and Bittnar [132] concluded that the elasticity and hardness values of cement paste usually decrease with the increase in indentation depth. Constantinides and Ulm [133] and Trtik et al. [134] found that the E-modulus values of hydrated Portland cement in the range of 17 and 34 GPa.

Nanoindentation is a promising approach to predict the nanomechanical properties of different phases such as clinker phases, hydrated phases, aggregates, interfacial transition zone and all other phases that may be present in the hydrated cementitious binders. The nano mechanical properties of geopolymer composites are considered to be a function of the characteristics of the hydrated geopolymer paste matrix. The final hydrated product of fly ash

based geopolymer are amorphous aluminosilicate [42,47, 135] C-S-H gel for slag based geopolymer [41] and composite gels (aluminosilicate and C-S-H gel) for blended series [35,36]. The modulus of elasticity of heat cured cylinder geopolymer specimens were reported by Sarker [136], Fernandez-Jimenez et al. [137], Sofi et al. [138], Hardjito et al. [139] and Wongpa et al. [140] in their studies. Nemecek et al. [141] found the elastic modulus and the hardness of geopolymer paste at the microscopic scale by nanoindentation and observed the elasticity in the range of 15 to 20 GPa.

Interfaces between the aggregate and hydrated gel often play a critical role in influencing the overall material performance of cement composites. Scrivener et al. [142] reported that a high volume of porous phase is generated in the vicinity of aggregate due to the incompatibility between this two phases commonly named as a wall effect. Recent investigation observed that the microstructures of cementitious binders markedly depends on the ITZ properties of hydrated paste. Akcaoglu et al. [143] and Erdem and Dawson [144] stated that the bigger the difference between the strengths of the ITZ and the surrounding matrix, the higher the tendency of micro-cracking in the ITZ. It was observed that addition of mineral admixtures such as silica fume, metakaolin, flyash and nanoparticles in the cementations binders' the interfacial bond strength and interfacial fracture energy is significantly increased [145,146].

2.8.5 Influence of nano particles in fly ash based geopolymer

Property evolution of nanosilica in fly ash based geopolymer can be reflected by the effects of nanosilica on hydration, gel property modification and pore structure refinement of the hydrated product. It was reported by Adak et al. [147] that addition of 6% colloidal nanosilica increased compressive strength of fly ash geopolymers. Gao et al. [148] showed that nanosilica

increased the strength of alkali activated slags. Bjeornstreom [149] observed that the higher specific surface area of nanosilica possess a highly reactive siliceous media in cementations material. Mackay et al. [150] reported that homogeneous and non-agglomerate dispersion of nano materials played a critical role in fabricating the polymeric nanocomposites. Li et al. [151] found that the mechanical and permeability properties of cementitious mortars can be improved with the different size of nano-particles. It is noteworthy that the nucleation effect, filler effect and pozzolanic reactivity of nanosilica played a important roles for the property development at nano-level [152,153,154,155].

2.9 Summary

General background information on cementitious binders, nanoparticle and fly ash based geopolymer are discussed in this chapter. Literature relevant to the fly ash based geopolymer development has been reported with a simplified conceptual model showing the geopolymerization reaction mechanism.

A brief review of nanosilica and ultrafine fly ash in the cementitious binders was also provided in this chapter. Its highlights some critical factors affecting the properties relating to setting time, workability, microstructure and strength of the hydrated cementitious binders. Despite the fact that the addition of nanosilica and ultrafine fly ash in Portland has many advantageous characteristics, however, it has not yet been used in fly ash based geopolymer as extensively as Portland cement.

It has been identified that there is a significant gap of research in the area of fly ash based geopolymer binders with and without nanosilica and ultrafine fly ash for ambient curing condition. Current drawbacks such as slow setting, high porosity and subsequent slow strength development of low calcium fly-ash geopolymers also pointed which might be altered with

these finer materials. Mixtures modified with additives have been designed and the methodology of experimental works has been detailed.

2.10 Reference

1. L.K.Turner, and F. G. Collins. Carbon dioxide equivalent (CO2-e) emissions: A comparison between geopolymer and OPC cement concrete. Constr. Build.Mater.43(2013)125-130
2. D.N. Huntzinger, and T.D. Eatmon, A life-cycle assessment of cement manufacturing: comparing traditional process with alternative technologies, J Clean Prod, 17 (7) (2009) 668–675
3. C. D. Lawrence. the Production of Low-Energy Cements. In: HEWEIT, P, C (ed.) Lea's Chemistry of Cement and Concrete, (Fourth Edition) (1998). (pp. 421-470). Oxford: Butterworth-Heinemann.
4. D. Baweja, and P. Nelson. Supplementary Cementing Materials: Their Acceptance in Australian Specifications. Sixth CANMET/ACI International Conference on Fly Ash, Silica.
5. A. Samarin., R.L. Munn, and J.B. Ashby. The Use of Fly Ash in Concrete - Australian Experience. First International Conference on the Use of Fly Ash, Silica Fume, Slag and Other Mineral By-Products in Concrete, ACI SP79, Montebello, Canada, pp. (1983) 143-172Ll
6. J. Davidovits. High-Alkali Cements for 21st Century Concretes. in Concrete Technology, Past, Present and Future. Proceedings of V. Mohan Malhotra Symposium, Editor: P. Kumar Metha

7. Duxson, P., and Fernandez-Jimenez, A. Geopolymer Technology: The Current State of the Art, J Mater Sci, 42 (9) (2007) 2917–2933
8. B.V. Rangan. Fly ash-based geopolymer concrete, Research Report GC 4, Engineering Faculty, Curtin University of Technology, Perth, Australia, 2008.
9. P. Duxson, A. Fernandez-Jimenez, J.L. Provis, G.C. Lukey, A. Palomo, and J.S.J. Deventer. Geopolymer technology: the current state of the art, J. Mater. Sci. 42 (9) (2007) 2917e2933.
10. D. Khale, and R. Chaudhary. Mechanism of geopolymerisation and factors influencing its development: a review, J. Mater. Sci. 42 (2007) 729e746.
11. P. Deb, P. Nath, and P.K. Sarker. The effects of ground granulated blast-furnace slag blending with fly ash and activator content on the workability and strength properties of geopolymer concrete cured at ambient temperature, Mater. Des.62 (2014) 32e39.
12. P.S. Deb, P. Nath, and P.K. Sarker. Strength and permeation properties of slag blended fly ash based geopolymer concrete, Adv. Mater. Res. 651 (2013)
13. A. Fernandez-Jimenez, A.G. Torre, A. Palomo, O.G. Lopez, M.M. Alonso, and M.A.G. Aranda. Quantitative determination of phases in the alkali activation of fly ash. Part I. Potential ash reactivity, Fuel 85 (2006) 625–634, http://dx.doi.org/10.1016/ j.fuel.2005.08.014.
14. W.C.T. Nigel, and A.V. Riessen. Determining the reactivity of a fly ash for production of geopolymer, J. Am. Ceram. Soc. 92 (2009) 881–887, http://dx.doi.org/ 10.1111/j.1551-2916.2009.02948.x.
15. J. Davidovits. Geopolymer Chemistry and Application, second ed., InstitutGéopolymère, Saint-Quentin: France, 2008.

16. J.G.S. Jaarsveld, J.S.J. Deventer, and L. Lorenzen. Factors affecting the immobilisation of metals in geopolymerised fly ash, Metall. Mater. Trans. B 29B (1998) 283–291.
17. P. Duxson, A. F. JimEnez, J.L. Provis, and G.C. Lukey, A. Palomo, J.S.J. van Deventer. Geopolymer technology: The current state of the art. J. Mater. Sci. 42 (2007) 2917–2933. http://dx.doi.org/10.1007/s10853-006-0637-z.
18. A. Palomo, M.W. Grutzeck, and M.T. Blanco. Alkali-activated fly ashes a cement for the future." Cem. Concr. Res., 29(2009) 1323–1329.
19. F. Collins, and J.G. Sanjayan. Effects of ultrafine materials on workability and strength of concrete containing alkali-activated slag as the binder, Cem. Concr. Res. 29 (1999) 459–462
20. M. Albitar, M.M. Ali, P. Visintin, and M. Drechsler. Effect of granulated lead smelter slag on strength of fly ash-based geopolymer concrete, Constr. Build. Mater., 83(2015) 128-135
21. ASTM Standard. Standard Specification for Coal Fly Ash and Raw or Calcined Natural Pozzolan for Use in Concrete. (ASTM C 618-2012), retrieved from http:// www.specs4.ihserc.com
22. A.F. JimEnez, and A, Palomo. Characterization of fly ashes. Potencial reactivity as alkaline cements. FUEL. 82(18) (2003) 2259–2265. http://dx.doi.org/10.1016/ S0016-2361(03)00194-7.
23. A.F. JimEnez, A, Palomo, A. I. Sobrados, and J. Sanz. The role played by the reactive alumina content in the alkaline activation of fly ashes. Microporous and Mesoporous materials. 91(2006) 111–119. http://dx.doi. org/10.1016/j.micromeso.2005.11.015.

24. B. Singh, G. Ishwarya, M. Gupta, and S.K. Bhattacharyya. Geopolymer concrete: A review of some recent developments. Construction and Building Materials, 85(15) (2015) 78-90
25. H. Rami, O. A. Haddad. Production of geopolymer concrete using natural pozzolan: A parametric study. Construction and Building Materials, 114 (2016) 699-707
26. A. Islam, U. Alengaram, M. Jumaat, I.I. Bashar, and S.M. Kabir. Engineering properties and carbon footprint of ground granulated blast-furnace slag-palm oil fuel ash-based structural geopolymer concrete. Construction and Building Materials, 101 (30)(2015) 503-521
27. A. Karthik, K. Sudalaimani, C.T.V. Kumar. Investigation on mechanical properties of fly ash-ground granulated blast furnace slag based self curing bio-geopolymer concrete. Construction and Building Materials, 149 (2017) 338-349
28. T. Sathanandam, P.O. Awoyera, V. Vijayan, and K. Sathishkumar. Low carbon building: Experimental insight on the use of fly ash and glass fibre for making geopolymer concrete. Sustainable Environment Research, 27 (2017) 146-153
29. W.K. Part, M. Ramli, C.B. Cheah. An overview on the influence of various factors on the properties of geopolymer concrete derived from industrial by-products. Construction and Building Materials, 77 (2015) 370-395
30. Provis J.L. Introduction to geopolymers. In: Geopolymers, structure, processing, properties and industrial applications. J.L. Provis and J.S.J. van Deventer (Eds.). Woodhead Publishing Limited, Oxford, U.K.
31. J. Davidovits. Geopolymer Chemistry and Application, second ed., InstitutGéopolymère, Saint-Quentin: France, 2008.

32. A. Fernandez-Jimenez, and A. Palomo. Characterisation of fly ashes potential reactivity as alkaline cements, Fuel 82 (2009) 2259–2265, http://dx.doi.org/10.1016/S0016-2361(03)00194-7.

33. D. Khale, and R. Chaudhary. Mechanism of Geopolymerization and Factors Influencing Its Development: A Review. J. Mater. Sci., 42 (2007)729-746.

34. H. XU, J. S. J. VAN DEVENTER. Int. J. Miner. Process. 59 (2000) 247

35. J.G.S. Jaarsveld, J.S.J. Deventer, and L. Lorenzen, The potential use of geopolymeric materials to immobilise toxic metals: Part I. Theory and applications. Miner Eng 10 (1997)659–69.

36. J.P. Hos, P.G. McCormick, and L.T. Byrne. Investigation of a synthetic aluminosilicate inorganic polymer. J Mater Sci 37 (2002) 2311–6

37. F.N. Okoye, J. Durgaprasad, N.B. Singh. Mechanical properties of alkali activated flyash/Kaolin based geopolymer concrete. Construction and Building Materials, 98 (2015) 685-691

38. A.A. Aliabdo, M. Elmoaty, A. Elmoaty, and H. Salem. Effect of cement addition, solution resting time and curing characteristics on fly ash based geopolymer concrete performance. Construction and Building Materials, 123 (2016) 581-593

39. L.N. Assi, E. Deaver, M.K. ElBatanouny, and P. Ziehl. Investigation of early compressive strength of fly ash-based geopolymer concrete. Construction and Building Materials, 112(2016) 807-815

40. Zaetang, Y., Wongsa, A., Sata, V., Chindaprasirt, P. Use of coal ash as geopolymer binder and coarse aggregate in pervious concrete. Construction and Building Materials, 96 (2015) 289-295

41. A. Islam, U.J. Alengaram, M. Jumaat, I.I. Bashar, and S.M. Kabir. Engineering properties and carbon footprint of ground granulated blast-furnace slag-palm oil fuel ash-based structural geopolymer concrete. Construction and Building Materials, Volume 101 (2015) 503-521
42. B. Panda, S.C. Paul, L.J. Hui, Y.D. Tay, and M.J. Tan. Additive manufacturing of geopolymer for sustainable built environment. Journal of Cleaner Production, Volume 167 (2017) 281-288
43. F.N. Okoye. Geopolymer binder: A veritable alternative to Portland cement. Materials Today: Proceedings, 4 (4) (2017) 5599-5604
44. A. Mehta, and R. Siddique. An overview of geopolymers derived from industrial by-products. Construction and Building Materials, 127 (2016) 183-198
45. K.M. Liew, A.O. Sojobi, and L.W. Zhang. Green concrete: Prospects and challenges. Construction and Building Materials, Volume 156 (2017) 1063-1095
46. E.M. Kumar, E. Ramamurthy. Influence of production on the strength, density and water absorption of aerated geopolymer paste and mortar using Class F fly ash. Construction and Building Materials, 156 (2017) 1137-1149
47. N. Toniolo, and A.R. Boccaccini. Fly ash-based geopolymers containing added silicate waste. A review. Ceramics International, 43 (2017) 14545-14551
48. N. Palankar, A.U.R. Shankar, and B.M. Mithun. Studies on eco-friendly concrete incorporating industrial waste as aggregates. International Journal of Sustainable Built Environment, 4 (2015) 378-390

49. A. Gharzouni, L. Vidal, N. Essaidi, E. Joussein, and E. Rossignol. Recycling of geopolymer waste: Influence on geopolymer formation and mechanical properties. Materials & Design, 94 (2016) 221-229
50. B. Bhardwaj, P. Kumar. Waste foundry sand in concrete: A review. Construction and Building Materials, 156 (2017) 661-674
51. S.Y. Oderji, B. Chen, and S.Y. Jaffar. Effects of relative humidity on the properties of fly ash-based geopolymers. Conscv/45dn.l;7yhgbv8ikjEQa,lType equation here.truction and Building Materials, 153 (2017) 268-273
52. W.M. Kriven. Geopolymer-Based Composites. Comprehensive Composite Materials II, 5 (2018) 269-280
53. P. Krivenko, and J. Skurchinskaya. In: Proceedings of the International Conference on the Utilization of Fly Ash and Other Coal Combustion By-products, Shanghai, (1991) 64.1–64.7.
54. A.R. Brough, and A. Atkinson. Sodium silicate-based alkali-activated slag mortars. Part I. Strength, hydration and microstructure. Cement Concrete Res 32 (2002)865–79.
55. K. Wang, and S. Shah, A. Mishulovich. Effects of curing temperature and NaOH addition on hydration and strength development of clinker-free CKD-fly ash binders. Cement and Concrete Composites, 34(2) (2004) 299–309
56. C.K.Yip, and S.J.S. Deventer. Microanalysis of calcium silicate hydrate gel formed within a geopolymeric binder. J Mater Sci 38(203) 3851–60
57. R.A. Feely, C.L. Sabine, K.Lee, W. Berelson, J. Kleypas, and V.J. Fabry. Impact of anthropogenic CO2 on the CaCO3 system in the oceans, Sci 305 (2004) 362–6

58. D. M. Roy, and G. M. Idorn. Hydration, Structure, and Properties of Blast- Furnace Slag Cements, Mortars, and Concrete. Journal of the American Concrete Institute, 79(6) (1982) 444-457.

59. P. Duxson, G. Lukey, and J. Deventer. Physical evolution of geopolymer derived from metakaolin up to 1000 °C. Journal of Materials Science, 42(9) (2007) 3044-3054, retrieved from http:// www.springerlink.com

60. F. Puertas, S. M.Ramirez, S. Alonso, and T. Vasquez, Alkali- activated fly ash/slag cement. Strength behaviour and hydration products. CemConcr Res 30 (2000)1625–32.

61. J. Tailby, and K.J.D. MacKenzie. Structure and mechanical properties of aluminosilicate geopolymer composites with Portland cement and its constituent mineralsCemConc Res, 40 (2010), pp. 787–794

62. A.R. Brough, A. Katz, G.K. Sun, L.G. Struble, R.J. Kirkpatrick, and J.F. Young. Adiabatically cured, alkali-activated cement-based waste forms containing high levels of fly ash: formation of zeolites and Al-substituted C–S–H. CemConcr Res 31(10) (2001) 1437–47.

63. M. Criado, A. F. Jiménez, A.G. Torre, M.A.G. Aranda, and A. Palomo. An XRD study of the effect of the SiO2/Na2O ratio on the alkali activation of fly ash. CemConcr Res 37(5) (2007) 671–9.

64. G. Steenbruggen, and G.G. Hollman. The synthesis of zeolites from fly ash and the properties of the zeolite products, J. Geochem. Explor. 62 (1998) 305–309.

65. A. Hajimohammadi, J.L. Provis, and J.S.J. van Devente. The effect of silica availability on the mechanism of geopolymerisation. CemConcr Res 41(3) (2011) 210–6.

66. P. Duxson, J.L. Provis, G.C. Lukeya, S.W. Mallicoat, W.M. Kriven, and J.S.J. Deventer. Understanding the relationship between geopolymer composition, microstructure and mechanical properties, Colloid Surf. A: Physicochem. Eng. Asp. 269 (2005) 47–58.
67. M. Rowles, and NB.O'Connor. Chemical optimisation of the compressive strength of aluminosilicate geopolymers synthesised by sodium silicate activation of metakaolinite. J Mater Chem 2003; 13: 1161.
68. A. Catherine, J.L. Provis, G.C. Lukey, and J.S.J. Deventer. In situ ATR-FTIR study of the early stages of fly ash geopolymer gel formation, Am. Chem. Soc. 23 (17) (2007) 9076–9082.
69. Puertas T. Bakharev. Geopolymeric materials prepared using Class F fly ash and elevated temperature curing. Ceme Concr Rese 35(2005) 1224–1232.
70. H. Rahier, B.V. Melle, M. Biesemans, J. Wastiels, and X.Wu. Low temperature synthesized aluminosilicate glasses. Part I. Low temper- ature reaction stoichiometry and structure of a model compound. J Mater Sci (1996) 31:71–9.
71. J.G.S. Jaarsveld, J.S.J. Deventer, and L. Lorenzen, The potential use of geopolymeric materials to immobilise toxic metals: Part I. Theory and applications. Miner Eng 10 (1997)659–69.
72. J.P. Hos, P.G. McCormick, and L.T. Byrne. Investigation of a synthetic aluminosilicate inorganic polymer. J Mater Sci 37 (2002) 2311–6.
73. A. Palomo, S. Alonso, A. Fernández-Jiménez, I. Sobrados, and J. Sanz. Alkaline activation of fly ashes: NMR study of the reaction products, J. Am. Ceram. Soc. 87 (2004) 1141–1145.

74. A. Fernández-Jiménez, A. Palomo. Composition and microstructure of alkali activated fly ash binder: effect of the activator, Cem. Concr. Res. 35 (2005) 1984–1992.

75. P. Deb, P. Nath, and P.K. Sarker. The effects of ground granulated blast-furnace slag blending with fly ash and activator content on the workability and strength properties of geopolymer concrete cured at ambient temperature, Mater. Des.62 (2014) 32e39.

76. P.S. Deb, P. Nath, and P.K. Sarker. Strength and permeation properties of slag blended fly ash based geopolymer concrete, Adv. Mater. Res. 651 (2013)

77. S.C. Pal, A. Mukherjee, and S.R. Pathak. Investigation of hydraulic activity of ground granulated blast furnace slag in concrete. Cem. Concr. Res. 33 (2003) 1481–1486. http://dx.doi.org/10.1016/S0008-8846(03)00062-0.

78. M. Steveson, and K. Sagoecrentsil. Relation between composition, structure and strength of inorganic polymers. Part2: fly ash derived in organic polymers, J. Mater. Sci. 40 (2005) 4247–4259.

79. J.S. Belkowitz, W.B. Belkowitz, K. Nawrocki, and F.T. Fisher. The impact of nano silica size and surface area on concrete properties, Mater. J. 112 (2015) 419–428.

80. A. Catherine, J.L. Provis, G.C. Lukey, and J.S.J. Deventer. In situ ATR-FTIR study of the early stages of fly ash geopolymer gel formation, Am. Chem. Soc. 23 (17) (2007) 9076–9082.

81. W.C.T. Nigel, and A.V. Riessen. Determining the reactivity of a fly ash for productionof geopolymer, J. Am. Ceram. Soc. 92 (2009) 881–887, http://dx.doi.org/10.1111/j.1551-2916.2009.02948.x.

82. M. Criado, A. Fernandez-Jimenez, A.G. Torre, M.A.G. Aranda, and A. Palomo. An XRD study ofthe effect of the SiO2/Na2O ratio on the alkali activation of fly ash, Cem. Concr.Res. 37 (2007) 671–679, http://dx.doi.org/10.1016/j.cemconres.2007.01.013.
83. E.D. Rodríguez, S.A. Bernal, J.L. Provis, J. Paya, J.M. Monzoa, and M.V. Borrachero. Effect of nanosilica-based activators on the performance of an alkali-activated fly ash binder, Cem. Concr. Comp. 35 (2013) 1–11, http://dx.doi.org/10.1016/j.cemconcomp.2012.08.025.
84. B.G. Kutchko, and A.G. Kim. Fly ash characterization by SEM-EDS, Fuel 85(2006)2537–44.
85. E.H. Chang, P.K. Sarker, N.Lloyd, and B.V. Rangan, Shear behaviour of reinforced fly ash-based geopolymer concrete beams Proc., 23rd Biennial Conf., Concrete Institute of Australia, Adelaide,
86. D.M.J Sumajouw, D. Hardjito, S.E. Wallah, and B.V. Rangan. Fly ash-based geopolymer concrete: Study of slender columns, J. Mater. Sci., 42(9) (2007) 3124–3130.
87. P.K. Sarker, and S. Mcbeath. Fire endurance of steel reinforcedfly ash geopolymer concrete elements." Constr. Build. Mater. 90(2015) 91–98.
88. E.I. Diaz, E.N. Allouche, and S. Eklund. Factors affecting the suitability of fly ash as source materials for geopolymers. Fuel 89 (2010) 992-996, retrieved from http:// www.sciencedirect.com
89. J.G.S. Jaarsveld, J.S.J. Deventer, and L. Lorenzen. Factors affecting the immobilisation of metals in geopolymerised fly ash, Metall. Mater. Trans. B 29B (1998) 283–291

90. P.S. Deb, P. Nath, and P.K. Sarker. Strength and permeation properties of slag blended fly ash based geopolymer concrete, Adv. Mater. Res. 651 (2013) 168–173. doi.org/10.4028/www.scientific.net/AMR.651.168.
91. P.S. Deb, P. Nath, and P.K. Sarker. Properties of fly ash and slag blended geopolymer concrete cured at ambient temperature. 7th International Structural Engineering and Construction Conference. Honolulu: USA; 2013.
92. P.S. Deb, P. Nath, and P.K. Sarker. The effects of ground granulated blast-furnace slag blending with fly ash and activator content on the workability and strength properties of geopolymer concrete cured at ambient temperature, Mater. Des. 62 (2014) 32–39, http://dx.doi.org/10.1016/j.matdes.2014.05.001.
93. S. Kumar, R. Kumar, T.C. Alex, A. Bandopadhyay, and S.P. Mehrotra. Effect of mechanically activated fly ash on the properties of geopolymer cement. In: Davidovits, J. (Ed.), Proceedings of the World Congress Geopolymer. Saint Quentin, France, 28 June–1 July, pp. 113–116 (2005)
94. V. F. F. Barbosa, and K. J. D. MacKenzie, C. Thaumaturgo. Synthesis and Characterization of Materials Based on Inorganic Polymers of Alumina and Silica: Sodium Polysialate Polymers. International Journal of Inorganic Materials, 2, 309
95. D. Hardjito, and B.V. Rangan. Development and Properties of Low Calcium Fly Ash Based Geopolymer Concrete. Research Report GC1, Faculty of Engineering, Curtin University of Technology
96. F. A.Jimenez, A. Palomo, I. Sobrados, and J. Sanz. The role played by the reactive alumina content in the alkaline activation of fly ashes. MicroporMesopor Mater 91 (2006)111–9.

97. J. Davidovits. Geopolymers: inorganic polymeric new materials, J. Thermal. Anal. 37 (1991) 1633–1656

98. J.E. Oh, P.J.M. Monteiro, S.J. Ssang, C. Sejin, and S.M. Clark. The evolution of strength and crystalline phases for alkali-activated ground blast furnace slag and fly ash-based geopolymers, Cem. Concr. Res. 40 (2010) 189–196, http://dx.doi. org/10.1016/j.cemconres.2009.10.010

99. P.K. Mehta. Studies on chemical resistance of low water/cement ratio concrete, Cem. Concr. Res. 15 (1985) 969.

100. P. Chindaprasirt, P. Paisitsrisawat, and U. Rattanasak. Strength and resistance to sulfate and sulfuric acid of ground fluidized bed combustion fly ashesilica fume alkali-activated composite, Adv. Powder Technol. 25 (2014) 1087e1093.

101. D.W. Breck. Zeolite Molecular Sieves: Structure, Chemistry and Use, Wiley- Inter Science, New York, 1974, pp. 415e418.

102. I. Ismail, S.A. Bernal, J.L. Provis, S. Hamdan, and J.S.J. Deventer. Microstructural changes in alkali activated fly ash/slag geopolymers with sulfate exposure, Mater. Struct. 46 (2013) 361e373.

103. T. Bakharev, Geopolymeric materials prepared using Class F fly ash and elevated temperature curing. Ceme Concr Rese 35(2005) 1224–1232.

104. Z. Bascarevic, Z. Miladinovic, N. Marjanovic, M. Komljenovic, V. Nikolic, and R. Petrovic. Impact of sodium sulfate solution on mechanical properties and structure of fly ash based geopolymers. Materials and Structures 48(2015) 683–697

105. M.K. Mohammed, A.R. Dawson, and N.H. Thom. Carbonation of filler typed self-compacting concrete and its impact on the microstructure by utilization of 100% CO2 accelerating techniques. Construction and Building Materials 50 (2014) 508–516

106. V.G. Papadakis, C.G. Vayenas, and M.N. Fardis. Fundamental modeling and experimental investigation of concrete carbonation. ACI Mater J 88 (1991)363–73.

107. S.A. Bernal, R.S. Nicolas, J.L. Provis, R.M. Gutie´rrez, and J.N.J Deventer. Natural carbonation of aged alkali-activated slag concretes. Mater Struc 47(2014) 693–707

108. K. Sobolev, and F. M. Gutiérrez. How nanotechnology can change the concrete world: Part 1. American Ceramic Society Bulletin, 10 (2005) 14–17.

109. F.Sanchez, and K. Sobolev. Nanotechnology in concrete – A review. Construction and Building Materials, 24 (11) (2010) 2060–2071.

110. P. Trtik, and P.J.M. Bartos. Nanotechnology and concrete: What can we utilise from the upcoming technologies? Proceeding of the 2nd Anna Maria workshop: Cement & Concrete: Trends & Challenges, pp. 109–12 (2001) Anna Maria, FL, USA.

111. S. Kawashima, J. W. Ted, D. Corr, C. Mark, and P.H. Surendra. Dispersion of CaCO3 nanoparticles by sonication and surfactant treatment for application in fly ash–cement systems. Mater and Struc. 47 (6) (2014) 011–1023

112. J. Jiang, G. Oberdorster, and P. Biswas. Characterization of size, surface charge, and agglomeration state of nanoparticle dispersions for toxicological studies. JNR11 (2008)77–89.

113. R. K. Chemistry of silica – Solubility, polymerization, colloid and surface Properties and biochemistry, 896 (1979) Wiley, New York.

114. S. Chen, G. Øye, and J. Sjöblom. Effect of pH and salt on rheological properties of aerosil suspensions. Journal of Dispersion Science and Technology, 28 (2007) 845–853.

115. P. Ding, and A.W. Pacek. De-agglomeration of silica nanoparticles in the presence of surfactants. J Disper Scie Tech 29(2008) 593–599.

116. W.U.L Jianbing, W. Baojun, M.A. Guozhang, and L. Lixia. Grafting of hyperbranched polymer onto the nanosilica surface and their effect on the properties of UV-curable coatings, Polym. Bull. 73(3) (2016) 859–873

117. Y. Xu, and D.D.L. Chung. Improving silica fume cement by using silane Cem. Concr. Res 30 (2000) 1305–1311

118. V. Aileen, and K. Wille. Understanding the Dispersion Mechanisms of Nanosilica in Ultra High Performance Concrete Nano Constr (2015) 311-316

119. F. Sanchez, and K. Sobolev. Nanotechnology in concrete-a review, Constr. Build. Mater. 24 (2010) 2060‑2071.

120. K. Sobolev, I. Flores, M.L.M. Torres, P.L. Valdez, E. Zarazua, and E.L. Cuellar. Engineering of SiO2 nanoparticles for optimal performance in nano cement based materials, Nanotech Constr. 3 (Spring 2009) 139e148.

121. P.S. Deb, P.K. Sarker, and S. Barbhuiya. Effects of nanosilica on the strength development of geopolymer cured at room temperature, Constr. Build. Mater. 10 (1) (2015) 675e683.

122. J.S. Dolado, I. Campillo, E. Erkizia, J.A. Ibanez, A. Porro, A. Guerrero, and S. Goni. Effect of nanosilica additions on belite cement pastes held in sulphate solutions, J. Am. Ceram. Soc. 90 (12) (2007) 3963–3976.

123. J.J. Gaitero, I. Campillo, and A.Guerrero. Reduction of the calcium leaching rate of cement paste by addition of silica nanoparticles. Cem Concr Res 38 (2008)1112–1118

124. .A. Jain, N. Neithalath. Beneficial effects of small amount of nanosilica on the chemical stability of cement pastes exposed to neutral pH environments. ACI Mater J 267 (2009) 59–74

125. W.C. Oliver, and G.M.R. Pharr. An improved technique for determining hardness and elastic modulus using load and displacement sensing indentation experiments. J Mater Res 7(1992)1564–83.

126. K. Zeng and C.-h Chiu. An analysis of load-penetration curves from instrumented indenta- tion, Acta Mater. 49 (2001) 3539–3551.

127. K. Zeng and L. Shen. A new analysis of nanoindentation load-displacement curves, Phil. Mag. A 82 10, 2002, pp. 2223–2229.

128. G. Constantinides, K.S.R. Chandran, F.J.Ulm, and K.J.V. Vliet. Grid indentation analysis of composite microstructure and mechanics: principles and validation. Mater SciEngA 430 (2006)189–202

129. F.-J. Ulm, M. Vandamme, C. Bobko, J.A. Ortega, K. Tai, and C. Ortiz. Statistical indentation techniques for hydrated nanocomposites: concrete, bone, and shale, Journal of the American Ceramic Society 90 (9) (2007) 2677–2692.

130. P. Mondal, S.P. Shah, and L. Marks. A reliable technique to determine the local mechanical properties at the nanoscale for cementitious materials, Cem. Concr. Res. 37(2007) 1440–1444

131. J. J. Hughes and P. Trtik. Micro-mechanical properties of cement paste measured by depth- sensing nanoindentation: a preliminary correlation of physical properties with phase type. Materials Characterization, 53(2-4) (2004) 223–231

132. V. Smilauer, and Z. Bittnar. Microstructure-based micromechanical prediction of elastic properties in hydrating cement paste. CemConcr Res 36 (2006)1708–18

133. G. Constantinides, and F.J. Ulm. The effect of two types of C–S–H on the elasticity of cement-based materials: results from nanoindentation and micromechanical modeling. CemConcr Res 34 (2004)67–80.

134. P. Trtik, J. Kaufmann, and U. Volz. On the use of peak-force tapping atomic force microscopy for quantification of the local elastic modulus in hardened cement paste. Cem Concr Res 42 (2012)215–21.

135. J.A. Jain, and N. Neithalath. Beneficial effects of small amount of nanosilica on the chemical stability of cement pastes exposed to neutral pH environments. ACI Mater J 267 (2009) 59–74

136. P. K. Sarker. .Analysis of geopolymer concrete columns, Materi Structu 42(2009) 715–724

137. A. F. Jimenez, and A. Palomo. Engineering properties of alkali-activated fly ash concrete. ACI Mater J 103(2) ,(2006) 106–112

138. M. Sofi, J.S.J van Deventer, and P.A. Mendis. Engineering properties of inorganic polymer concretes (IPCs). Cement Concr Res 37(2007) 251–257. doi:10.1016/j.cemconres. 2006.10.008

139. D. Hardjito, S.E. Wallah, and M.J. Sumajouw. The stress–strain behaviour of fly ash-based geopolymer concrete. In: Developments in mechanics of structures and materials. A ABalkema Publishers, The Netherlands, (2005) 831–834

140. J. Wongpa, K. Kiattikomol, C. Jaturapitakkul, and P. Chindaprasirt. Compressive strength modulus of elasticity, and water permeability of inorganic polymer concrete. Mater Des 31(2010) 4748–54.

141. J. Nemecek, V. Šmilauer, and L. Kopecky. Nanoindentation characteristics of alkali-activated aluminosilicate materials. CemConcr Compos 33 (2011)163–70.

142. K. Scrivener, A.K. Crumbie, and P. Laugesen. The Interfacial Transition Zone (ITZ) Between Cement Paste and Aggregate in Concrete. Interface Sci 12(2004) 411–21.

143. R. Akcaoglu, M. Tokyay, and T. Celik. Assessing the ITZ microcracking via scanning electron microscope and its effect on the failure behavior of concrete, Cem. Concr. Res. 35 (2005) 358–363.

144. S. Erdem, A.R. Dawson, and N.H. Thom. Influence of the micro- and nanoscale local mechanical properties of the interfacial transition zone on impact behavior of concrete made with different aggregates, Cem. Concr. Res. 42 (2012) 447–458.

145. K. Mitsui, Z.J. Li, D.A. Lange, and S.P. Shah. Relationship between microstructure and mechanical-properties of the paste-aggregate interface, J. Aci. Mater. 91 (1994) 30–39.

146. A.H. Asbridge, G.A. Chadbourn, and C.L. Page. Effects of metakaolin and the interfacial transition zone on the diffusion of chloride ions through cement mortars, Cem. Concr. Res. 31 (2001) 1567–1572.

147. D. Adaka, M. Sarkarb, and S. Mandala. Effect of nanosilica on strength and durability of fly ash based geopolymer mortar, Constr. Build Mater. 70 (2014) 453–459.

148. X. Gao, Q.L. Yu, and H.J.H. Brouwers. Characterization of alkali activated slag flyash blends containing nanosilica, Constr. Build. Mater. 98 (2015) 397e406.

149. J. Bjornstrom, A. Martinelli, J.R.T. Johnson, A. Matic, and I. Panas. Chem. Phys. Lett. 380 (2003) 165.

150. M.E. Mackay, A. Tuteja, P.M. Duxbury, C.J. Hawker, B.V. Horn, and Z.B. Guan. General strategies for nanoparticle dispersion. Science 1(2006) 311:1740.

151. H. Li, H.G.Xiao, J. Yuan, and J. Ou. Microstructure of cement mortar with nano-particles. Compos Part B 1(2003) 35.

152. J.Y. Shih, T.P. Chang, and T.C. Hsiao. Effect of nanosilica on characterization of Portland cement composite, Mater. Sci. Eng. A-Struct. 424 (2006) 266–274.

153. G. Quercia, G. Hüsken, and H.J.H. Brouwers. Water demand of amorphous nano silica and its impact on the workability of cement paste, Cem. Concr. Res. 42 (2012) 344–357.

154. M.H. Zhang, and J. Islam. Use of nanosilica to reduce setting time and increase early strength of concretes with high volumes of fly ash or slag, Constr. Build. Mater. 29 (2012) 573–580.

155. Y.Qing, Z. Zenan, K. Deyu, and C. Rongshen. Influence of nano-SiO2 addition on properties of hardened cement paste as compared with silica fume. Constr Build Mater 21(3) (2007) 539–45.

CHAPTER 3

GEOPOLYMER DESIGN, MIXING, CURING AND EXPERIMENTAL CONDITION

3.1 Overview

Despite the fact that geopolymer mechanism was developed over a couple of decades ago and has many advantageous characteristics, it has not yet been used in concrete as extensively as Portland cement. Widespread use of low calcium fly-ash geopolymers is hindered due to some of its limitations such as slow setting, high porosity and subsequent slow strength development. Improvement of these properties is essential in order to increase the use of geopolymers in concrete as an alternative to energy-intensive OPC binders. The effects of nanosilica and ultra-fine fly ash in OPC systems are widely investigated and it was found as an effective additive to improve the microstructure and mechanical and durability properties. However, research on the effects of nanosilica and ultra- fine fly ash on the properties of geopolymers is scarce in literature. Therefore, this study aimed to investigate the effect of nanosilica and ultra- fine fly ash on the properties of fly ash geopolymers. Geopolymer mixes suitable for room temperature curing were selected after a number of trials for fly ash only, OPC and GGBFS blended fly ash based mixes with 0–3% nanosilica and 0-15% ultra-fly ash contents. Commercially available materials were used in all the mixes.

3.2 Experimental programme

A low-calcium ‘Class F’ fly ash was used as the main aluminosilicate source material. Other ingredients used in this study included nanosilica, ultrafine fly ash, ordinary Portland cement (OPC), ground granulated blast furnace slag (GGBFS), alkaline solutions (sodium hydroxide

and sodium silicate), water and coarse and fine aggregates. Properties of the binder materials and aggregate were tested in accordance with the Australian and ASTM standard. Twenty one fly ash based geopolymers with different amount of nanosilica (0-3%) and twelve fly ash based geopolymers with different amount of ultrafine fly ash (0-15%) were prepared in laboratory. The effects of nanosilica and ultrafine fly ash on the fresh and hardened properties of ambient cured geopolymers were investigated. The fresh geopolymer properties were workability and setting times, and the hardened geopolymer properties were mechanical strength, microstructure, nanostructure, pore distribution and durability properties.

3.3 Descriptions of materials

3.3.1 Fly ash

The chemical and mineral compositions of the fly ash were determined by X-Ray Fluorescence (XRF) analysis and are given in Table 3.1. The specific surface area was measured by the BET method on dry and degassed fly ash using the TriStar 3000 machine. The BET specific surface area for class F fly ash (Gladstone) was observed 1.501±0.036 m^2/g.

Table 3.1 Chemical compositions of fly ash, OPC, GGBFS and nanosilica

Chemical analysis	Fly ash (Wt. %)	OPC (Wt. %)	GGBFS (Wt. %)	Nanosilica (Wt. %)
SiO_2	46.69	21.1	29.96	99.5
Al_2O_3	29.14	4.7	12.25	0.001
Fe_2O_3	13.81	2.7	0.52	0.001
CaO	3.29	63.6	45.45	-
MgO	1.4	2.6	-	-
MnO	0.16	-	-	-
K_2O	0.72	-	0.38	-
Na_2O	0.86	-	0.31	-
P_2O_5	1.63	-	0.04	-
TiO_2	1.34	-	0.46	-
SO_3	0.43	2.5	3.62	-
LOI[a]	0.68	2.0	2.39	-

[a] Loss on ignition

3.3.2 GGBFS and Ordinary Portland cement

GGBFS conforming to the AS 3582.2 Standard [1] was used in the study. GGBFS is a glassy granular material and a non-metallic product which consist of silicates and aluminosilicate of calcium. Ordinary Portland cement (OPC) conforming to AS 3972 [2] was used to blend with fly ash. The chemical compositions of OPC consist of calcium, silica, alumina and iron. Calcium is usually derived from limestone, marl or chalk, while silica, alumina and iron come from the sands, clays & iron ores. The chemical compositions of GGBFS and OPC are given in Table 3.1.

3.3.3 Ultrafine fly ash

The potential for using ultrafine fly ash in fly ash based geopolymer may be of particular interest due to its beneficial effects in OPC based cementitious systems. Use of finer particles in cementitious binders are being increasingly developed due to their economic and environmental benefits. The ultrafine fly ash was produced by grinding the regular fly ash in a ball mill. The blaine's surface areas of the ultrafine fly as was increased from 340 m^2/kg to 523 m^2/kg after the milling.

3.3.4 Nanosilica

Commercial nanosilica with an average particle size of 15 nm with hydrophilic natures was used in the study. The Specific surface areas of the nanosilica was observed 640 m^2/g. The chemical compositions of nanosilica are given in Table 3.1.

3.3.5 Aggregates

Fine aggregate used in this study was locally available clean natural sand with rounded or sub-rounded particles. The grain size distribution curve for the fine aggregate was performed according to AS2758.1-2014 [3]. The fine aggregate had an average fineness modulus of 2.67 and the absorption value of fine aggregate was 0.99% which was within the acceptable limit of 2% as per AS 2758.1-2014 [3].

Crushed granite coarse aggregates with nominal maximum sizes of 7mm, 10mm and 20mm of were used in the concrete mixes. A suitable grading of aggregates was determined in accordance with the AS 2758.1 -2014 [3] (Standards Australia, 1998). The combined aggregate volume was a combination of 41% 20mm, 9% 10mm aggregate and 15% 7mm aggregate and 35 % sand. The fineness modulus of combined aggregates was found 6.12. Moreover, the absorption value of combined aggregate was found below the acceptable limit of 2% according to the AS 2758.1 section 3.7.2 [3].

3.3.6 Alkaline liquid

The alkaline liquid of the geopolymer mixes consisted of the same proportion of alkaline solution (40%) with a sodium silicate to sodium hydroxide ratio of 2.0. The concentration of the NaOH solution was kept 8 M throughout the study. The NaOH used in this study was in pellets from with 97-98% purity and was dissolved in water at least 24 hours prior to mixing. The sodium silicate solution was obtained from a commercial supplier in Australia. The properties and composition of the sodium silicate solution (Na_2SiO_3) supplied by the producer are shown in Table 3.2.

Table 3.2 Chemical composition of sodium silicate.

Grade	NA46
NaOH (w/w)	14.9
Na_2O (wt %)	11.6
Si_2O (wt %)	30.1
Wt. ratio SiO_2/Na_2O	2.61
Specific gravity (gm./ml @ 20° C)	1.46
Appearance	Viscous clear to light yellow liquid
P^H	12.8
Solubility (water)	Soluble
% volatiles	> 60% (water)

3.3.7 Water and super plasticiser

Potable tap water taken from the Curtin university concrete laboratory which is originally supplied by water distributing authority of Perth, Australia was used in the mixes. A Naphthalene-based superplasticizer supplied by BASF chemicals commonly known as Rheobuild 1000 was used during the mixing. The superplasticizer complies with ASTM C494-12 [4] as Class A and F admixture and has a specific gravity of 1.2 with a solid content of 40%.

3.4 Mix design of fly ash based geopolymer

3.4.1 Mixes with nanosilica

The binder compositions of the geopolymer paste mixes were proportioned based on the previous works on geopolymers cured at room temperature. Twenty-one geopolymer paste mixes in 3 series (fly ash only, GGBFS blended fly ash and OPC blended fly ash) were mixed in the laboratory. The mix proportions are given in Appendix A. In the fly ash only series, fly ash was used as the main binder with 0–3% nanosilica. In the GGBFS blended fly ash series, 0–3% nanosilica was included with 15% GGBFS and 82–85% fly ash. The binder composition of the OPC blended fly ash series was 0–3% nanosilica, 10% OPC and 87–90% fly ash. The GGBFS and OPC contents of 15% and 10% respectively were used since these proportions

were found in previous studies [5, 6, 7] as the optimum blending with low-calcium fly ash for reasonable setting times. The alkaline liquid content of each mix consisted of the same proportion of alkaline solution (40%) with a sodium silicate to sodium hydroxide ratio of 2.0. The concentration of the NaOH solution was 8M. The samples containing different binders were named according to the type of binder used in the mix. For example, FA-PC-NS3 represents a geopolymer paste mix having 3% nanosilica (NS) in the Portland cement (PC) blended fly ash based geopolymer paste. Similarly, the mix designations of FA-NS and FA-S-NS represent the fly ash only and GGBFS blended fly ash series respectively.

3.4.2 Mixes with ultrafine fly ash

Total of twelve geopolymer mixes were prepared by varying the ultrafine fly ash content from 0 to 15%. The mixes are divided into three main series as fly ash-only (FA), OPC blended fly ash (FA-PC) and GGBFS (slag) blended fly ash (FA-S). The binder to alkaline liquid ratio was kept constant at 0.4 with a constant sodium silicate to sodium hydroxide ratio of 2.0 and NaOH molarity of 8M. In the fly ash-only (FA) series, fly ash was used as the main binder with 0-15% ultrafine fly ash. In the slag blended (FA-S) series, 0-15% ultrafine fly ash was added with 15% GGBFS and 70-85% fly ash. Similarly, in the OPC blended (FA-PC) series, 0-15% ultrafine fly ash was added to 10% OPC and 75-90% fly ash.

3.4.3 Geopolymer concrete mix design

The numbers of parameters remained constant during the study were aggregate content, alkaline activator solution, sodium silicate to NaOH ratio, molarity of NaOH solution and the method of curing. An alkaline solution to binder ratio 0.40 was shown to give good strength and microstructure of the geopolymer concrete. Sodium silicate to sodium hydroxide ratios of 2.0 was shown to be appropriate. The geopolymer concrete was wet-mixed for at least 3-4

minutes and all the concrete samples were ambient-cured (15-20 ^{o}C) after casting until tested. The following steps were followed in the design of geopolymer concrete mixes.

Step 1. Calculate the content of binder materials

In GGBFS blended fly ash based geopolymer binder, the fly ash was replaced by GGBFS at 15%. In order to determine the required quantity of different ingredients in geopolymer mixes, a constant amount of binder was used. In this study, the total binder content of the geopolymer mixes was kept constant at 400 kg/m^3, for both the nanosilica and ultrafine fly ash based series. There was 340 kg / m^3 of fly ash and 60 kg / m^3 of GGBFS in the mixes with 15% GGBFS.

Step 2. Select the maximum size of aggregate

ACI 318 [8] section 3.3.2 states the nominal maximum size of coarse aggregate should not exceed (a) 1/5 the narrowest dimension between sides of forms, (b) 1/3 the depth of slabs, nor (c) 3/4 the minimum clear spacing between individual reinforcing bars or wires, bundles of bars, or prestressing tendons or ducts. The combined aggregates may be selected to match the standard grading curves used in the design of Portland cement concrete mixes. Based on the previous studies, a maximum size of coarse aggregate of 20 mm was used in this study. A combination of 20 mm, 10 mm and 7 mm nominal size aggregate were used in all mixes.

Step 3. Select optimum coarse aggregate content

Mass of alkaline activator content= 0.4*400= 160 kg/m^3

Mass of aggregate =2400-400-160= 1840 kg/m^3

Where 2400 kg/m^3 unit weight of the geopolyner concrete

A combination of 41% of 20mm, 9% of 10mm and 15% of 7 mm nominal size of coarse aggregate and 35% of sand was used in this study for all mixes.

Mass of 20mm aggregate= 0.41*1840= 754.4 kg/m^3

Mass of 10mm aggregate= 0.09*1840= 165.6 kg/m^3

Mass of 7mm aggregate= 0.15*1840= 276 kg/m^3

Mass of sand = 0.35*1840= 644 kg/m^3

Step 4. Estimate the alkaline liquid content

Mass of alkaline liquid for was taken as 40% of the binder.

Mass of alkaline liquid content= 0.4*400 = 160 kg/m^3

The sodium silicate solution-to-sodium hydroxide ratio varied from 2.0For SS/SH ratio 2.0

Mass of sodium hydroxide solution = 160/ (1+2.0) = 53.3 kg/m^3

Mass of sodium silicate solution = 160-55.3 = 1064.7 kg/m^3

Step 6. Estimate the nanosilica and ultrafine fly ash

Mass of 3% nanosilica = 400*0.03 = 12 kg/m^3

Mass of 15% ultrafine fly ash = 400*0.15 = 60 kg/m^3

3.5 Manufactures of test specimens

3.5.1 Preparation and mixing of nanosilica in alkaline solution

The alkaline solution was prepared in the laboratory by mixing sodium silicate and sodium hydroxide solutions at the required ratio at least 2 hrs prior to mixing. Sodium hydroxide solution of 8M concentration was prepared by mixing 97-98% pure pallets with tap water. The sodium silicate was added to enhance the formation of geopolymer precursors or the polymerization process [9]. The mass of NaOH solids was measured as 8×40 = 320 grams per

litre of NaOH solution of 8M concentration. Sodium silicate solution with SiO_2 to Na_2O ratio by mass of 2.61 (SiO_2 = 30.1%, Na_2O = 11.6% and water = 58.3%) was used in this study.

Usually, nanosilica may not get dispersed well after wetting and add microbubbles to the mix during mixing. A uniform dispersion of the nanoparticles is essential to avoid agglomeration and promote the reaction. Use of ultrasound was found to be the most effective way of dispersion of nanosilica particles. Therefore, ultra-sonication was used to disperse the nanosilica particles in the alkaline solution to avoid the agglomeration during wetting and mixing. Operating conditions of the UP400S (400 W, 24 kHz) ultrasonic device were set at 24 kHz and amplitude 100% with 80% pulse range for 30 min. The nanosilica particles were found evenly distributed in the alkaline liquid after ultra-sonication, as shown in Fig. 3.1.

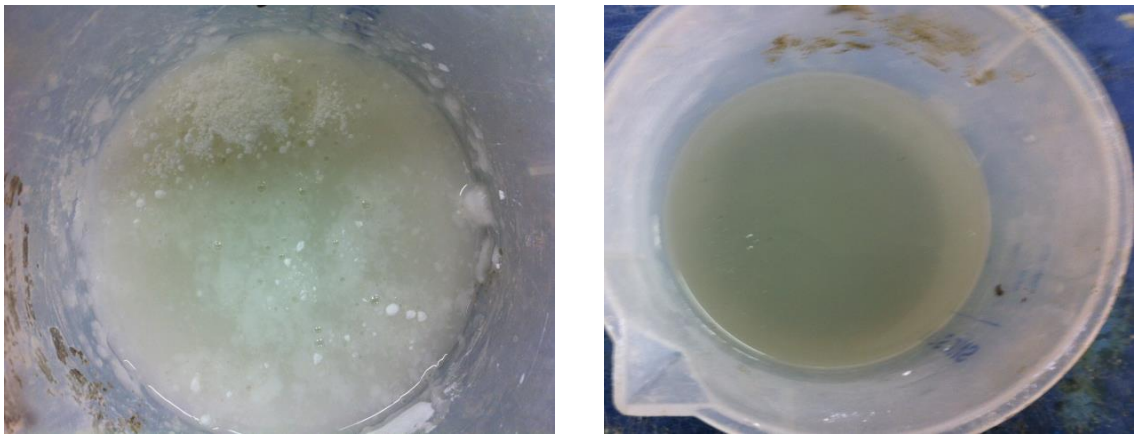

Fig. 3.1 Alkaline solution with nanosilica (a) before ultra-sonication (b) after ultra-sonication

3.5.2 Preparation of aggregate

Both the coarse and fine aggregates were prepared to saturated surface dry (SSD) condition. The aggregates were stored in sealed containers when they reached to SSD condition. The actual moisture content of aggregates was tested before each batching of the geopolymer mixture. For this, approximately 1 kg of aggregate was placed in a pan. Then the pan was stored

in the oven at 105^{0}C for a period 24 hours. After 24 hours, the pan was removed from the oven and the weight of the pan was deducted to get the weight of oven dried (OD) aggregate. The difference in weight represents the total moisture content of the aggregate. Similar procedure of coarse aggregate was applied for the fine aggregate to check moisture content prior to mixing.

3.5.3 Manufacture of geopolymer paste, mortar and concrete specimens, demoulding and curing

The mixing for all geopolymer paste, mortar and concrete were undertaken using a 10-litre Hobart mixer and 70-litre mixer. For geopolymer paste and mortar all dry ingredients were first added in a Hobart mixer following by addition of the activator solutions to the dry materials and mixing it further for 3 to 5 minutes. The geopolymer concrete mixing was done according to the mixing procedure outlined in AS 1012.2 [10]. The mixing pan was cleaned to remove any foreign material before each mixing. The coarse aggregates were first loaded in the mixing pan and followed by sand followed by the sand, fly ash, GGBFS or OPC for the geopolymer concrete mixes. All dry materials in the pan mixer were mixed for about three minutes. Then alkaline solution was added to the dry mix and mixed for 3-4 minutes to get a uniform geopolymer mixes.

Cube mortar specimens of size 50 × 50 × 50 mm were cast for compressive strength tests. Cylindrical specimens (100 × 200 mm) were cast for compressive strength, sulphate attack and sorptivity tests. Velsof was used as a demolding agent and the specimens were demolded at 24 hours after casting and then cured at room temperature (15-20 ^{0}C) at a relative humidity of 70 ± 10%.

3.6 Test procedure

3.6.1 Particle size distribution

Sieve analysis was used to determine the proportion of particles of different sizes within a particular coars aggregate. The test used a tower of interlocking sieves with apertures that decreased in size from top to bottom. Sieve analysis was conducted as per the AS 1289.3.6.1-2009 [12]. Similar procedure as in the fine aggregate was applied for sieve analysis of the coarse aggregate.

3.6.2 Setting time and Workability test

The setting time tests were conducted at 20^{o}C in accordance with ASTM C191 [13] and the specimens for other tests were cured at the same temperature. Flow test of fresh geopolymer mortar was conducted in accordance with ASTM C1437-13 standard [14]. Testing for workability of fresh concrete was done in accordance with ASTM C 143 [15].

A mould with the dimensions of 300mm in height, 100mm diameter at the top and 200mm diameter at the bottom is used to measure the slump of the fresh concrete.

3.6.3 Compressive strength test

Geopolymer samples were kept in room temperature conditions until tested. Compressive strength test was carried out on mortar cube (50 × 50 × 50 mm) and concrete cylindrical specimens of 100 mm diameter and 200 mm height according to AS1012.9-2016 [16]. Sulphur capping in accordance with ASTM C 617-12 [17] was used to provide a uniform load distribution for cylinder specimens. Finally, the test was carried out in MCC8 machine on three specimens at different age with a constant rate of 0.333 MPa/sec and the average value to the nearest 0.5 MPa has been recorded.

3.6.4 Mercury Intrusion Porosimetry (MIP) test

Total porosity and pore size distribution were tested for different geopolymer samples (10×10×5 mm) using an Autoscan mercury intrusion porosimeter. The equipment can generate a maximum pressure of 60 ksi. The contact angle and surface tension for the tests were 140° and 480 dyn/cm, respectively.

3.6.5 X-ray powder diffraction (XRD)

X-ray diffraction (XRD) tests of geopolymer samples were conducted on a Siemens D500 Bragge Brentano diffractometer in a 2 h-range of 5e80Θ. Operating conditions for the XRD were set a 40 kV and 30 mA using a Cu ka X-ray source. Crystalline phases of the geopolymers were identified by comparison with a Powder Diffraction File (PDF). Rietveld refinement with XRD data was used to obtain quantitative phase abundance of the geopolymer paste samples.

3.6.6 Scanning electron microscope (SEM) and energy-dispersive X-ray spectroscopy (EDX)

Scanning electron micrographs (SEM) and energy dispersive X-ray (EDX) spectroscopy were conducted to examine the localized morphology and elemental distributions at the microscopic scale for small cut paste samples using the MIRA3 TESCAN from platinum coated exposed surfaces. The samples were put in the vacuum desiccator for 24 hours before putting the samples for SEM and EDX.

3.6.7 Sample preparation and nano-indentation testing

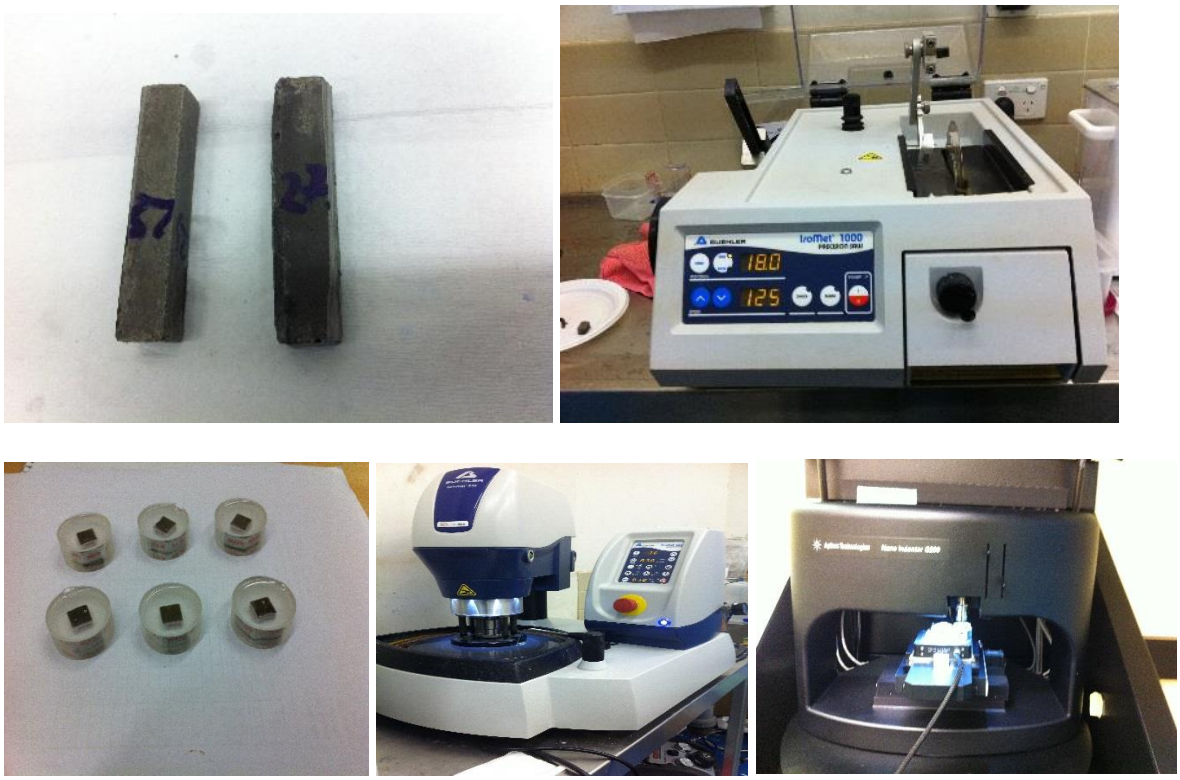

Fig. 3.2 Sample preparation for nano indentation testing

A Berkovich indenter was used for the indentation. Geopolymer specimens with the dimensions of 10 mm × 10 mm × 10 mm were cut using an Iso-Met 1000 precision saw at a speed of 1200 rpm. Since the accuracy of nano-indentation results need very low roughness on the surface of the samples, emery paper discs were used for grinding in order to reduce the surface roughness [18]. The samples were then polished using a suspension solution ranging from 6.0 millimicron to 0.1 millimicron for 1 hour. After polishing, a microscope was used to check the surface of the sample. Polished samples were also ultrasonically cleaned after each polishing step to remove polishing debris from the surface. The nano-indentations were carried out at 8 locations diagonally in a load control mode (1.0 mN) with 20 millimicron grid spacing.

3.6.8 Acid resistance test

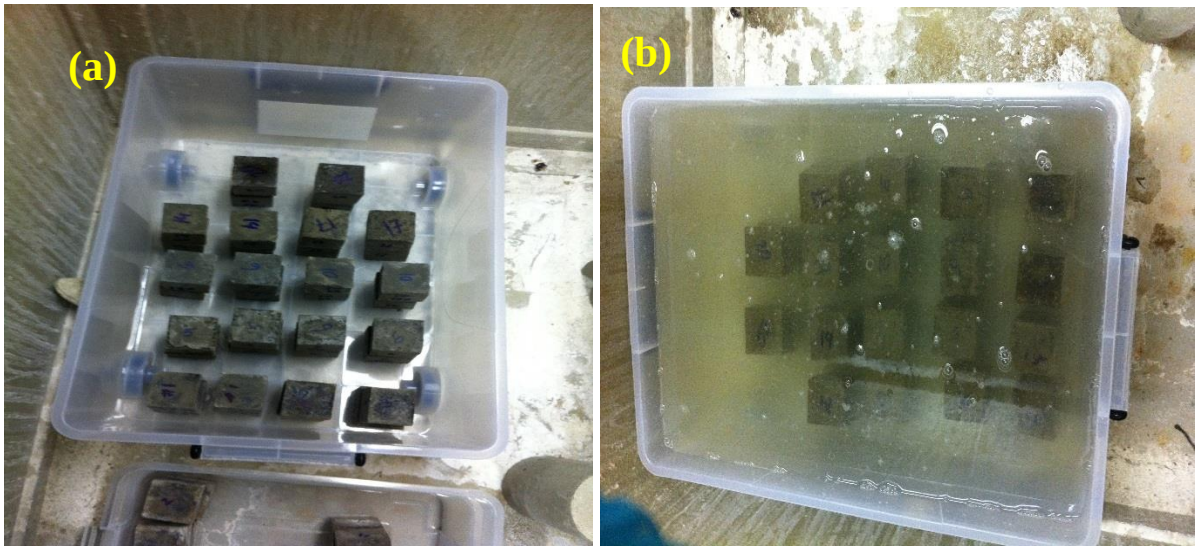

Fig. 3.3 Samples before (a) and after (b) sulphuric acid submerged.

Resistance to sulfuric acid was determined by the modified test method B of the ASTM C 267 Standard [22]. The geopolymer cube mortar specimens were fully immersed in 3% sulfuric acid solution at the age of 28 days for 12 consecutive weeks. The acid solution was replaced weekly and the pH level was monitored regularly to maintain the designated pH of 3.0. The specimens were removed from the acid solution after the exposure period and brushed carefully to remove the loose particles from its surface. They were then left for drying under room temperature for 1hr before recording the mass changes. Strength and microstructure of the geopolymer specimens were also investigated after different exposure periods.

3.6.9 Sulphate resistance test

Geopolymer cylinder specimens (100 mm diameter and 200 mm height) with an OPC concrete core (60 mm diameter and 150 mm height) were cast to check the variation of compressive strength according to AS1012.9-2016 [16] after 28, 56, 90 and 120days. Changes in mass and length (25 mm ×25 mm ×150 mm) as per the standard were also carried out in 5% sodium and

magnesium sulfate solutions. After, the selected exposure period, the samples were removed from the sulphate solution and wiped clean prior to the measurement. Mass of the specimen was taken by a laboratory scale and was returned to the sulphate solution container immediately after the measurement was done. The reported mass change was the average value for two samples.

3.6.10 Carbonation test

Carbonation test was carried out for nanosilica and ultrafine fly ash blended geopolymer specimens. Three 50 mm thick slices were sawn from each cylinder (100 x 200) after 28 days curing and air dried for 72hrs to remove the free water from the surface. Once coated, all slices were left into an accelerated carbonation chamber at 5.0% CO_2 concentration (RH 98% and 23 ± 2 ^{0}C) [21] until tested at 28 days, 56 days and 90 days. The carbonation depth on the face exposed to CO_2 was examined by spraying 1% phenolphthalein pH-indicator after the completion of each exposure periods. The depth of carbonation was measured by averaging at 4-5 points' perpendicular to one face of the split mortar specimens.

3.6.11 Water sorptivity

ASTM C1585-2011 [20] standard guideline was followed for sorptivity testing of geopolymer mortar samples. The tests were done at 28 days and 90days after casting of the specimens. The specimen used in the testing was consisted of 100 mm diameter with 50 mm in thickness.

Three specimens were retrieved from three different cylinders for each mixture. Specimens were put in the oven for 24 hours at a temperature of 105 °C and checked for constant mass at every 24 hours. The procedure was continued until the difference between two successive weights was not greater than 1gm. Then, the side and top of each specimen's surface was sealed

with the epoxy coating. The samples were then placed at the top of water supported by three pins and the water was allowed to inflow into the bottom surface over the time. The water level was maintained not more than 3 mm from the bottom face of the specimen during the test. The quantity of absorbed fluid was measured by weighing the specimen at different intervals. The mass of the specimen was recorded at an interval of 1, 5, 10, 20, 30 minutes and every hour up to 6 hours of initial contact to water.

3.7 Summary

Mix design of fly ash based geopolymer with different amount of finer materials such as nanosilica and ultrafine fly ash is described in this chapter. Preparation, mixing and curing condition of fly ash only, GGBFS and OPC based fly ash based geopolymer paste, mortar and concrete specimens are explained in detail in this chapter. Added to this, testing procedures for setting time, workability, strength, microstructure, nano indentation, MIP and ITZ testing are explained. Geopolymer specimens in aggressive chemical testing condition such as carbonation, sulphuric acid and sulphate (sodium and magnesium) are also described in this chapter.

3.8 Reference

1. Standard Australia. Supplementary cementitious materials for use with portland and blended cement - Slag - Ground granulated iron blast-furnace .(AS 3582.2-2001), retrieved from http:// www.saiglobal.com
2. Standard Australia. General purpose and blended cements. (AS 3972-2010), retrieved from http:// www.saiglobal.com
3. Standard Australia. Aggregates and rock for engineering purposes - Concrete aggregates. (AS 2758.1-2014), retrieved from http:// www.saiglobal.com

4. ASTM Standard. Standard Specification for Chemical Admixtures for Concrete. (C494/C494M-2012), retrieved from http:// www.specs4.ihserc.com
5. P.S. Deb, P. Nath, P.K. Sarker, Strength and permeation properties of slag blended fly ash based geopolymer concrete, Adv. Mater. Res. 651 (2013) 168– 173. doi.org/10.4028/www.scientific.net/AMR.651.168.
6. P.S. Deb, P. Nath, P.K. Sarker. Properties of fly ash and slag blended geopolymer concrete cured at ambient temperature. 7th International Structural Engineering and Construction Conference. Honolulu: USA; 2013.
7. P.S. Deb, P. Nath, P.K. Sarker, The effects of ground granulated blast-furnace slag blending with fly ash and activator content on the workability and strength properties of geopolymer concrete cured at ambient temperature, Mater. Des. 62 (2014) 32–39, http://dx.doi.org/10.1016/j.matdes.2014.05.001.
8. American Concrete Institute (ACI 318-08). Building Code Requirements for Structural Concrete and Commentary. (ACI318-2008), American Concrete Institute, MI, USA.
9. H. Xu, J.S.J. van Deventer, The Geopolymerisation of Alumino-silicate Minerals. International Journal of Mineral Processing, 59 (3) 2000) 247-266.
10. Standard Australia. Methods of testing concrete - Preparation of concrete mixes in the laboratory. (AS 1012.2-2014), retrieved from http:// www.saiglobal.com
11. ASTM Standard. Standard Test Method for Compressive Strength of Hydraulic Cement Mortars (Using 2-in. or [50-mm] Cube Specimens). (ASTM C109/C109M-2016), retrieved from http:// www.specs4.ihserc.com
12. Standard Australia. Methods of testing soils for engineering purposes - Soil classification tests - Determination of the particle size distribution of a soil - Standard

method of analysis by sieving .(AS 1289.3.6.1-2009), retrieved from http:// www.saiglobal.com

13. American Society of testing materials. Standard Test Methods for Time of Setting of Hydraulic Cement by Vicat Needle. ASTM C191-2014
14. American Society of testing materials. Standard Test Method for Flow of Hydraulic Cement Mortar. ASTM C1437e13-2014
15. American Society of testing materials. Standard Test Method for Slump of Hydraulic-Cement Concrete. ASTM C143/C143M-2014
16. Standard Australia. Methods of testing concrete - Determination of the compressive strength of concrete specimens. (AS 1012.9-2016), retrieved from http:// www.saiglobal.com
17. American Society of testing materials. Standard Practice for Capping Cylindrical Concrete Specimens. ASTM C 617-2016
18. M. Miller, C. Bobko, M. Vandamme, F.-J. Ulm, Surface roughness criteria for cement paste nanoindentation, Cem. Concr. Res. 38 (4) (2008) 467–476, http:// dx.doi.org/10.1016/j.cemconres.2007.11.014.
19. American Society of testing materials. Standard Test Methods for Chemical Resistance of Mortars, Grouts, and Monolithic Surfacings and Polymer Concretes. ASTM C 267
20. ASTM Standard. (2011a). Standard test method for measurement of rate of absorption of water by hydraulic cement concretes, (ASTM C 1585-2011), retrieved from http:// www.specs4.ihserc.com
21. D.W.S. Ho, Lewis, R.K. LewisCarbonation of concrete and its prediction. Cem. Concr. Res., 17 (1987), pp. 489-504

22. ASTM Standard. Standard Test Methods for Chemical Resistance of Mortars, Grouts, and Monolithic Surfacings and Polymer Concretes, (ASTM C 267—01 2012), retrieved from http:// www.specs4.ihserc.com

CHAPTER 4

GEOPOLYMER PASTE WITH NANOSILICA AND ULTRAFINE FLY ASH

4.1 Overview

The results of fly ash based geopolymer paste with nanosilica and ultrafine fly ash are discussed in this chapter. The geopolymer samples are divided into different series based on the binder's composition such as fly ash only, GGBFS blended fly ash and OPC blended fly ash. The effects of inclusion of nanosilica and ultrafine fly ash on setting time, mechanical properties, microstructure development and pore structure properties with respect to their corresponding control mixes at different ages are studied.

4.2 Critical factors affecting the geopolymer process

Materials rich in silicon and aluminium are the primary requirements for geopolymerization process. The presence of highly reactive silica in the base material is the most significant factor in producing a mechanically-sound cementitious material via the geopolymerization process. Added to this, the aluminium content of a base material also plays a critical role to the hardening properties of a geopolymer binder. It was observed that macrocroscopic characteristics and microstructure properties are also influenced by several other factors such as the fineness of the base material, presence of calcium in the base material, amount and concentration of the alkali and the curing conditions. The effects of small proportions of very fine materials such as nanosilica and ultrafine fly ash on the properties of fly ash geopolymer paste cured at room temperature are presented in this chapter.

4.3 Effects of ultrafine fly ash and nanosilica on fly ash based geopolymer

4.3.1 Setting time of fly ash based geopolymer with nanosilica and ultrafine fly ash

4.3.1.1 Fly ash only geopolymer

Setting times of fly ash-only geopolymers with 0% - 3% nanosilica and 0 - 15% ultrafine fly ash are presented in Fig. 4.1.

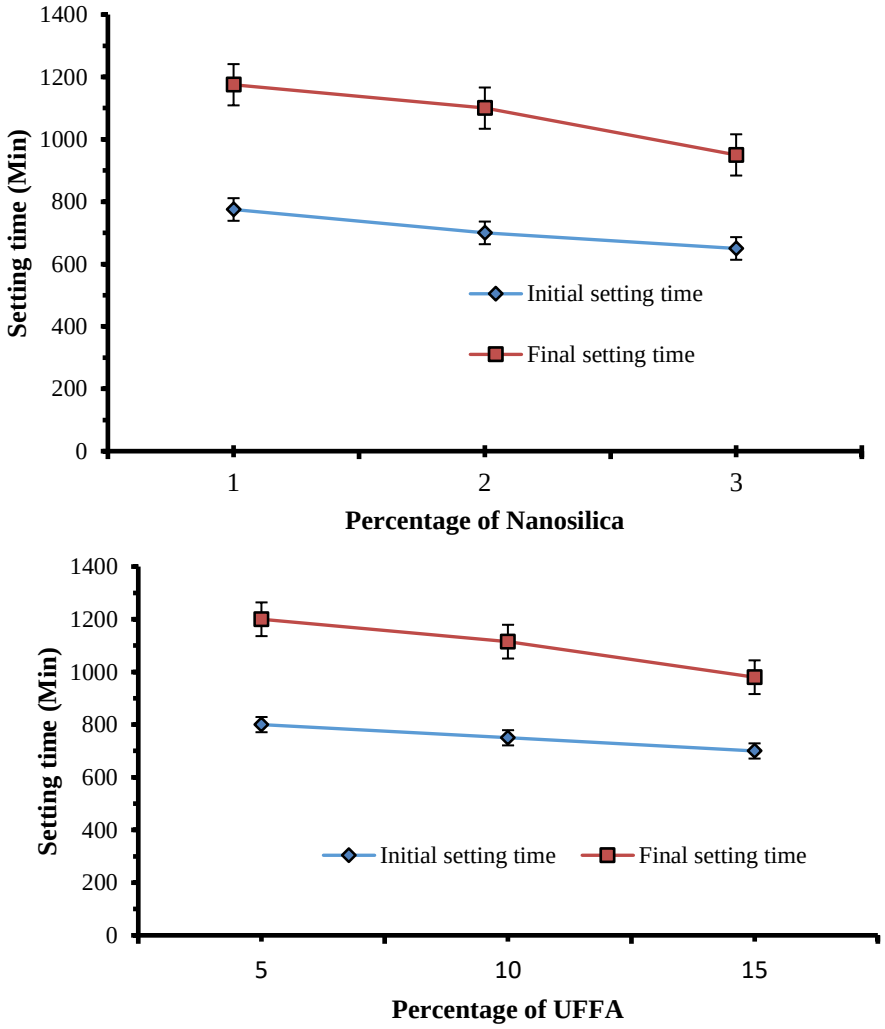

Fig. 4.1 Effect of nanosilica and ultrafine fly ash on setting times of fly ash-only geopolymers

It was reported by different researchers [1, 2, 3] that low-calcium fly ash based geopolymers cured at room temperature generally takes a long time (>24 hours) to set due to its slow rate of chemical reaction. Fernandez-Jimenez et al. [4] also noted that initial curing temperature played a critical role for the reaction kinetics of fly ash based geopolymer paste.

The initial and final setting times of fly ash based geopolymer without nanosilica and ultrafine fly ash was observed 1,535 and 2,220 min, respectively and didn't include in the Fig. 4.1 for clarity. It is noted from the Fig. 4.1 shows that the addition of nanosilica and ultrafine fly ash significantly reduced the initial and final setting times of geopolymer pastes. The initial setting times of the geopolymers of this series with 1, 2 and 3 % nanosilica were 775, 700 and 650 minutes, and the corresponding final setting times were 1175,1100 and 950 minutes, respectively. The initial setting times of the mixes using 5%, 10% and 15% ultrafine fly ash were 800 min, 750 min and 700 min, respectively. While the reduction in setting time was very large by 2% nanosilica and 5% ultrafine fly ash, it was relatively small with further increase in the percentage of nanosilica and ultrafine fly ash. This reduction in the setting time is caused by the accelerated reaction of the nanosilica and ultrafine fly ash due to the higher values of specific surface area. It was shown by Jaarsveld et al. [5] and Chindaprasirt et al. [6] that the surface charge and fineness of binder particles influenced the initial setting properties of geopolymer mixes. Thus, the high fineness of nanosilica and ultrafine fly ash reduced the setting times by accelerating the geopolymerisation process.

4.3.1.2 OPC and GGBFS blended fly ash based geopolymers

The effect of nanosilica and ultrafine fly ash on the setting times of the GGBFS blended fly ash geopolymers are presented in Fig. 4.2. A noteworthy reduction of setting time was seen in GGBFS blended fly ash based geopolymers with 2% and 3 % nanosilica and 5%, 10% and

15% ultrafine fly ash than that of control mixture (without ultrafine fly ash). As shown in this figure, the initial setting time of the GGBFS blended fly ash geopolymers reduced almost linearly from 71 minutes for no nanosilica to 51 minutes for 2% nanosilica. The corresponding final setting times were 320 minutes and 180 minutes for 0% and 2% nanosilica, respectively. Similar phenomenon was observed for 10% ultrafine fly ash in the GGBFS blended fly ash geopolymer mixture. For 10% increase of ultrafine fly ash, the initial and final setting times decreased by approximately 28% and 29%, respectively.

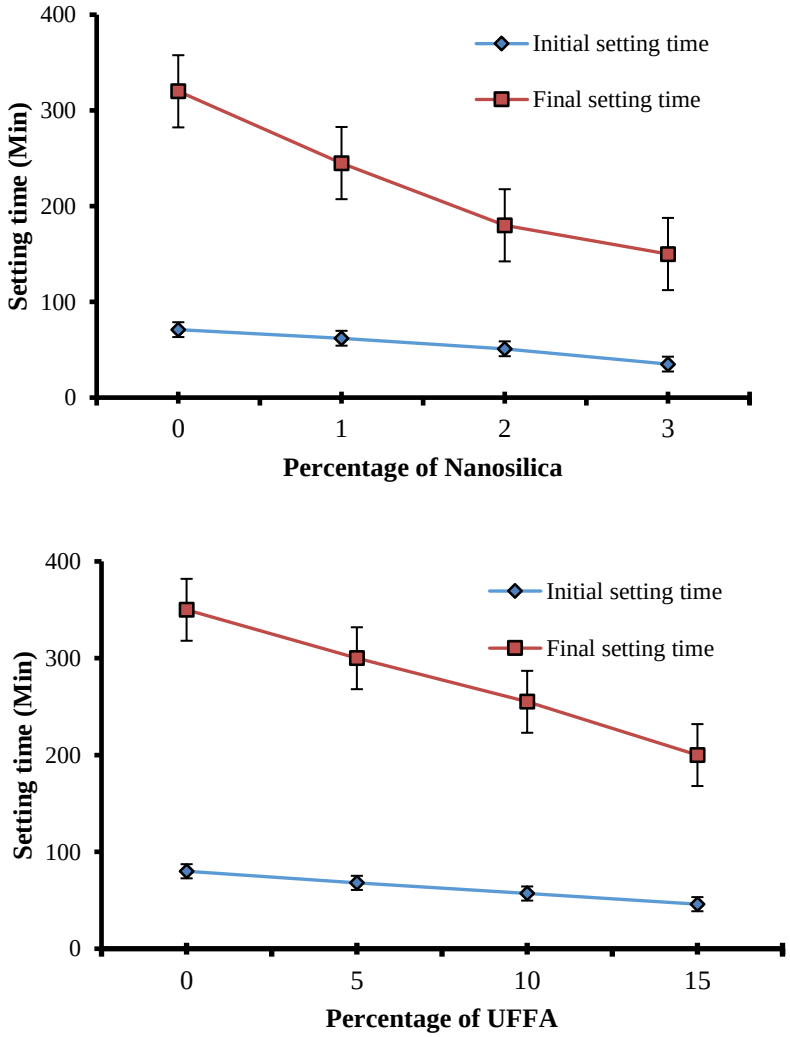

Fig. 4.2 Effect of nanosilica and ultrafine fly ash on setting times of GGBFS blended fly ash based geopolymers

According to Duxon et al. [7] initial setting of geopolymer binder occurred when the rate of dissolution was surpassed by the rate of condensation and precipitation of aluminosilicate species. It is clearly noted from Fig. 4.2 that increasing the amount of finer base materials significantly reduced the setting time GGBFS blended fly ash geopolymer as compared to that of the corresponding control mixes (FA-S-NS0 and FA-S-UF0).

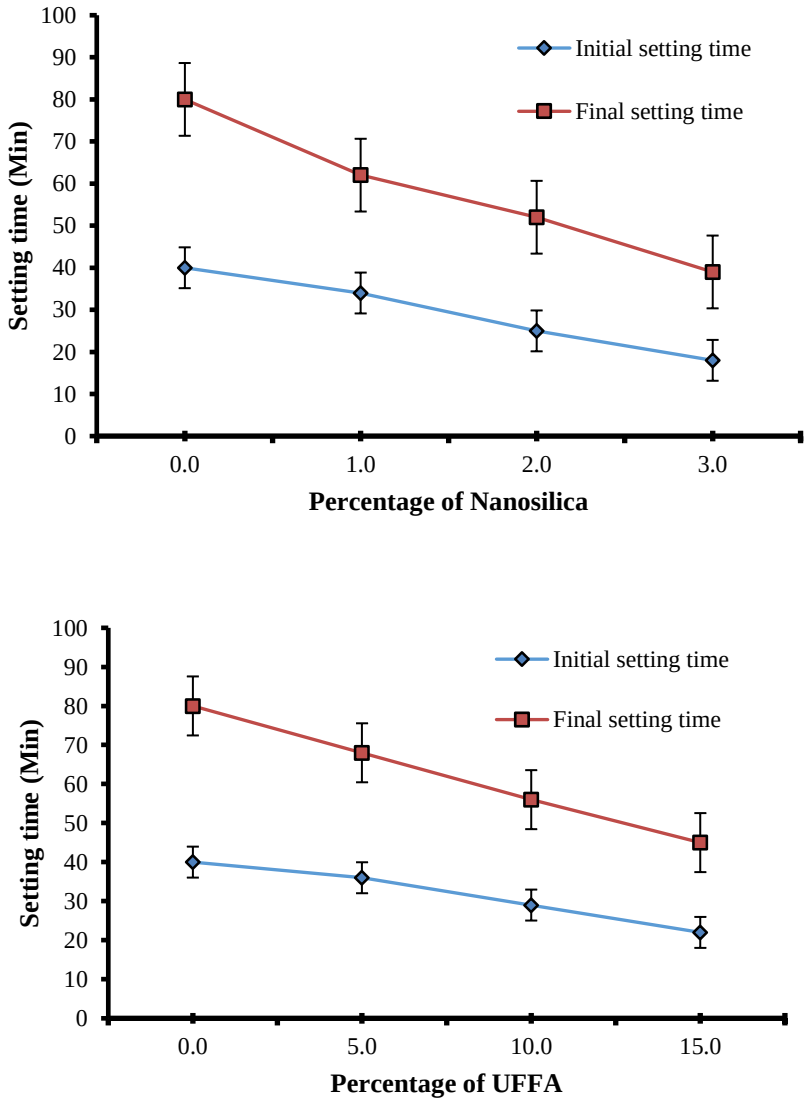

Fig. 4.3 Effect of nanosilica and ultrafine fly ash on setting times of OPC blended fly ash based geopolymers

The setting times of the OPC blended fly ash geopolymers are presented in Fig. 4.3. As shown in this figure, the initial setting time reduced from 40 minutes for no ultrafine fly ash to 22 minutes for 15% ultrafine fly ash. The corresponding final setting times were 80 minutes and 45 minutes, respectively. The initial and final setting times also decreased with an increase in nanosilica concentration (0-3%) in the OPC blended fly ash geopolymer mixes. The final setting times were 80 min, 62 min, 52 min and 39 min for 0%, 1%, 2% and 3% nanosilica, respectively. Palomo et al. [9] reported that the heat released hydration of OPC favoured the rate of chemical reactions of ash dissolution, setting and hardening process. Fig. 4.3 indicates that the reductions in the setting times are almost linear with the increase of the finer materials.

It is shown by the comparison of the setting times of three geopolymer series that the higher amount of calcium in the GGBFS and OPC blended geopolymers resulted in accelerated setting as compared to the fly ash-only geopolymers. Previous research [2,3,8] found that setting time of fly ash based geopolymers could be controlled by varying the amount of CaO in the mixes. The faster setting of GGBFS and OPC blended fly ash based geopolymers are attributed to the formation of calcium silicate hydrate (CSH) and calcium aluminate hydrate (CAH) by the presence of calcium. Similar behaviour was also observed in previous studies by Nath and Sarker [3], Deb at al. [10] and Temuujin et al. [11] on geopolymers cured in room temperature. The inclusion of the nanosilica and ultrafine fly ash in GGBFS and OPC blended fly ash based geopolymers further accelerated the setting process. It can also be noticed from Fig. 4.2 and Fig. 4.3 that the difference between initial and final setting times is reduced with the increase of finer materials. This shows the combined role of calcium and the higher surface area of ultrafine fly ash on setting of geopolymers at room temperature.

Thus, the results establish that the combined role of calcium and the higher surface area of finer materials is an effective way to control the setting of geopolymers in ambient curing conditions. It is noteworthy that the higher amount of calcium in the OPC blended series (Fig. 4.2) together with the higher nanosilica and ultrafine fly ash content resulted in a much faster setting than the GGBFS blended geopolymers (Fig. 4.3).

4.3.2 Compressive strength of fly ash based geopolymers

4.3.2.1 Fly ash only geopolymer

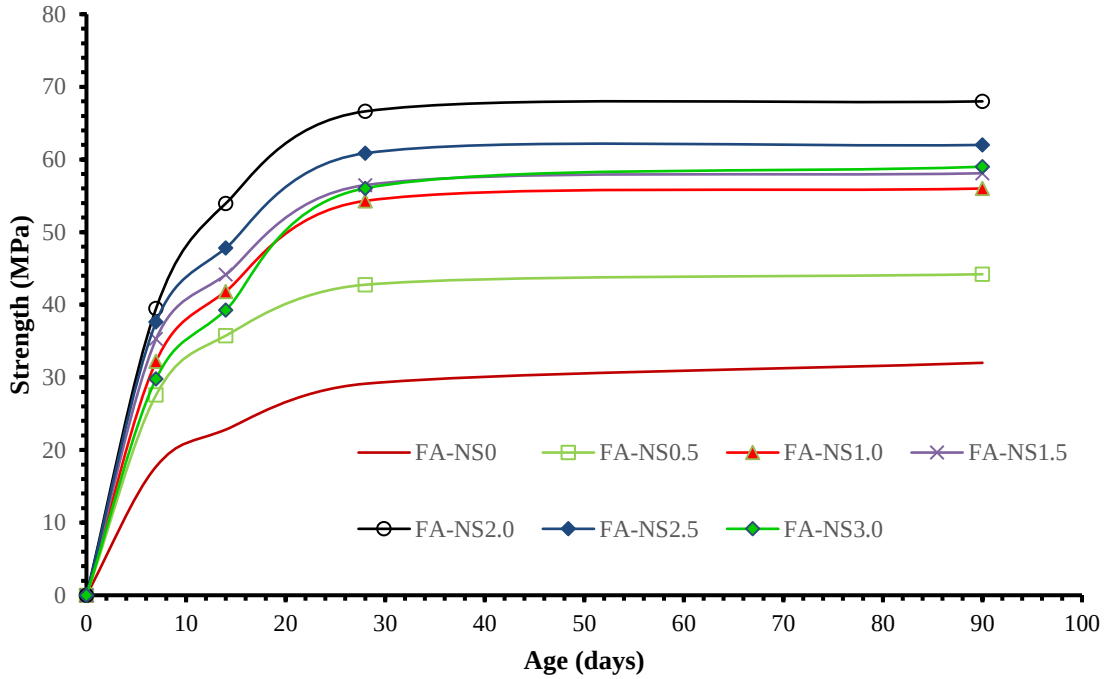

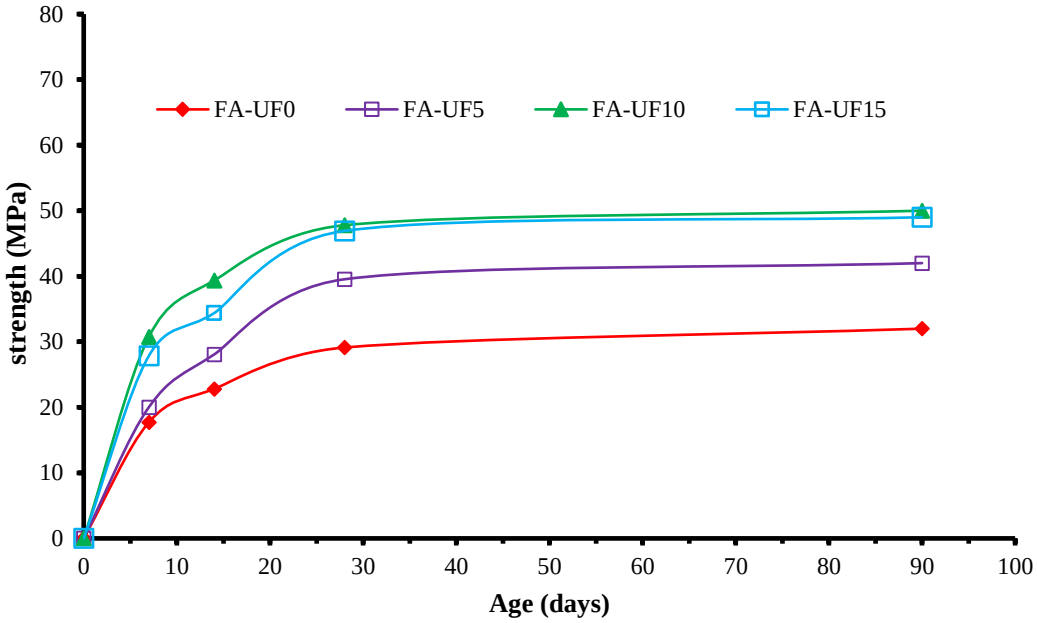

Fig. 4.4 Effect of nanosilica and ultrafine fly ash on compressive strength of fly ash only geopolymers

The compressive strengths of fly ash only geopolymer pastes with 0 to 3% nanosilica are plotted in Fig. 4.4. The 28-day compressive strength of the control mix was 29.0 MPa which increased up to 67 MPa by the inclusion of nanosilica. It can be seen from the figure that compressive strengths of the mixes containing 0.5 to 3% nanosilica were significantly higher than that of the control mix. Mixes FA-NS1.0, FA-NS2.0 and FA-NS3.0 exhibited 87%, 129% and 93% higher 28-day compressive strength values than the mix FA-NS0.0. This shows that the binder became stronger with the increase of soluble silica or silica concentration in the mixes. The highest 28-day compressive strength in this series was observed in mix FA-NS2.0. The strength increase declined for nanosilica contents in excess of 2%. This is mainly because the nanosilica content of 2% was sufficient for reaction to its entirety due to its high surface area. An addition of nanosilica in excess of 2% did not participate in the reaction process and

hence did not increase the strength any further. The effect of nanosilica is found to follow the same trend on the compressive strengths at 7, 14 and 28 days of age, as shown in Fig. 4.4.

The developments of compressive strength with age for fly ash-only geopolymers paste containing different percentages of ultrafine fly ash are presented in Fig. 4.4. It can be seen from the graph that strength of geopolymers mixes increased with the increases of ultrafine fly ash in the mixes. For example, the compressive strength of mixture FA-UF0 without ultrafine fly ash at 28 days was 29 MPa, which gradually increased to 47.0 MPa when 10% of ultrafine fly ash was added. Compressive strength then decreased to 39.0 MPa when the ultrafine fly ash was increased to 15%.

The observed strength variations suggest that there is a relationship between the amount of finer particles and strength development of fly ash based geopolymer paste. Addition of nanosilica and ultrafine fly ash in fly ash based geopolymer paste probably increased dissolution rate of the aluminosilicates. Chindaprasirt et al. [12] and Temmujin et al. [13] observed an increased dissolution rate of the source materials by increasing fineness. Xu and van Deventer [14] concluded that higher dissolution rate of the source materials leads to develop higher compressive strength in geopolymers. It was also previously observed by Fernandez-Jimenez and Palomo [15] that higher amount of aluminosilicate gel can be generated in fly ash based geopolymers with the addition of highly reactive silica in the mixes that eventually gives higher strength. Similar behavior was also observed by other researchers [6, 8, 9]. Xu and Deventer [30] showed that the addition of soluble silicates accelerated the reaction process at a higher rate and helped build the long-chain silicate oligomers in the geopolymer matrix and eventually increased the mechanical strength. Fernandez-Jimenez and

Palomo [15] showed that the extent of the soluble silicon concentration is a critical variable controlling the geopolymerization process.

It appears from Fig. 4.4 that 2% nanosilica and 10% ultrafine fly ash in the fly ash-only geopolymer paste reacted almost entirely and their further increases were not effective in the improvement of strength. It is believed that the unreacted particles caused excessive self-desiccation and cracking in the matrix that eventually reduced the strength, as described by Hajimohammadi [18].

4.3.2.2 OPC and GGBFS blended fly ash based geopolymer

Previous research showed that high amount of OPC (> 12%) [3] and GGBFS (>20%) [10, 19] in fly ash geopolymer mixes cause rapid setting and rapid loss of workability during the casting process. Hence, the amount of OPC and GGBFS contents were kept at 10% and 15% respectively in this study to avoid fast setting.

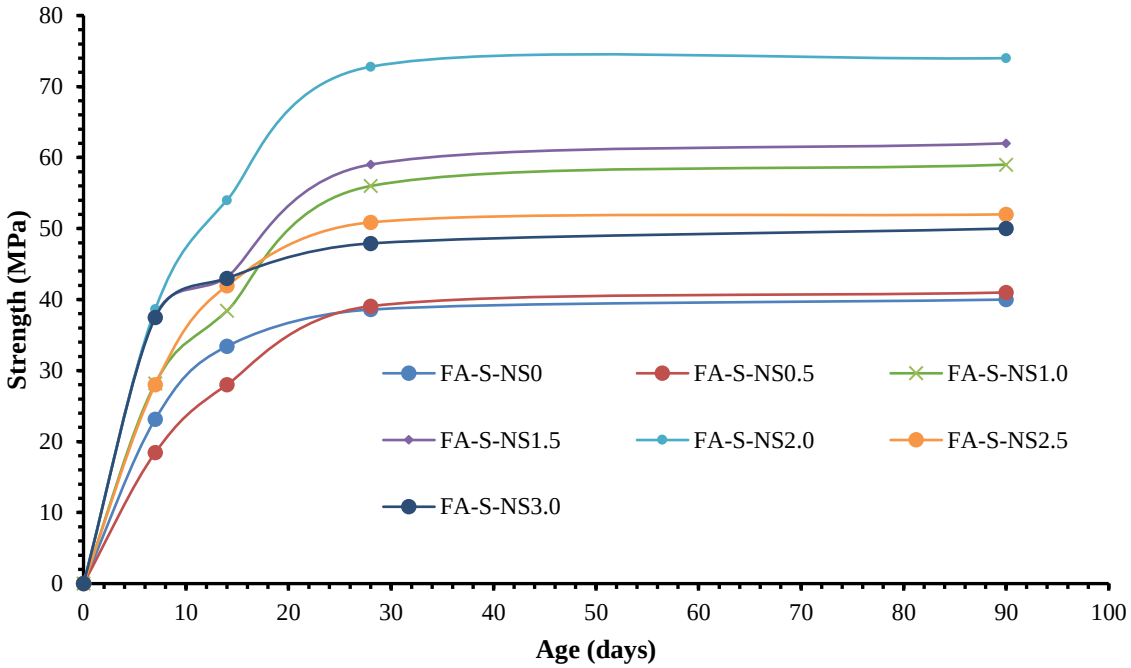

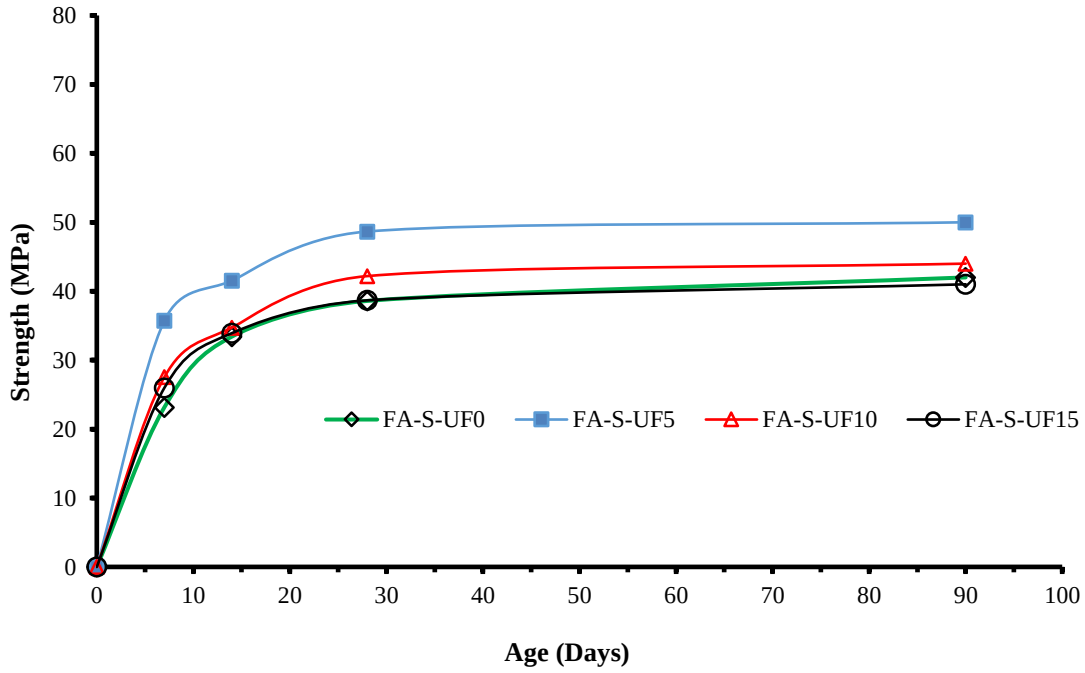

Fig. 4.5 Effect of nanosilica and ultrafine fly ash on compressive strength of GGBFS blended fly ash based geopolymers

The variations in compressive strength with addition of nanosilica in the 15% GGBFS blended fly ash geopolymers are presented in Fig. 4.5. Addition of higher amount of GGBFS content (20%) with the lower SS/SH ratio (1.5) along with higher molarity of NaOH (14M) in the fly ash based system generally exhibited higher strength. However, it can be seen from the current experimental results that the strength can be further increased with the addition of nanosilica in the mixes even with lower molarity (8M) of NaOH and GGBFS content of 15% in the mixes.

At 28 days, mix FA-S-NS1 containing 1% nanosilica achieved 45% higher compressive strength than the control mix (FA-S-NS0). The effect of nanosilica addition on the strength development is shown to be maximized at the rate of 2% that was also observed in the other two mixture series. The increase in strength is seen to decline for the nanosilica dosage

exceeding 2%. The strength of the mixture containing 2% of nanosilica reached to 73.0 MPa which is 88% higher than that of the control mix (39.0 MPa). However, the compressive strength for 3% nanosilica (mix FA-S-NS3) addition was observed only 24% higher than that of the control mix (FA-S-NS0) but 51% less than the strength for 2% nanosilica (mix FA-S-NS2).

The strength results plotted in Fig. 4.5 show that the compressive strength (73 MPa) with 2% nanosilica in the GGBFS blended fly ash geopolymers (FA-S-NS2) is significantly higher than that (29.0MPa) of the mix without GGBFS and nanosilica (FA-NS0). This is because the presence of calcium increased the strength of geopolymer due to the formation of Ca–Al–Si amorphous structures. Similar effect of the presence of calcium bearing compounds was also observed by Yip and Deventer [23].

The compressive strengths of the GGBFS blended fly ash containing different percentages of ultrafine fly ash at 7, 14 and 28 days are plotted in Fig. 4.5. It can be seen from the results that the 7-day compressive strength of the GGBFS blended fly ash geopolymers increased from 23 MPa to 35 MPa by the inclusion of 5% ultrafine fly ash. Similarly, the 14-day and the 28-day strengths increased from 33 MPa to 41 MPa and from 38 MPa to 48 MPa, respectively. Fernandez-Jimenez and Palomo [15] and Criado et al. [16] observed that the presence of reactive and soluble silica modifies the reaction kinetics and rate of crystallization of geopolymer precursor. When ultrafine fly ash is increased from 0% to 5%, the amount of soluble silica is increased in the mixture. As the amount of soluble silica is increased, the polymerization processes is accelerated. Khale and Chaudhary [20] noted that the presence of highly reactive silica in the mixes generate higher amount of alkali aluminosilicate gel giving higher mechanical strength. However, the strength-age graphs for the geopolymers with 10%

and 15% ultrafine fly ash show that the strengths of these mixes were less than those of the mixture with 5% ultrafine fly ash. This shows that 5% ultrafine fly ash is adequate for strength enhancement of the GGBFS blended fly ash geopolymers. Further increase in the ultrafine fly ash content did not have any negative effect on the strengths as compared to those of the mixture with no ultrafine fly ash (FA-S-UF0). Therefore, a small amount of ultrafine fly ash is enough for strength enhancement of the GGBFS blended fly ash geopolymers than in the fly ash-only geopolymers. This is likely because the GGBFS blended geopolymers have 15% GGBFS, which has a higher surface area (450 m^2/kg) than that of fly ash (340 m^2/kg). Thus, the GGBFS blended geopolymers have finer particles than the fly ash-only geopolymers, and inclusion of 5% ultrafine fly ash is found to be adequate for reasonable setting time and strength enhancement.

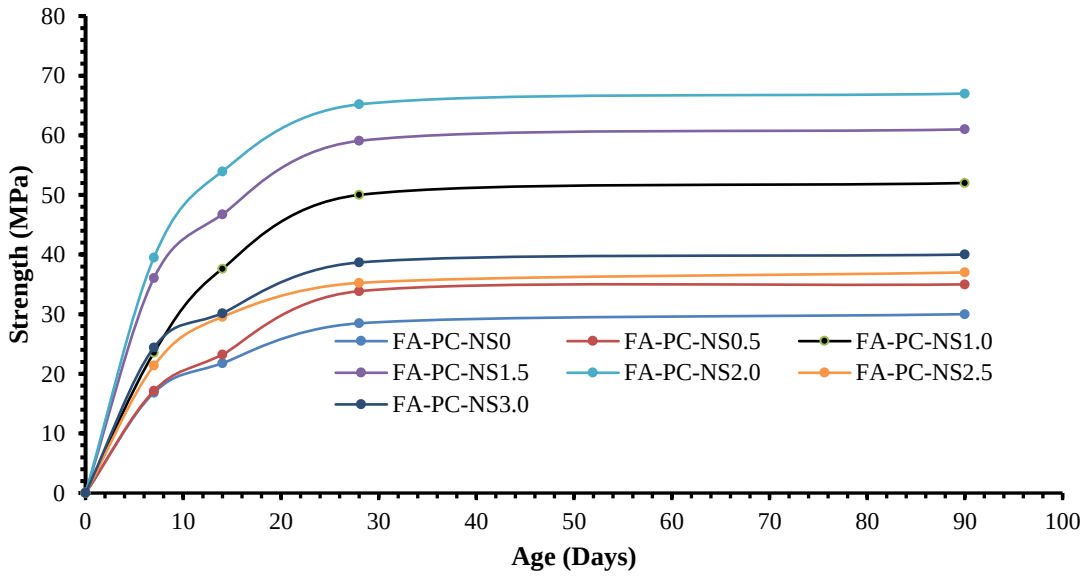

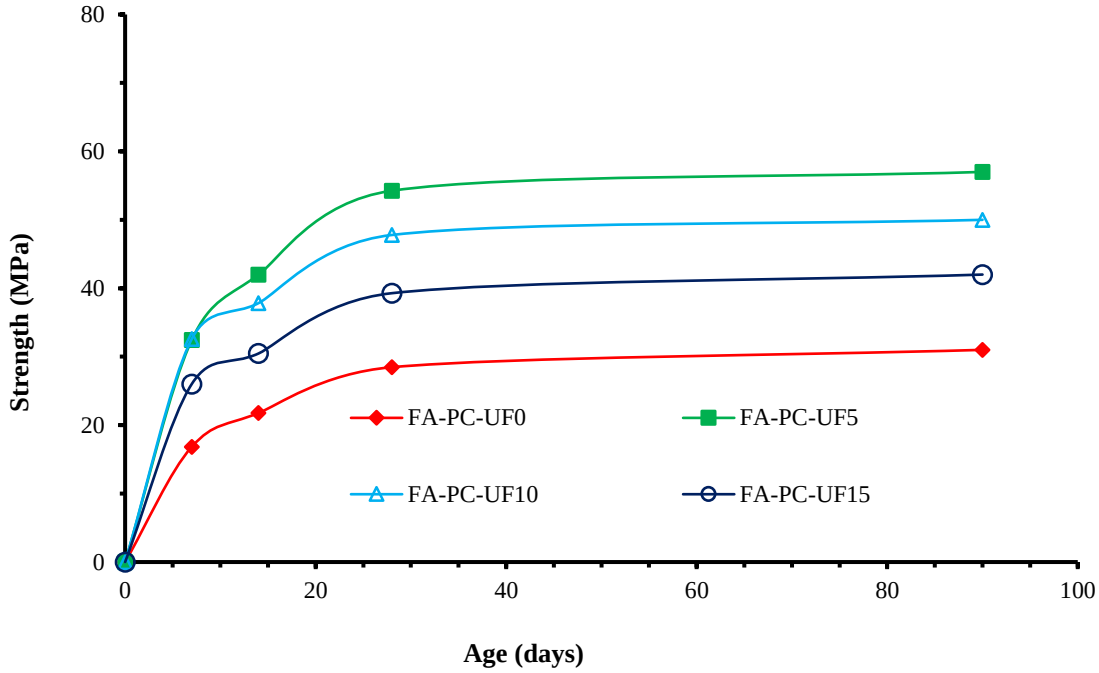

Fig. 4.6. Effect of nanosilica and ultrafine fly ash on compressive strength of OPC blended fly ash based geopolymers

Fig. 4.6(a) presents the effect of nanosilica on the compressive strengths of the 10% OPC blended fly ash geopolymer mixes. It is noted from the figure that compressive strengths of the mixes with nanosilica are significantly higher than that of the control mix at 28th day. The addition of the nanosilica significantly increased the strength of the mixes.

The compressive strength continuously increased with the increase of nanosilica dosage from 0.5% to 2% and then reduced with further increase in the percentage of nanosilica. For example, FA-PC-NS1 exhibited 75% higher strength than the control mix (FA-PC-NS0). The highest 28-day compressive strength in this series was 65.0 MPa obtained for the mix FA-PC-NS2. This strength is significantly higher than that of the control mix (28.5 MPa). It is observed from the results (Fig. 4.6) that the rate of strength development can be controlled by the addition of nanosilica in the mixes. However, increasing the dosage of nanosilica above 2% did not

further increase strength. Mix FA-PC-NS3 with 3% nanosilica showed 35% higher strength than the mix FA-PC-NS0 but 90% less than the mix FA-PC-NS2. These results indicate that the optimal content of nanosilica for maximum compressive strength is 2% for the fly ash only and OPC-blended fly ash mixes.

The strength developments of the OPC blended fly ash geopolymers with different amounts of ultrafine fly ash are plotted in Fig. 4.6(b). In this series, the OPC content was constant at 10%. It can be seen that the strength development of mixture FA-PC-UF0 with no ultrafine fly ash was relatively slow. When ultrafine fly ash was included in the mixture, the strength development rate increased significantly from the early ages and continued to 28 days. Tailby and Mackenzie [21] and Suwan and Fan [22] showed that addition of OPC in fly ash based geopolymer generates heat which eventually strengthened its polymeric structure. Addition of ultrafine fly ash in OPC blended series might further enhance its geopolymerization process. The higher compressive strength development in OPC blended geopolymer mixes might be attributed to the addition of the ultrafine fly ash, which acted as a reactive filler and provided additional soluble silica in the geopolymer pastes.

At 28 days, the geopolymers FA-PC-UF5, FA-PC-UF10 and FA-PC-UF15 achieved 54MPa, 48MPa and 39MPa of compressive strength, respectively, which are 91%, 67% and 38% higher, than the strength of the geopolymer without ultrafine fly ash (FA-PC-UF0). Further increase in the ultrafine fly ash did not contribute to further increase of strength development. The likely reason is that 5% ultrafine fly ash is enough for the reaction in these blended mixes and its addition in higher percentages leaves more unreacted fly ash to act as defect sites causing a decline in strength. This leads to the understanding that the geopolymerization and the strength development rate of ambient cured fly ash based

geopolymer can be controlled and accelerated with the optimum amount of ultrafine fly ash in the mixes.

The percentage of nanosilica and ultrafine fly ash required to maximise the compressive strengths for the GGBFS and OPC blended geopolymers are found as 2% and 5%, respectively. The compressive strengths of the geopolymers containing these optimum percentages of ultrafine fly ash are compared in Figs 4.5 and 4.6. It can be seen from the figure that the 7-day, 14-day and 28-day compressive strengths of these geopolymers varied in the ranges of 31 to 36 MPa, 39 to 42 MPa and 48 to 54 MPa, respectively. Nanosilica, with its high surface area to volume ratio strongly also influenced the compressive strengths of all types of OPC and GGBFS blended fly ash based geopolymer mixes. It is noted from Figs 4.5 and 4.6 that the addition of 2% nanosilica resulted in similar compressive strengths in the mixes of each series at a given age between 7 and 28 days when cured at room temperature. However, at 28 days of age the GGBFS blended fly ash based geopolymer mix exhibited 12% higher strength than the OPC blended fly ash geopolymer.

These compressive strengths are considered suitable for various in-situ and precast concrete applications. Therefore, low-calcium fly ash geopolymers of these ranges of compressive strength can be designed for ambient curing using a small proportion of ultrafine fly ash, GGBFS and OPC in the mixture.

4.3.3 Microstructures of fly ash based geopolymer

4.3.3.1 Fly ash only geopolymer

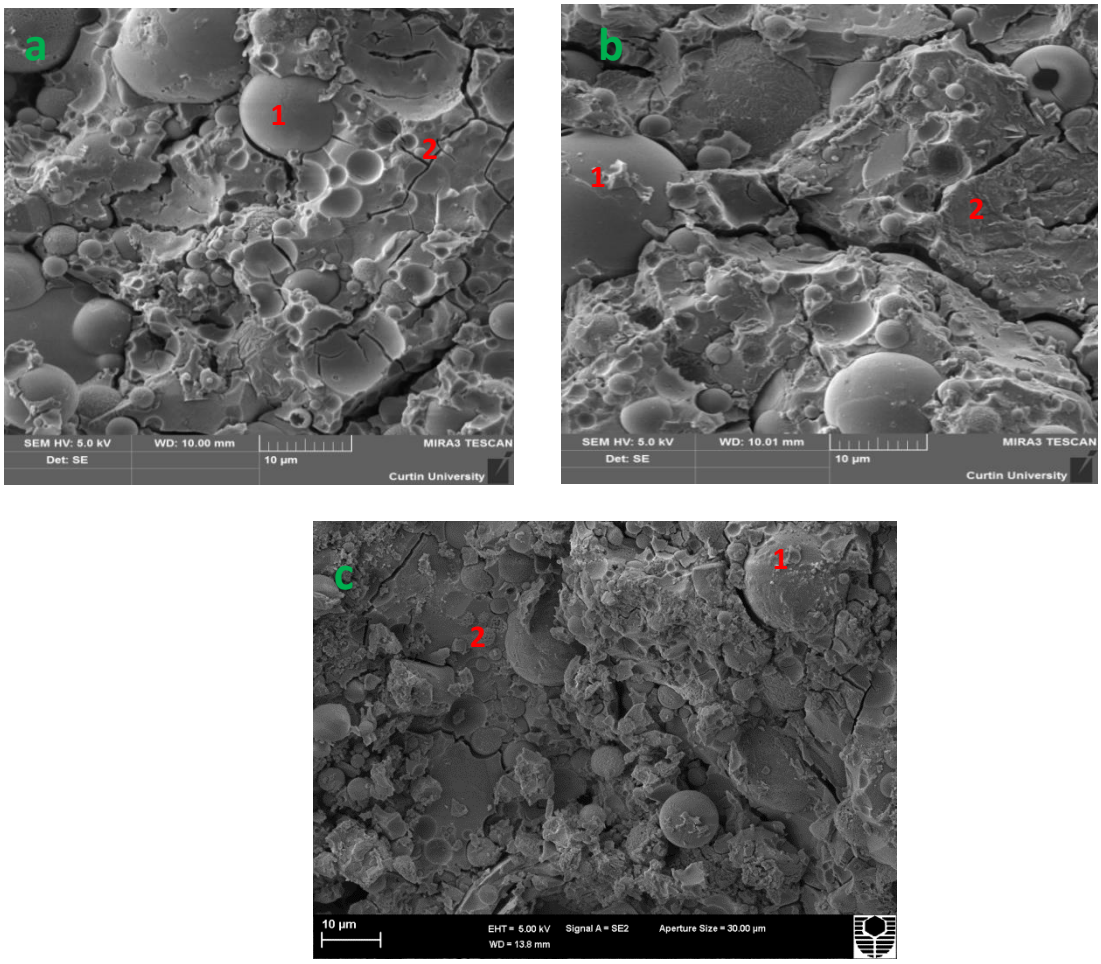

Fig 4.7 SEM images of fly ash only geopolymer containing nanosilica: (a) 0 wt. % (FA-NS0), (b) 2 wt. % (FA-NS2) and (c) 3 wt. % (FA-NS3)

Fig. 4.7 shows the SEM images of the fly ash only geopolymer paste samples after 28 days. Incorporation of nanosilica was noticed to influence the microstructure of the hardened geopolymer paste samples. A key difference between the microstructures of FA-NS2 (2% NS) and FA-NS0 (0% NS) is that FA-NS2 is denser than FA-NS0 with less number of unreacted particles. The zone surrounding the unreacted particles appears compact, although few micro cracks were detected in the vicinity of the particles. It is also observed that nanosilica acted as

a filler material in this case to fill the spaces inside the skeleton of hardened microstructure of geopolymer paste to increase its compactness. This agrees with the observations on fly ash based geopolymers by Shih et.al [24].

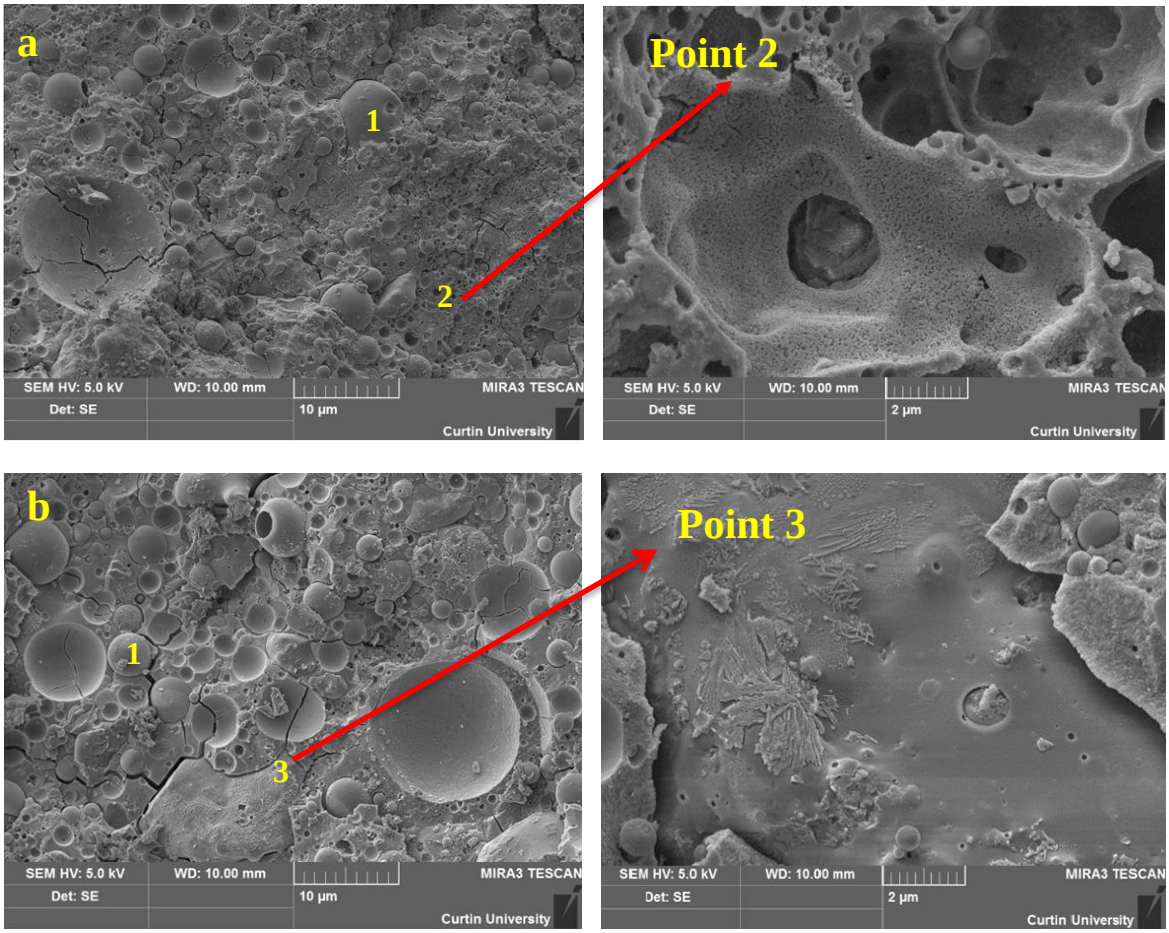

Fig. 4.8 SEM images of fly ash-only geopolymers: a) no ultrafine; b) with 10% ultrafine.

The backscattered SEM images of the hardened geopolymer specimens with and without ultrafine fly ash are shown in Fig. 4.8. It can be seen from the comparisons of the figures that generally there are less pores in the geopolymer containing ultrafine fly ash (point 3, Fig. 4.8) as compared to that with no ultrafine fly ash (point 2, Fig. 4.8a). A relatively more compact microstructure can be observed in the geopolymer containing ultrafine fly ash. Though some unreacted fly ash particles (point 1) can be seen in both the geopolymers, they mostly

appear to be well connected by the reaction product in the geopolymer containing ultrafine fly ash.

This is mainly attributed to the higher dissolution rate of the source materials due to the higher fineness of the ultrafine fly ash and the presence of sufficient amount aluminium species in the source material. Formation of sodium aluminosilicate gel was noticed which was also found by other researchers [25, 26, 27]. According to Divya and Chaudhary [20] curing conditions played an essential role in development of the microstructure of fly ash based geopolymers. The microstructural development is accelerated with higher curing temperature and time. Other researchers [11, 12, 28, 29] observed a slower microstructure development of class F fly ash geopolymers due to its lower dissolution rate at ambient temperatures. However, it can be seen from the SEM images (Figs. 4.7 and 4.8), that the addition of finer materials (nanosilica and ultrafine fly ash) enhanced the microstructure development of the geopolymer paste samples at room temperature.

An EDS analysis for fly ash only based geopolymer with 2% nanosilica (Fig. 4.9a) and 10% ultrafine fly ash (Fig. 4.9b) indicates a silicon, sodium and aluminium-rich compound.

This compound is an indication of the presence of sodium aluminosilicate gel in the mixes. This is consistent with the observations made by other researchers on fly ash geopolymers [7, 15, 30].

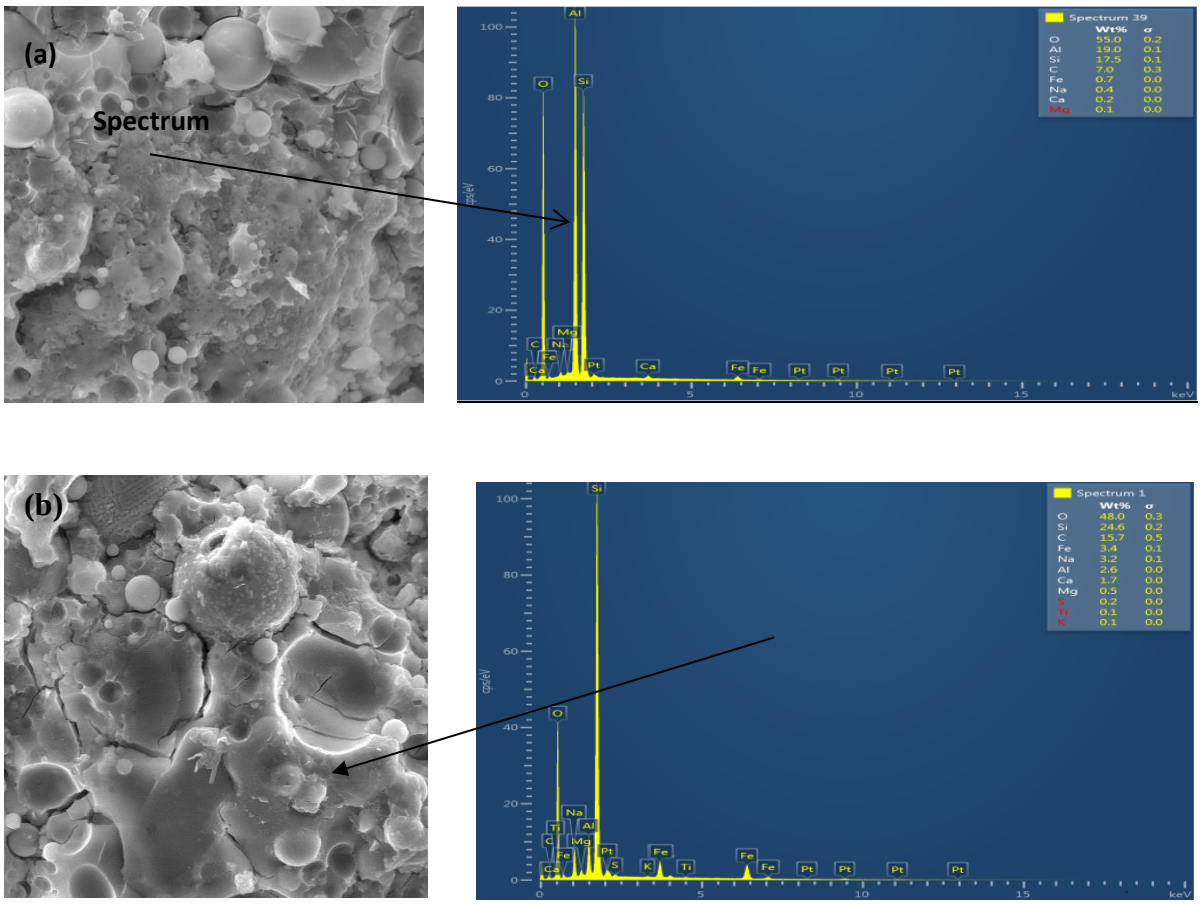

Fig. 4.9 EDX spectra of geopolymers (a) with 2% nanosilica in fly ash only (b) fly ash only with 10% ultrafine fly ash.

4.3.3.2 OPC and GGBFS blended fly ash based geopolymer

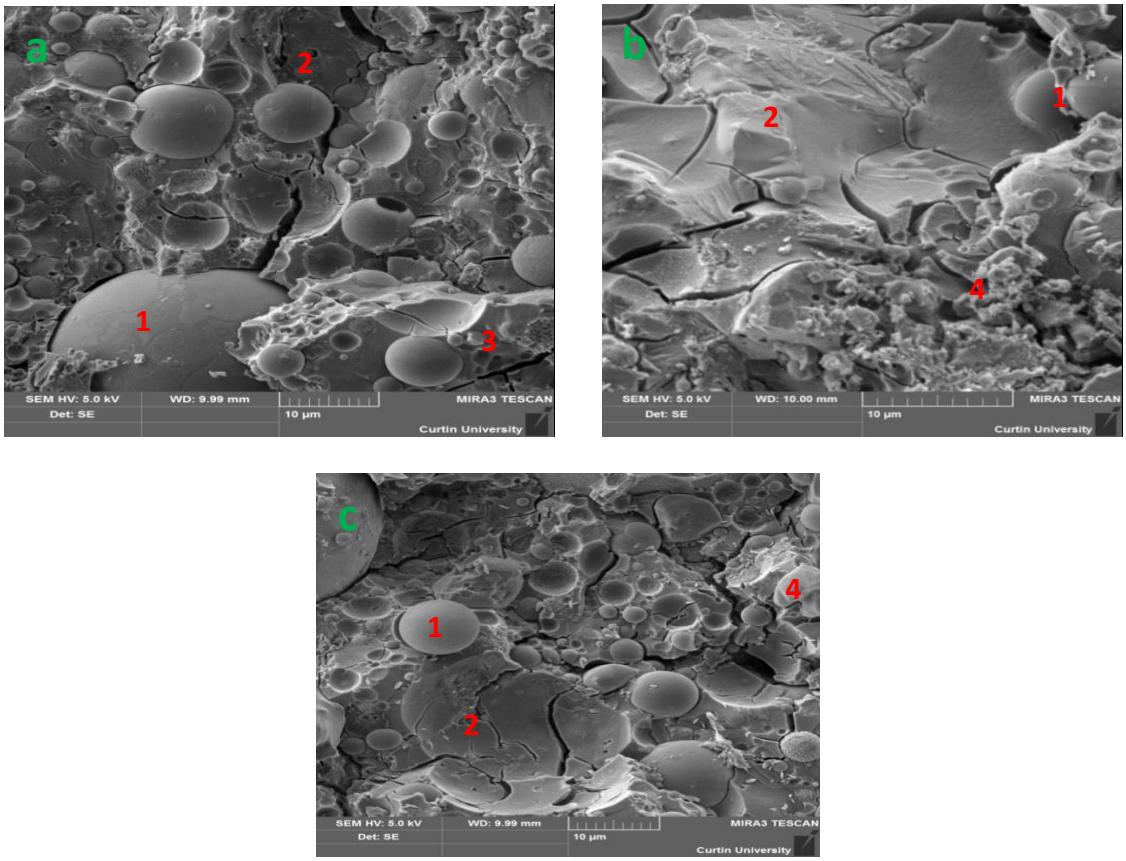

Fig. 4.10 SEM image of GGBFS blended fly ash geopolymers containing nanosilica: (a) 0 wt.% (b) 2 wt.% and (c) 3 wt.%.

The SEM images of the GGBFS blended fly ash geopolymers are shown in Fig. 4.10. The microstructure of the GGBFS blended fly ash geopolymer with 2% nanosilica (Fig. 4.10b) is seen to be much more compacted and dense with less pores as compared to the other two mixes. The microstructures of mixes FA-S-NS0 and FA-S-NS3 are similar to those of mixes FA-NS0 and FA-NS3.

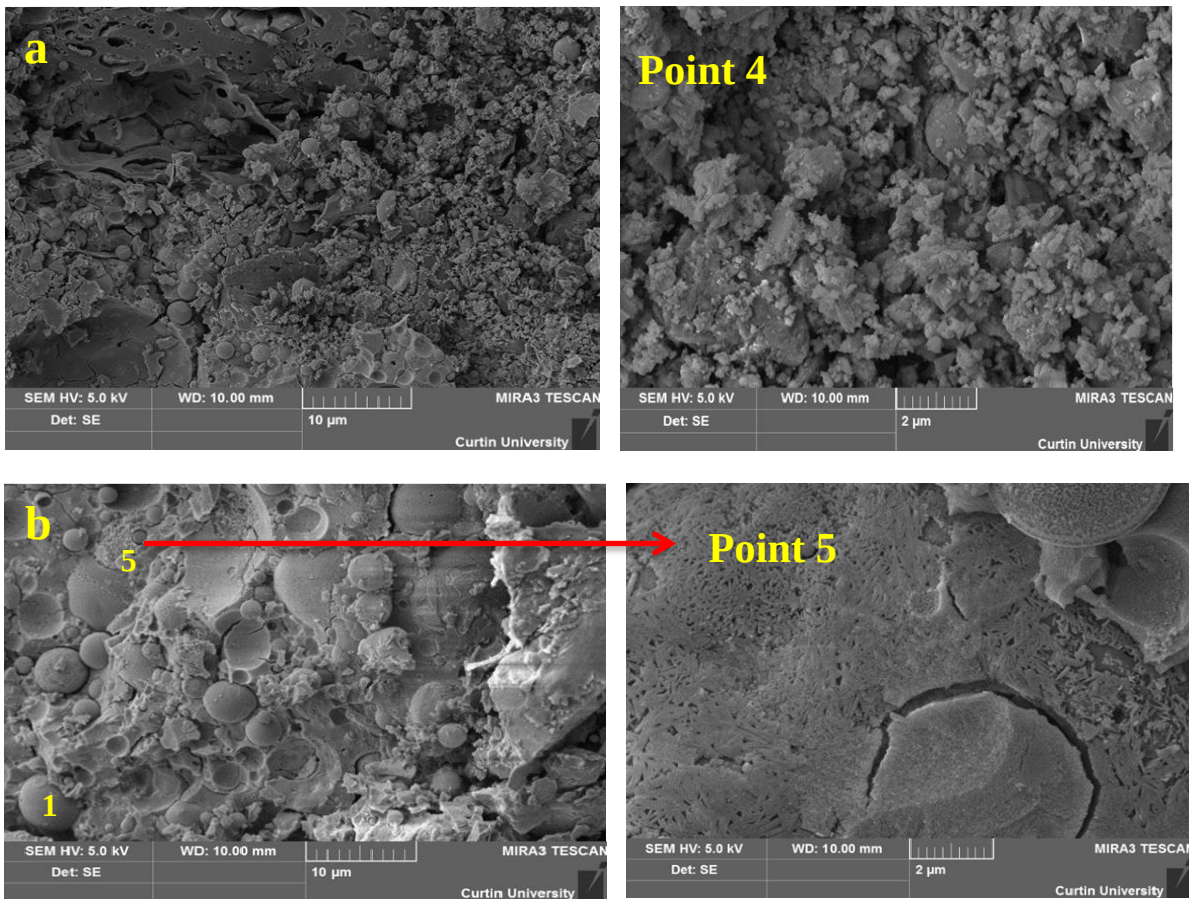

Fig. 4.11 SEM pictures of GGBFS blended geopolymers: a) no ultrafine fly ash; b) with 5% ultrafine fly ash

Figs. 4.11a and 4.11b show the micrographs of the GGBFS blended fly ash based geopolymers with no ultrafine fly ash and with 5 % ultrafine fly ash, respectively. It can be seen from Fig. 4.11b that the ultrafine fly ash reduced the pore size and increased the amount of reaction product as compared to the geopolymer with no ultrafine fly ash (Fig. 4.11a). A relatively more compact reaction product can be seen in the geopolymers with ultrafine fly ash (Fig. 4.11b) as compared to that on the geopolymer without ultrafine fly ash (point 4, Fig. 4.11b). The visual appearance of the matrix of FA-S-UF5 (Fig. 4.11b) appears to be dense and the remaining unreacted particles are well attached to the matrix. On the other hand, mixture

FA-S-UF0 (Fig. 4.11b) exhibited a relatively loose connection around the unreacted fly ash particles.

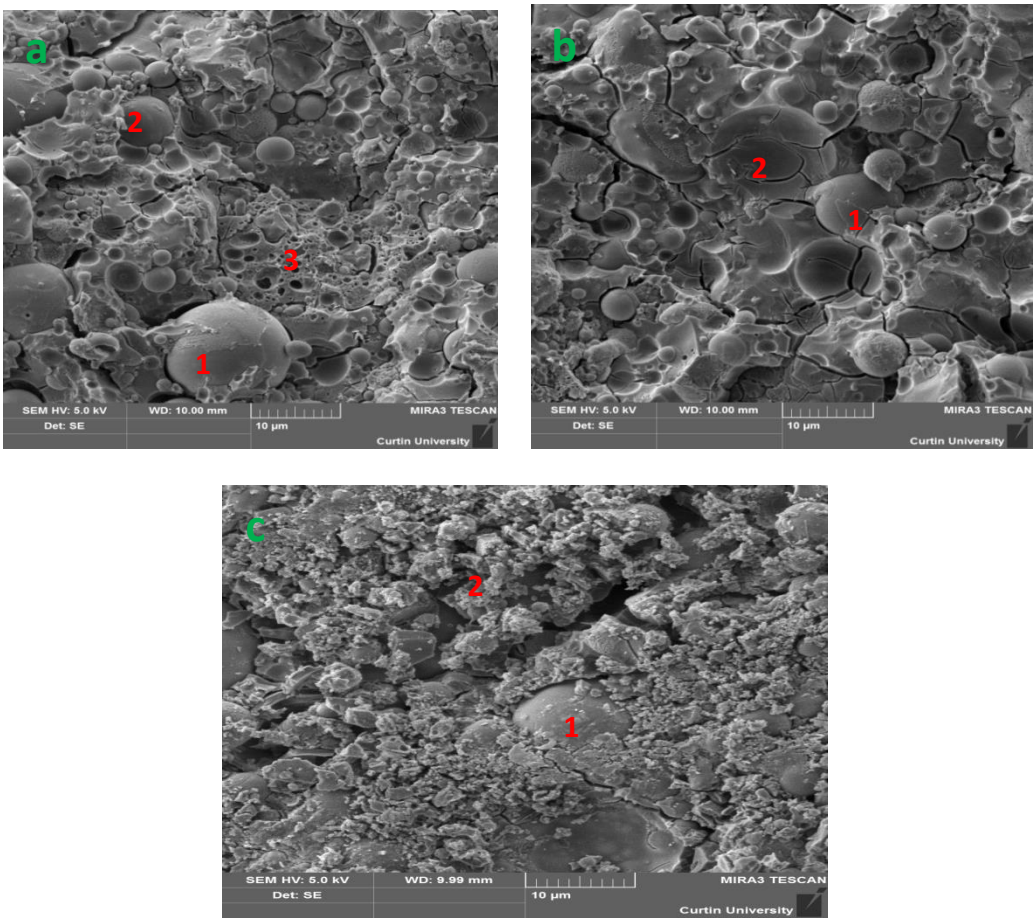

Fig. 4.12 SEM image of OPC blended fly ash based geopolymer paste containing different amounts of nanosilica (a) 0 wt.% (b) 2 wt.% and (c) 3 wt.%.

The SEM images of OPC blended fly ash based geopolymers with different amount of nanosilica are presented in Fig. 4.12. Significant differences in the microstructures were observed with the addition of nanosilica in OPC blended fly ash based geopolymers. In mix FA-PC-NS0, a large amount of unreacted particles (point 1 of Fig. 4.12a) with a large amount of small pores (point 3 of Fig. 4.12a) was observed.

Fig. 4.12 shows that the addition of 2% nanosilica (FA-PC-NS2) in the OPC blended fly ash geopolymer, the voids between the unreacted particles and pores in the hydrated matrix were filled with amorphous hydrated gel and resulted in denser microstructure. No portlandite (calcium hydroxide) was observed and can be considered to have been fully converted into C–S–H by the pozzolanic reaction. However, the structure of the FA-PC-NS3 (3% NS) was observed less dense than FA-PC-NS2 (2% nanosilica) and a loose connection of unreacted fly ash particles was noticed in this case. It is noteworthy that the increase in nanosilica form 2% to 3 % in the mixes resulted in an increase in the amount of partially hydrated gel (Fig. 4.12c) and are not well connected in the geopolymer matrix due to its excess amount in the mixes.

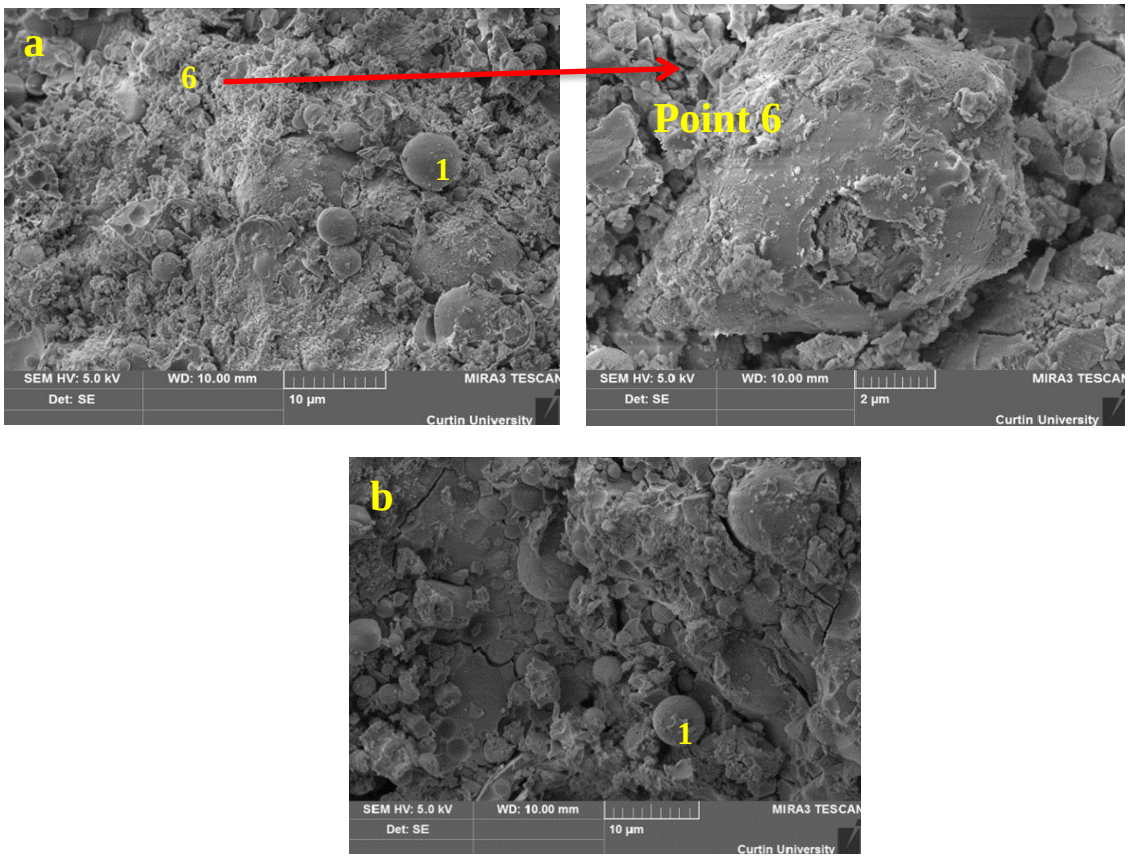

Fig. 4.13 SEM image of OPC blended fly ash based geopolymer paste containing different amounts of ultrafine fly ash (a) 0 wt.% (b) 5 wt.%

The SEM photographs of the OPC blended fly ash geopolymers without and with 5% ultrafine fly ash are shown in Figs 13a and 13b, respectively. Similar to the microstructures of the GGBFS blended geopolymers, ultrafine fly ash resulted in a relatively more compact microstructure in the OPC blended geopolymer.

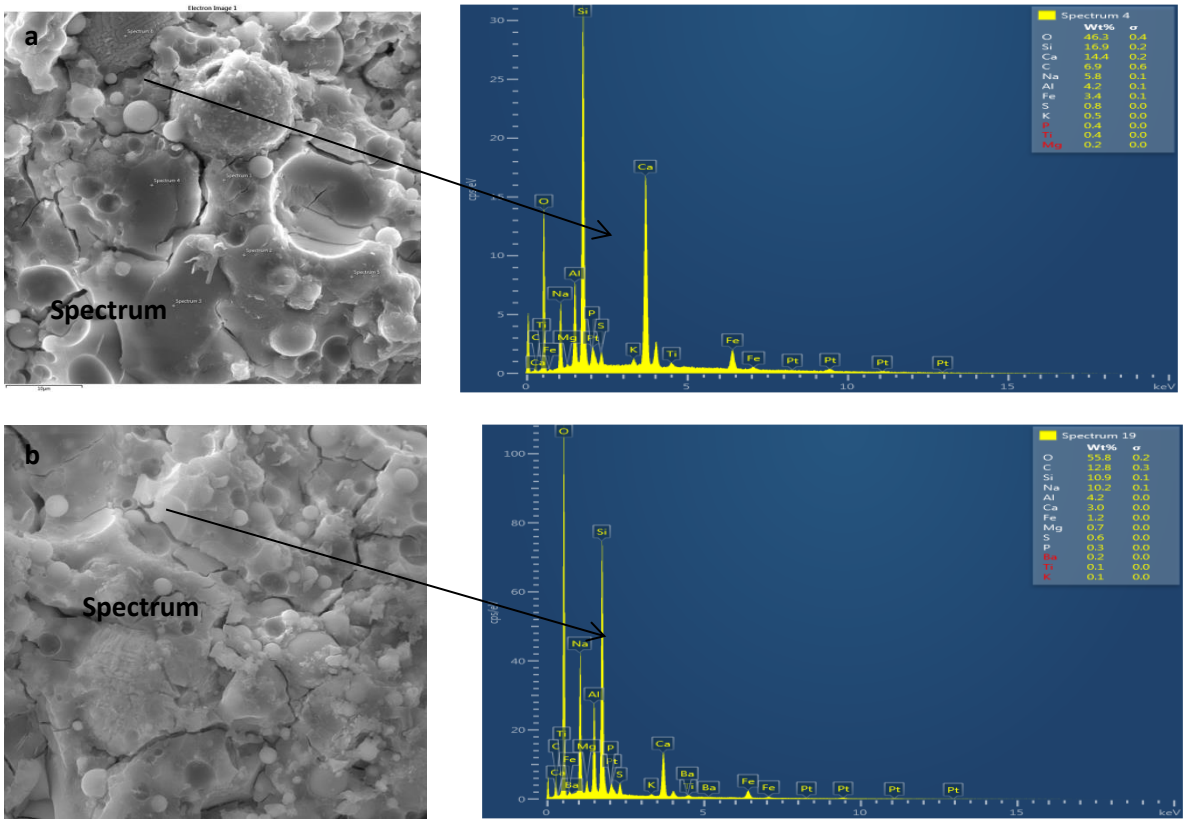

Fig. 4.14 EDX spectra of geopolymers with 2% nanosilica (a) OPC blended fly ash and (b) GGBFS blended fly ash

Fig. 4.14, shows the EDX spectra with identified elements in the hydrated geopolymer paste. The spectrum of EDX provided valuable information on the change of the phase composition of the geopolymer pastes. High concentrations of silicon, oxygen and aluminium can be observed in all the geopolymer paste samples indicating formation of aluminosilicate gels.

Relatively high concentrations of calcium and sodium are also observed in the EDX spectra of the OPC and GGBFS blended fly ash geopolymers (Fig. 4.14a and 14b). These high concentrations of calcium and sodium in addition to silicon, oxygen and aluminium are attributed to the formation of additional calcium silicate (CSH) or calcium aluminosilicate (CASH) and sodium aluminosilicate (NASH) hydrates in these two mixes. Formations of these additional products have resulted in the more compact and dense microstructures. Thus, the unreacted particles of these mixes are seen to be well connected by the reaction products as shown in Figs. 4.14a and 4.14b.

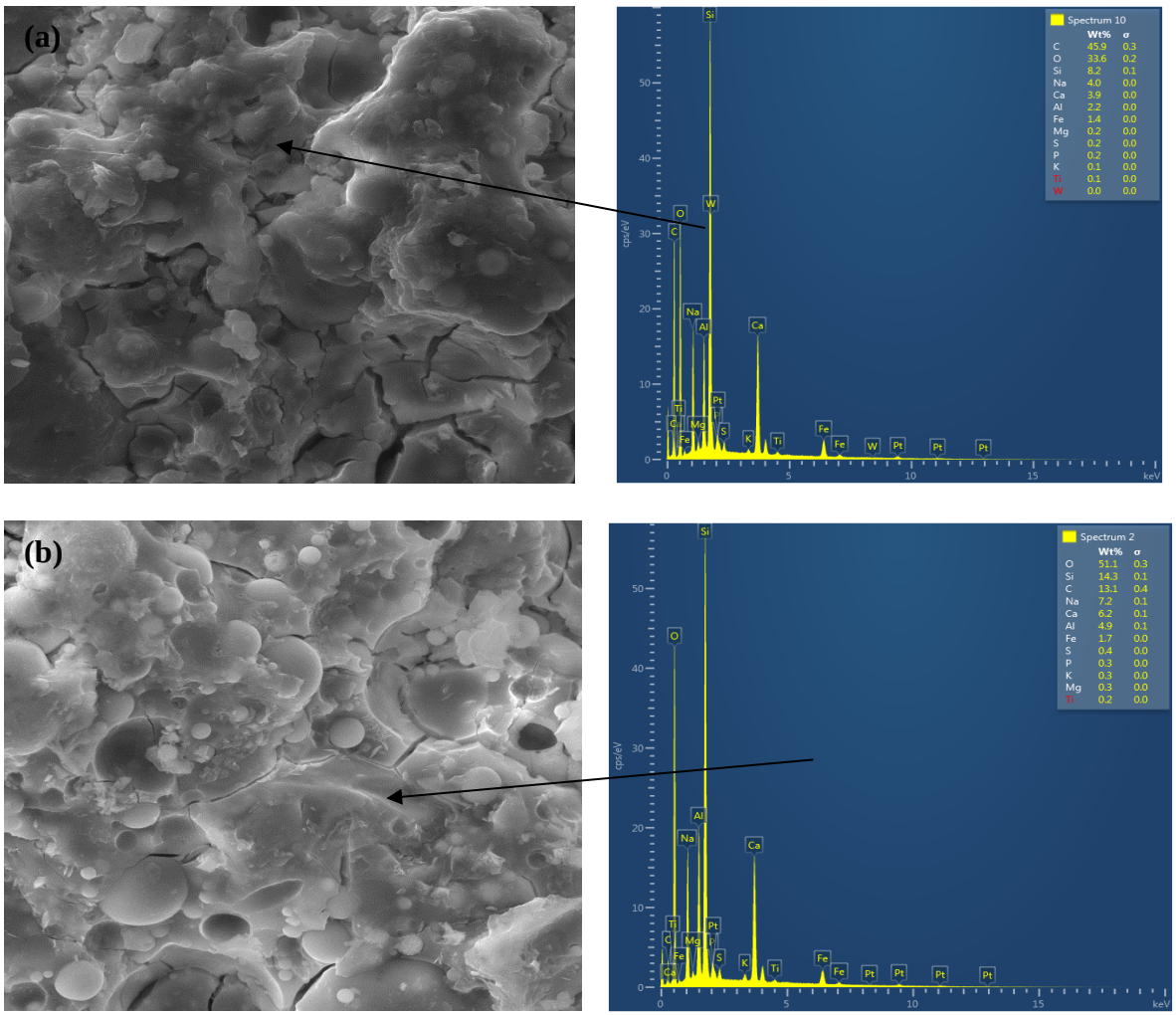

Fig. 4.15 EDX spectra of geopolymers paste with ultrafine fly ash (a) OPC blended fly ash

with 5% ultrafine fly ash and (b) GGBFS blended fly ash with 5% ultrafine fly ash. EDS analysis (Fig. 4.15b) indicates that the elemental composition of GGBFS blended with ultrafine fly ash (FA-S-UF5) is different from the fly ash only geopolymer mixes (FA-UF10). It can be seen that the elements are mostly composed of silicon and aluminium components. In Fig. 4.15b, calcium is also detected apart from the other elements. The presence of calcium can be explained by the formation of sodium aluminosilicate amorphous gels with minor CH gel or in the form of calcium sodium aluminosilicate gel. Observation of these products matches well with those reported in the literature on similar systems [13, 28, 29, 31].

SEM photographs of the three series of geopolymers show that the inclusion of optimum amounts of nanosilica and ultrafine fly ash resulted in a denser microstructure of the reaction product with reduced amount of pores as compared to the mixes without ultrafine fly ash. Fernandez-Jimenez and Palomo [32] pointed out that the considerable amount of unreacted or not totally consumed spheres indicate a moderate degree of reaction in the system. Jimenez and Palomo [15] showed that a considerable amount of unreacted or partially reacted fly ash spheres are the indications of moderate degree of reaction in the system. From the above comparison of the microstructures, it can be seen that the mixes with 2% nanosilica resulted in more compact and dense product as compared to those with no or 3% nanosilica. This more compact microstructure resulted in the highest compressive strength of the mixes containing 2% nanosilica as presented in Figs. 4.5 and 4.10. Also, the most compact microstructure with the least amount of pores observed in the GGBFS blended fly ash mix with 2% nanosilica (Fig. 9(b)) resulted in the highest compressive strength (72 MPa) among all the mixes of this study.

4.3.4 XRD and Quantitative X-ray Diffraction Analysis (QXDA) of fly ash based geopolymer

Fig. 4.16 shows the XRD patterns of nanosilica and ultrafine fly ash blended geopolymer samples cured in room temperature at the age of 28 days. The peaks of minor crystalline phases such as quartz, mullite, hematite and magnetite that are observed in geopolymers without nanosilica did not change significantly with 2% nanosilica in the mixes.

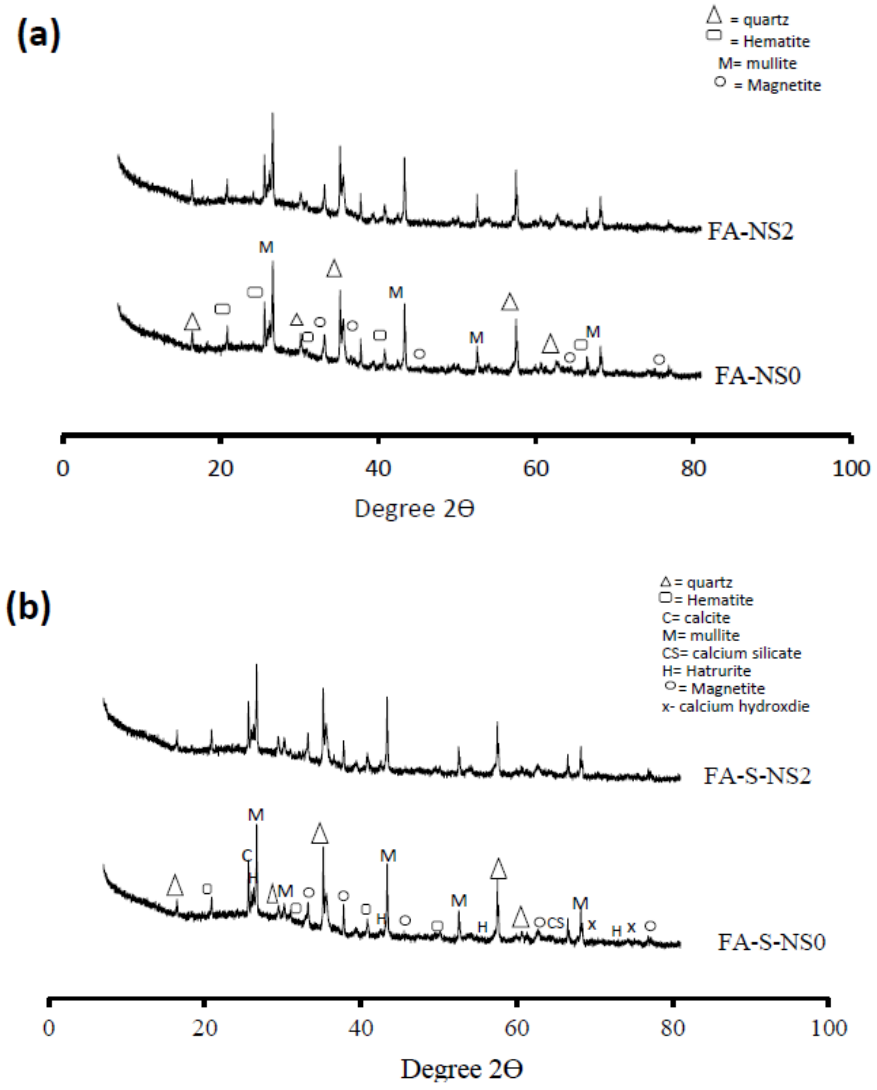

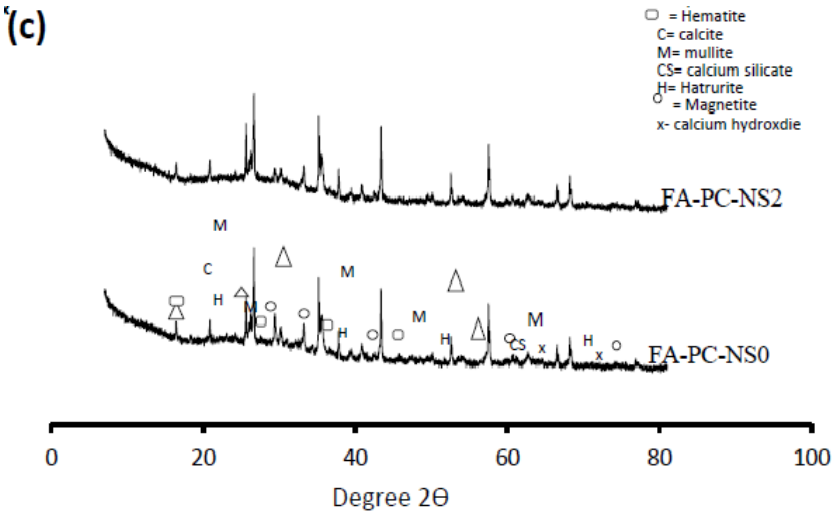

Fig. 4.16 X-ray diffraction patterns of geopolymers with 0% and 2% nanosilica (a) Fly ash only (b) GGBFS blended fly ash (c) OPC blended fly ash.

The peaks characterizing the calcium silicate observed in OPC and GGBFS blended fly ash based geopolymers apart from other common phases were noticed in fly ash only geopolymer. However, Portlandite ($Ca(OH)_2$) crystal peaks were only observed in OPC and GGBFS blended fly ash based geopolymer mixes without nanosilica (FA-S-NS0 and FA-PC-NS0). It appears that the $Ca(OH)_2$ crystals in control mixes (FA-S-NS0 and FA-PC-NS0) were modified and converted into calcium silicate hydrate due to the inclusion of 2% nanosilica in the geopolymer mixes. This is in a good agreement with the findings by other researchers for calcium reached binder samples [25, 28]. Yip et al. [23] indicated that the higher amount of reactive silica reduces the alkalinity of the activating solution and reduced the precipitation of $Ca(OH)_2$ that eventually lead to formation of calcium silicate gel to a greater extent.

Table 4.1 Phase abundance (weight %) of fly ash based geopolymer

Phase	Weight % (esd)								
	FA-NS0	FA-NS2	FA-UF5	FA-PC-NS0	FA-PC-NS2	FA-PC-UF5	FA-S-NS0	FA-S-NS2	FA-S-UF5
Calcite	-	-	-	2.2	1.2	1.7	1.2	1.5	1
Hatrurite	-	-	-	2.4	1.5	2.1	1.5	1.8	-
Hematite	2.5	2.2	2.2	2.4	1.9	2.4	2.1	2.6	2.2
Magnetite	3.9	3.9	3.9	3.4	3.0	3.2	3.0	3.5	3
Mullite	8.6	8.7	8.7	7.7	6.7	7.7	6.8	7.9	7
Quartz	4.7	4.6	4.6	4.0	4.0	4.1	3.9	4.1	3.9
Amorphous Content	80	81	81	78	82	79	79	81	83

The phase compositions of the geopolymers as determined by the Rietveld analysis are given in Table 4.1. Based on the quantitative data, Hematite [Fe_2O_3] (PDF# 01-076-4579), Magnetite [Fe_3O_4] (PDF# 04-007-2718), Mullite [$Al_{4.64}Si_{1.36}O_{9.68}$] (PDF# 01-079-1453) and Quartz [SiO_2] (PDF# 00-046-1045) were recorded in all three types of geopolymers. However, as shown in Table 4.1, Calcite [Ca (CO_3)] (PDF# 01-083-0578) and Hatrurite [Ca_3 (SiO_4) O] (PDF# 01-070-8632) were also formed in the OPC and GGBFS blended fly ash geopolymers, along with the previously mentioned crystalline phases. The values of calcite and hatrurite are noted to vary with the incorporation of ultrafine fly ash in OPC and GGBFS blended fly ash geopolymers. It can be seen that the incorporation of 2% nanosilica and 5% ultrafine fly ash reduced the amount of calcite and Hatruritein the OPC and GGBFS blended geopolymers. It is also noted from Table 4.1 that the amount of quartz, mullite hematite and magnetite did not vary significantly with the addition of ultrafine fly ash. This means that the crystalline phases are barely affected by the addition of nanosilica and ultrafine fly ash.

4.3.5 Pore structures of fly ash based geopolymer

4.3.5.1 Fly ash only geopolymer

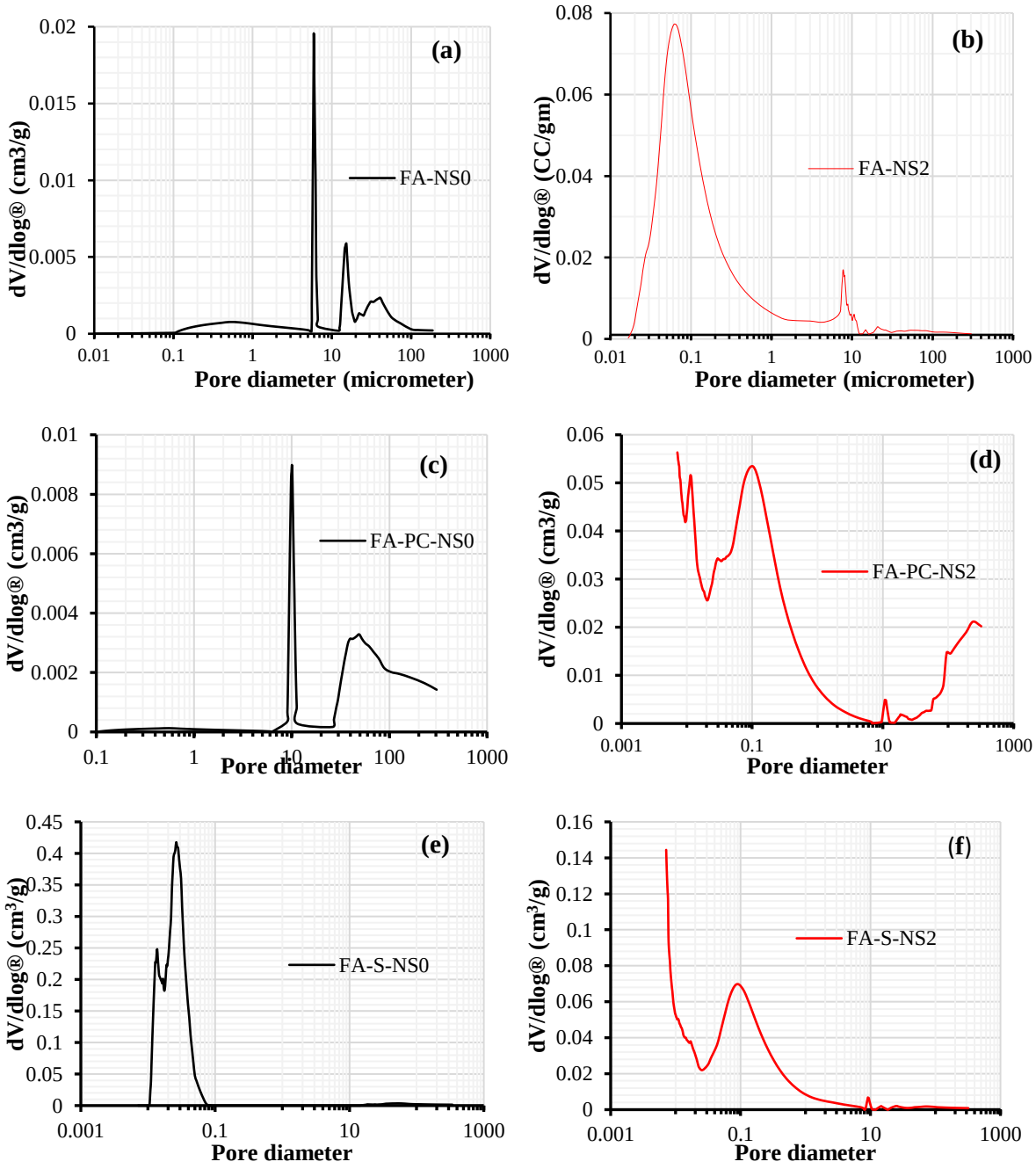

Fig.4.17 Pore Structures of fly ash based geopolymer with and without nanosilica (a) FA-NS0, (b) FA-NS2,(c) FA-S-NS0,(d) FA-S-NS2,(e) FA-PC-NS0, (f) FA-PC-NS2,

The pore size distribution differential curve of different fly ash based geopolymer series are obtained by taking the slope of the pore size distribution curve dV/dlogd against logd (Figs. 4.17a -f). It is noticed that the skeleton of the differential curve with 0% and 2% nanosilica exhibited different intensity with respect to various pore diameter. For example, in mix FA-NS0 (0% nanosilica), two peaks were observed at 5.92 µm and 15 µm (Fig.4.17a). However, the distribution of the pore sizes was different for the specimen containing 2% nanosilica. In fact, the major peak of the geopolymer with 2% nanosilica shifted to a diameter of 0.07 µm. Generally, pore distributions with the peak corresponding to a diameter of 0.01 µm to 10 µm is considered as capillary pores and those with the peak corresponding to 0.001 µm to 0.01 µm are considered as gel pores [30, 31]. Puertas et al. [29] reported that the pore size distribution and porosity value played critical roles in controlling the pore structures of cementitious binders.

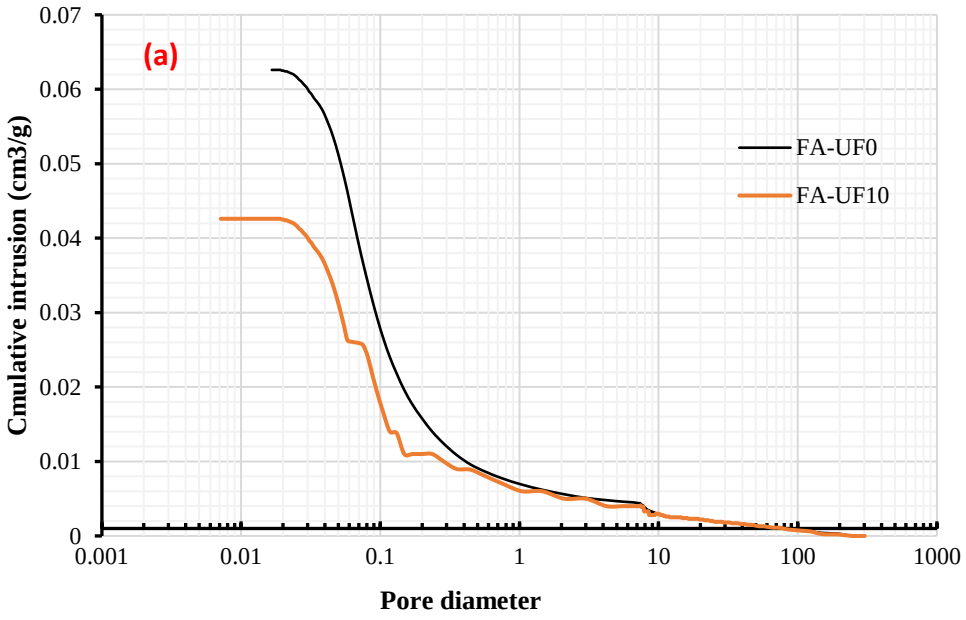

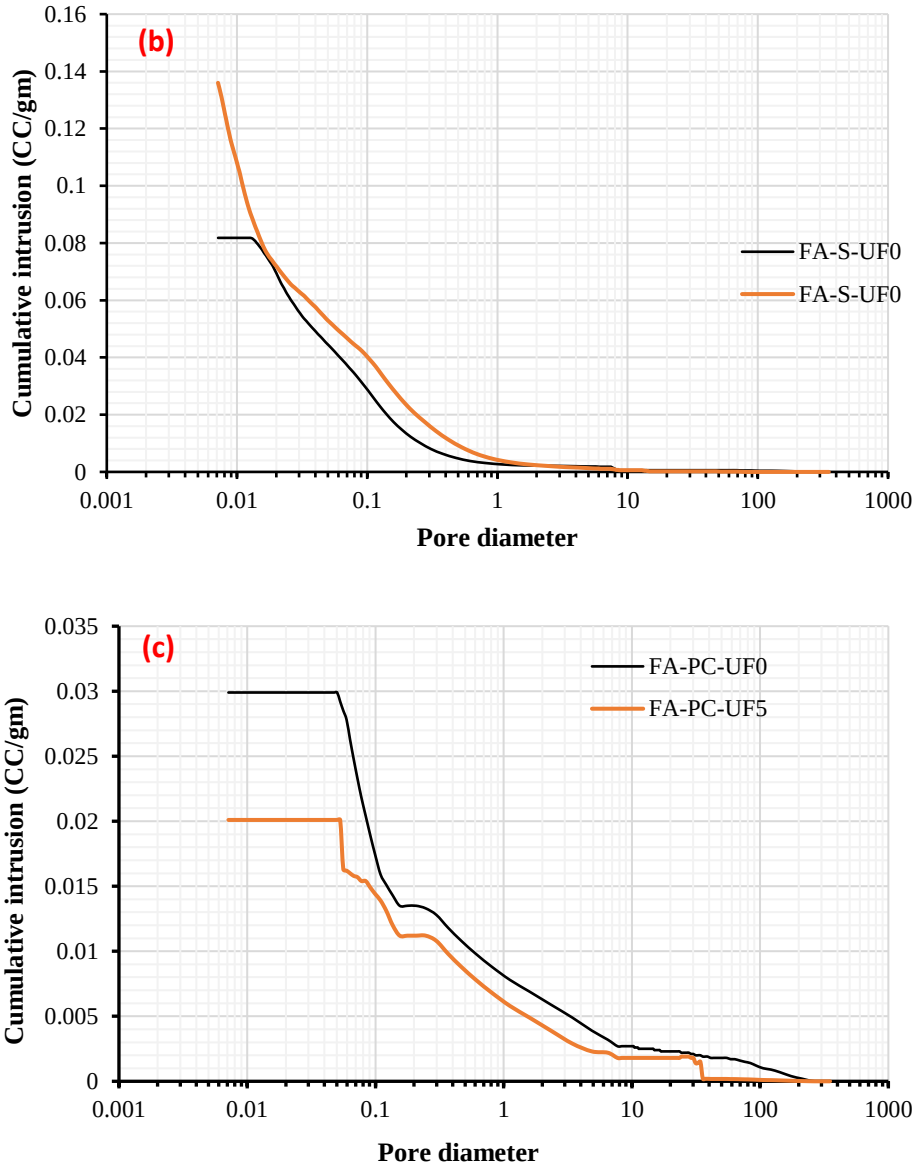

Fig.4.18 Pore Structures of fly ash based geopolymer with and without ultrafine fly ash (a) FA-UF0, FA-UF10 (b) FA-S-UF0, FA-S-UF5,(c) FA-PC-UF0, FA-PC-UF5.

The porosity values in the geopolymer specimens with and without ultrafine fly ash at the age of 28 days were determined by mercury intrusion porosimetry and the result is presented in Fig. 4.18. It is noted from the Figs that the porosity of fly ash-only geopolymer paste reduced from 12.8% to 9.1% by the inclusion of 10% ultrafine fly ash.

The threshold value of the pore diameter was also found to decrease from 0.061 μm for the geopolymer with no ultrafine fly ash (FA-UF0) to 0.008 μm for the geopolymer with 10% ultrafine fly ash (FA-UF10). Fernandez-Jimenez et al. [32] demonstrated that the size of the aluminosilicate gel ultimately determines the pore patterns of fly ash geopolymers. The reduction of pore volume and the sizes are attributed to the formation of additional aluminosilicate gel in mixture FA-UF10 which eventually filled the larger pores; the size of ultrafine fly ash also act as a filler material in this case where the ultrafine fly ash particles bridge the spaces between unreacted grains.

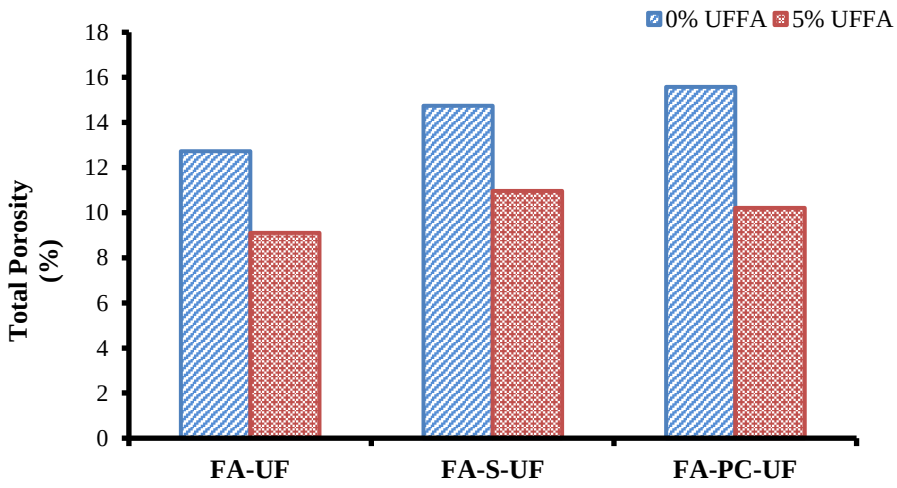

Fig. 4.19. Total porosity (%) of the geopolymers with and without ultrafine fly ash

The total porosity values of the GGBFS blended fly ash based geopolymers reduced from 14.74% to 10.97% by the inclusion of 5% ultrafine fly ash Fig. 4.19. Addition of 5% ultrafine fly ash in GGBFS blended fly ash geopolymer produced more binding gel to fill up the pores. Similarly, the porosity value reduced from 15.58% to 10.21% in the OPC blended geopolymer by the inclusion of 5% ultrafine fly ash. The threshold diameters were found as 0.018 □m and 0.013□m respectively for GGBFS and OPC blended geopolymers with 5%

ultrafine fly ash in the mixes. The results indicate that the inclusion of optimum ultrafine fly ash reduced the total porosity and the threshold pore diameter for all the geopolymer mixes. This means that ultrafine fly ash, with its high surface area to volume ratio strongly influenced the geopolymerisation process of all types of geopolymer and resulted in precipitation of higher amount of reaction product in the pores than that of the control mixes. These results are in good agreement with compressive strength data. It can be observed from Figs. 4.4 and 4.5 that 10% ultrafine fly ash in the OPC blended geopolymers exhibited higher strength (54.0 MPa) with lower porosity (10.21%) than its corresponding control mixture (FA-PC-UF0). Therefore, the durability of geopolymers can be improved by addition of ultrafine fly ash as this reduced porosity of the binder.

4.4 Summary

The effects of incorporating 0-3% nanosilica and 0-15% ultrafine fly ash in geopolymer pastes on the compressive strengths and microstructures are presented in this section. The results showed that the finer particles with the optimum dosages significantly improved the mechanical and microstructural properties of geopolymer paste. It is observed that the initial and final setting time of the geopolymer paste decreased with the increase of the finer materials in the mixes due to the surface effect, small size, and high surface energy of the finer materials. The obtained compressive strengths were observed between 32 to 54 MPa in the mixes using ultrafine fly ash and 32 to 75 MPa in the mixes using nanosilica. However, the finer particles greater than the optimum values exhibited decline of strength and rapid setting, especially, for the OPC and GGBFS blended fly ash geopolymer mixes. Denser microstructures and reduced porosity values were also observed in the specimens using the optimum nanosilica and ultrafine

fly ash. The optimum percentage of nanosilica was foundas 2% and that of ultrafine fly ash was 10% for fly ash-only and 5% for GGBFS and OPC blended fly ash based geopolymers.

4.5 Reference

1. D. Khale, R. Chaudhary, Mechanism of Geopolymerization and Factors Influencing Its Development: A Review. J. Mater. Sci., 42 (2007)729-746.
2. P. Nath, P. K. Sarker, Effect of GGBFS on setting, workability and early strength properties of fly ash geopolymer concrete cured in ambient condition Constr. Build. Mater., 66 (2014) 163–171.
3. P. Nath, P.K. Sarker, Use of OPC to improve setting and early strength properties of low calcium fly ash geopolymer concrete cured at room temperature." Cem. Concr. Comp., 55 (2015) 205–214.
4. A. Fernandez-Jimenez, M. Monzo, M. Vicent, A. Barba, A. Palomo, Alkaline activation of metakaolin–fly ash mixtures: Obtain of Zeoceramics and Zeocements."Micro.Mesopo.Mater., 108 (2008) 41–49
5. V.J.G.S. Jaarsveld, V. J.S.J. Deventer, G.C. Lukey, The characterisation of source materials in fly ash-based geopolymers. Mater. Lett., 57(7) (2003)1272–1280
6. P. Chindaprasirt, C. Jaturapitakkul, T. Sinsiri, Effect of fly ash fineness on microstructure of blended cement paste." Constr. Build Mater., 21 (2007)1534–41.
7. P. Duxson, F.A. Jimenez, J.L. Provis, G.C. Lukey, A. Palomo, V.J.S.J. Deventer, Geopolymer technology: the current state of the art. J. Mater. Sci., 42 (2007) 2917–33.
8. E.I. Diaz, E.N. Allouche, S. Eklund, Factors affecting the suitability of fly ash as source material for geopolymers. Fuel, 89 (2010) 992–996.

9. A. Palomo, P. Krivenko, L.I. Garcia, E. kavalerova, O. Maltseva, F.A. Jiménez, Review on alkaline activation: new analytical perspectives. Mater.De. Constr., 64(315), (2014) e022
10. P. Deb, P. Nath, P.K. Sarker, The effects of ground granulated blast-furnace slag blending with fly ash and activator content on the workability and strength properties of geopolymer concrete cured at ambient temperature, Mater. Des.62 (2014) 32e39.
11. J. Temuujin J, R.P. Williams, A.V. Riessen, Effect of mechanical activation of fly ash on the properties of geopolymer cured at ambient temperature. J Mater Process Technol 209(2009)5276–80.
12. P. Chindaprasirt, C. Jaturapitakkul, T. Sinsiri, Effect of fly ash fineness on microstructure of blended cement paste." Constr. Build Mater., 21 (2007)1534–41.
13. J. Temuujin, R.P. Williams, V.A. Riessen, Influence of calcium compounds on the mechanical properties of fly ash geopolymer pastes. J. Haza. Mater. 167(1-3) (2009) 82–88.
14. H. Xu, V.J.S.J. Deventer, Geopolymerisation of multiple minerals." Miner. Eng., 15 (2002) 1131
15. A. Fernandez-Jimenez, A. Palomo, Characterisation of fly ashes. Potential reactivity as alkaline cements. Fuel. 82 (2003) 2259–2265.
16. M. Criado, A. F. Jiménez , A.G. Torre, M.A.G. Aranda, A. Palomo , An XRD study of the effect of the SiO2/Na2O ratio on the alkali activation of fly ash. CemConcr Res 37(5) (2007) 671–9.
17. H. Xu, J.S.J. Deventer, The geopolymerisation of alumino-silicate minerals." Int. J. Miner. Process. 59 (3) (2000) 247–266.

18. Hajimohammadi, J.L. Provis, J.S.J. van Deventer, The effect of silica availability on the mechanism of geopolymerisation. CemConcr Res 41(3) (2011) 210–6.
19. P.S. Deb, P. Nath, P.K. Sarker, Strength and permeation properties of slag blended fly ash based geopolymer concrete, Adv. Mater. Res. 651 (2013) 168–173. doi.org/10.4028/www.scientific.net/AMR.651.168.
20. K. Divya, R. Chaudhary, Mechanism of Geopolymerization and Factors Influencing Its Development: A Review. J Mater Sci, 42 (2007) 729-746, retrieved from http:// www.springerlink.com
21. J. Tailby, K.J.D. MacKenzie. Structure and mechanical properties of aluminosilicate geopolymer composites with Portland cement and its constituent mineralsCemConc Res, 40 (2010), pp. 787–794
22. T. Suwan, M. Fan, Influence of OPC replacement and manufacturing procedures on the properties of self-cured geopolymer. Constr. Build. Mater., 73 (2014) 551–561
23. C.K. Yip, J.S.J. Deventer, Microanalysis of calcium silicate hydrate gel formed within a geopolymeric binder, J. Mater. Sci. 38 (2003) 3851–3860.
24. J.Y. Shih, T.P. Chang, T.C. Hsiao, Effect of nanosilica on characterization of Portland cement composite, Mater. Sci. Eng. A-Struct. 424 (2006) 266–274.
25. J.E. Oh, P.J.M. Monteiro, S.J. Ssang, C. Sejin, S.M. Clark, The evolution of strength and crystalline phases for alkali-activated ground blast furnace slag and fly ash-based geopolymers, Cem. Concr. Res. 40 (2010) 189–196, http://dx.doi. org/10.1016/j.cemconres.2009.10.010

26. E.D. Rodríguez, S.A. Bernal, J.L. Provis, J. Paya, J.M. Monzoa, M.V. Borrachero, Effect of nanosilica-based activators on the performance of an alkali-activated fly ash binder, Cem. Concr. Comp. 35 (2013) 1–11
27. K. Scrivener, A.K. Crumbie, P. Laugesen, The Interfacial Transition Zone (ITZ) Between Cement Paste and Aggregate in Concrete. Interface Sci 12(2004) 411–21.
28. S. Kumar, R. Kumar, T.C. Alex, A. Bandopadhyay, S.P. Mehrotra, Effect of mechanically activated fly ash on the properties of geopolymer cement. In: Davidovits, J. (Ed.), Proceedings of the World Congress Geopolymer. Saint Quentin, France, 28 June–1 July, pp. 113–116 (2005)
29. F. Puertas, S. M.Ramirez, S. Alonso, T. Vasquez, Alkali- activated fly ash/slag cement. Strength behaviour and hydration products. CemConcr Res 30 (2000)1625–32
30. A.Criado, F.A.Jimenez, A.Palomo, Alkali activation of fly ash: Effect of the SiO2=Na2O ratio. Part I: FTIR study. Micro. Mesop. Mater., 106(1–3) (2007) 180–191
31. R.R. Lloyd, J.L. Provis, J.S.J. Deventer, Acid resistance of inorganic polymer binders. 1. Corrosion rate, Mater. Struct. 45 (2012) 1e14
32. A. Fernandez-Jimenez, A. Palomo, Characterisation of fly ashes potential reactivity as alkaline cements, Fuel 82 (2009) 2259–2265, http://dx.doi.org/10.1016/S0016-2361(03)00194-7.

CHAPTER 5

GEOPOLYMER MORTAR WITH ULTRAFINE FLY ASH AND NANOSILICA.

5.1 Overview

The effects of nanosilica and ultrafine fly ash on fly ash based geopolymer mortar are presented in this chapter. The base materials used are fly ash (FA), ground granulated blast furnace slag (GGBFS) and Ordinary Portland cement, curing temperature and the amount of alkaline solution were kept constant with varying the percentages of nanosilica and ultrafine fly ash in the mixes. The test results show that strength and durability properties of fly ash based geopolymer mortar significantly depends on the type and amount of finer materials present in the binder. Geopolymer mixes with each specific series has an optimum amount of nanosilica and ultrafine fly ash values that helps them achieve the desired properties such as higher compressive strength and lower porosity and higher resistances to acid attack and carbonation.

5.2 Workability of fly ash based geopolymer with ultrafine fly ash and nanosilica

5.2.1 Fly-ash only geopolymer

The flowability of fresh geopolymer mortar incorporating nanosilica and ultrafine fly ash is shown in Fig. 5.1. It can be seen that the flow behaviour of fly ash based geopolymer mortar is influenced by the amount of finer materials in the mixes.

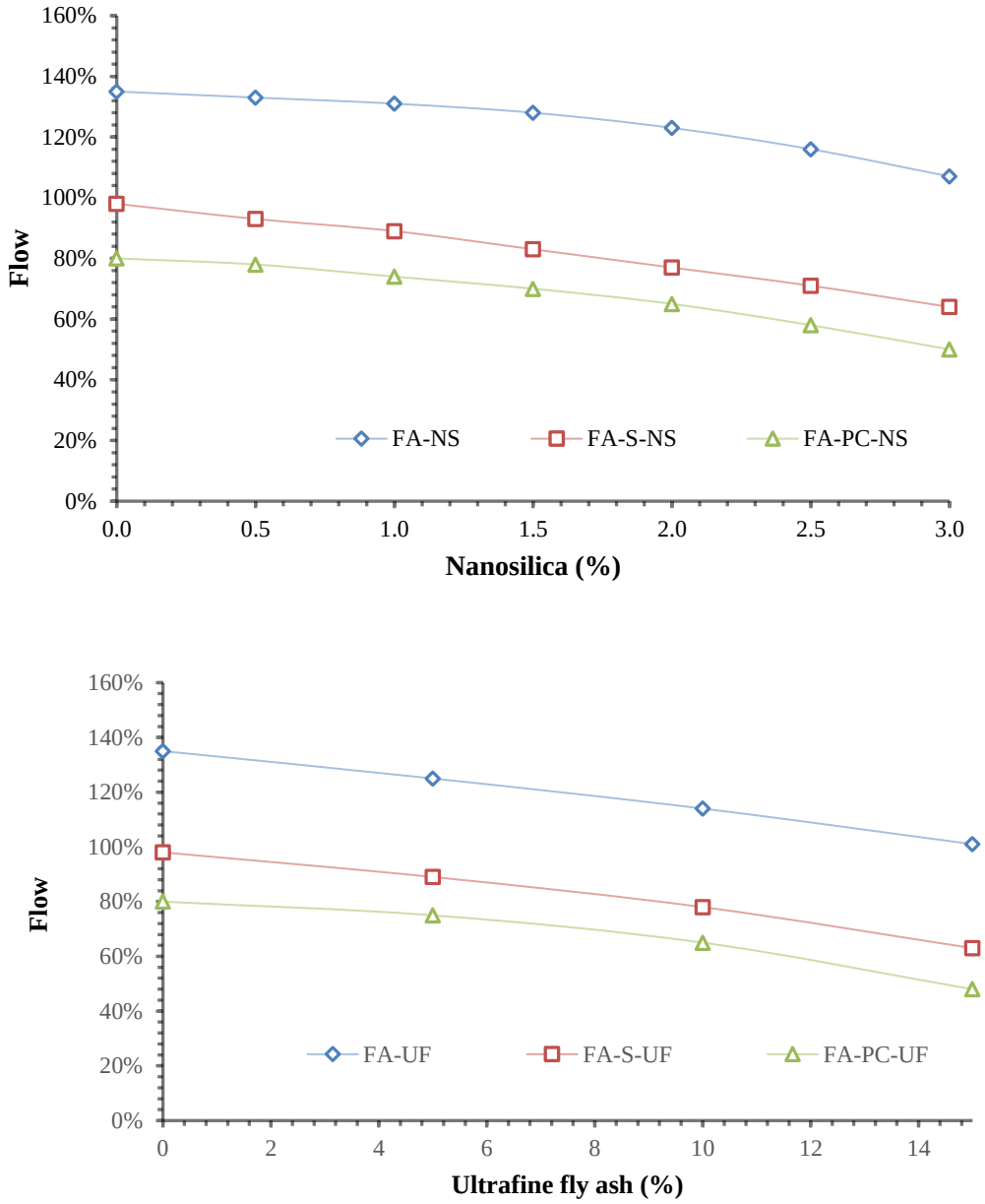

Fig. 5.1 Effect of nanosilica and ultrafine fly ash on workability of fly ash based geopolymer

It can be seen that the increase of nanosilica in the mixes increased the cohesiveness of fresh geopolymer mortar. As seen from Fig. 5.1, the flow of fly ash only geopolymer mortar FA-NS0 reduced from 135% to 107% with 3% nanosilica (FA-NS3.0). This can be attributed mainly to the higher specific surface area of nanosilica than that of regular fly ash. The higher surface area of binders need a higher amount of of alkaline liquid to maintain the same level of

workability. The same scenarios were also observed for fly ash onlygeopolymer mortar with ultrafine fly ash. It is apparent from Fig. 5.1 that the control mix without ultrafine fly ash (FA-UF0) showed 135% flow whereas it was 125% for 5% ultrafine fly ash geopolymer mortar (FA-UF5.0). Similarly, the flow value also decreased as the ultrafine fly ash content was increased to 10% and 15%.

5.2.2 OPC and GGBFS blended fly ash based geopolymer

It can be seen that flow values of the mortar mixes containing GGBFS and OPC were less than those of the fly ash only mixes. The decrease in flow is because of the early reaction of the calcium contained in GGBFS and OPC. The trend is similar to the observations in previous works [1, 2 3, 4]. Nath and Sarker [4] and Provis et al. [5] reported that the flow of fly ash geopolymer mortars decreased with the increase of calcium bearing components in the binder. Gao et al. [6] noted that lower slag content provided a better flowability due to their morphological differences. It can be seen from Fig.5.1 that the flow of geopolymer mortars gradually decreased with the increase of nanosilica. The flow of OPC blended fly ash geopolymer mortars decreased from 80% (FA-PC-NS0) to 50% (FA-PC-NS3.0) with the addition of 3% nanosilica. The flow decreased from 98% to 64% by the addition of 3% nanosilica in the GGBFS blended fly ash geopolymer mortar. Similarly, flow decreased from 80% to 48% by 15% ultrafine fly ash in the OPC blended fly ash geopolymer mortar. The decrease of flow in the mixes of all three series by the inclusion of nanosilica and ultrafine fly ash are attributed to the increased liquid demand and accelerated reaction due to increased specific surface area. The geopolymer mortars based on GGBFS and OPC blended fly ash containing 3% nanosilica and 15 % ultrafine fly ash were relatively stiff in nature and showed low workability.

5.3 Strength of fly ash based geopolymer mortar with ultrafine fly ash and nanosilica

5.3.1 Fly-ash only geopolymer

The compressive strength developments of the fly ash geopolymer mortars with 0% to 3% nanosilica and 0% to 15% ultrafine fly ash are shown in Fig. 5.2. Each value is an average of the results obtained from 3 identical specimens.

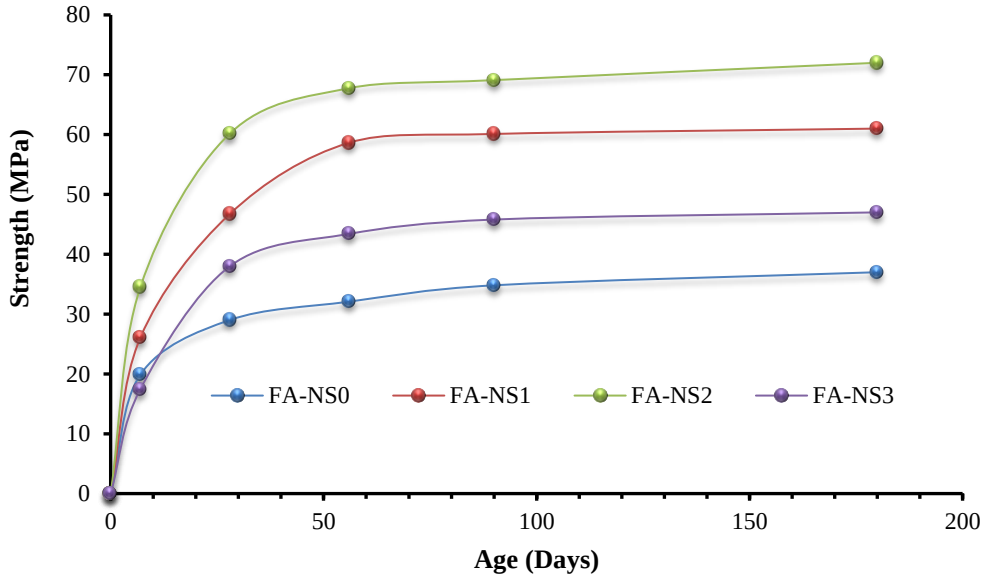

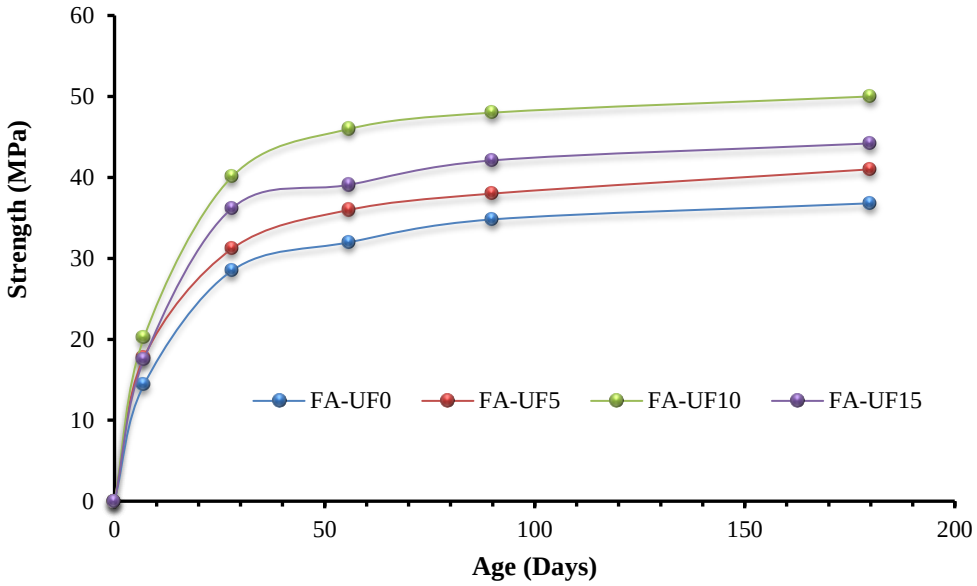

Fig. 5.2 Effect of nanosilica and ultrafine fly ash on compressive strength of fly ash only geopolymer mortar.

It can be seen from the figure that the rate of strength development slowed down significantly after 28 days and it was negligible after the age of 56 days. Noticeable increase of strength can be seen in the fly ash geopolymer mortars containing nanosilica. The extent of the increase in strength is dependent on the percentage of nanosilica. The highest strengths at all ages up to 28 days were found in the mortars with 2% nanosilica. While the strength of the mortar with 3% nanosilica was higher than that of the control mix (FA-NS0), it was less than that of the mix with 2% nanosilica. Fernandez and Palomo [7] reported that the fineness of the source material played an important role in the strength development of geopolymer binders. Temuujin et al. [8] also showed that the reduction of particle size and change in morphology increased the dissolution rate which eventually increased the compressive strength of geopolymer binder.

For ultrafine fly ash incorporated geopolymer mortars, it can be seen from Fig. 5.2 that FA-UF10, FA-S-UF5.0 and FA-PC-UF5.0 mortars with 10% and 5% ultrafine fly ash developed higher compressive strengths compared to those of the corresponding mixes without

ultrafine fly ash. This observation is same with those found in previous section for nanosilica incorporated fly ash based geopolymer paste, and it can be explained by the fact that the degree of polymerization increased with the use of ultrafine fly ash.

It was shown in previous works [1, 3, 4] that curing temperature, molarity of sodium hydroxide and the reactivity of the source materials played crucial roles on the strength development of fly ash geopolymers. Generally, geopolymers based on fly ash only and cured at room temperature showed low compressive strength because of the slow geopolymerisation process. The strength development in the mortar specimens without nanosilica and ultrafine fly ash showed similar trend in Fig. 5.2. The finer particles took partin the reaction process from an early age because of their high specific surface. A greater degree of reaction of the aluminosilicate source materials is expected to give higher strength [9]. However, the results of this study suggest that there is a limiting value on the percentage of nanosilica and ultrafine fly ash beyond which no further increase in mortar strength is achieved. Thus, the optimum dosage of nanosilica and ultrafine fly ash for is the mortar mixtures is found to be 2% and 10% respectively. Belkowitz et al. [10] noted that the unreacted nanosilica caused an excessive self-desiccation and cracking in the matrix that eventually caused decline of strength. Therefore, the reduced strength of the mortar with 3% nanosilica than that with 2% nanosilica is attributed to the presence of unreacted particles acting as defect sites.

5.3.2 OPC and GGBFS blended fly ash based geopolymer

The strength developments of OPC and GGBFS blended series with the different amounts of nanosilica are shown in Figs 5.3 and 5. 4. As mentioned earlier, low-calcium fly ash was blended with either 10% OPC or 15% GGBFS in order to accelerate the setting of these mixes.

As other ingredients remained constant, Fig. 5.3 and Fig. 5.4 show the influence of nanosilica and ultrafine fly ash addition on the strength development.

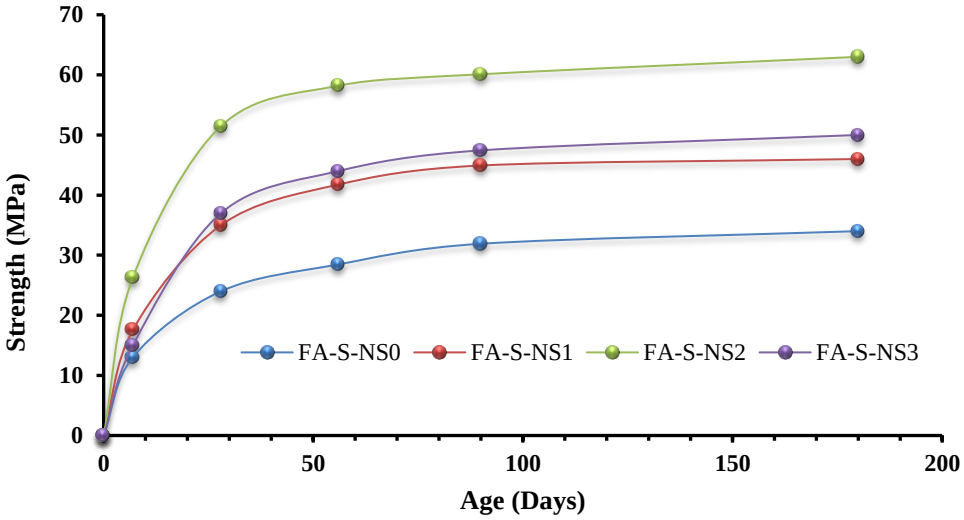

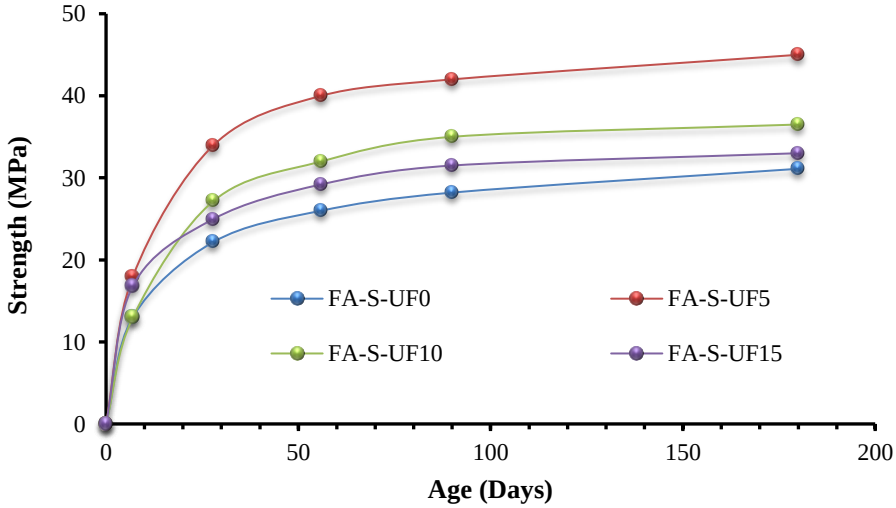

Fig. 5.3 Effect of nanosilica and ultrafine fly ash on compressive strength of GGBFS blended fly ash based geopolymer mortar,

It is noteworthy that inclusion of nanosilica from 0 to 3% in the OPC and GGBFS blended series increased compressive strength by 40 to 64% as compared to the corresponding control mixes. Chindaprasirt et al. [11] and Somna et al. [12] reported that larger surface area of the source materials increased the geopolymerization process and eventually increased the

strength. It is noted from Fig. 5.4 that mixes with 1%, 2% and 3% nanosilica; in the OPC blended series exhibited 41%, 63% and 50% higher strength respectively than the mix without nanosilica. Similar trend was also observed for GGBFS blended geopolymer mortars. The pore refinement process of nanosilica has resulted in higher strength of the geopolymer mixes. The addition of nanosilica increases the supply of the Si required for the geopolymerization process. It is noteworthy that due to its very large specific surface, nanosilica is highly reactive as compared to that of other cementitious materials such as fly ash, OPC and GGBFS. The main effect of the nanosilica addition in OPC and GGBFS blended series was the acceleration of the interconnected structure growth due to higher geopolymerization process that eventually resulted in higher compressive strength. The effect of nanosilica on strength development was similar in all the three series of mixes and the optimum percentage of nanosilica was found as 2%.

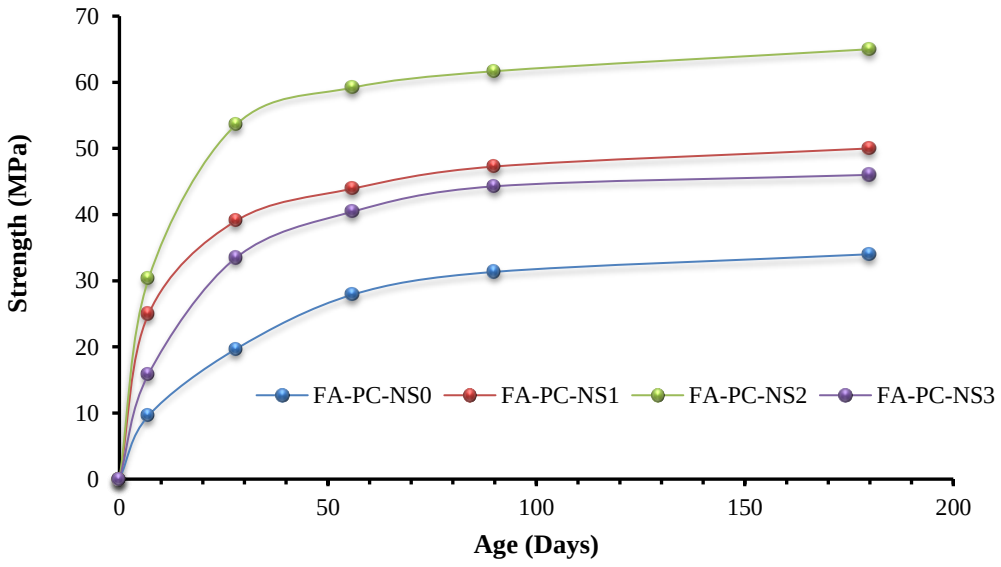

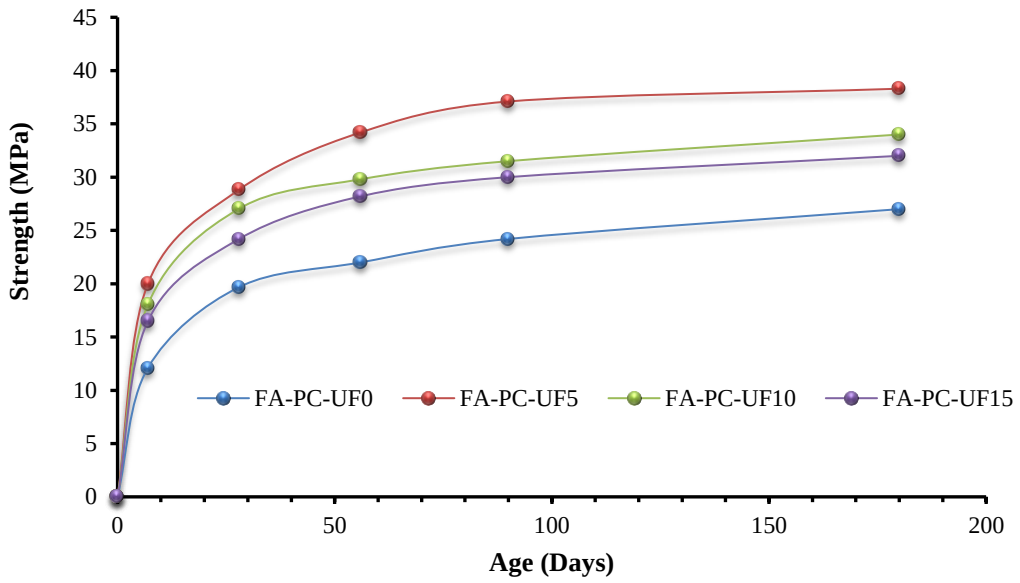

Fig. 5.4 Effect of nanosilica and ultrafine fly ash on compressive strength of OPC blended fly ash based geopolymer mortar.

Figs. 5.3 and 5.4 also provide a comparison of compressive strengths of the fly ash based geopolymer mortars with 0% to 15% ultrafine fly ash at 28, 56, 90 and 180 days. As expected, strength increased with partial replacements of regular fly ash by 5% to 15% ultrafine fly ash. At 28 days, the strength of the mortar FA-PC-UF5.0 was 30% higher than that of FA-PC-UF0. Although the strength improvement of mortar FA-PC-UF15 wassignificantly higher than mortar FA-PC-UF0 at 28 days, the improvement declined to 17% at 28 days when the mixture is compare with FA-PC-UF5.0. The 180-day strength of mortar FA-PC-UF5.0 was 38.3 MPa, which was the highest strength achieved for the OPC blended fly ash mortar series. The compressive strength of GGBFS blended fly ash based geopolymer mortars incorporating 5% (FA-S-UF5.0), 10% (FA-S-UF5.0) and 15% (FA-S-UF15) ultrafine fly ash were higher than that of control mixture. However, when the content of ultrafine fly ash increased above 5%, the compressive strength of geopolymer mortar declined. This trend is the same as that

shown by the OPC blended fly ash geopolymer mortar with 5% ultrafine fly ash. The optimum dosage of ultrafine fly ash for this mortar series was found to be 10% for fly ash only geopolymer and 5% for OPC and GGBFS blended fly ash mortar series.

5.4 Sorptivity of fly ash based geopolymer mortar with ultrafine fly ash and nanosilica

Sorptivity tests were conducted for the geopolymer mortar mixes without nanosilica, 2% nanosilica, 5% and 10% ultrafine fly ash. Nanosilica dosage of 2% for all geopolymer series, 10% ultrafine fly ash for fly ash only and 5% for OPC and GGBFS blended geopolymer were selected for the sorptivity and acid resistance tests since this percentage was found to maximise the compressive strength. The sorptivity coefficients of the fly ash only, OPC and GGBFS blended fly ash geopolymer mortars are given in Fig. 5.5.

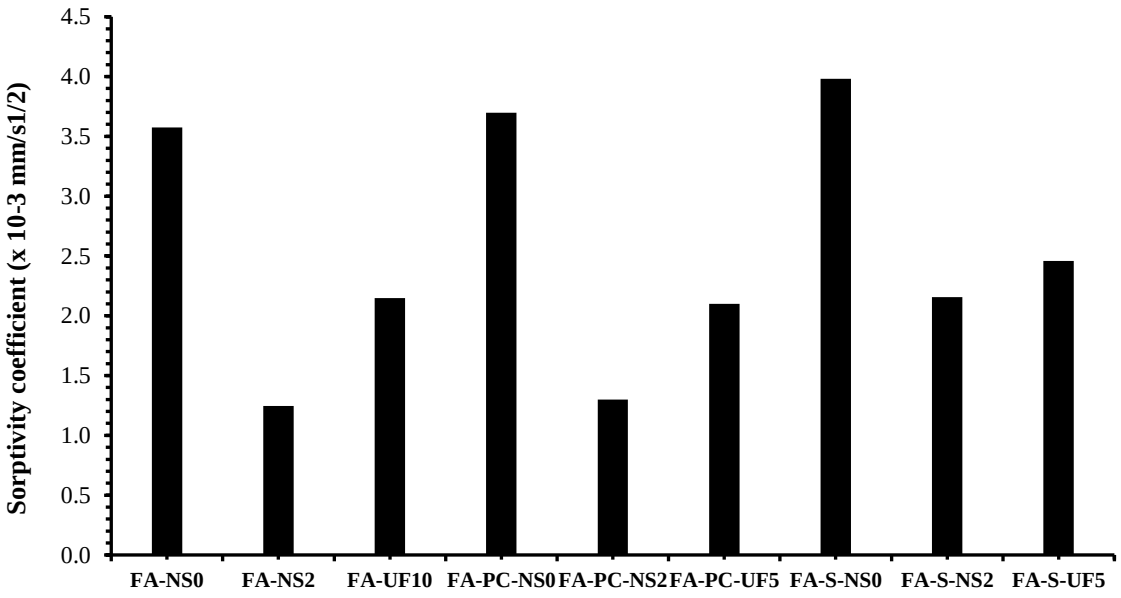

Fig. 5.5 Sorptivity coefficient of geopolymer mortars with nanosilica.

As shown by the results, sorptivity coefficient of the mixes without nanosilica was in the range of 3.575 $\times 10^{-3}$ mm/s$^{1/2}$ to 3.980$\times 10^{-3}$ mm/s$^{1/2}$ and that of the mixes with 2% nanosilica

was in the range of 1.247×10^{-3} mm/s$^{1/2}$ to 2.157×10^{-3} mm/s$^{1/2}$ and 2.099×10^{-3} mm/s$^{1/2}$ to 2.457×10^{-3} mm/s$^{1/2}$ for ultrafine fly ash based series. Thus, it is apparent from the results that the sorptivity coefficient decreased with finer materials in the mortar mixes of all the three series. For example, sorptivity coefficient decreased from 3.575×10^{-3} mm/s$^{1/2}$ to 1.247×10^{-3} mm/s$^{1/2}$ by 2% nanosilica in the fly ash only geopolymer mortar. Sorptivity reduced by ultrafine fly ash and nanosilica in the GGBFS and OPC blended fly ash geopolymer mortars in a similar way. The decrease in sorptivity of the specimens indicates a reduction in the porosity by inclusion of finer materials (nanosilica and ultrafine fly ash) in the binder.

The improvement of porosity for fly ash based geopolymer series are attributed to two reasons. Firstly, the particle packing of finer particles in the wide distribution of binder particle sizes resulted in a denser matrix. Secondly, the reaction of nanosilica and ultrafine fly ash in geopolymerization process produced further amount of aluminosilicate gel along with the reaction products from the main source materials. It is likely that additional reaction product precipitated in the available pore structures. As described by Law et al. [13], an increase in SiO_2 increases the density of the matrix. Therefore, the combined filling effect of nanosilica/ ultrafine fly ash by the improved particle packing and the additional reaction product produced a denser binding matrix that reduced the porosity and increased compressive strength as seen in Figs. 5.2 to 5.4.

5.5 Durability properties of fly ash based geopolymer mortar with ultrafine fly ash and nanosilica

5.5.1 Resistance to carbonation of fly ash based geopolymer

An accelerated carbonation test was conducted on the geopolymer samples. The test method followed is similar to that presented in literature [27]. It is noted from Figs.5.6 to 5.8 that fly

ash based geopolymer mortar with 2% nanosilica and 10% ultrafine fly ash displayed no clear border between the coloured (purple colour) and colourless area when sprayed with phenolphthalein indicator. The carbonation depth for fly ash only geopolymer mix without nanosilica or ultrafine fly ash (FA-NS/UF0) after 28, 56 and 90 days were recorded as 15 mm, 20mm and 26 mm, respectively. However, it is noted from Table 5.1 that the carbonation penetration depth was significantly reduced at the same ages with inclusion of 2% nanosilica and 10% ultrafine.

For example, mortar FA-NS2.0 exhibited carbonation depths of 5mm, 9mm and 15mm and mortar FA-UF10 showed 6mm, 10mm and 14 mm that are significantly less than that of their corresponding control mix (FA-NS/UF0). The decrease in the measured carbonation depth is attributed to the refinement of pores by the finer particles (nanosilica/ultrafine fly ash). Puertas et al. [14] noted that pores filled with hydrated gel or other precipitated materials usually prevents the passage of CO2 into deeper layers of the cementitious binder. Deja [15] also observed that the lower values of total porosity and average pore diameter improved the resistance to carbonation of cementitious binders.

However, it is noted from Fig. 5.6 that the graduation of colour in the outer part was lighter as compared to the inner parts and the penetration depth in this occasion was not giving a clear idea about carbonation resistance of fly ash based geopolymer mortar. Hence, PH and microstructure analysis were carried out for fly ash based geopolymer mortars to find a better understanding of carbonation resistance after different exposure periods.


(a)


(b)

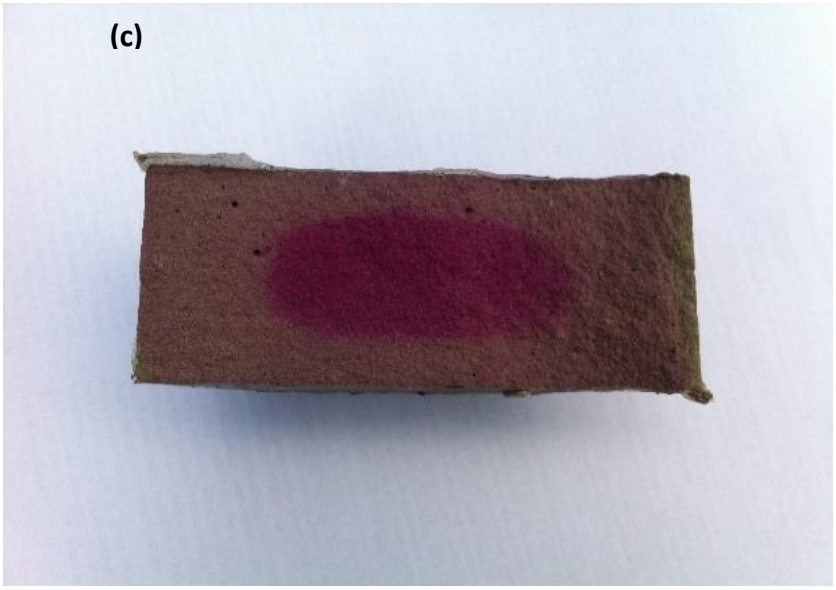

Fig. 5.6 Carbonation depth of fly ash only based geopolymer with (a) control mix (FA-NS/UF0) (b) FA-NS2 and (c) FA-UF10.

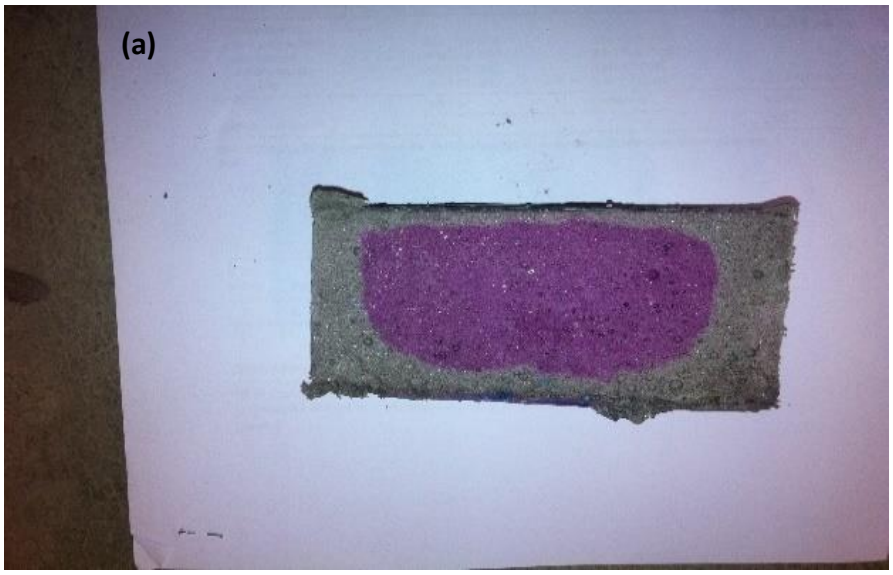

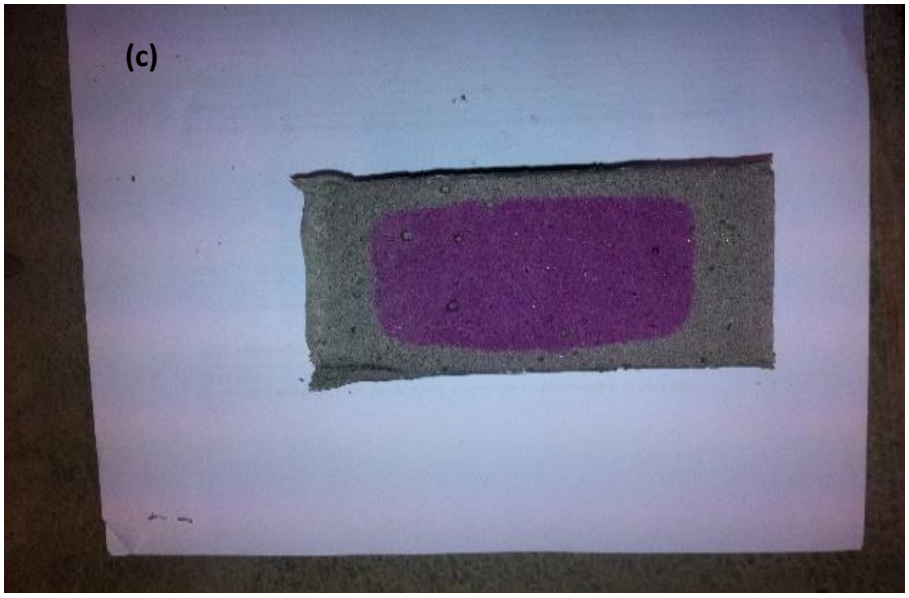

Fig. 5.7 Carbonation depth of OPC blended fly ash based geopolymer with (a) control mix (FA-S-NS/UF0) (b) FA-S-NS2 and (c) FA-S-UF10.


(a)

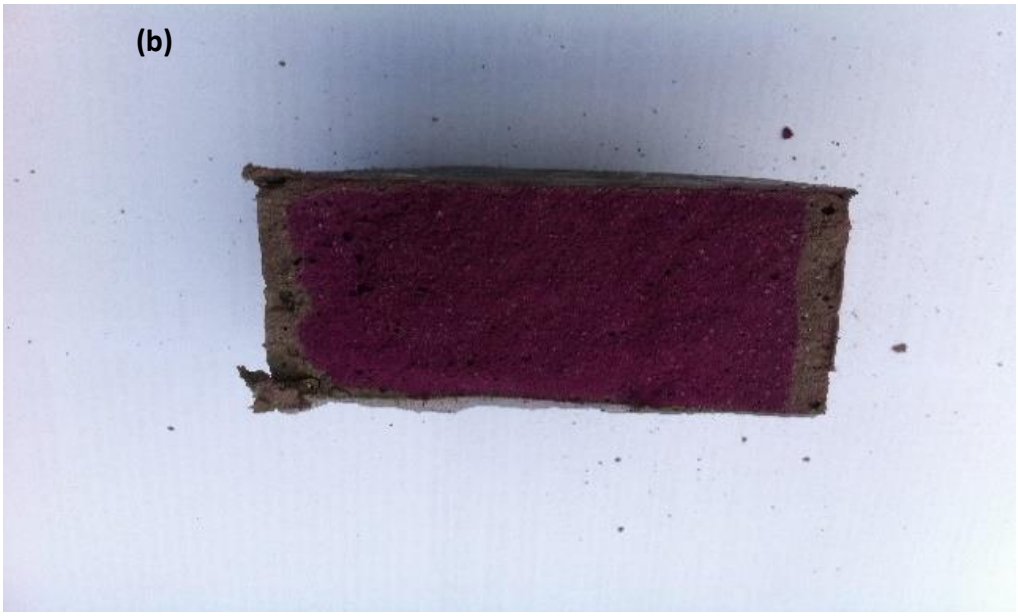
(b)

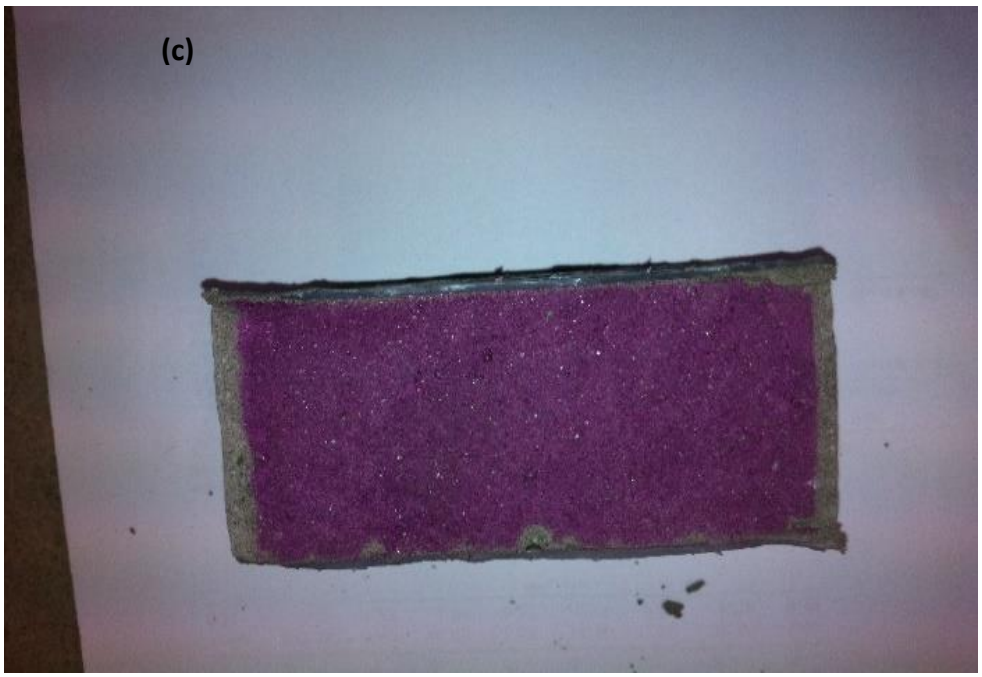

Fig. 5.8 Carbonation depth of OPC blended fly ash based geopolymer with (a) control mix (FA-PC-NS/UF0) (b) FA-PC-NS2 and (c) FA-PC-UF10.

It has been reported by other researchers [15, 16] that the pH values of OPC and alkali activated hardened mortar after the CO_2 exposure can be used as an indicator to assess the severity of carbonation attacks. It is noteworthy that differences in the dissolved carbonate/bicarbonate equilibrium after the carbonation exposure leads to change the pH values of the hydrated phases. For this reason, in this study, pH values for all geopolymer mixes before and after the CO_2 exposure (28d, 56d and 90days) were recorded. The initial pH values for all geopolymer mixes before the CO2 exposure were observed in the range of 11.0 to 12.0 that are in line with the findings of other researchers [15, 17]. However, it is noted from Table 1 that pH values of all geopolymer series were significantly decreased with prolonged CO_2 exposure (90days) and noted in the range of 10.5-11.00. Law et al. [13] also observed the lower pH value in fly ash based geopolymer binder after longer carbonation exposure periods. Silva et al. [17]

found that the pH value of cementitious binder were reduced due to its physical and chemical reaction in cementitious binder with available carbon dioxide in pore structure. It is observed from Table 5.1 that control mixture of fly ash only based geopolymer showed lower value of pH than that of FA-NS2 (2% nanosilica) and FA-UF10 (10% ultrafine fly ash).

Table 5.1 P^H values and carbonation depth of fly ash based geopolymer mortar.

Mix ID	pH value Before carbonation			pH value After carbonation			Carbonation depth (mm)		
Days	28	56	90	28	56	90	28	56	90
FA-NS0	11.70	11.50	11.15	11.00	10.70	10.51	15	20	26
FA-NS2	11.80	11.65	11.35	11.20	10.91	10.75	5	9	15
FA-UF10	11.90	11.75	11.45	11.30	10.99	10.85	6	10	14
FA-PC-NS0	11.90	11.70	11.55	11.10	10.72	10.55	11	22	30
FA-PC-NS2	11.92	11.70	11.45	11.15	10.80	10.65	8	13	19
FA-PC-UF5	11.99	11.80	11.55	11.25	10.90	10.75	7	15	22
FA-S-NS0	11.85	11.55	11.25	11.00	10.75	10.50	16	20	28
FA-S-NS2	11.90	11.68	11.52	11.05	11.68	11.52	7	12	17
FA-S-UF5	11.99	11.78	11.62	11.15	11.78	11.62	8	14	19

Carbonation depth, pH values along with the scanning electron microscope (SEM) was used as a reference for predicting and assessing the carbonation effects of FA-NS2 and FA-UF10 mixes.

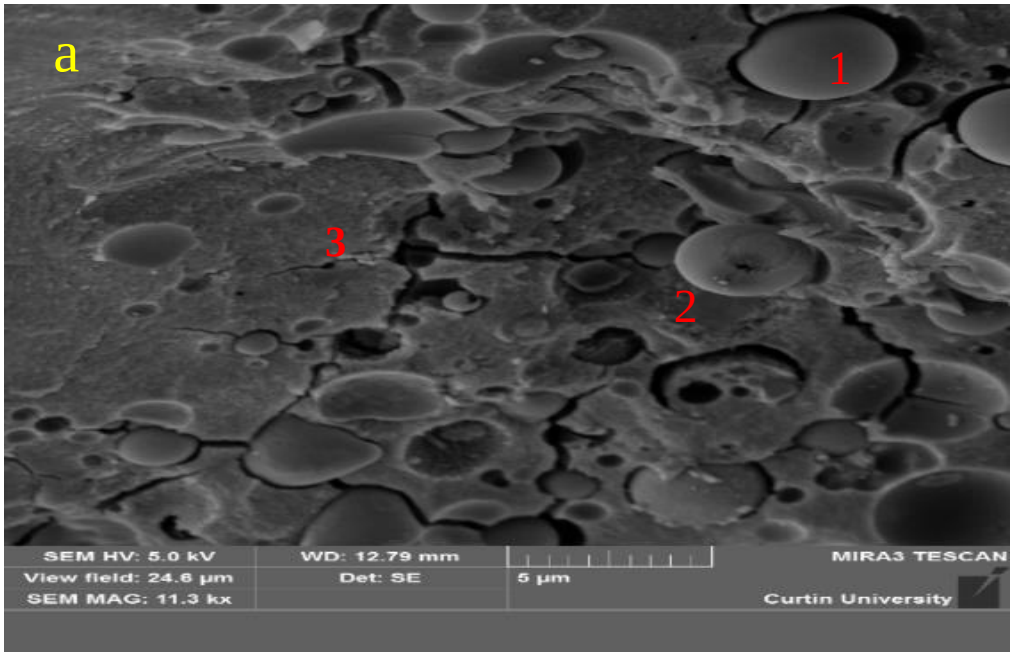

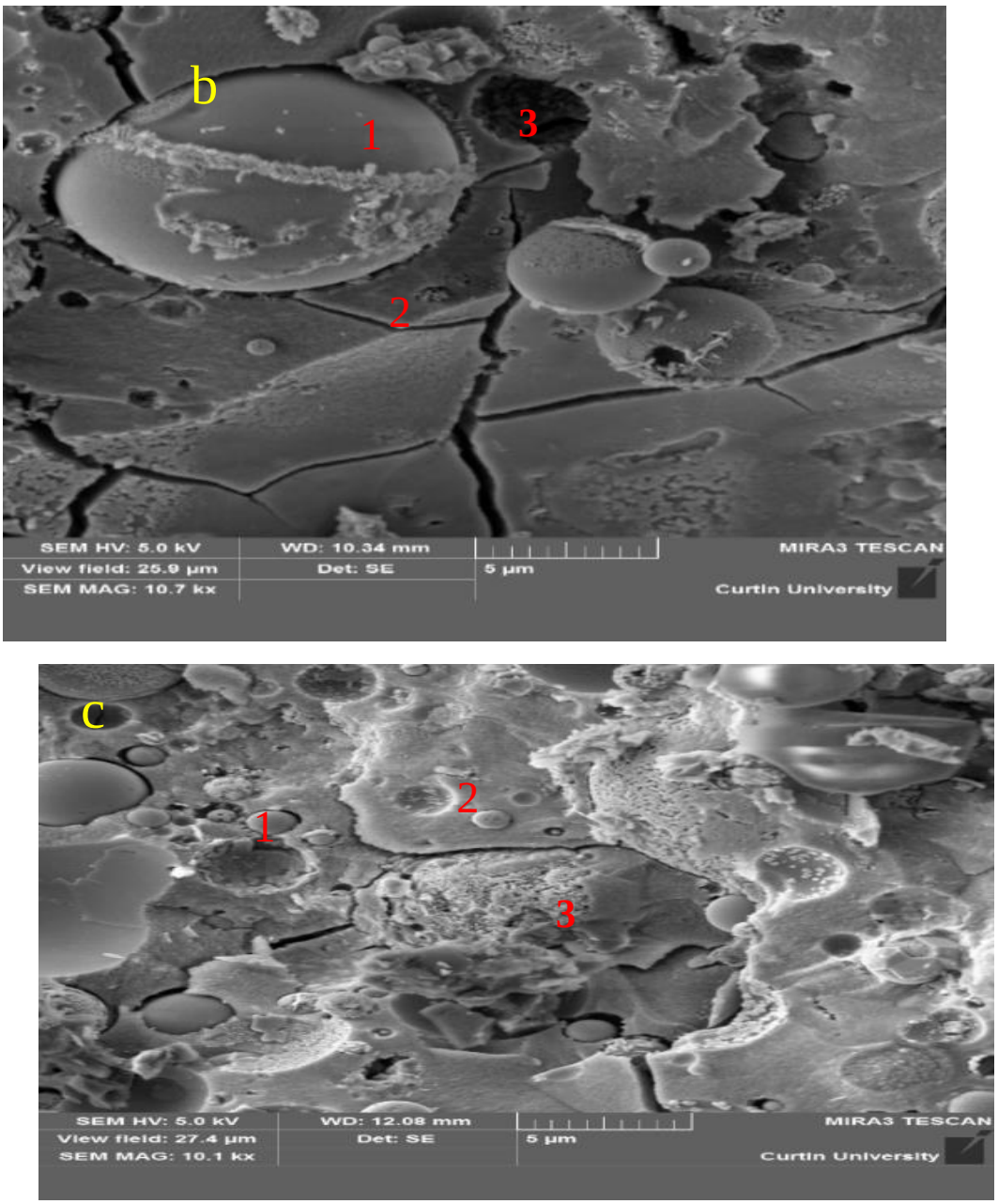

Fig. 5.9 SEM images of fly ash only based geopolymer mortar after 28days CO_2 exposure (a) control mix (FA-NS/UF0) (b) FA-NS2 and (c) FA-UF10.

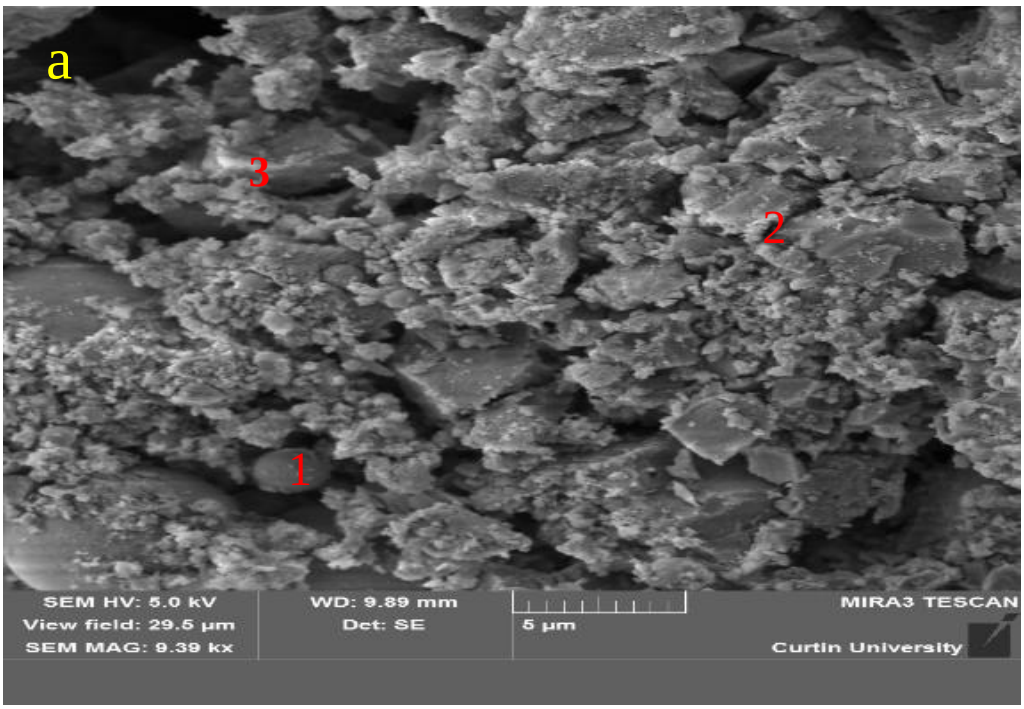
a
3
2
1
SEM HV: 5.0 kV
View field: 29.5 µm
SEM MAG: 9.39 kx
WD: 9.89 mm
Det: SE
5 µm
MIRA3 TESCAN
Curtin University

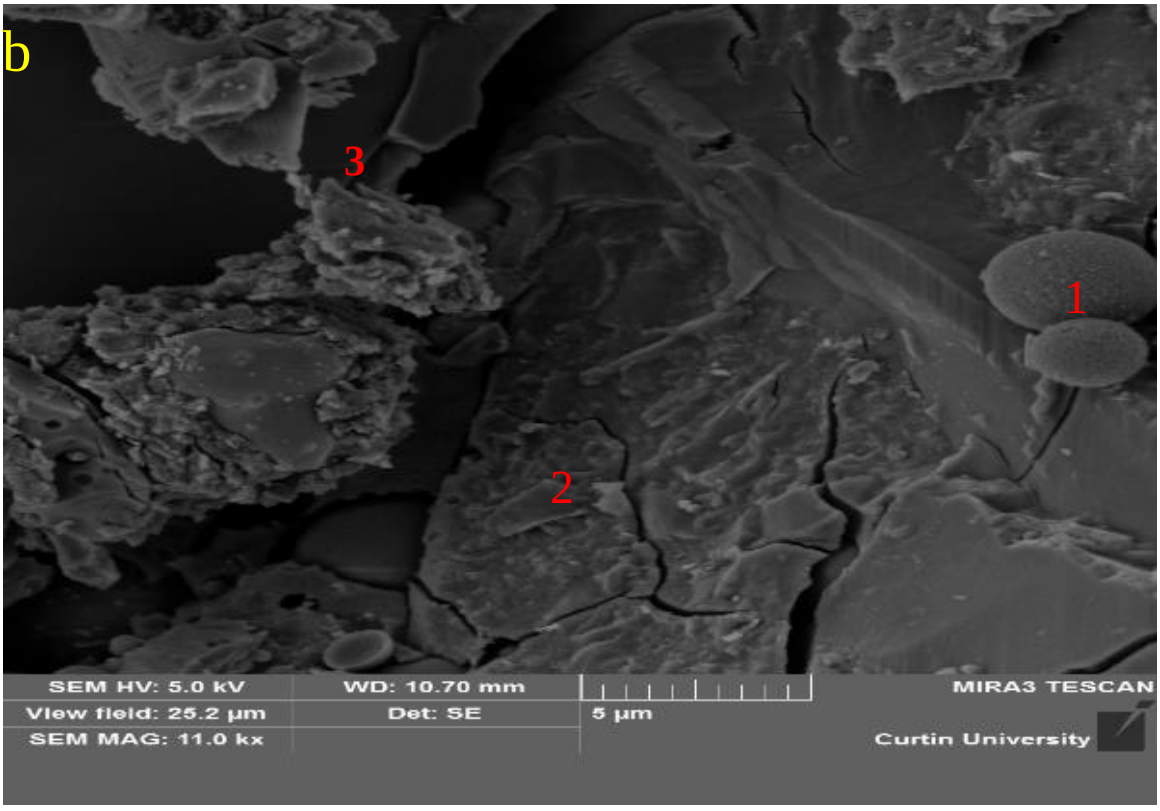
b
3
1
2
SEM HV: 5.0 kV
View field: 25.2 µm
SEM MAG: 11.0 kx
WD: 10.70 mm
Det: SE
5 µm
MIRA3 TESCAN
Curtin University

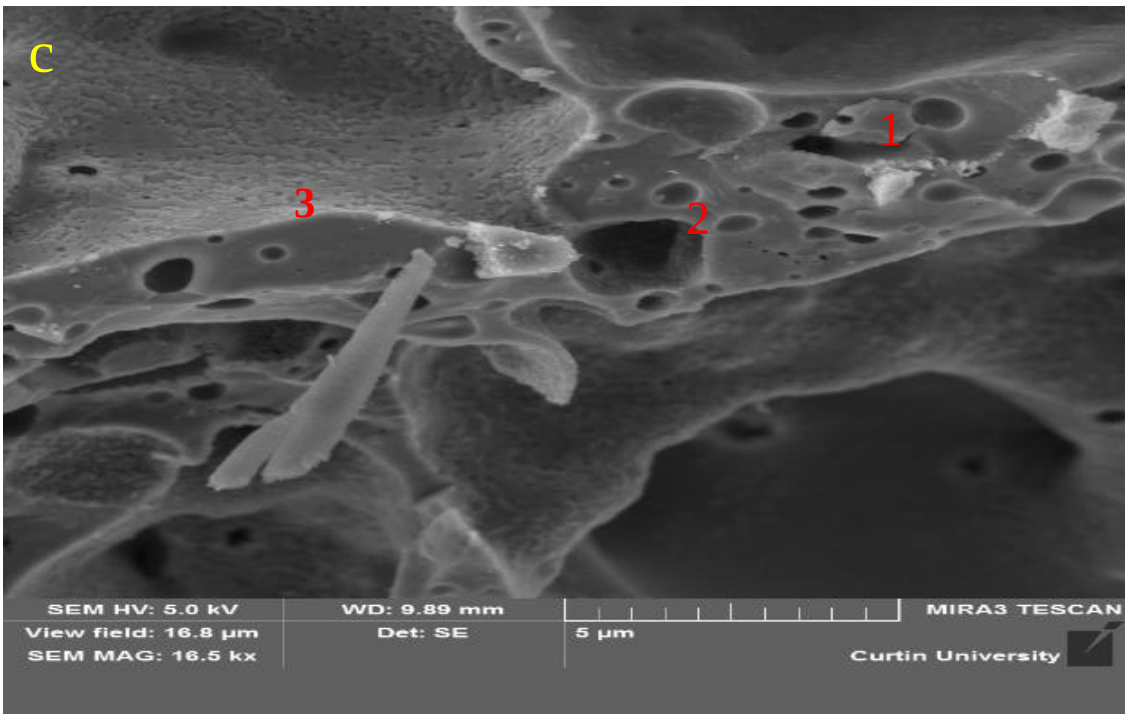

Fig. 5.10 SEM images of fly ash only based geopolymer mortar after 28days CO_2 exposure (a) control mix (FA-S-NS/UF0) (b) FA-S-NS2 and (c) FA-S-UF10.

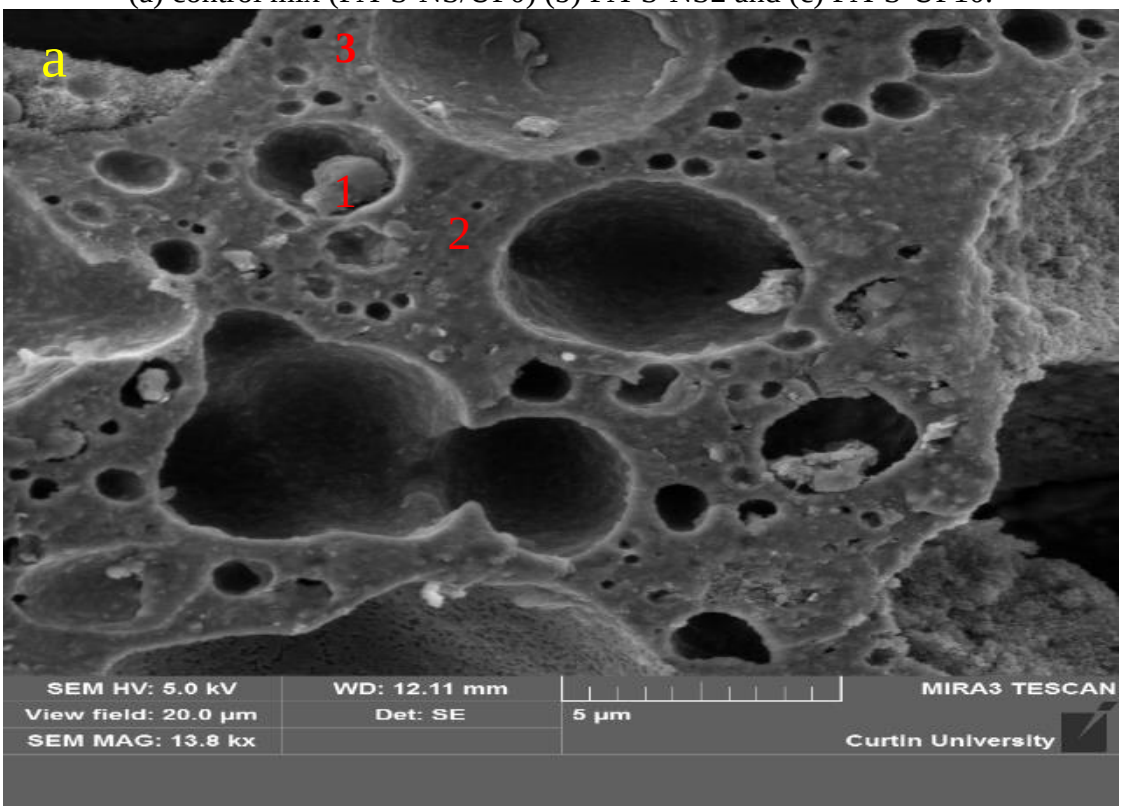

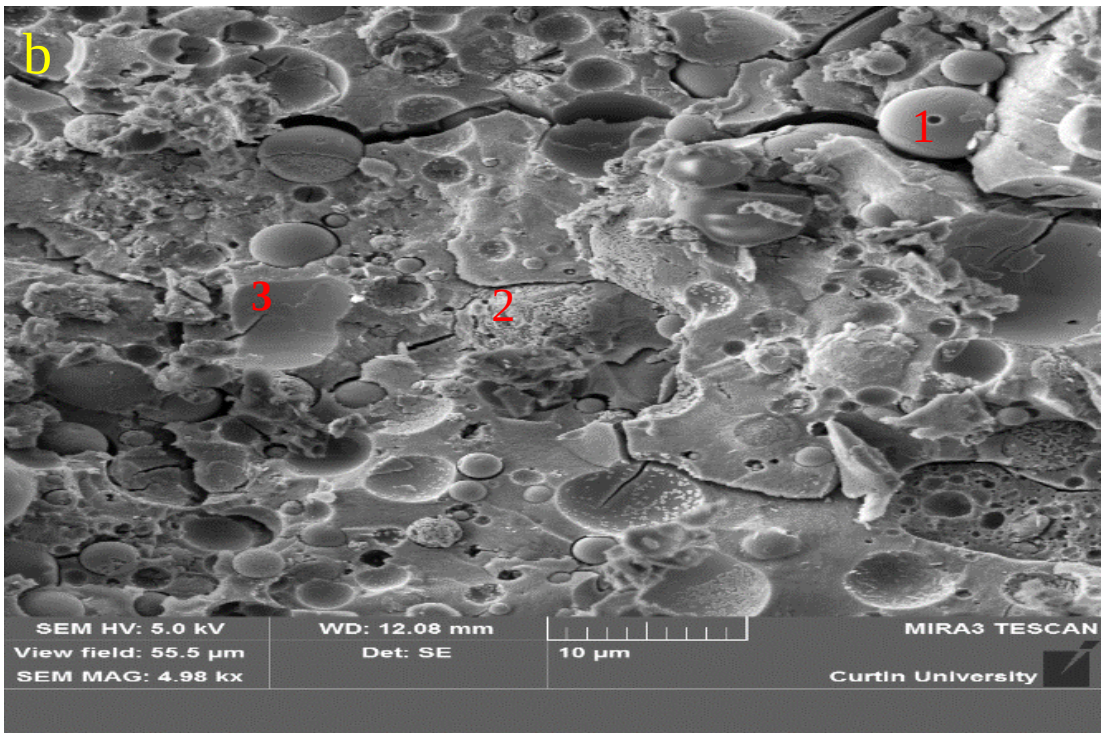

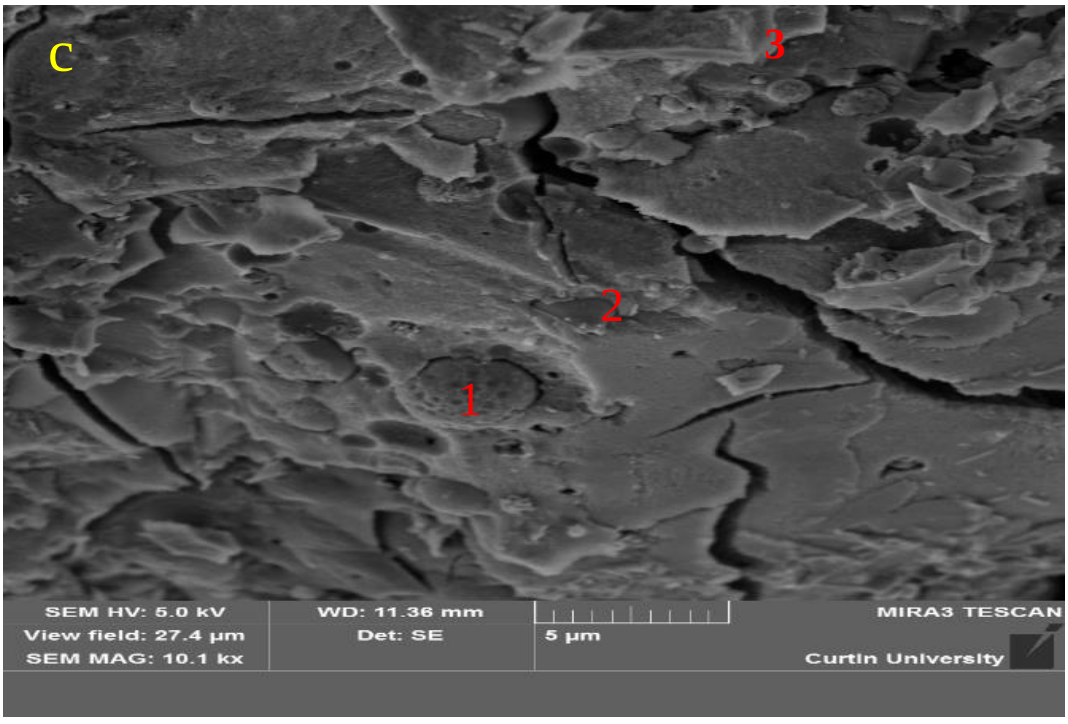

Fig. 5.11 SEM images of fly ash only based geopolymer mortar after 28days CO_2 exposure (a) control mix (FA-PC-NS/UF0) (b) FA-PC-NS2 and (c) FA-PC-UF10.

Figs. 5.9 to 5.11 shows the SEM images of 2% nanosilica and 10% ultrafine fly ash incorporated fly ash only, OPC and GGBFS blended fly ash based geopolymer mortar samples near the exposed surface after 28 days. It is noted from the figures that the light areas are particles of unreacted fly ash (Point 1) and the grey areas pointed with 2 are geopolymer hydrated phase, and the dark areas are pores or disintegrated phase (Point 3). It can be seen that existence of pores or disintegrated phase in geopolymer mixes allows carbonation to proceed in the normal diffusion process. The figure shows the formation of $CaCO_3$ agglomerates in and around the pores (Point c) and the formation of dense carbonate layers on the pore surface also observed. It is noted from Figs. 5.9 (b, c), 5.10 (b, c) and 5.11 (b, c) that the addition of 2% nanosilica and 10% ultrafine fly ash particles in the fly ash based geopolymer series, the voids between the unreacted particles and pores in the hydrated matrix were filled with amorphous hydrated gel along with the finer particles. However, free entries of CO_2 to the available pores in the geopolymer specimens are still possible, apart from the dense hydrated matrix as the CO_2 is a continuation process. As shown in Fig. 5.5, the porosity of the fly ash based geopolymer are reduced with 2% nanosilica, 5% and 10% ultrafine fly ash and the pore structure are modified showing smaller pores and better resistance in CO_2 exposures. It is also noted from the figure that no extremely deteriorated condition were observed in any of the geopolymer mixes even after 90 days of CO_2 exposure.

5.5.2 Acid resistance of fly ash based geopolymer

5.5.2.1 Change in mass

The geopolymer mortar specimens were immersed in 3% sulfuric acid solution for 90 days and the changes in mass were determined on a weekly basis. The change in mass of a specimen was calculated by comparing mass measured after exposure to acid solution to the initial mass

before the exposure. The specimens were visually inspected for any deterioration by the exposure to acid solution. Photographs of the specimens without and with 2% nanosilica and 10% ultrafine fly ash after 90 days immersion in the acid solution are shown in Fig.5.12. Photographs of the specimens before acid exposure are also shown in this figure for comparison. Generally, some minor erosion could be observed in all the specimens by the acid attack.

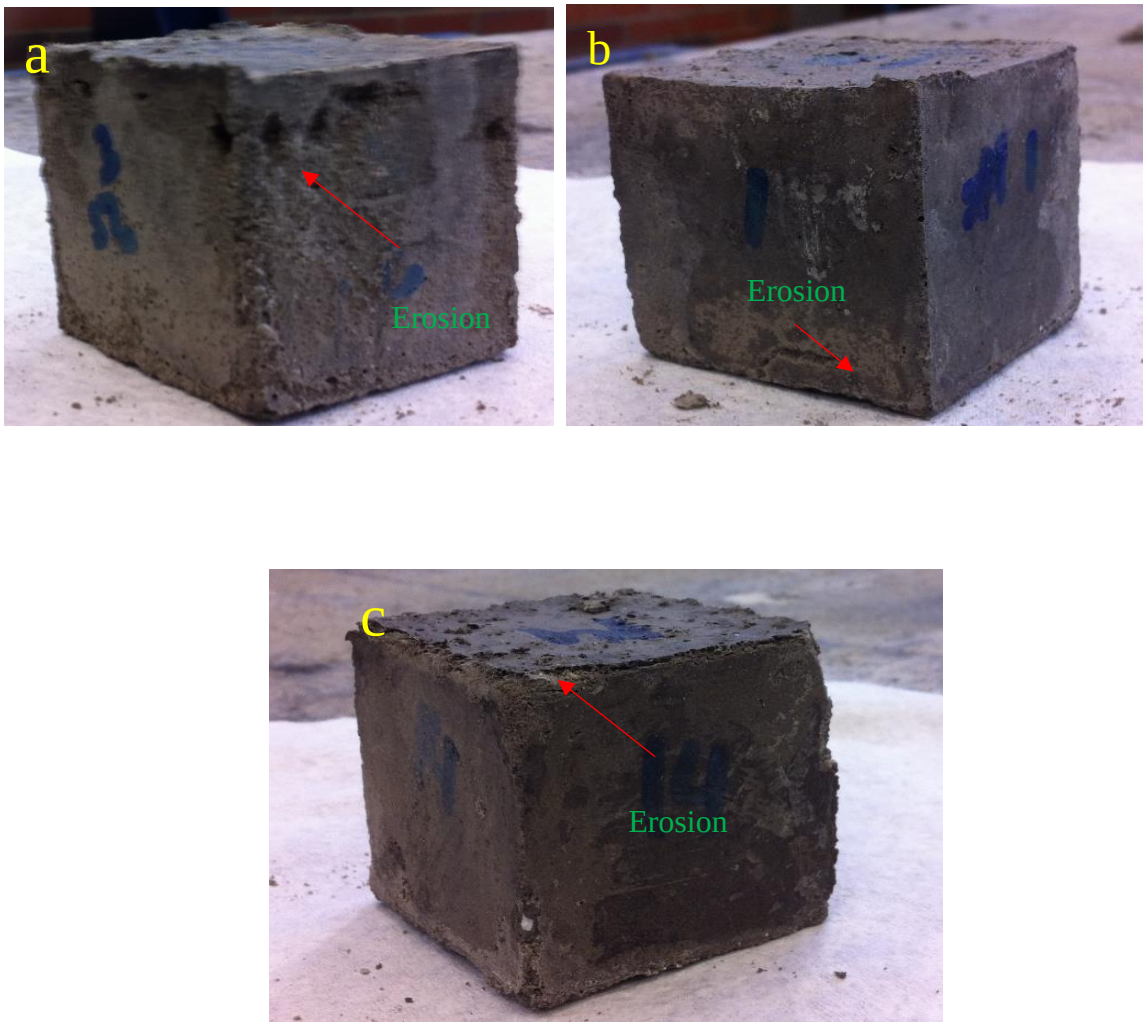

Fig. 5.12 Visual appearance of geopolymer specimens after 90 days of acid submerged (a): FA-S-NS0/UF0, (b) FA-NS2 and (c) FA-UF10.

The visual inspection led to the conclusion that there were different intensities of deterioration in the OPC and GGBFS blended fly ash based geopolymer mortar specimens. There were relatively more damages, especially at the corners of specimens without nanosilica and those containing OPC and GGBFS Figs 5.13 and 5.14. However, the specimens with optimum nanosilica and ultrafine fly ash were seen to remain structurally intact. The surface became a little softer as the duration of the test progressed but could not be easily scratched with finger nails. The deterioration of the surface was seen to increase with time though the extent of deterioration among the samples could not be easily differentiated through visual inspection.

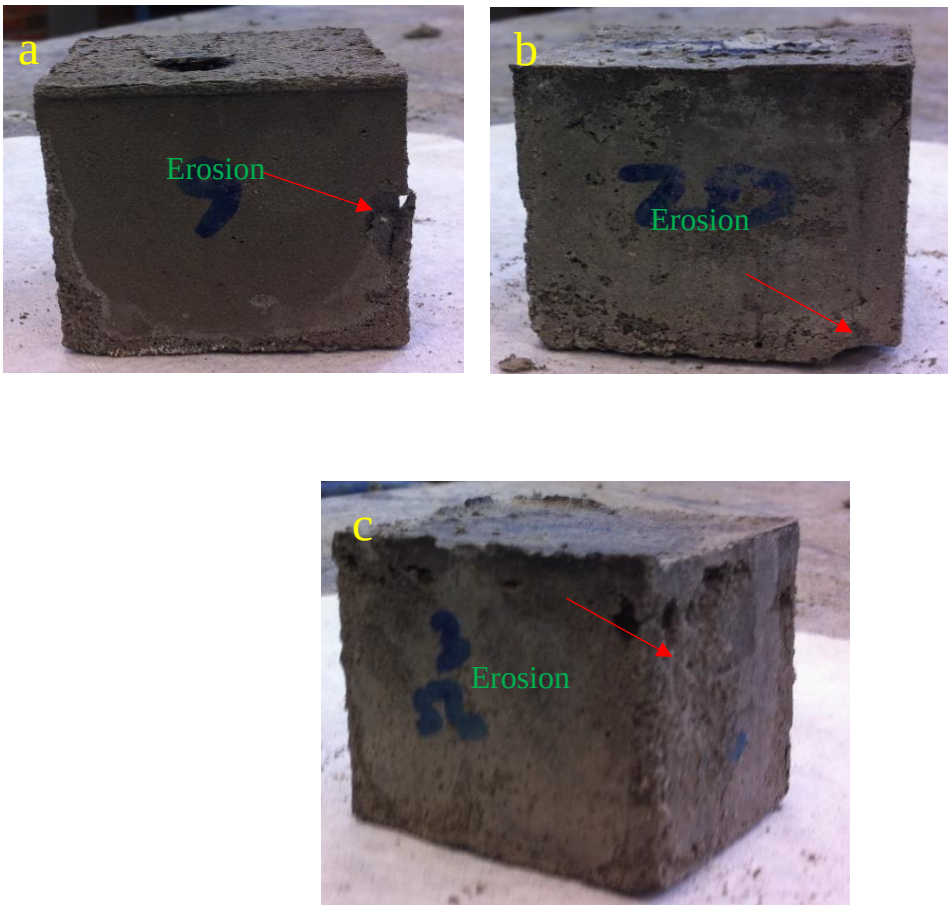

Fig. 5.13 Visual appearance of geopolymer specimens after 90 days of acid submerged (a): FA-S-NS0/UF0, (b) FA-S-NS2.0 and (c) FA-S-UF10.

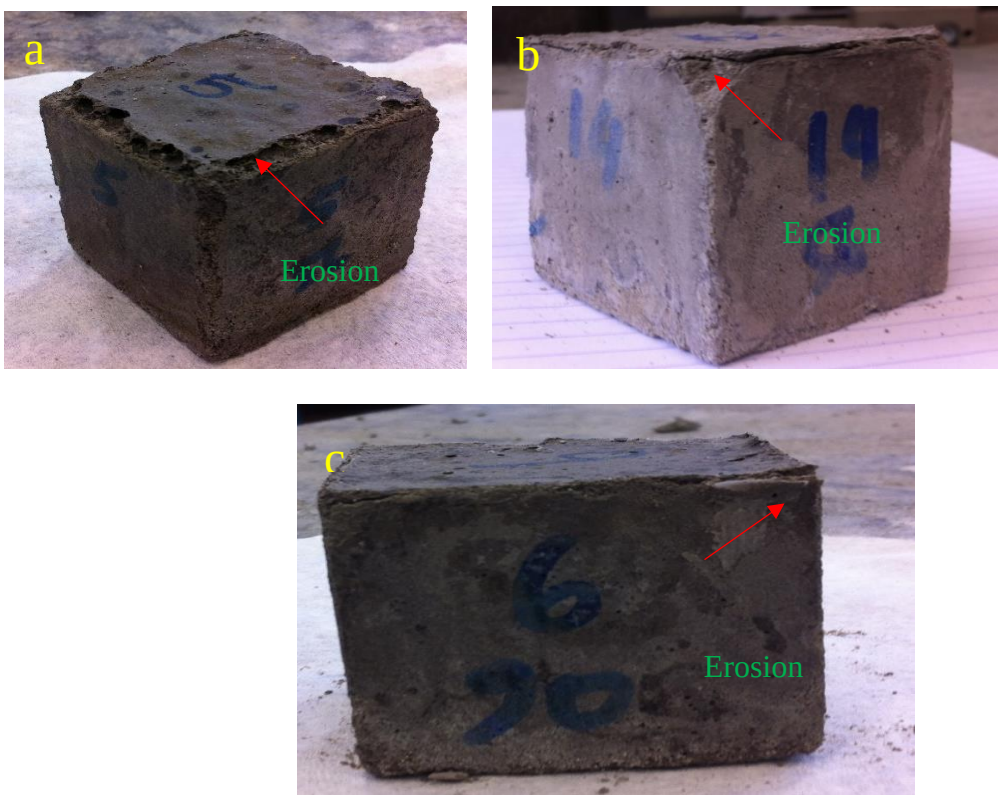

Fig. 5.14 Visual appearance of geopolymer specimens after 90 days of acid submerged (a): FA-PC-NS0/UF0, (b) FA-PC-NS2 and (c) FA-PC-UF10.

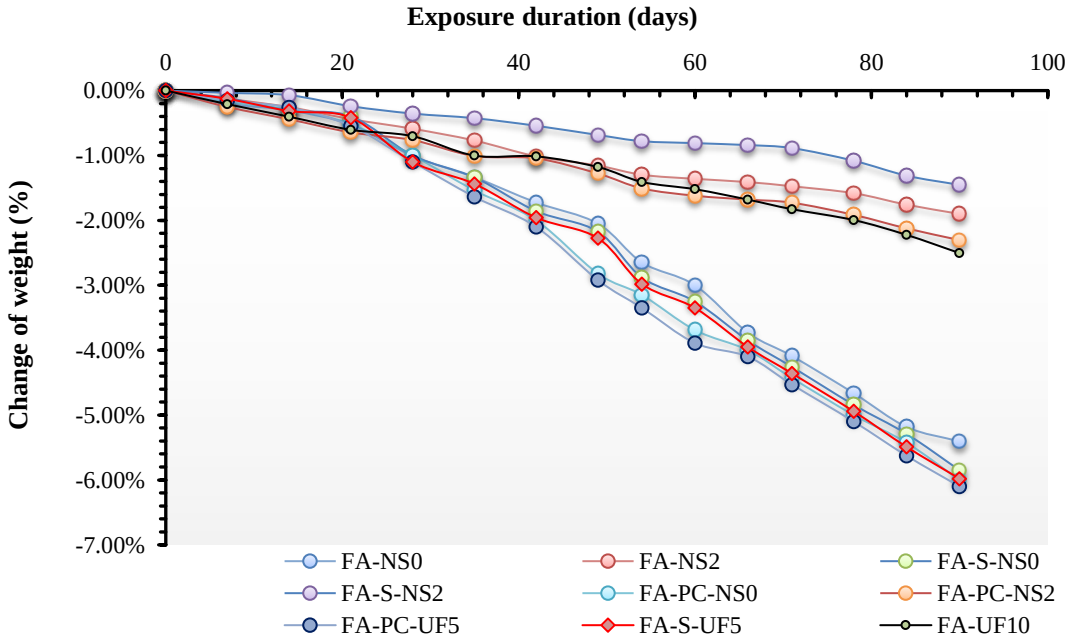

Fig 5.15 Change in mass of mortar specimens after immersion in 3% sulfuric acid solution.

Changes in mass for specimens of all the geopolymer mortars are presented in Fig 5.15. The results show that mass of the geopolymer specimens gradually decreased with the increase of acid exposure time. It can be seen that the mass loss after 90 days of acid exposure for fly ash only geopolymer mortar without nanosilica was 5.41% as compared to 1.9% for the mix with 2% nanosilica and 2.5% with 10% ultrafine fly ash. After the same exposureperiod, mass loss of the OPC blended fly ash geopolymer mortar without nanosilica (FA-PC-NS0) and with 2% nanosilica (FA-PC-NS2.0) were 6.0% and 2.3%, respectively. Similarly, the 90-day mass losses for the GGBFS blended fly ash geopolymer mortars were 5.8 % without nanosilica (FA-S-NS0) and 1.5% with 2% nanosilica (FA-S-NS2.0). Overall, the mass loss varied from 1.9% to 6.00% for all the geopolymer mortars. These mass losses of the nanosilica / ultrafine fly ash incorporated geopolymer mortars are very small as compared to the mass losses usually shown by OPC based cementations materials [21, 23]. Previous studies [23, 24] on OPC based binders showed that sulfuric acid has a highly deleterious effect on mass loss. This is because sulfuric acid causes decomposition of the Ca(OH)2 and forms gypsum that deteriorates the matrix by scaling and softening. Though the penetration of sulfuric acid can be reduced, the formation of gypsum in the regions close to surface causes progressive disintegration of the matrix [24]. Therefore, the mass losses observed in the geopolymer specimens without finer particles were much smaller than that can be expected in OPC based binders under the same exposure condition. However, inclusion of optimum nanosilica and ultrafine fly ash has further reduced the mass loss of geopolymer specimens.

5.5.2.2 Change in compressive strength

The 28-day compressive strength of each geopolymer mix before exposure to acid solution is used as a benchmark to calculate the strength loss after each exposure period of 28, 56 and 90 days. The compressive strengths of the mortar specimens from 9 mixes are presented in Fig. 5.13. It can be seen from the figure that loss of strength occurred in all the geopolymer mixes and it increased with the increase of exposure period. It is noteworthy from Fig. 5.13 that fly ash only, OPC and GGBFS blended fly ash geopolymer specimens without nanosilica/ultrafine fly ash exhibited higher strength loss as compared to those with nanosilica/ ultrafine fly ash.

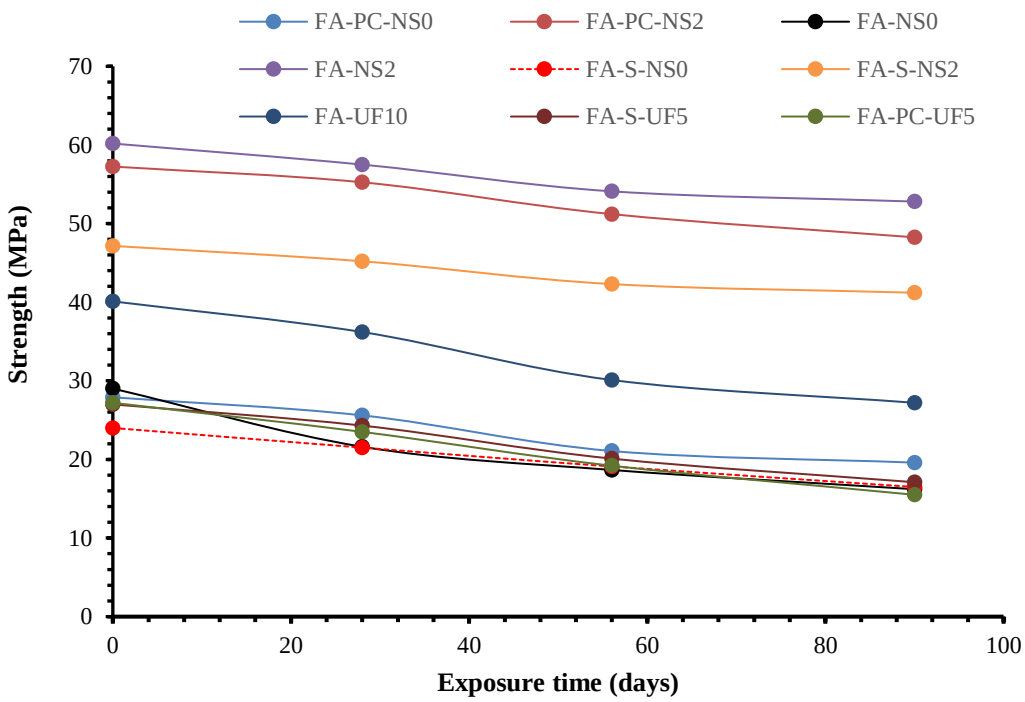

Fig. 5.13 Change in compressive strength of geopolymer mortars in sulfuric acid exposure.

The strength loss in the specimens without nanosilica ranged from 30% to 41% while that in the specimens with nanosilica ranged from 9% to 11% and 20% to 30% with ultrafine fly ash. For example, the strength value of mix FA-NS2 (2% nanosilica) after 90 days of

sulfuric acid exposure was 54.0 MPa, as compared to 60.0 MPa prior to acid exposure and 40.1 MPa down to 32.0 MPa for FA-UF10 mix. Whereas, the compressive strength of mix FA-NS0 (0% nanosilica) reduced from 29.0 MPa to 19.1 MPa after 90 days of immersion in sulfuric acid. Bakharev [18] showed that depolymerisation of the aluminosilicate polymers in acidic media resulted in a significant strength loss of alkali activated binders. Chindaprasirt [19] noted that the oxy-aluminium bridge (–Al–Si–O) of geopolymeric gel probably gets destroyed in acidic environment and leads to strength reduction of alkali activated binders.

Reduction of permeability helps reduce the ingress of acid in to geopolymer matrix and thus improves the resistance to acid attack [20]. It is apparent from Fig. 5.13 that incorporation of 2% nanosilica and 10% ultrafine fly ash in fly ash based geopolymer can effectively reduce the rate of acid attack expressed in terms of strength loss. Belkowitz et al. [21] noted that the pore refinement process by finer particles usually prevents the passage of aggressive elements into the deeper layers of hydrated gel structure. It means that the optimum amount of nanosilica and ultrafine fly ash present in the geopolymer mixes produces a denser structure that reduces the degradation by an acid. The results of the present study are also supported by the findings of Fattuhi and Hughes [22], and Israel et al. [23] that the lower porosity improved the acid resistance of hydrated gel.

As shown in Fig.5.16, the strength loss in OPC blended fly ash geopolymer mortar without nanosilica was higher than those with 2% nanosilica (FA-PC-NS2.0) and 5% ultrafine fly ash (FA-PC-UF5.0). Strength loss of the OPC blended geopolymer mortar reduced from 11.5 MPa (FA-PC-NS0) to 6.5 MPa (FA-PC-NS2.0) by 2% nanosilica and from 27.2 MPa to 19.5 MPa by 5% ultrafine fly ash. This highlights the poor resistance of mix FA-PC-NS0

(without nanosilica) against a highly corroding and aggressive environment as compared to mixes FA-PC-NS2.0 and FA-PCUF5.

Incorporation of 2% nanosilica and 5% ultrafine fly ash produced a denser and less permeable pore structure prolonging the negative effects of acid attack. This observation correlates well with the findings of Hartman and Fogler [24] that showed that an increased amount of soluble silica produced a denser layer and helped to reduce the extent of damagein the aluminosilicate structure with removal of each of the aluminium atoms under acid attack.

Similarly, In the GGBFS blended mortar series, the strength loss after 90 days of immersion reduced from 7.5 MPa (FA-S-NS0) to 4.0 MPa (FA-S-NS2.0) by 2% nanosilica and from 27.1 MPa to 20.2 MPa with 5% ultrafine fly ash (Fig.5.13). The results of this study show that inclusion of 2% nanosilica and 5% ultrafine fly ash made a significant improvement in the strength loss in all the three geopolymer mortar series.

5.5.2.3 Change in microstructure after sulfuric acid exposure

The SEM images of the fly ash only, OPC and GGBS blended fly ash based geopolymer mortars with and without nanosilica after 90 days exposure to sulfuric acid are presented in Fig. 5.17(a) to (i). Images of the specimens before acid exposure are also shown in the figure.

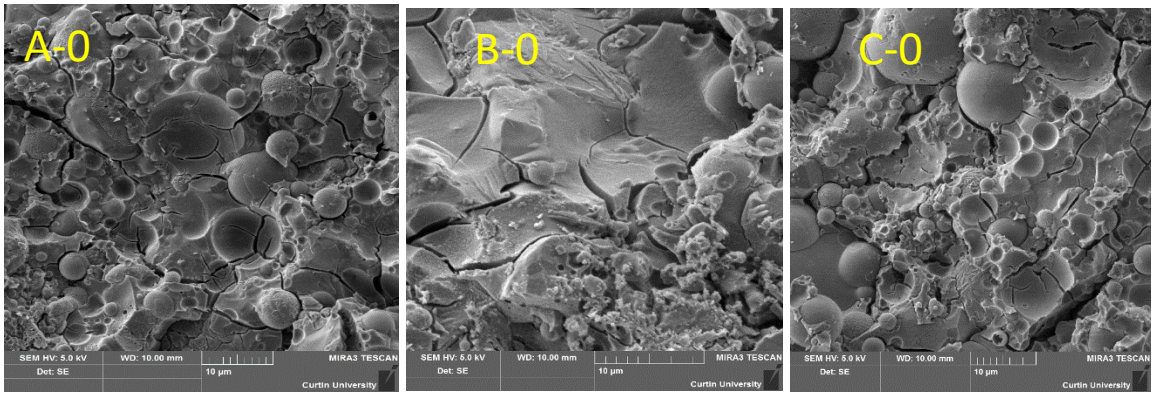

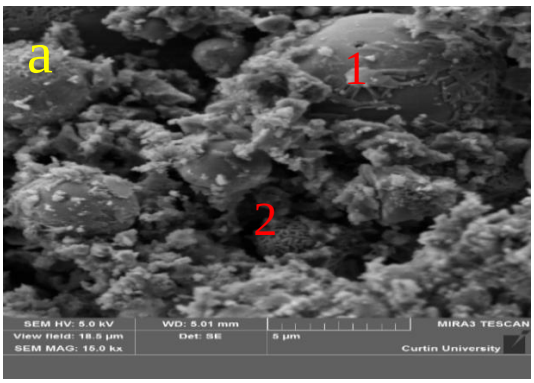
a
1
2
SEM HV: 5.0 kV
View field: 18.5 µm
SEM MAG: 16.0 kx
WD: 5.01 mm
Det: SE
5 µm
MIRA3 TESCAN
Curtin University

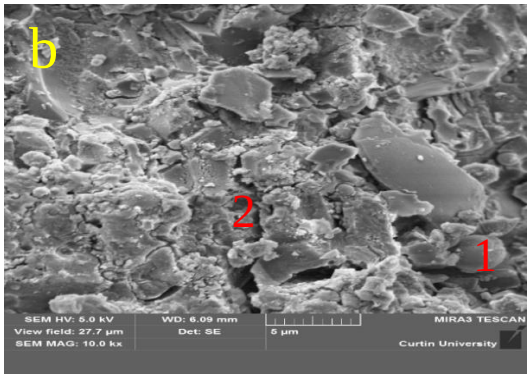
b
2
1
SEM HV: 5.0 kV
View field: 27.7 µm
SEM MAG: 10.0 kx
WD: 6.09 mm
Det: SE
5 µm
MIRA3 TESCAN
Curtin University

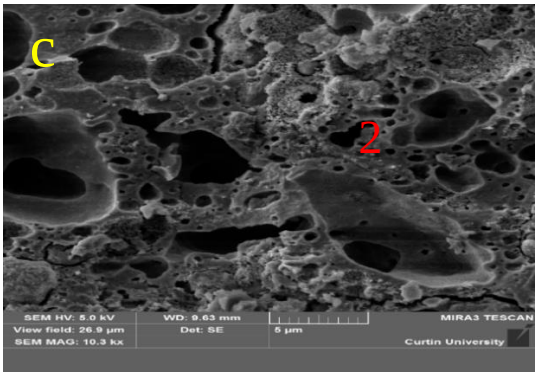
c
2
SEM HV: 5.0 kV
View field: 26.9 µm
SEM MAG: 10.3 kx
WD: 9.63 mm
Det: SE
5 µm
MIRA3 TESCAN
Curtin University

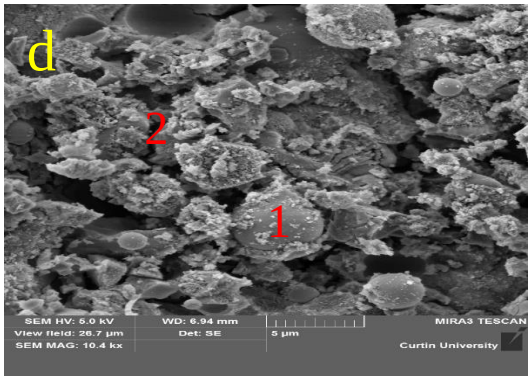
d
2
1
SEM HV: 5.0 kV
View field: 26.7 µm
SEM MAG: 10.4 kx
WD: 6.94 mm
Det: SE
5 µm
MIRA3 TESCAN
Curtin University

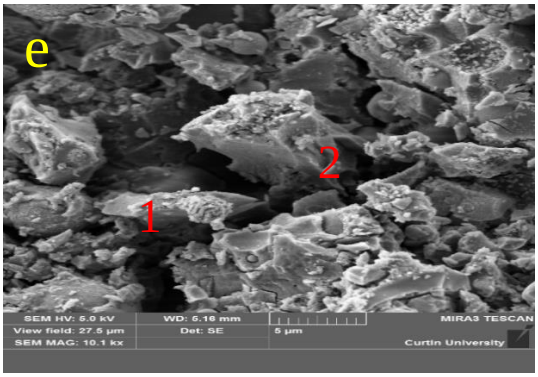
e
2
1
SEM HV: 5.0 kV
View field: 27.5 µm
SEM MAG: 10.1 kx
WD: 5.16 mm
Det: SE
5 µm
MIRA3 TESCAN
Curtin University

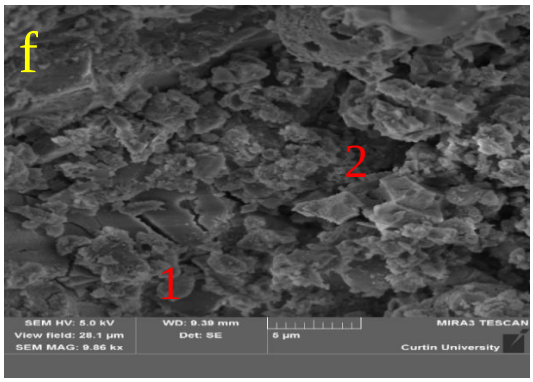
f
2
1
SEM HV: 5.0 kV
View field: 28.1 µm
SEM MAG: 9.86 kx
WD: 9.39 mm
Det: SE
5 µm
MIRA3 TESCAN
Curtin University

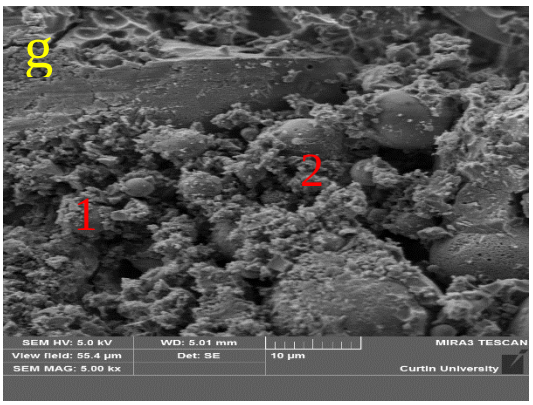
g
2
1
SEM HV: 5.0 kV
View field: 55.4 µm
SEM MAG: 5.00 kx
WD: 5.01 mm
Det: SE
10 µm
MIRA3 TESCAN
Curtin University

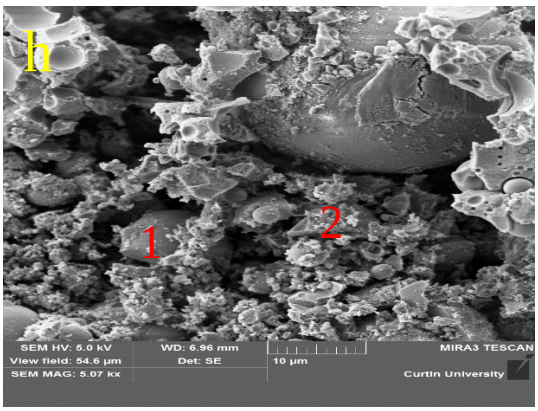
h
1
2
SEM HV: 5.0 kV
View field: 54.6 µm
SEM MAG: 5.07 kx
WD: 6.96 mm
Det: SE
10 µm
MIRA3 TESCAN
Curtin University

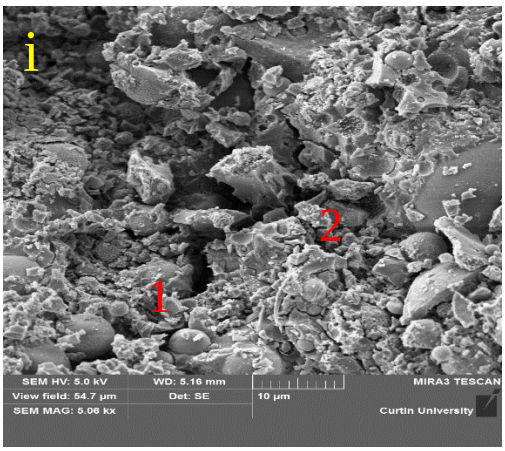

Fig. 5.17 SEM images of geopolymer mortars before acid submerged (A-0: FA-NS2, B-0: FA-PC-NS2, C-0: FA-S-NS2) and after 90 days acid exposure (a) FA-NS0, (b) FA-NS2, (c) FA-PC-NS0, (d) FA-PC-NS2, (e) FA-S-NS0 ,(f) FA-S-NS2 (g) FA-UF10, (h)FA-S-UF5and (i) FA-PC-UF5

Significant differences in microstructure were observed in all the specimens after 90 days of sulfuric acid exposure. It can be seen that the relatively compact microstructure of geopolymers before the acid exposure became more porous after the exposure to sulphuric acid. However, geopolymer mortar with nanosilica showed less deterioration than the fly ash geopolymer mortar without nanosilica. It is noted from Fig 5.17(a) that fly ash only geopolymer mortar without nanosilica (FA-NS0) immersed in sulfuric acid for 90 days exhibited porous and disintegrated gel clusters (point 2) around the unreacted particles (point 1). Similar observations can also be noted in the microstructures of the OPC and GGBFS blended fly ash geopolymer mortars. More compact and less porous structures can be observed in the mixes with nanosilica when comparisons are made between the microstructure of Fig. 5.17(d) to that in Fig. 5.17(c) and the microstructure of Fig. 5.17(e) to that in Fig. 5.17(f). Bakharev [18] pointed out that disintegration of microstructure along with significant loss of strength in geopolymer materials is due to low inter crystalline bond strength.

In a similar study, Ismail et al. [25] also noted that the presence of H^+ could destroy the alumino-silicate network of geopolymer materials and eventually lead to disintegration of the polymer gel. The findings of Lloyd et al. [20] concluded that H_3O^+ and HSO_4^- ions from the sulfuric acid could diffuse into the gel phase, where H_3O^+ attacks the gel and severely damage the gel network. However, Fig 5.17(b) indicates that inclusion of 2% nanosilica in the fly ash only geopolymer reduced acid aggravation due to its additional reaction products. The mechanisms involved in the process are related to mechanical percolation along with pore filling effects of nanosilica. It appears that the aluminosilicate gel of the mix with 2% nanosilica (FA-NS2, Fig. 5.17(b)) was more compact than that of the control mix (FA-NS0, Fig. 5.17(a)). Similar differences are also observed in the mixes of the other two series. This observation on the differences in microstructures is consistent with the less strength loss of the mixes with 2% nanosilica and 5% ultrafine fly ash, as shown in Fig. 5.13. It suggests that the introduction of optimum finer materials reduced the porosity and increased the acid resistance in terms of strength loss and disintegration of the microstructure. The dense microstructure formed by nanosilica/ ultrafine fly ash provides resistance to the penetration of acidic ions reducing the extent of disintegration in the microstructure and eventual less strength loss.

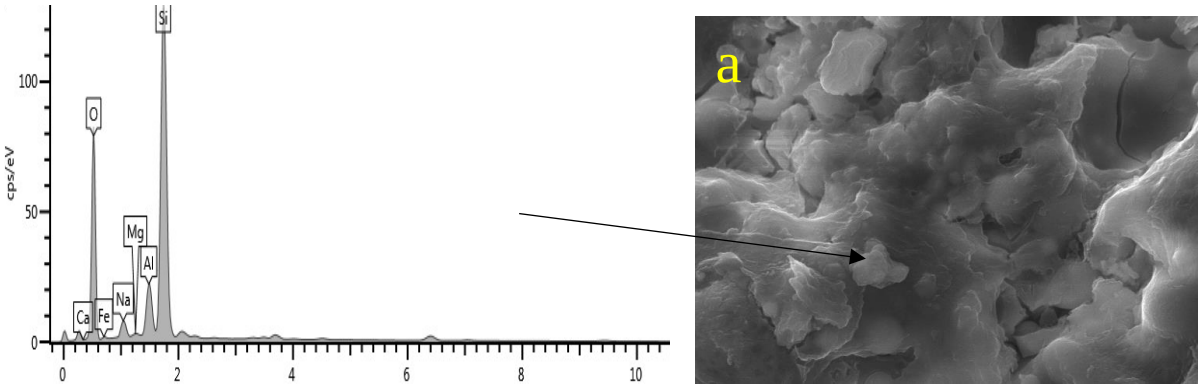

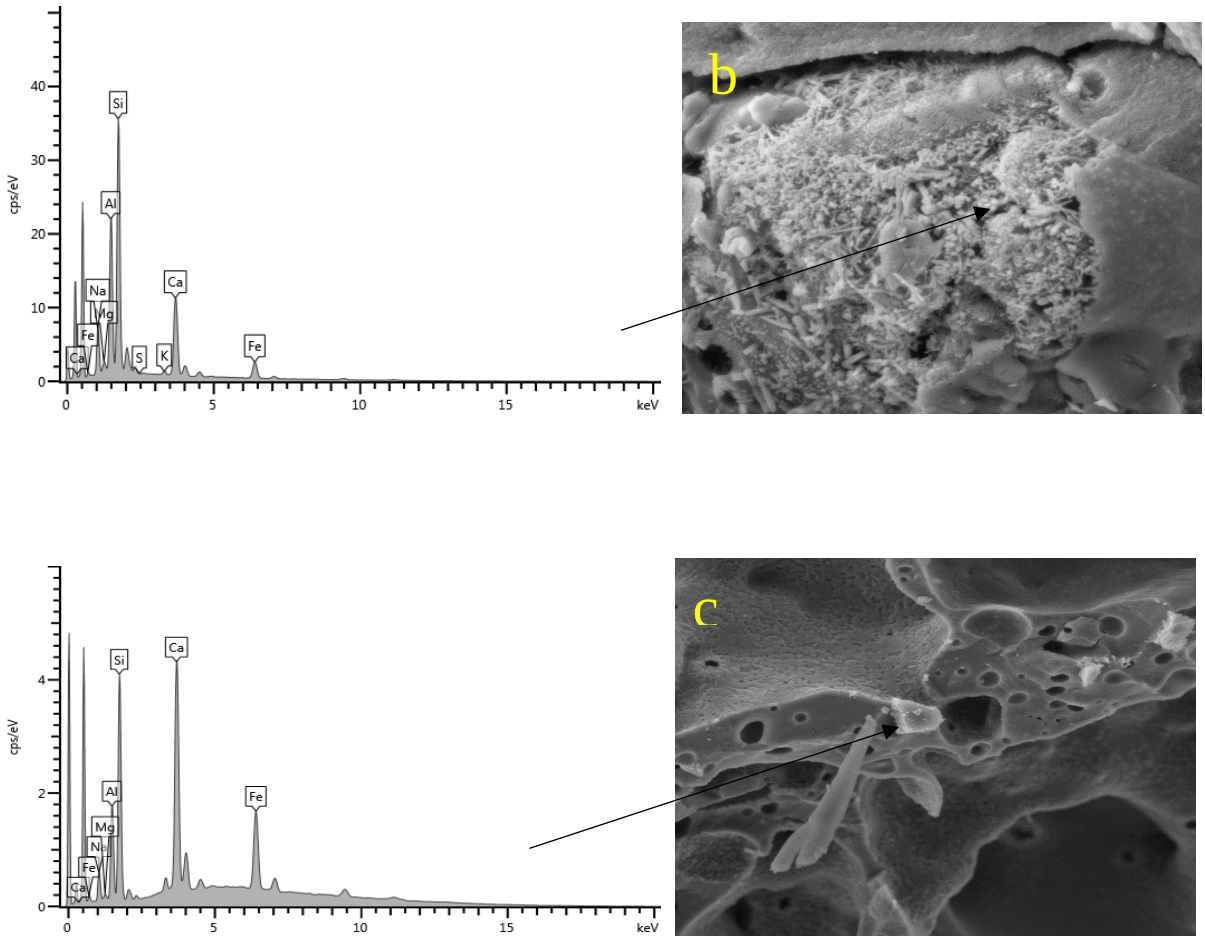

Fig. 5.18 EDX spectra of geopolymers mortar without nanosilica under acid exposure (a) Fly-ash only, (b) OPC blended fly-ash and (c) GGBFS blended fly-ash

The energy dispersive X-ray patterns for fly ash only, OPC and GGBFS blended fly ash based geopolymers without nanosilica are shown in Figs. 5.18(a) to 5.18(c). Notable traces of silicon, sodium, aluminium and calcium elements were observed in the EDX patterns of the OPC and GGBFS blended fly ash geopolymers. Presence of the first three elements is from the sodium aluminosilicate gel, whereas the calcium is from gypsum formed in OPC and GGFBS blended geopolymers. Strong peaks of calcium were observed in the OPC and GGBFS blended geopolymers without nanosilica (Figs. 5.18(b) and 5.18(c)).

These phenomena agreed well with the studies reported by other researchers [14, 20] that the exchanged calcium ions diffusing toward the acid solution react with the counter-diffusing sulfate anions resulting in the formation and deposition of gypsum crystals inside the corroding layer. The XRD patterns (Figs. 5.19(b) and 5.19(c)) also suggest a possible alteration and restructuring of the polymer network in the OPC and GGBFS blended geopolymers without nanosilica.

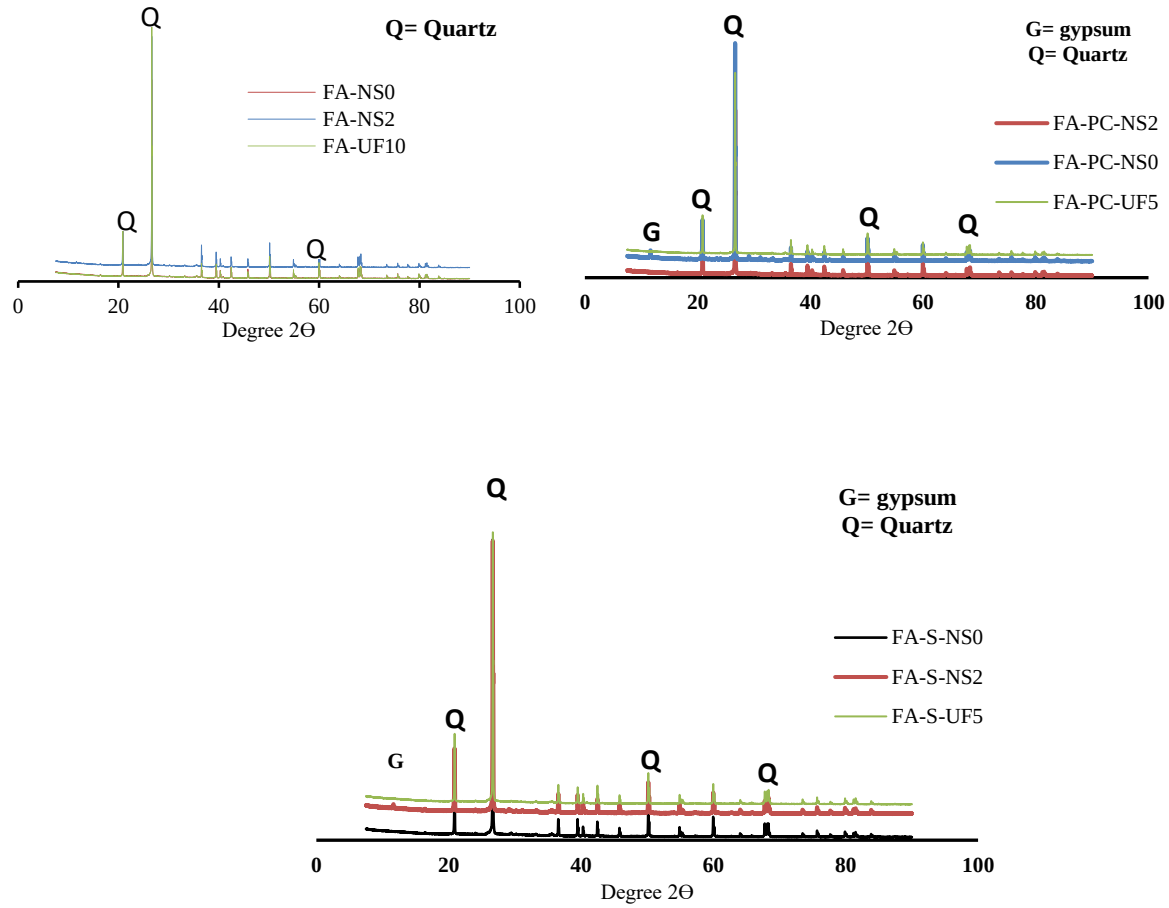

Fig. 5.19 X-ray diffraction patterns of geopolymers mortar under sulfuric acid exposure: (A) fly ash only with 0%, 2% nanosilica and 10% ultrafine fly ash. (B) OPC blended fly ash with 0%, 2% nanosilica and 5% ultrafine fly ash (C) GGBFS blended fly ash with 0%, 2% nanosilica and 5% ultrafine fly ash.

The XRD spectra of the samples after 90 days exposure to acid solution are shown in Figs. 5.19(a) to 5.19(c). It is confirmed from the XRD spectrum that the formation of gypsum takes place in both OPC and GGBFS blended fly ash geopolymers without nanosilica. The traces of gypsum are likely due to the reaction between available depleted calcium from the OPC and GGBFS with sulphur ions from the sulfuric acid. However, it is noted from Figs. 5.19(b) and 5.19(c) that the traces of gypsum entirely disappeared for both OPC and GGBFS blended geopolymers with 2% nanosilica. It seems Ca^{2+} that was released from the dissolution of OPC and GGBFS interacted with silicate ions and formed calcium silicate oligomers. However, no peaks of gypsum traces were observed for fly ash only geopolymers with and without nanosilica. Bakharev [18] and Lloyd et al. [20] noted that the acid resistance kinetics of polymer modified mortars depends on its material composition. In the current study [26] formation of aluminosilicate and CSH gel as final hydrated products were observed in GGBFS and OPC blended fly ash geopolymers. The presence of calcium silicate hydrate (CSH) in mixes FA-PC-NS0 and FA-S-NS0 might have reacted with H_2SO_4 and disintegrated in the form of calcium sulfate or as an amorphous silica gel at the end [39, 40]. Puertas et al. [14] and Wallah and Rangan [26] also concluded that the higher calcium content in the alkali activated binder generates greater amounts of gypsum during acidic exposure and might precipitate into and cover the pores of the mortar.

5.6 Summary

Systematic experiments were carried on fly ash based geopolymer mortar with and without nanosilica and ultrafine fly ash to evaluate the setting time, workability, mechanical, microstructure and durability properties at different ages. It was noted that inclusion of nanosilica and ultrafine fly ash in fly ash based geopolymer mortar reduced setting time. It is

noteworthy that the role of optimum nanosilica and ultrafine ash in geopolymer mortar exhibited the same phenomenon as fly ash geopolymer paste series.

It is observed that the addition of finer materials (nanosilica and ultrafine fly ash) above the optimum level leads to decrease the compressive strength of the geopolymer mortar. However, the rate of strength development still higher than that of their corresponding control mixes. The SEM imaging indicates that the interlocking mechanism and the spaces between two particles were dense with 2% nanosilica and 10% ultrafine fly ash for fly ash only based geopolymer mortar. It is noted from the sorpitivity data that the permeation capacity of the geopolymer mortar increases significantly after the optimum nanosilica and ultrafine fly ash was incorporated. Added to this, the durability properties such as the acid and carbonation resistance of the geopolymer mortar also significantly increased with 2% nanosilica and 10% ultrafine fly ash for fly ash only based geopolymer mortar.

5.7 Reference

1. P. Deb, P. Nath, P.K. Sarker, The effects of ground granulated blast-furnace slag blending with fly ash and activator content on the workability and strength properties of geopolymer concrete cured at ambient temperature, Mater. Des., 62 (2014) 32-39
2. P.S. Deb, P. Nath, P.K. Sarker, Strength and permeation properties of slag blended fly ash based geopolymer concrete, Adv. Mater. Res., 651 (2013), 168-173
3. P. Nath, P.K. Sarker, Effect of GGBFS on setting, workability and early strength properties of fly ash geopolymer concrete cured in ambient condition, Constr. Build. Mater., 66 (2014) 163-171

4. P. Nath, P.K. Sarker, Use of OPC to improve setting and early strength properties of low calcium fly ash geopolymer concrete cured at room temperature, Cem. Concr. Comp., 55 (2015), 205-214
5. J.L. Provis, P. Duxson, J.S.J. Deventer, The role of particle technology in developing sustainable construction materials, Adv. Powder Technol., 21 (2010) 2-7
6. X. Gao, Q.L. Yu, H.J.H. Brouwers, Characterization of alkali activated slag–fly ash blends containing nanosilica, Constr. Build. Mater., 98 (2015), 397-406
7. A. Fernandez-Jimenez, A. Palomo, Characterisation of fly ashes. Potential reactivity as alkaline cements, Fuel, 82 (2003), 2259-2265
8. J. Temuujin, R.P. Williams, A. Riessen, Effect of mechanical activation of fly ash on the properties of geopolymer cured at ambient temperature, J. Mater. Process. Tech., 209 (2009), 5276-5280
9. A. Fernandez-Jimenez, M. Monzo, M. Vicent, A. Barba, A. Palomo, Alkaline activation of metakaolin–fly ash mixtures: obtain of Zeoceramics and Zeocements, Microporous Mesoporous Mater., 108 (2008), 41-49
10. J.S. Belkowitz, W.B. Belkowitz, K. Nawrocki, F.T. Fisher, The impact of nano silica size and surface area on concrete properties, Mater. J., 112 (2015), 419-428
11. P. Chindaprasirt, C. Jaturapitakkul, T. Sinsiri, Effect of fly ash fineness on microstructure of blended cement paste, Constr. Build. Mater., 21 (2007), 1534-1541
12. K. Somna, C. Jaturapitakkul, P. Kajitvichyanukul, P. Chindaprasirt, NaOH- activated ground fly ash geopolymer cured at ambient temperature, Fuel, 90 (6) (2011) 2118-2124

13. D.W. Law, A.A. Adam, I. Patnaikuni, T.K. Molyneaux, A. Wardhono, Long term durability properties of class F fly ash geopolymer concrete, Mater. Struct., 48 (2015), pp. 721-731
14. F. Puertas, G.R. Mejía, J.A. Fernández, S. Delvasto, J. Maldonado, Alkaline cement mortars. Chemical resistance to sulfate and seawater attack,Mater. Constr., 52 (2002), pp. 55-71
15. J. Deja, Carbonation aspects of alkali activated slag mortars and concretes. Silic Ind 67(1) (2002)37–42
16. F. PUERTAS, M. PALACIOS, T.V. AZQUEZ, Carbonation process of alkali-activated slag mortars. J MATER SCI 41 (2006) 3071–3082Mm
17. R.V. Silva, R. Neves, J. Brito, R.K. Dhir, Carbonation behaviour of recycled aggregate concrete. Cement & Concrete Composites 62 (2015) 22–32
18. T. Bakharev, Resistance of geopolymer materials to acid attack, Cem. Concr. Res., 35 (2005), pp. 658-670
19. P. Chindaprasirt, S. Taebuanhuad, U. Rattanasak, Resistance to acid and sulfate solutions of microwave-assisted high calcium fly ash geopolymer, Mater. Struct., 46 (2013) 375-381
20. R.R. Lloyd, J.L. Provis, J.S.J. Deventer, Acid resistance of inorganic polymer binders. 1. Corrosion rate, Mater. Struct., 45 (2012), pp. 1-14
21. J.S. Belkowitz, W.B. Belkowitz, K. Nawrocki, F.T. Fisher, The impact of nano silica size and surface area on concrete properties, Mater. J., 112 (2015), 419-428

22. N. Fattuhi, B. Hughes, The performance of cement paste and concrete subjected to sulphuric acid attack, Cem. Concr. Res., 18 (4) (1988), pp. 545-553
23. D. Israel, D.E. Macphee, E.E. Lachowsk, Acid attack on pore-reduced cements,J. Mater. Sci., 32 (1997), pp. 4109-4116
24. R.L. Hartman, H.S. Fogler, Understanding the dissolution of zeolites, Langmuir, 23 (10) (2007), pp. 5477-5484
25. I. Ismail, S.A. Bernal, J.L. Provis, S. Hamdan, J.S.J. Deventer, Microstructural changes in alkali activated fly ash/slag geopolymers with sulfate exposure, Mater. Struct., 46 (2013), pp. 361-373
26. S.E. Wallah, B.V. Rangan, Low Calcium Fly Ash Based Geopolymer Concrete: Long Term Properties". Research Report GC2 Faculty of Engineering, Curtin University of Technology, Perth, Australia (2006), pp. 01-9

CHAPTER 6

GEOPOLYMER CONCRETE WITH NANOSILICA AND ULTRAFINE FLY ASH

6.1 Overview

The properties of fly ash based geopolymer concretes using nanosilica and ultrafine fly ash are presented in this chapter. The geopolymer concrete samples are divided into three different series based on the binder's composition such as fly ash only, GGBFS and OPC blended fly ash based geopolymer. All concrete specimens were cured at room temperature. Addition of nanosilica and ultrafine fly in different fly ash based geopolymer series on the workability, compressive strength and shrinkage properties were evaluated at different ages.

6.2. Workability of fly ash based geopolymer concrete with nanosilica and ultrafine fly ash

To investigate the effect of nanosilica and ultrafine fly ash on workability of fly ash based geopolymer concrete, a slump test [1] was carried out immediately after mixing of the fresh concrete. The workability of the geopolymer concrete mixes with nanosilica and ultrafine fly ash, in terms of the slump value, are given in Tables 6.1 and 6.2, respectively. It is noted from the tables that mixes produced with higher nanosilica and ultrafine fly ash exhibited decreased workability when compared with the control mixes.

Table 6.1 Slump values of different geopolymer mixes with nanosilica**.**

	Fly ash				Slag				OPC			
Mix id	FA-NS0	FA-NS1	FA-NS2	FA-NS3	FA-S-NS0	FA-S-NS1	FA-S-NS2	FA-S-NS3	FA-PC-NS0	FA-PC-NS1	FA-PC-NS2	FA-PC-NS3
Slump (mm)	220	210	190	165	190	185	165	155	180	168	152	146

For example, slump of mixes of FA-NS series reduced from 220mm for 0% nanosilica (FA-NS0) to 165mm for 3% nanosilica (FA-NS3). Similarly, mix FA-S-NS2 with the 15% slag and 2% nanosilica had a slump value of 165 mm as compared to 190 mm for the mix FA-S-NS0 with 0% nanosilica. It is noteworthy from Table 6.1 that mixes FA-NS3, FA-S-NS3 and FA-PC-NS3 exhibited the lowest slump values in their respective mix series since they had the highest percentage of nanosilica (3%) as compared to the other mixes. The decrease of workability in the mixes of all three series by the inclusion of nanosilica is attributed to the increased liquid demand and accelerated reaction because of its high specific surface. Added to this, alkaline solution (combination of sodium silicate (SS) and sodium hydroxide (SH)) which is more viscous than water, usually makes geopolymer concrete more cohesive and sticky.

Table 6.2 Slump values of different geopolymer mixes with ultrafine fly ash.

	Fly ash				Slag				OPC			
Mix id	FA-UF0	FA-UF05	FA-UF10	FA-UF15	FA-S-UF0	FA-S-UF5	FA-S-UF10	FA-S-UF15	FA-PC-UF0	FA-PC-UF5	FA-PC-UF10	FA-PC-UF15
Slump (mm)	220	215	190	170	190	182	168	153	180	170	158	143

The workability behaviour of geopolymer mixes changed significantly in distinct levels when the ultrafine fly ash was used. It is observed from the Table 6.2 that geopolymer concrete mixes with higher ultrafine fly ash (15%) showed similar behaviour to those with 3% nanosilica. Mix FA-UF15 with 15% ultrafine fly ash showed less slump value that that of FA-

UF0 (0% ultrafine fly ash). Similar effects were also noticed in the mixes FA-S-UF15 and FA-PC-UF15. The slump values of the mixes FA-S-UF15 and FA-PC-UF15 were observed 153mm and 143mm and found to have reasonable workability during the casting time. Moreover, no segregation or bleeding was observed in the mixes during mixing, compaction and finishing of the concrete.

6.3 Strength of fly ash based geopolymer concrete with nanosilica and ultrafine fly ash

6.3.1 Fly ash-only geopolymer concrete

Compressive strengths of the fly ash-only geopolymer concrete mixes with 0-3% nanosilica and 0-15% ultrafine fly ash up to 90 days are shown in Figs. 6.1 and 6.2, respectively. It can be seen from these figures that strength development of the geopolymer concrete slowed down after the age of 28 days. It is noted from the figures that the inclusion of 3% nanosilica and 15% ultrafine fly ash in fly ash-only geopolymer mixes has increased compressive strength as compared to that of the respective control mix.

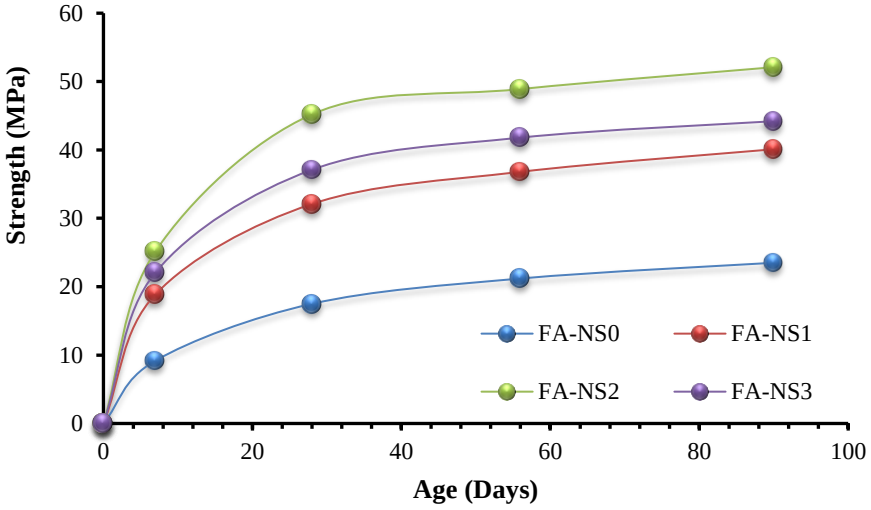

Fig. 6.1 Effect of nanosilica on compressive strength of fly ash only geopolymer concrete.

In geopolymer mixes with nanosilica, mix FA-NS1 containing 1% nanosilica achieved 36.8 MPa compressive strength at 56 days which is 70% higher than that of FA-NS0 containing 0% nanosilica. Similarly, mix FA-NS3 with 3% nanosilica exhibited 14 % higher compressive strength than that of geopolymer mix FA-NS1. However, the rate of strength development appeared to be more pronounced with 2% nanosilica in the fly ash-only geopolymer concrete mixes. In this series, the highest strength increase was observed in mixture FA-NS2 with 2% nanosilica and the compressive strength reached 48.9 MPa at 56 days. It is noteworthy that addition of nanosilica in the fly-ash based geopolymer binder increased the dissolution rate of Si and Si–Al phases, which strongly affects the rate of polymerization. Khater et al. [6] reported that the presence of nanosilica in fly-ash based geopolymer mixes are the key factor to enhance the strength properties due to its amorphous property and the high specific area.

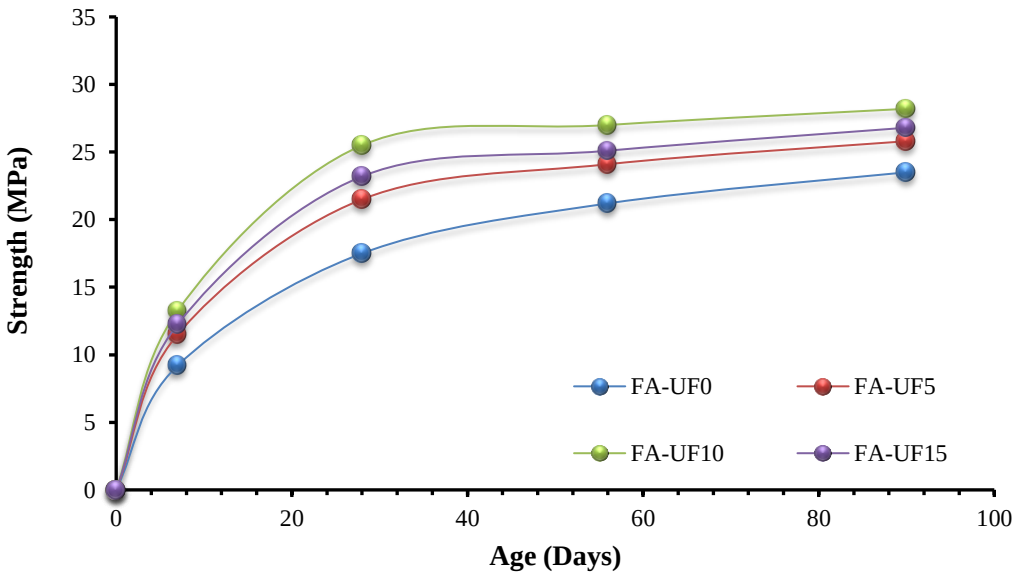

Fig. 6.2 Effect of ultrafine fly ash on compressive strength of fly ash only geopolymer concrete.

In the geopolymer concrete mixes with ultrafine fly ash, FA-UF0 with no ultrafine fly ash in the binder showed a slower rate of strength development as compared to the other mixes.

When ultrafine fly ash was incorporated in the fly-ash only geopolymer mixes keeping the other parameters constant, the strength was significantly increased at the initial ages and continued to gain up to 28 days. At 28 days, mixes FA-UF5 and FA-UF10 with 5% and 10% ultrafine fly ash respectively, achieved 24% and 33% higher strength, than the geopolymer mix without ultrafine fly ash (FA-UF0). The highest strength increase was observed in this series with 10% ultrafine fly ash (FA-UF10) that reached 28.2 MPa at 90 days.

6.3.2 OPC and GGBFS blended fly ash based geopolymer concretes

As can be seen from the results presented in Figs. 6.3 to 6.4, GGBFS blended fly ash based geopolymer with 2% nanosilica (FA-S-NS2) and 5% ultrafine fly ash (FA-S-UF5) developed higher compressive strengths compared to those of the companion mixes without nanosilica and ultrafine fly ash (FA-NS0/FA-UF0). Similar trend is also observed in the OPC blended fly ash based geopolymer series (Figs. 6.5 to 6.6) with 2% nanosilica (FA-PC-NS2) and 5% ultrafine fly ash (FA-PC-UF5).

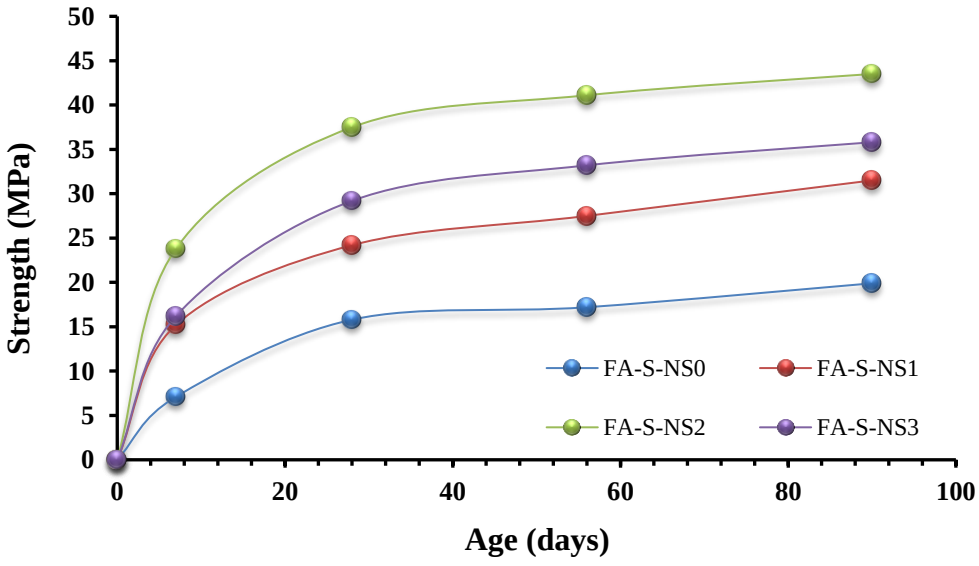

Fig. 6.3 Effect of nanosilica on compressive strength of GGBFS blended fly ash based geopolymer concrete.

A relatively high compressive strength (37.5 MPa) was noted to increase with the increment of 1% to 3% nanosilica in GGBFS blended fly ash based geopolymer concretes than that of its corresponding control mix (FA-S-NS0). The mix FA-S-NS1 containing 1% nanosilica achieved 24.2MPa at 28 days which is 55% higher than the strength of FA-S-NS0 containing 0% nanosilica. However, the compressive strength declined when the amount of nanosilica was increased from 2% to 3% (FA-S-NS3). Mix FA-S-NS3 showed 28% less strength than that of mix FA-S-NS2 with 2% nanosilica.

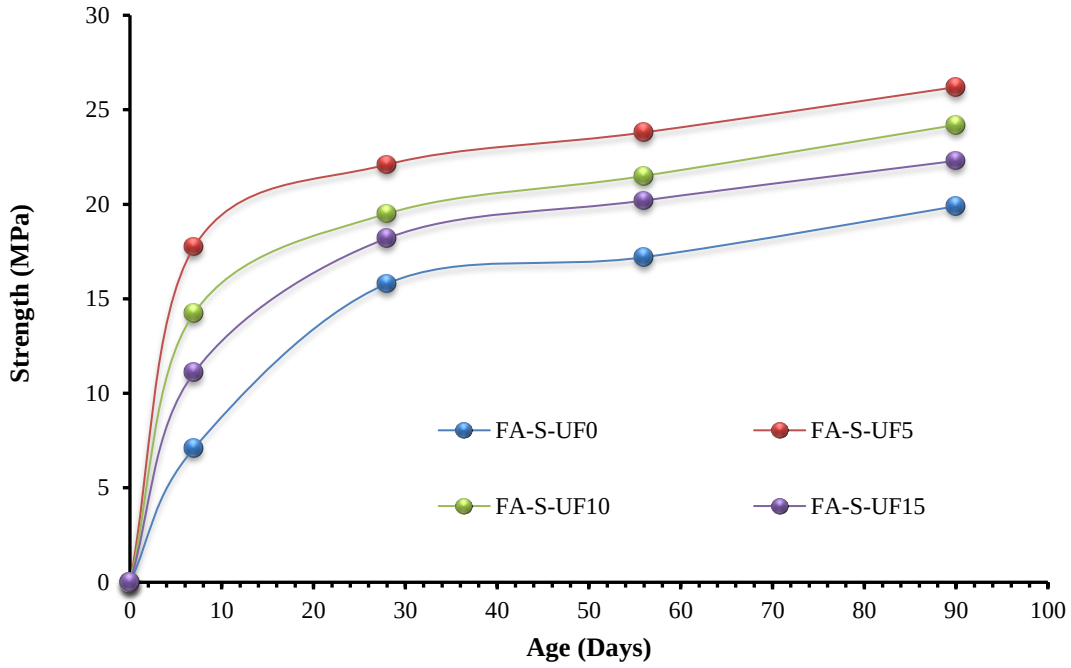

Fig. 6.4 Effect of ultrafine fly ash on compressive strength of GGBFS blended fly ash based geopolymer concrete.

Fig. 6.4 provides a comparison of compressive strengths of GGBFS blended fly ash based geopolymer mix with and without ultrafine fly ash at 28, 56 and 90 days. As expected, with ultrafine fly ash, the strengths of all the UFA incorporated mixes were higher than that of its control mix at 28 days. The strength of the mix FA-S-UF5 (5% UFA) was 40% higher than

that of the FA-S-UF0 (0% UFA). Similarly, the 28-day compressive strengths were 18% and 22% higher for 10% and 15% UFA, respectively, than that of the control mix.

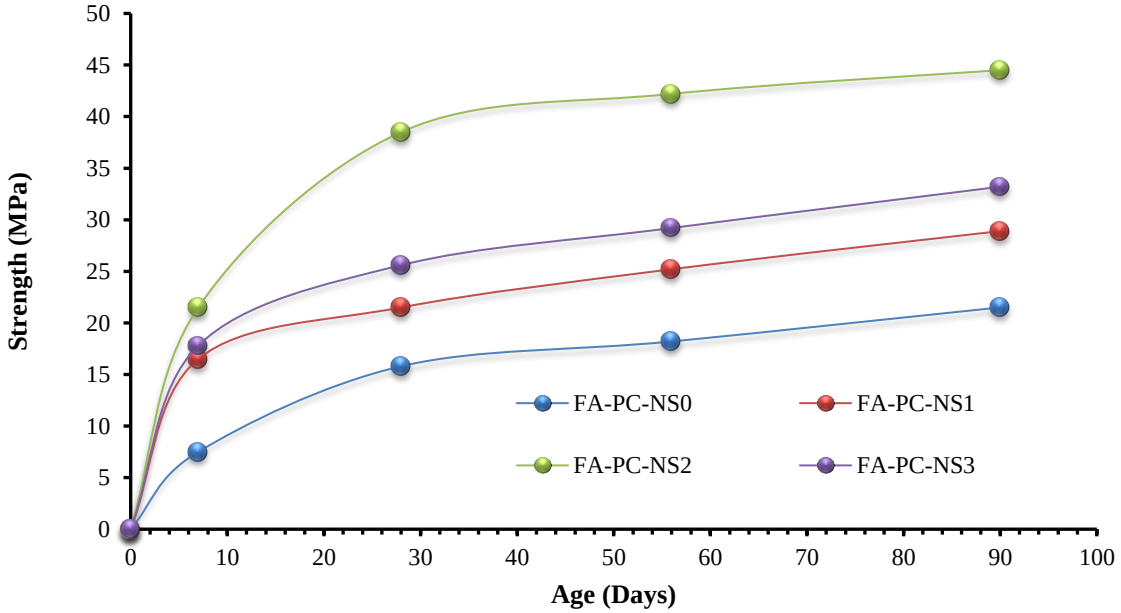

Fig. 6.5 Effect of nanosilica on compressive strength of OPC blended fly ash based geopolymer concrete.

Compressive strengths of the OPC blended fly ash based geopolymer concretes with and without nanosilica up to 90 days are presented in Fig. 6.5. Strength of FA-PC-NS concrete mixes similar trends of strength development as in the FA-S-NS mix series. Geopolymer concrete mixes FA-PC-NS1 (1% nanosilica), FA-PC-NS2 (2% nanosilica) and FA-PC-NS3 (3% nanosilica) showed increases of 28-day compressive strengths by 35%, 130% and 60%, respectively as compared to the control mix (FA-PC-NS0).

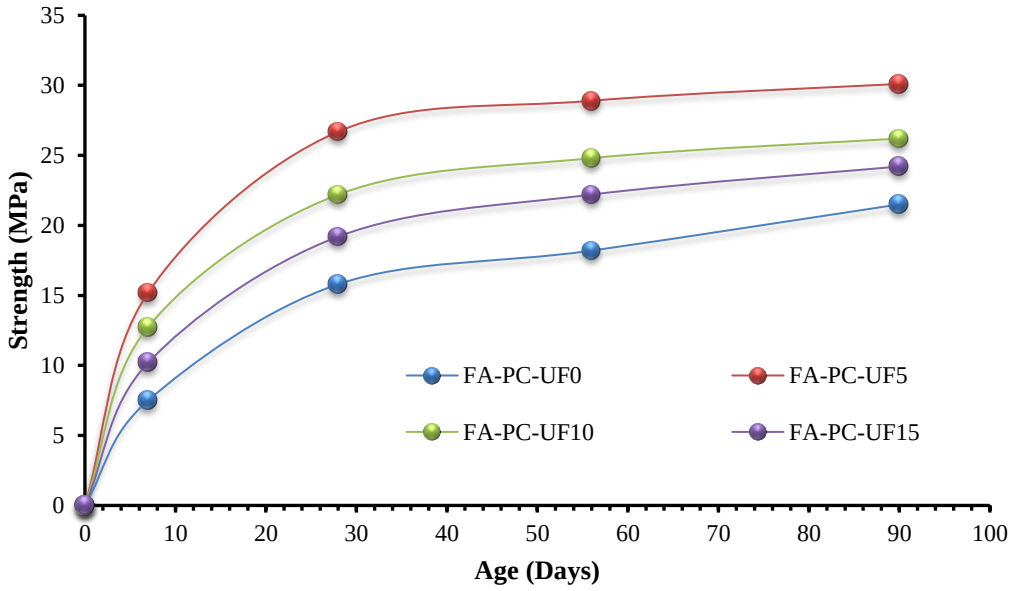

Fig. 6.6 Effect of ultrafine fly ash on compressive strength of OPC blended fly ash based geopolymer concrete.

The compressive strengths of the OPC blended fly ash based geopolymer mixes with and without ultrafine fly ash are presented in Fig. 6.6. It is noted from the figure that at 28-day the compressive strengths of FA-PC-UF5 (5% UFA), FA-PC-UF10 (10% UFA) and FA-PC-UF15 (15% UFA) geopolymer are higher than that of controlled mix (FA-PC-UF0).

Compressive strength of geopolymer concrete is significantly influenced by the amount of fine materials in the mixes. According to the results (Figs. 6.1 to 6.6), maximum compressive strengths were observed with the 2% nanosilica in all geopolymer mix series. In the mix series with ultrafine fly ash, the maximum compressive strengths were found for 10% ultrafine fly ash in the fly ash-only mixes, and 5% ultrafine fly ash for GGBFS and OPC blended fly ash mixes (Fig. 6.7).

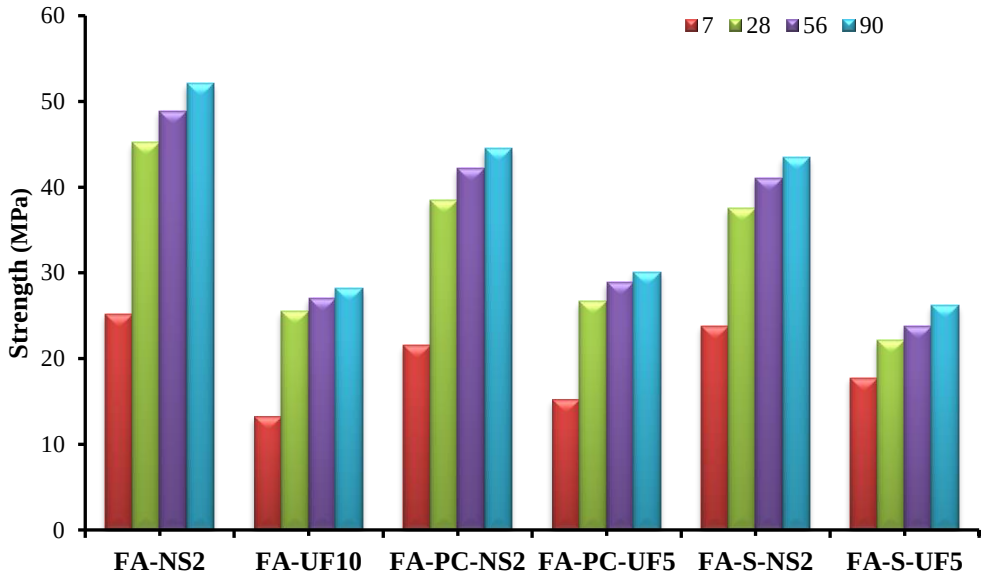

Fig. 6.7 Effect of optimum nanosilica and ultrafine fly ash on compressive strength of fly ash based geopolymer concrete.

Comparing the strengths of nanosilica and ultrafine fly ash mix series up to 90 days of age, as shown in Fig. 6.7, it can be seen that 2% nanosilica exhibited higher compressive strength than the corresponding mixes with 5% or 10% ultrafine fly ash. This was due to the higher surface area of the nanosilica as compared to that of ultrafine fly ash. It can be seen from Fig. 6.7 that increase in the fineness of materials up to a certain level (optimum) in fly ash based geopolymer concrete mixes resulted in a significant increase in strength, especially during the early age of 7 to 28 days. For example, fly ash only geopolymer mix with 2% nanosilica (FA-NS2.0) exhibited 45.2 MPa compressive strength at 28 days which is significantly higher than that of its optimum ultrafine fly ash mix (25.5 MPa). Similarly, the 28-day compressive strengths of the GGBFS and OPC blended mixes with 2% nanosilica were 37.5 MPa and 38.5 MPa, respectively, as compared to 22.1 MPa and 26.7 MPa with 5% ultrafine fly ash.

6.4 Shrinkage properties of fly ash based geopolymer concrete with ultrafine fly ash and nanosilica

6.4.1 Fly ash-only geopolymer concrete

The mean drying shrinkage values of the geopolymer concrete specimens with 0% nanosilica or UFA (FA-NS0/FA-UF0), 2% nanosilica (FA-NS2) and 10% UFA (FA-UF10) are plotted in Fig. 6.8. It can be seen that the rate of shrinkage was high during the early ages up to 28 days and the rate decreased after this age. The 120-day drying shrinkage of the geopolymer concrete specimens varied between 650 and 790 microstrain. It is noteworthy that the 28-day drying shrinkage values of the geopolymer specimens were below the limit of 1000 microstrain as recommended by the AS1379-2007 standard [2] for normal concrete.

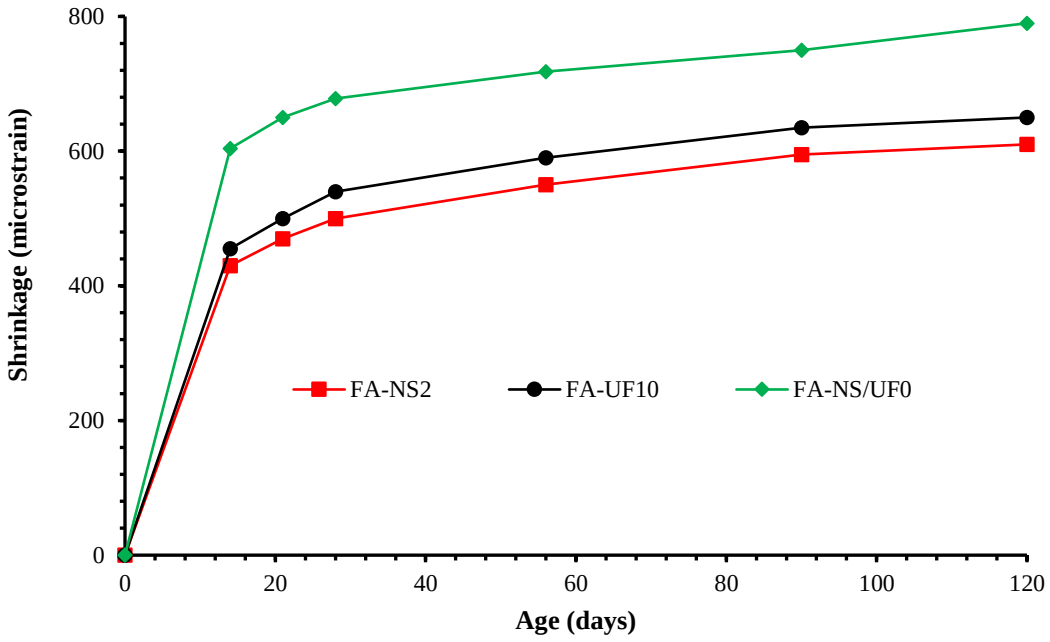

Fig. 6.8 Drying shrinkage of fly ash only geopolymer concrete for control mix, with 2% nanosilica and 10% ultrafine fly ash.

It can be seen from Fig. 6.8 that for a constant SS/SH ratio of 2.0, drying shrinkage decreased with the optimum values of nanosilica (2%) and ultrafine fly ash (10%) in the fly ash only geopolymer mixes. The 120-day drying shrinkage values of the mixes FA-NS2 and FA-UF10 were 610 and 650 microstrain, respectively, which are significantly lower than that of the control mix (790 microstrain for FA-NS0/FA-UF0). However, the effect of the type of finer material appears to be more pronounced on the strength development of concrete.

6.4.2 OPC and GGBFS blended fly ash based geopolymer concretes

The drying shrinkage of OPC and GGBFS blended fly ash based geopolymer concrete with 0% nanosilica / UFA (FA-S-NS0/FA-S-UF0), 2% nanosilica (FA- S-NS2) and 5 % UFA (FA- S-UF5) are plotted in Fig.6.9.

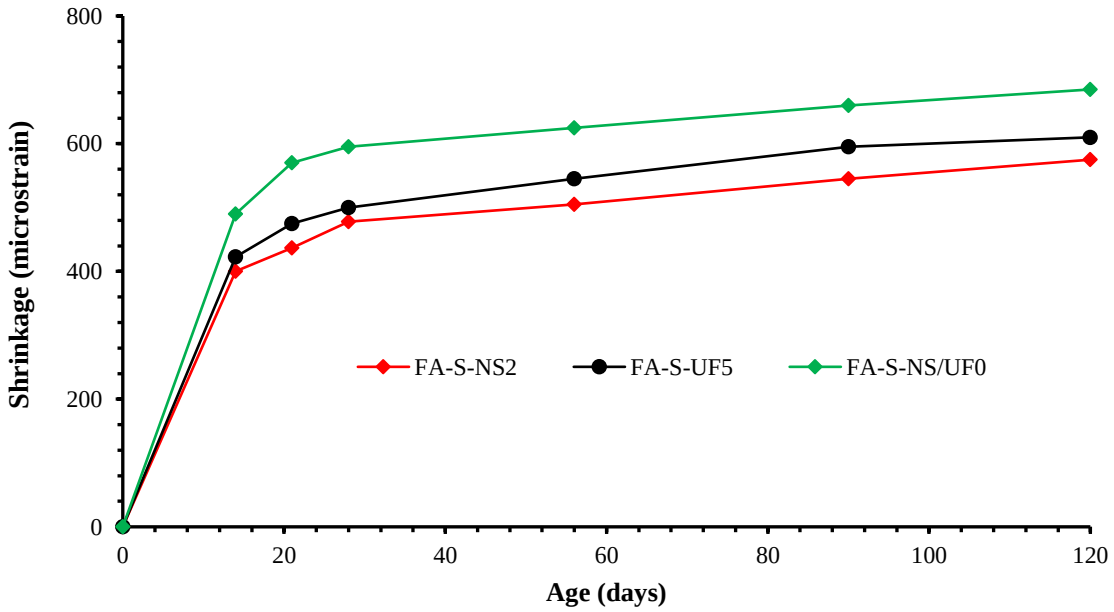

Fig. 6.9 Drying shrinkage of GGBFS blended fly ash based geopolymer concrete for control mix, with 2% nanosilica and 5% ultrafine fly ash**.**

It is noted from the figure that the shrinkage values of geopolymer mixes with optimum nanosilica and UFA fluctuated slightly over the period of measurement and considerably reduced than that of the respective control mixes. The 120-day shrinkage for FA-S-NS2 (2% nanosilica) reduced almost 16% than FA-S-NS0 (0% nanosilica). Similarly, geopolymer mix FA- S-UF5 (5% ultrafine fly ash) exhibited 12% less shrinkage than that of FA- S-UF0 (0% UFA) at 120 days (Fig. 6.9). However, it is also observed that the rate of drying shrinkage can be reduced with the types of finer material in the mixes. Mix FA- S-NS2 which has the same amount of alkaline solution with slag content as in mixture FA- S-UF5 exhibited 4% less shrinkage value at 120 days. The lower drying shrinkage of the geopolymer concrete with the optimum nanosilica and UFA is attributed to the presence of less interconnected capillary network of the geopolymer matrix. This observation is consistent with the finding reported by Ma and Ye [3].

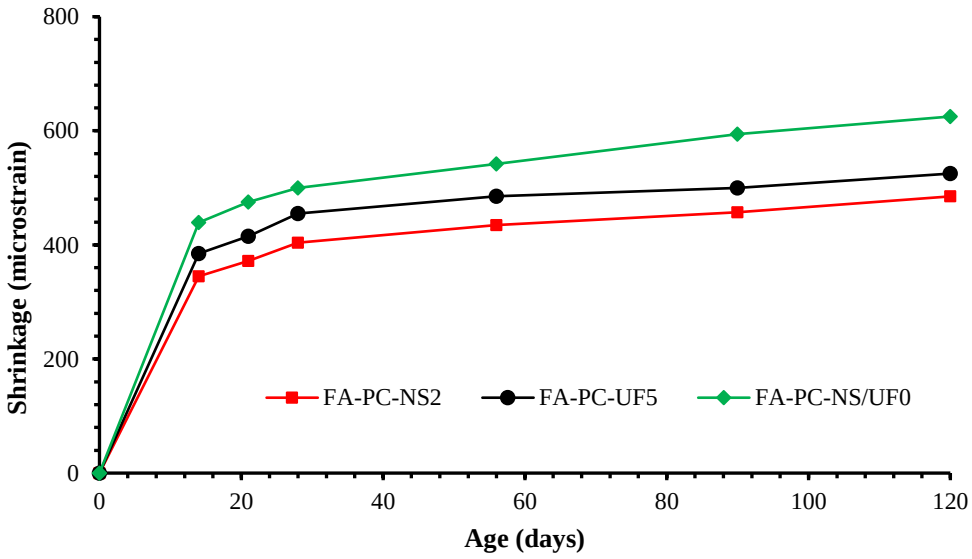

Fig. 6.10 Drying shrinkage of OPC blended fly ash based geopolymer concrete for control mix, with 2% nanosilica and 5% ultrafine fly ash.

Drying shrinkage values of the OPC blended fly ash based series with optimum nanosilica (2%) and UFA (5%) are plotted in Fig. 6.10. Comparing the shrinkage values of FA-

PC-NS2, FA- PC-UF5 and the corresponding control mix (FA- PC-NS0), it can be seen from the figure that shrinkage reduced by the optimum value of nanosilica and UFA in the mix. Mix FA-PC-NS2 (2% nanosilica) 22% less shrinkage, respectively, than that of FA- PC-NS0/UF0 (control mix). However, the shrinkage values of FA-PC-UF5 which contained 5% UFA were significantly higher than those of FA-PC-NS2 with 2% nanosilica. For example, geopolymer mix FA-PC-UF5 (5% UFA) exhibited 11% less shrinkage reduction value at 120 days of age as compared to FA-PC-NS2 with the same alkaline content, OPC and SS/SH ratio in the mix. The shrinkage value of the geopolymer concrete mix FA-PC-NS2, which has a similar compressive strength of the GGBFS based exhibited 5% higher shrinkage at 28 days. The drying shrinkage value of FA-S-NS2 at 28 days was found 575 macrostrain as compared to the value of 485 macrostrain of the OPC blended geopolymer specimens.

6.4.3 Comparison with the design shrinkage calculated by the Australian Standard

Concrete shrinkage models are intended to provide an estimate of the shrinkage strain at different ages. Clause 3.1.7.2 of the Australian Standard AS 3600 [4] describes a procedure for calculating the design shrinkage of OPC concrete. The calculation is based on the characteristic compressive strength of concrete, thickness of the member, the surrounding environment and the age of concrete. The value calculated using the standard has a range of ±30%.

The equations proposed by Gilbert (2002) [7] that have been developed to estimate the shrinkage of concrete and used in this study as a comparison to the experimental results.

The total shrinkage strain is given by Equation 1 and the endogenous shrinkage at any time t (in days) after concrete placement is given by Equation 2.

$$\varepsilon_{cs} = \varepsilon_{cse} + \varepsilon_{csd} \quad (1)$$

Where, ε_{cs} = Design Shrinkage Strain, ε_{cse} = Chemical (autogenous) Shrinkage, ε_{csd} = Drying Shrinkage strain and t = time (in days).

$\varepsilon_{cse} = \varepsilon^*_{cse}$ x (1.0- e-0.1t) ---------- (2)

Where ε^*_{cse} is the final endogenous shrinkage and may be taken as

ε^*_{cse} = (0.06fc'- 1.0) x 50 x 10-6----------(3)

In which f'c is in MPa. The drying shrinkage at time t (in days) after the commencement of drying may be taken as

ε_{csd} = k1 k4 εcsd.b ----------(4)

$\varepsilon_{csd.b}$ = (1.0-0.008fc') x ε*csd.b---------- (5)

$\varepsilon_{csd.b}$ = Basic drying shrinkage strain, $\varepsilon^*_{csd.b}$ = Final drying basic shrinkage strain, K1= (σ1t0.8)/(t0.8+0.15th) and σ1= 0.8+1.2e-0.005th where, th= hypothetical thickness and k4= 0.65 for interior environment

Where εcsd.b* depends on the quality of the local aggregates and may be taken as 800 x 10^{-6} for Sydney and Brisbane, 900 x 10-6 for Melbourne and 1000 x 10^{-6} elsewhere.

This procedure was used to calculate the design shrinkage of the specimens of different geopolymer mixes with and without nanosilica and UFA of this study. The measured mean shrinkage value and the corresponding calculated value for each mixture at different ages are given in Table 6.3. It can be seen that the experimental values for the geopolymer concrete mixes for optimum nanosilica and UFA are lower than the calculated values. The measured values for the control geopolymer concrete mixes are higher than the calculated value. The

measured shrinkage of FA-NS2 and FA-UF10 are the lowest among all the geopolymer concrete mixes.

Table 6.3 Drying shrinkage values of different geopolymer mixes with nanosilica and ultrafine fly ash.

Mix id		Ages (Days)			
	Method	28	56	90	120
FA-NS0	Experimental	678	718	750	790
	AS3600	695	755	790	820
FA-NS2	Experimental	500	550	595	610
	AS3600	525	570	598	638
FA-UF10	Experimental	540	590	635	650
	AS3600	558	625	675	701
FA-PC-NS0	Experimental	545	578	602	625
	AS3600	560	590	629	657
FA-PC-NS2	Experimental	489	515	550	575
	AS3600	522	568	604	650
FA-PC-UF05	Experimental	508	545	587	610
	AS3600	528	580	620	660
FA-S-NS0	Experimental	595	625	660	685
	AS3600	627	680	721	780
FA-S-NS2	Experimental	478	505	545	575
	AS3600	505	539	591	625
FA-S-UF05	Experimental	500	545	595	610
	AS3600	527	580	526	680

Castel et al. [5] studied the shrinkage behaviour of fly ash geopolymer concrete mixes with an alkaline liquid to binder ratio of 0.6 and curing at different temperatures. It was shown in their study that curing at 40^0C for 3 days was necessary for the shrinkage of fly ash geopolymer concrete to meet the design shrinkage requirement of AS 3600. The results of this

study, as presented in Table 6.3, show that shrinkage of geopolymer concrete cured at room temperature could be reduced by the addition of optimum nano-slica (2%) and ultrafine fly ash (5%). Therefore, these mix design considerations of can reduce drying shrinkage of geopolymer concrete to meet the required design values when cured at lower temperatures.

6.5 Summary

Inclusion of optimum nanosilica and ultrafine fly ash showed significant effects on the development of mechanical and shrinkage properties of fly ash based geopolymer concrete when cured at room temperature.

Noticeable increase of strength can be seen in the fly ash geopolymer concrete with nanosilica and ultrafine fly ash in the mixes. The highest strengths at all ages up to 90 days were found in the mixes with 2% nano-silica and 10 % ultrafine fly ash for fly ash-only geopolymer series. While the strength of the concrete mixes with optimum nanosilica and ultrafine fly ash was higher than that of the control mixes, however, it was less than that of its corresponding paste and mortar.

For example, the strength value of mix FA-NS2 (concrete) after 28 days was 45.0 MPa, as compared to 67.0 MPa for the corresponding paste and 60.0 MPa for mortar. Same phenomenon has been observed for ultrafine fly ash-based series. Compressive strength of mix FA-UF10 reduced from 47.0 MPa for paste to 25.0 MPa for Concrete at 28 days

Furthermore, it is shown that 2% nanosilica has the greatest effect on reducing the drying shrinkage values of geopolymer concretes. The results show that, in general, the workability, strength and shrinkage of fly ash-only geopolymer concrete with 2% nanosilica and 10% ultrafine fly ash are superior to those of the control concrete. Similarly, 5% ultrafine

fly ash improved the strength and shrinkage of the GGBFS or OPC blended fly ash geopolymer concretes.

6.5 Reference

1. ASTM Standard. Standard Test Method for Slump of Hydraulic-Cement Concrete. (ASTM C 143/C143M -2015). retrieved from http:// www.specs4.ihserc.com
2. Standards Australia, AS 1379. Specification and Supply of Concrete. (2007).
3. Y. Ma, G. Ye, The shrinkage of alkali activated flyash, Cem and Concre Res 68 (2015) 75–82.
4. Standards Australia. Concrete Structures.(AS 3600-2009), retrieved from http:// www.saiglobal.com on 29 May 2015
5. A. castel, S Foster, J Aldred, Time- dependent behavior of a class F fly ash based geopolymer concrete, procee. NTCC2014: international Confer. on Non-Traditional cement and concrete, June 2014.
6. H.M. Khater, B.A. El-Sabbagh, M. Fanny, Effect of nanosilica on alkali activated water cooled slag geopolymer ARPN J. Sci. Technol., 02 (2012), p. 2
7. R.I. Gilbert. Creep and shrinkage models for high strength concrete - proposal for inclusion in AS3600 Australian Journal of Structural Engineering, 4(2) (2002), 95-106.

Every reasonable effort has been made to acknowledge the owners of copyright material. I would be pleased to hear from any copyright owner who has been omitted or incorrectly acknowledged.

CHAPTER 7
NANOMECHANICAL PROPERTIES OF FLY ASH BASED GEOPOLYMER

7.1 Overview

The properties of a material can be improved by enhancement of its microstructure which consists of phases such as hydrated gel, unreacted particles and the porous phase. Therefore, assessment of these three phases and creating their relationships to the nanomechanical properties of a material is critically important. Nemecek et al. [1, 7] investigated into the micromechanical properties of fly ash and metakaolin based geopolymer binders by using nano-indentation techniques. Since previous studies [2,3,4] showed that blending of OPC and GGBFS with class F fly ash can significantly improve the setting and hardening behaviour of geopolymers cured in ambient condition, it is necessary to investigate into the micro properties and volume fractions of different phases developed in the reaction products using these blended aluminosilicate sources. Moreover, a small percentage of nanosilica was shown to improve the mechanical properties of fly ash geopolymers. Thus, it is necessary to investigate into the developed phases by nanosilica in order to understand its effect on the mechanical properties. Therefore, the principal aim of this part of the study was to experimentally determine the micromechanical properties of different geopolymer mixtures, with particular emphasis on the addition of nanosilica and the connectivity of the solid phases. Statistical analysis of grid nano-indentation data was used to determine the elastic modulus and hardness of the produced phases and their volume fractions.

7.2 Mathematical formulation to determine mechanical properties from nanoindentation

7.2.1 Oliver and Pharr Method

Oliver and Pharr [5] proposed a method to analyse the indentation data based on analytical solutions. It was observed that the direct measurement of the contact area is not always accurate and convenient, and proposed a procedure to determine the contact area based on the depth of indentation and indenter shape function.

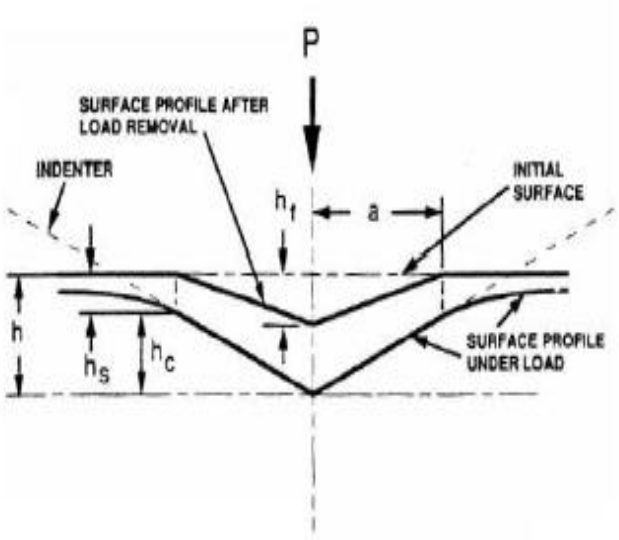

Fig. 7.1 Schematic representation of a section through an indenter [5]

Fig. 7.1 shows that the cross-section of an indentation. At any time during loading, the total displacement *h* is expressed by Equation 1.

$$h = h_c + h_s \text{ ---------- (1)}$$

Where h_c is the vertical distance along which contact is made, called the contact depth. h_s is the displacement of the surface at the perimeter of the contact. At the peak load, P_{max}, displacement is h_{max} and the radius of contact circle is ***a.*** During unloading, elastic displacement

is recovered and the final depth of the residual hardness impression once the indenter is fully withdrawn is h_f.

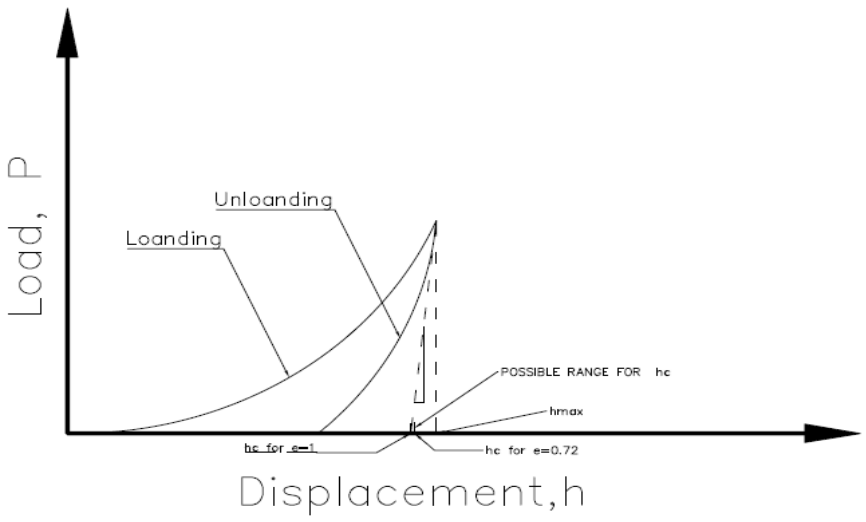

Fig. 7.2 Schematic Representation of Load vs Indenter Displacement

The typical nano-indentation load-deflection curves are shown in Fig. 7.2. The indentation modulus is determined from the slope of the unloading curve corresponding to the maximum load. The contact stiffness (S) is evaluated as the initial slope of the unloading curve at the peak load and maximum depth h_{max}. Thus, the relationship is given by Equation 2.

$$S = \frac{dp}{dh}\ (h = h_{max}) \quad \text{---------- (2)}$$

The indentation modulus is a function of dP/dh and the area of contact (A_c). Equation 3 was derived from the Hertzian theory of contact mechanics taking into the effect of the area of contact [6].

$$E_r = \frac{S\sqrt{\pi}}{2\sqrt{A_C}} \quad \text{---------- (3)}$$

The elastic modulus of the indenter and the specimen is generally referred to as the combined modulus (E_r) [8] and related to the elastic modulus and Poisson's ratio of the two bodies which can be described by Equation 4.

$$\frac{1}{Er} = \frac{1-\nu^2}{E} + \frac{1-\nu'^2}{E'} \quad \text{---------- (4)}$$

Where ν and ν' are the Poisson's ratios of the testing material and the indenter respectively. Similarly, E and E′ are the elastic moduli of the testing material and the indenter respectively. At the peak load (P_{max}), the projected contact area (A), can be determined as a function of the contact depth (h_c), as Equation 5.

$$A = f(h_c) \quad \text{---------- (5)}$$

Where $h_c = h_{max} - h_s$, and h_s is the displacement of the surface at the perimeter of the contact which can be calculated by Equation 6.

$$hs = € \frac{Pmax}{S} \quad \text{---------- (6)}$$

Where € is the geometric constant and its value is taken as 0.75 for a paraboloid revolution. The perfect area function for a Berkovich indenter can be calculated by Equation 6, where the Berkovich indenter face angle θ = 65.27° [12]

$$A(h_c) = 3\sqrt{3}h_c^2 \tan^2\theta = 24.5h^2_c \quad \text{---------- (7)}$$

The mean contact pressure or hardness value (H) is given by Equation 8.

$$H = \frac{P_{max}}{A(h_c)} = \frac{P}{24.5h_{c2}} \quad \text{..... (8)}$$

7.2.2 Deconvolution of grid indentation data

Researchers [8, 9, 10] have considered the deconvolution of indentation load–displacement (P–h) data to obtain the elastic modulus (E) and hardness values of the cementitious binders. The individual phase properties of the analyzed data were determined by applying the statistical

deconvolution to elastic modulus and hardness histograms. The deconvolution technique was carried out manually by fitting a number of probability density functions (PDF) to the experimental frequency plot (normalized histogram) of the measured quantity.

Statistical analysis of the large amount of data collected from grid indentation provides an insight on the mechanical properties of the multiple phases [9, 10]. A proper statistical analysis of the indentation data is required to calculate the volume fraction of each material phase. The distribution of each phase is assumed to follow a normal distribution. If a random variable such as X denotes the presence of an individual mechanical property, the probability distribution of X in phase *i* can be written as in Equation 9.

$$\varphi_i(x) = \frac{1}{\sqrt{2\pi\sigma_i}} \exp\left(-\frac{1}{2\sigma^2}((x-\mu_i)^2\right) \ldots\ldots\ldots (9)$$

Where μ_i and σ_i^2 are the mean and variance of the distribution, respectively. Considering X_1, X_2…..X_m as the independent and identically distributed mechanical property of each phase with volume fractions of f_1, f_2. . . f_m respectively, the theoretical probability distribution of each mechanical phase for the specimen can be written as in Equation 10.

$$\varphi(x) = \sum_{i=1}^{m} (f_i \varphi_i(x)) \ldots\ldots\ldots (10)$$

Again considering $X_{(1)}$, $X_{(2)}$. . . $X_{(N)}$ are sample data obtained from grid indentation, the expression for the empirical cumulative distribution function (CDF) is given by Equation 11.

$$G(x_{(i)}) = i/N - 1/2N \text{ for } i \in [1, N] \ldots\ldots\ldots (11)$$

Where μ_i is the mean and σ_i is the variance of the distribution. The function $\varphi_i(x)$ can be found by minimising the error function given by by Equation 12.

$$\min \sum_{j=1}^{N} \left(\sum_{i=1}^{n} f_i \varphi_i(x_j) - G(x_j)\right)^2 \ldots\ldots\ldots (12)$$

The total volume fraction can be expressed by a summation of all single phases f_i , as given by Equation 13.

$$\sum_{i=1}^{n} f_i = 1 \ldots\ldots\ldots (13)$$

7.3 Nanoindentation Data Analysis

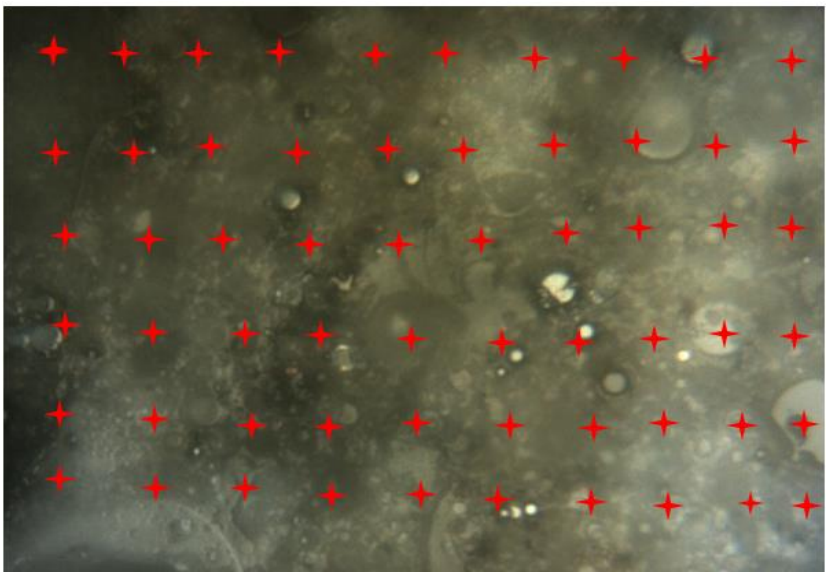

Fig. 7.3 Image of 60 µm × 60 µm indent locations.

Grid indentation was performed on 28 days geopolymer samples with 0% and 2% nanosilica. On each geopolymer sample, 4 different locations were chosen randomly to minimize site specific properties on the indentation data set. On each location, 60 indents were made in an array where 10 indents were made in each of the 6 rows. Spacing between the indents were 10 µm. A huge volume of indent data was analysed statistically to determine the phase properties and volume fraction of different phases in the hydrated geopolymers.

7.3.1 Force–indentation depth behaviour

The typical load-indentation curves of fly ash geopolymer specimens are presented in Figs. 7.4 -7.6 (a-d). It can be seen from the curves that there were changes in the gradient and plastic deformation with respect to the maximum indentation loads (0.5 mN – 1.0 mN) after each cycle. This phenomenon is attributed to the presence of different phases in that particular vicinity of the indenter.

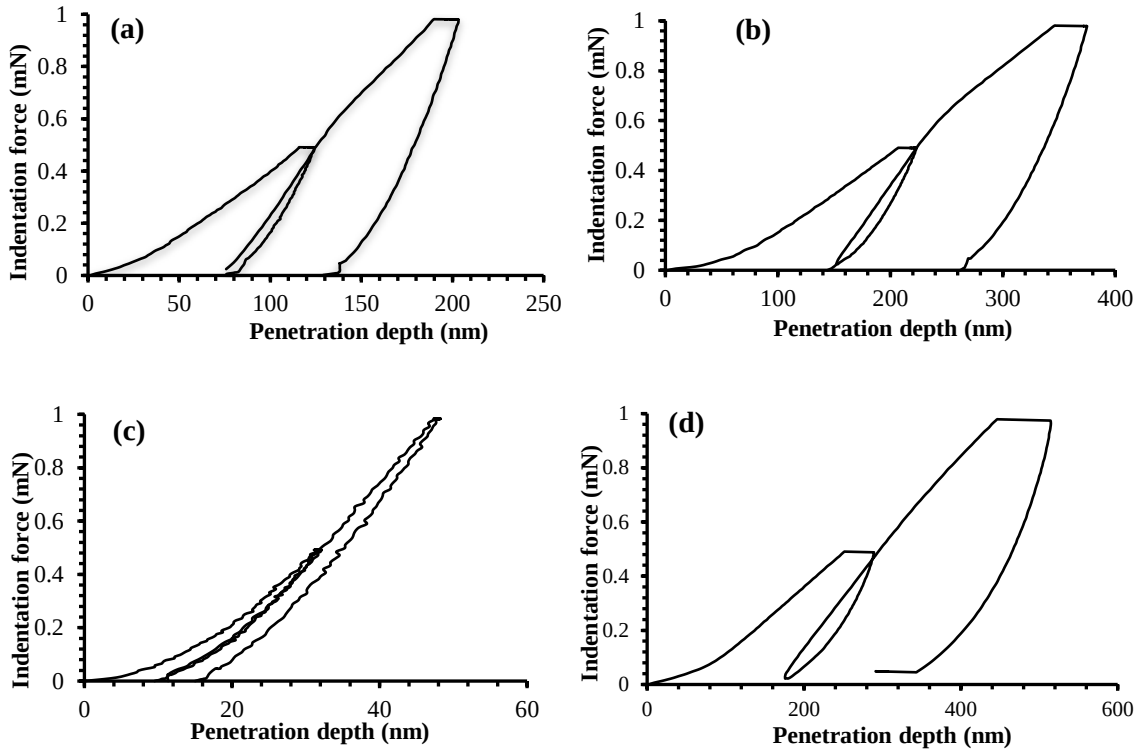

Fig. 7.4 Typical load–indention curves of fly ash only geopolymer (a) partially activated (b) activated, (c) unreacted and (d) porous

For example, penetration of the matrix at the maximum load shown in Fig. 7.4b is higher than that in Fig. 7.4a. It is noteworthy that the partially activated geopolymer source materials generally showed higher load bearing capacity than that of pure aluminosilicate gel product. Unreacted particles of geopolymer matrix (Fig. 7.4c) generally shows higher load

bearing capacity than other phases of the reaction product (Figs. 7.4a, 7.4b and 7.4d). On the other hand, the vicinity of the cementitious area in Fig.7.4d showed a greater displacement due to the presence of porous or loosened matrix in that area. These aspects will be discussed further in terms of the elasticity and hardness properties in the following sections. Elastic modulus was evaluated from the final unloading region of the load vs. indentation curve using the Oliver and Pharr method [5], as described earlier.

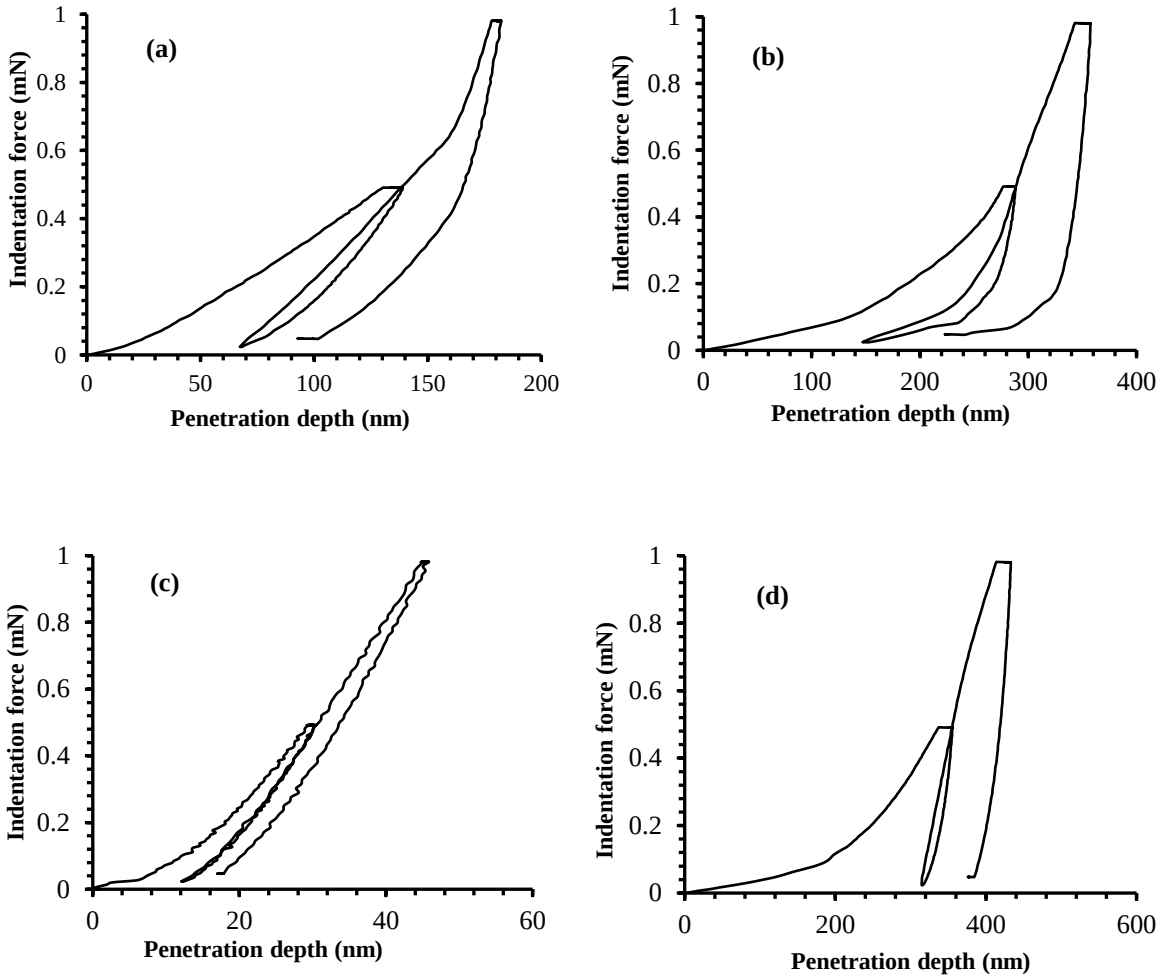

Fig. 7.5 Typical load–indention curves of GGBFS blended fly ash based geopolymer

Figs. 7.5 and 7.6 indicated that the schematic load–unload–reload–unload curves of GGBFS and OPC blended fly ash based geopolymer with 0% and 2% nanosilica. Partially

activated phase shown on the Fig. 7.5a exhibited less penetration depth than that of its hydrated phase showed in Fig. 7.5b. On the other hand, lowest penetration depth for GGBFS blended fly ash based geopolymer is noted in Fig. 7.5c. Porous or disintegrated phase, as in Fig. 7.5d, showed the highest penetration depth for the blended geopolymer.

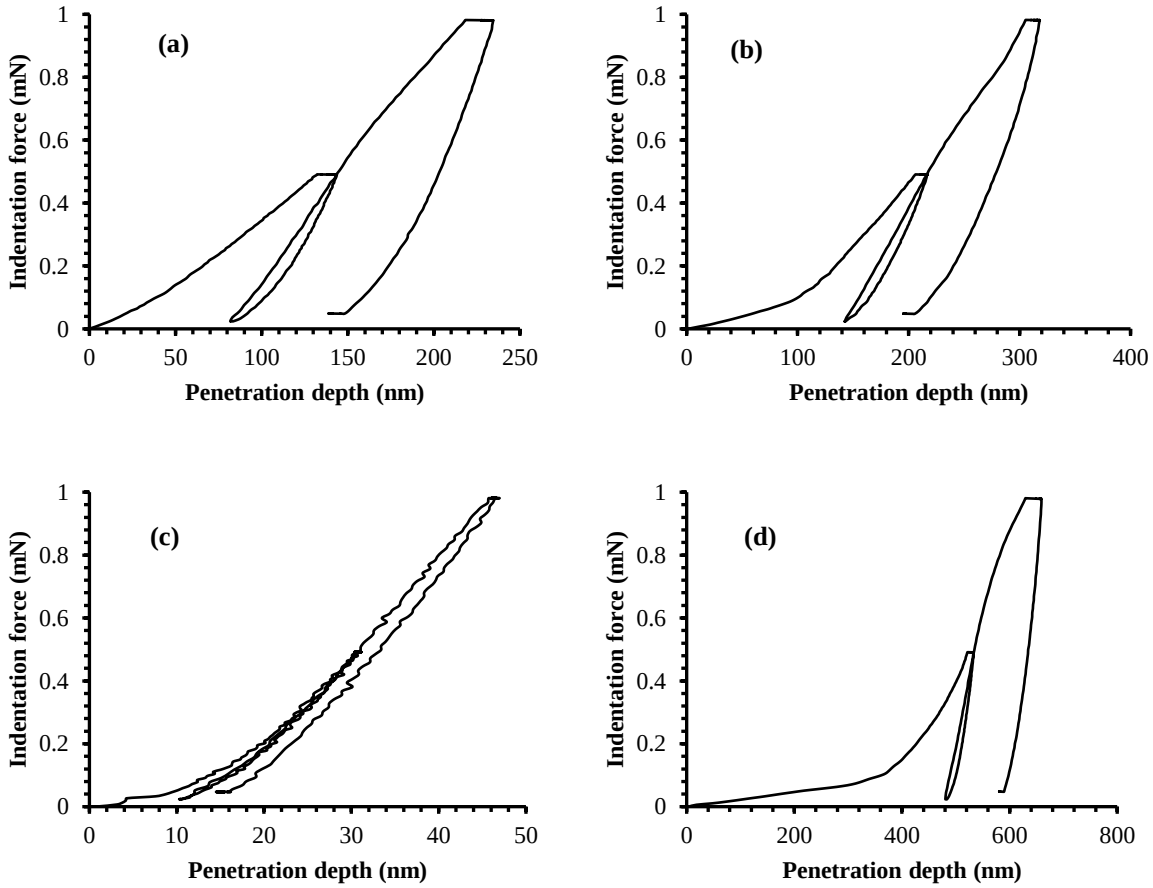

Fig. 7.6 Typical load–indention curves of OPC blended fly ash based geopolymer

Similar force-penetration behaviour was also observed for OPC blended fly ash geopolymer series (Fig. 7.6a to d).

7.3.2 Variation of indentation depth with elastic modulus

Fig. 7.7 shows the variation of indentation depths of the fly ash-only geopolymer specimen with respect to E-modulus. It can be seen from the figure that the indentation depth varied from about 100 nm to 400 nm at 0.5 mN to 1.0 mN loading cycles. The average E-modulus varied in a range of 5.0 to 100 GPa. Deconvolution of the indentation data show the presence of four distinct phases with a typical range of indentation depth for each phase.

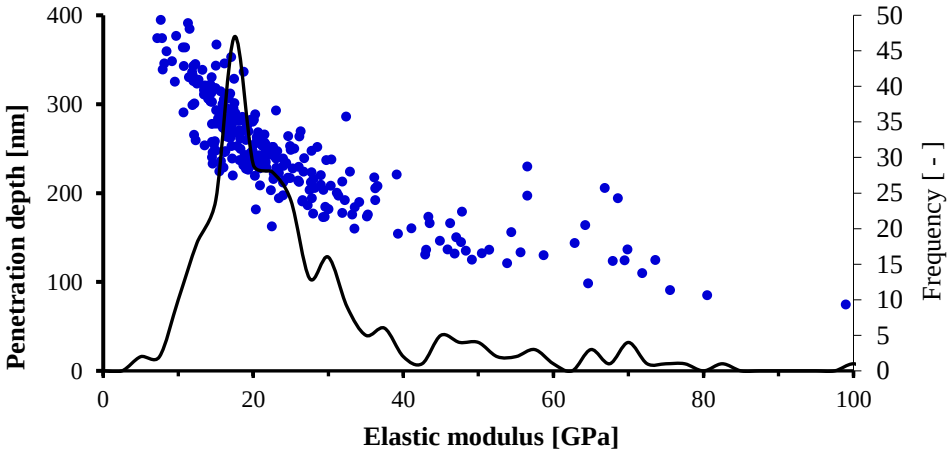

Fig. 7.7 Indentation depth vs. elastic modulus and frequency of fly ash only geopolymer

The mean indentation depths in the non-activated and partially activated aluminosilicate phases were found in the ranges of 65 nm to 80 nm and 154 nm to 168 nm respectively. The indentation depths in the hydrated sodium aluminosilicate gel phase were noted in the range of 260 to 280 nm. A decrease in E-modulus was also observed at mean higher depths of 390 to 410 nm indicating the presence of porous regions. These observed indention depths are similar to those previously reported by Nemecek [1] and lee [11] for alkali activated geopolymers. The increases in the elasticity value at lower penetrations as shown in

Figs. 7.7 and 7.9 are considered to be due to the presence of unreacted or partially reacted fly ash particles.

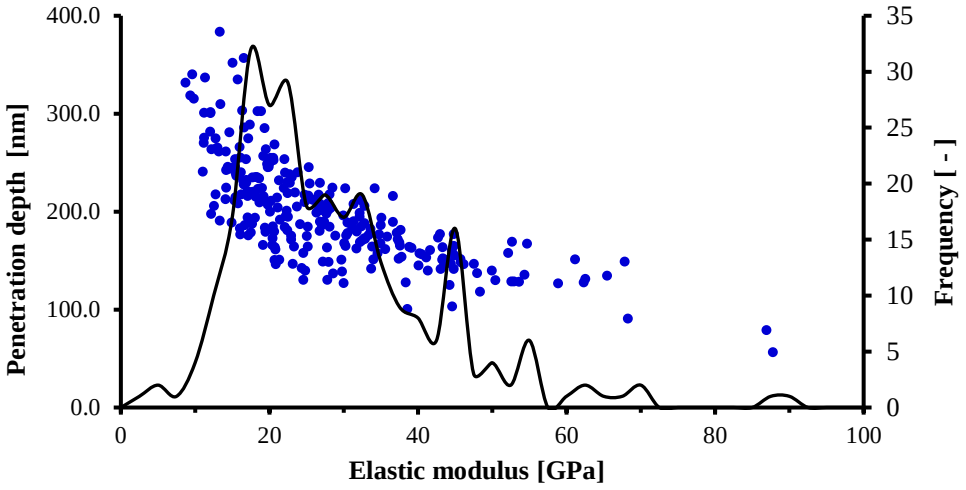

Fig. 7.8 Indentation depth vs. elastic modulus and frequency of GGBFS blended fly ash based geopolymer

Fig. 7.8 shows the schematic representation of the penetration depth vs elastic modulus of GGBFS blended fly ash based geopolymer. It is observed from the figure that the modulus values of the mix decreased with the increase in indentation depth and approached to similar values observed in fly ash only geopolymers. The smaller indentation depths in the ranges of 65 nm to 80 nm represented the unreacted phase with higher elastic value. It is noted from the figure that as the indentation depth increased, the value of elastic modulus decreased. For example, the indentation depths in the hydrated gel phase were noted in the range of 260 to 280 nm.

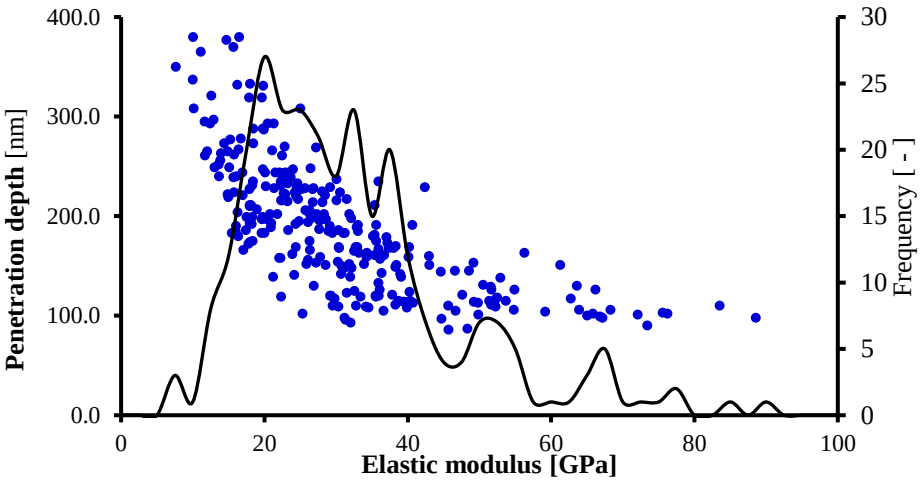

Fig. 7.9 Indentation depth vs. elastic modulus and frequency of OPC blended fly ash based geopolymer

Fig. 7.9 shows a typical penetration depth vs elastic modulus of OPC blended fly ash based geopolymer paste sample. Corresponding variation in depth of indentation was noted from 65 nm to 500 nm for different elastic values. It is noteworthy from the Fig. 7.9 that the elastic values corresponding to its indentation depth are similar to the values observed in previous section for different geopolymer series and reported by different researchers in their studies [9, 10, 11, 12].

7.3.3 Elasticity, hardness and phase volume fractions of geopolymer specimens

The frequency distributions of the elastic modulus and hardness values obtained from the naoindentation data of the fly ash-only geopolymer specimen are plotted in Figs. 7.10a to 7.10d. It was recognised by previous studies [11 to 15] that separation of hydration products into two or three distinctive phases using the deconvolution technique is very difficult since the histograms do not present an apparent bimodal or trimodal distribution, as shown in these figures. For this reason, the elasticity and hardness values of different phases reported by other studies [1, 11] are considered as reference values in the analysis of the test data.

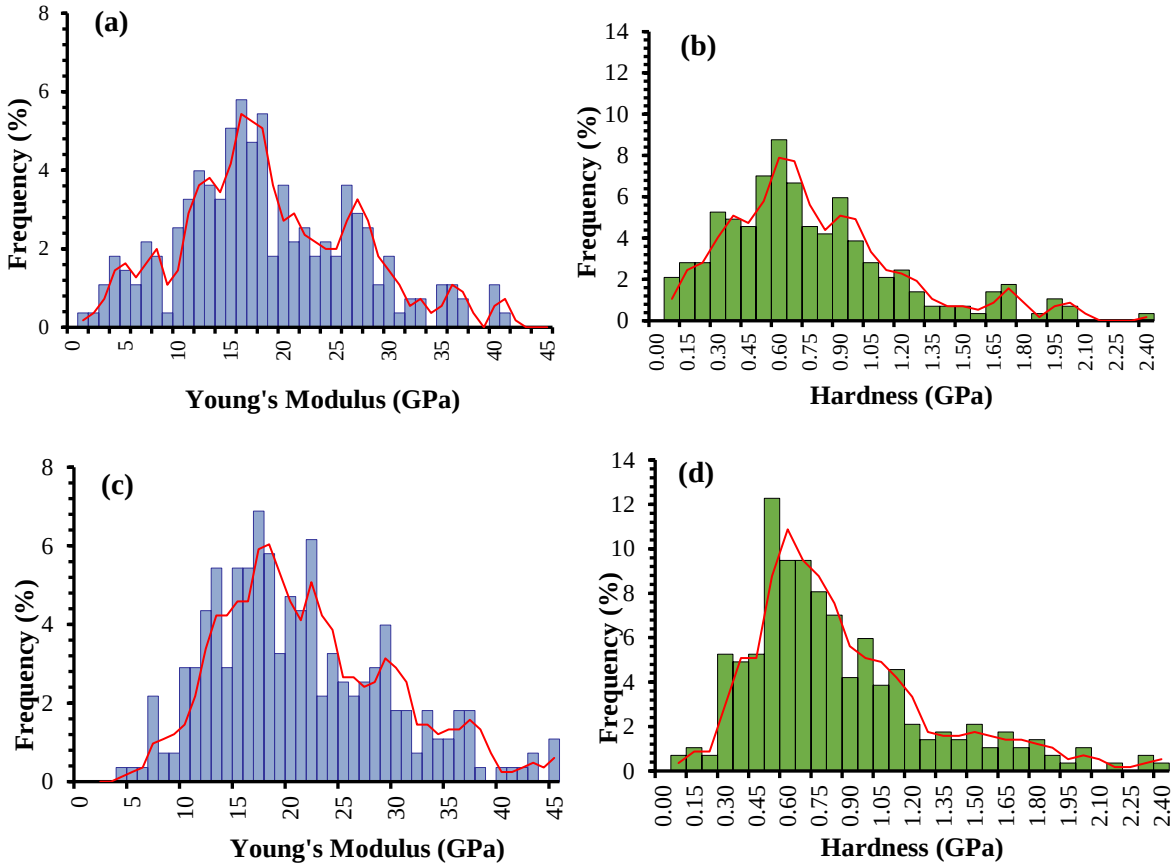

Fig. 7.10 Frequency distribution of elastic modulus and hardness of the fly ash geopolymer: (a, b) FA-NS0 and (c, d) FA-NS2.

It can be seen from the figures that most of the elasticity values (peaks) are laid within a range of 5.0 GPa to 30.0 GPa and hardness values are in the range of 0.3 GPa to 1.1 GPa. These values match well with the elasticity and hardness values reported by previous studies [42, 56]. The average values of modulus of elasticity and hardness for hydrated aluminosilicate gel found by Nemecek [1] were in a range of 17 to 21 GPa and 0.4 to 1.0 GPa, respectively. A significant difference in elastic modulus and hardness values for unreacted, amorphous and porous phases can be seen in Figs. 7.10a and 7.10b. It can be noted that higher stiffness of the unreacted phases and lower stiffness of the porous phases as compared to the amorphous phase were reported for cementitious systems [19, 20]. Since the frequencies of the modulus of

elasticity values higher than 45 GPa were relatively low, they are not shown in Fig. 7.10a and 7.10c; however they were included in calculations of the total volume fractions of different phases. It can be expected that each phase would have a unique set of elastic modulus and hardness value. Hence, the values of elastic modulus with corresponding hardness values are collected together in order to understand the relationship between this two mechanical properties.

It can be seen from Figs. 7.10a to 7.10d that the ranges of E-modulus and hardness values for different phases of the fly ash-only geopolymer with 2% nanosilica (FA-NS2) are comparable to the range of values obtained for the mix without nanosilica (FA-NS0). The E-modulus and hardness of the aluminosilicate gel phase are mostly found to vary in the ranges of 5.0 GPa to 30.0 GPa and 0.3 GPa to 1.1 GPa, respectively. However, despite the similar ranges of elasticity and hardness values, a significant difference in the volume fractions of different phases can be observed in the two mixes. The volume fractions of the four distinct phases such as the aluminosilicate gel phase, partially reacted phase, unreacted phase and porous phase of the geopolymers were calculated by using the typical range of the values of E-modulus of these phases and the frequency distributions of Fig.7.10. The volume fractions of the phases calculated using the elasticity values is given in Table 7.1. The compressive strengths and the different molar ratios are also given in this table to understand the correlations.

Table 7.1 Indentation elasticity and proportions of different phases in fly ash based geopolymer paste obtained from nanoindentation.

Mix	Compressive Strength [16]	Porosity (%)	Si/Al	Na/Al	Porous phase (Volume Fraction %)		Aluminosilicate gel phase (Volume Fraction %)		Partially activated phase (Volume Fraction %)		Unreacted particles (Volume Fraction %)	
					Elasticity	Hardness	Elasticity	Hardness	Elasticity	Hardness	Elasticity	Hardness
FA-NS0	29	14.0	1.22	3.22	13.0	14.0	70.0	48.9	8.5	-	7.5	23.1
FA-NS2	67	8.0	1.33	3.27	7.1	8.33	84.9	63.6	3.0	-	5.0	29.2
FA-S-NS0	25	15.5	1.38	3.45	12.5	16.5	68.0	46.7	8.9	-	10.6	26.3
FA-S-NS2	73	9.5	1.40	3.55	9.1	10.2	81.1	62.5	6.5	-	2.3	28.3
FA-PC-NS0	26	16.0	1.37	3.50	15.6	17.4	69.0	45.4	9.2	-	7.5	36.7
FA-PC-NS2	65	10.0	1.39	3.53	8.7	10.0	78.2	65.2	10.4	-	4.0	24.8

It can be seen from Table 7.1 that the volume fraction of hydrated aluminosilicate gel increased from 70.0% to 84.9% with 2% nanosilica. The volume fraction of the porous phase for mix FA-NS2 decreased from 13.0% to 7.1%. The volume fractions of the partially reacted phase and unreacted phase reduced from 8.5% to 3.0% and 7.5% to 5.0%, respectively. Therefore, the increased reaction rate and nucleation effect of nanosilica has increased the hydrated phase and reduced the porous phase of geopolymer. Moreover, a relationship can also be observed in Table 7.1 among the compressive strength, Si/Al and Na/Al molar ratios and volume fractions of different phases. Previous studies [2, 3, 4] showed that fly ash based geopolymer mixes with optimum molar ratios of Si/Al and Na/Al exhibited a higher degree of geopolymerization, which eventually influenced the micromechanical characteristic of the final hydrated product. Rowles and O'Connor [22] observed a correlation among the nanostructure, molar ratio and the mechanical properties of geopolymer binders. It can be seen from Table 7.1 that the Si/Al and Na/Al molar ratios increased with the addition to 2% nanosilica that has influenced the geopolymerisation reaction rate. Thus the inclusion of nanosilica increased the

volume of hydrated phase, reduced the volume of porous phase and eventually increased compressive strength from 29 MPa to 66 MPa. This is a significant improvement of the microstructure and compressive strength of the fly ash-only geopolymer by the inclusion of 2% nanosilica.

Table 7.2 Phase abundance (weight %) of geopolymers of different mixes.

Phase	Weight % (esd)					
	FA-NS0	FA-NS2	FA-PC-NS0	FA-PC-NS2	FA-S-NS0	FA-S-NS2
Calcite	-	-	2.2	1.2	1.2	1.5
Hatrurite	-	-	2.4	1.5	1.5	1.8
Hematite	2.5	2.2	2.4	1.9	2.1	2.6
Magnetite	3.9	3.9	3.4	3.0	3	3.5
Mullite	8.6	8.7	7.7	6.7	6.8	7.9
Quartz	4.7	4.6	4.0	4.0	3.9	4.1
Amporphous content	80.0	81.0	78.0	82.0	81.0	83.0

The phase compositions of the geopolymers as determined by the rietveld analysis are given in Table 7.2. Based on the quantitative data hematite [Fe_2O_3], magnetite [Fe_3O_4], mullite [$Al_{4.64}Si_{1.36}O_{9.68}$] and quartz [$SiO_2$] were recorded in both FA-NS0 and FA-NS2 mixtures. It can be seen from Table 7.2 that the amounts of quartz, mullite, hematite and magnetite did not very significantly with the addition of 2% nanosilica in the mix. Moreover, comparison of the total volume fraction of unreacted phase from Table 7.1 with the QXRD data from Table 7.2 supports that the crystalline phases are not affected significantly by the addition of nanosilica. Elasticity values for these unreacted phases such as magnetite (150 GPa), hematite (148 GPa), mullite (220 GPa) and quartz (76.5 GPa), as reported by other researchers [20, 21, 22], were observed in relatively low frequencies in the nanoindentation test data.

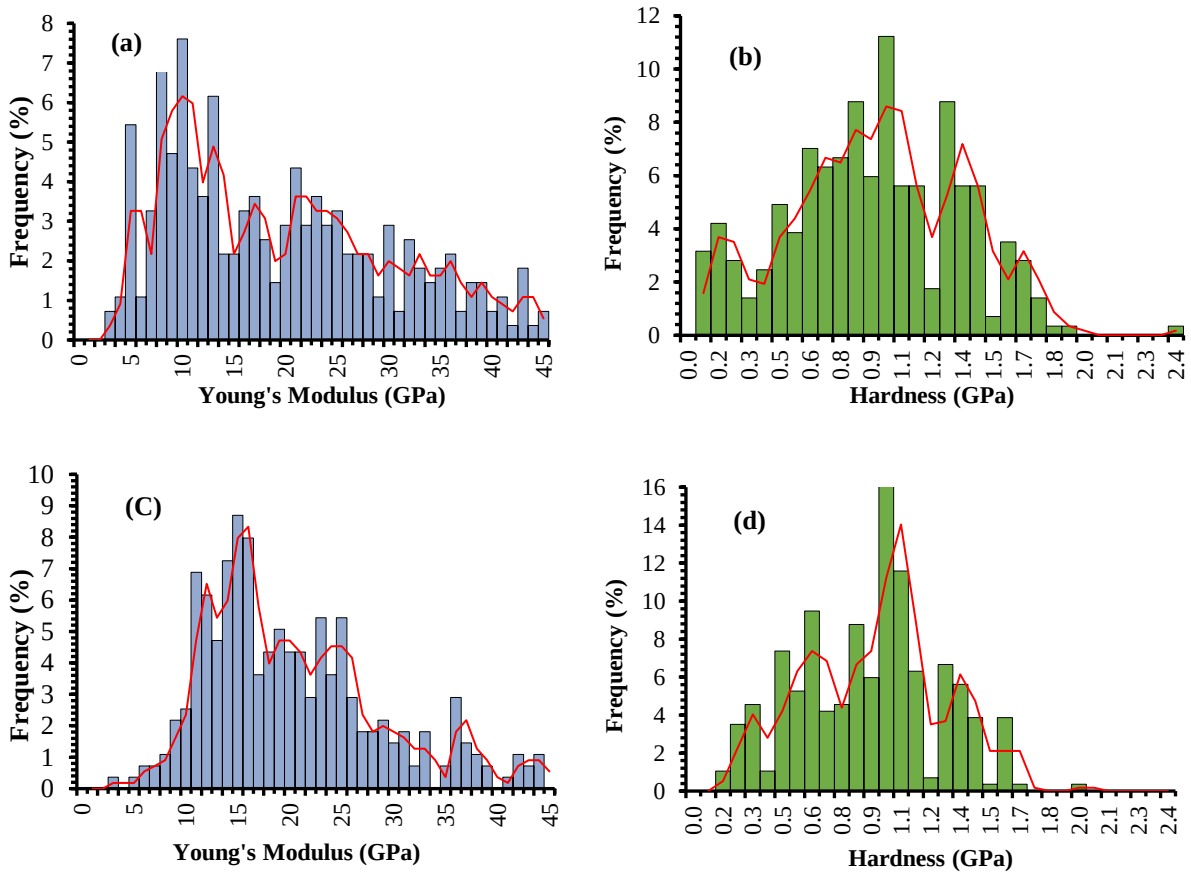

Fig. 7.11 Experimental elastic modulus and hardness frequency of GGBFS blended fly ash geopolymer:(a) and (b) FA-S-NS0, and (c) and (d) FA-S-NS2.

As shown in Figs.7.11 and 7.12, the nanoindentation of the specimens containing 10% OPC (FA-PC-NS) or 15% GGBFS (FA-S-NS) showed the similar trend of indentation depth to elastic modulus relationship as in the fly ash-only specimens. A decrease in modulus of elasticity and hardness values were observed with an increase in indentation depths. The average indentation depths of hydrated gel for OPC or GGBFS blended fly ash based geopolymer specimens were in the range of 160–210 nm, while the average indentation depth of unhydrated and porous phases were observed in the ranges of 50–80 nm and 555–700 nm, respectively (Fig7.8 and Fig.7.9).

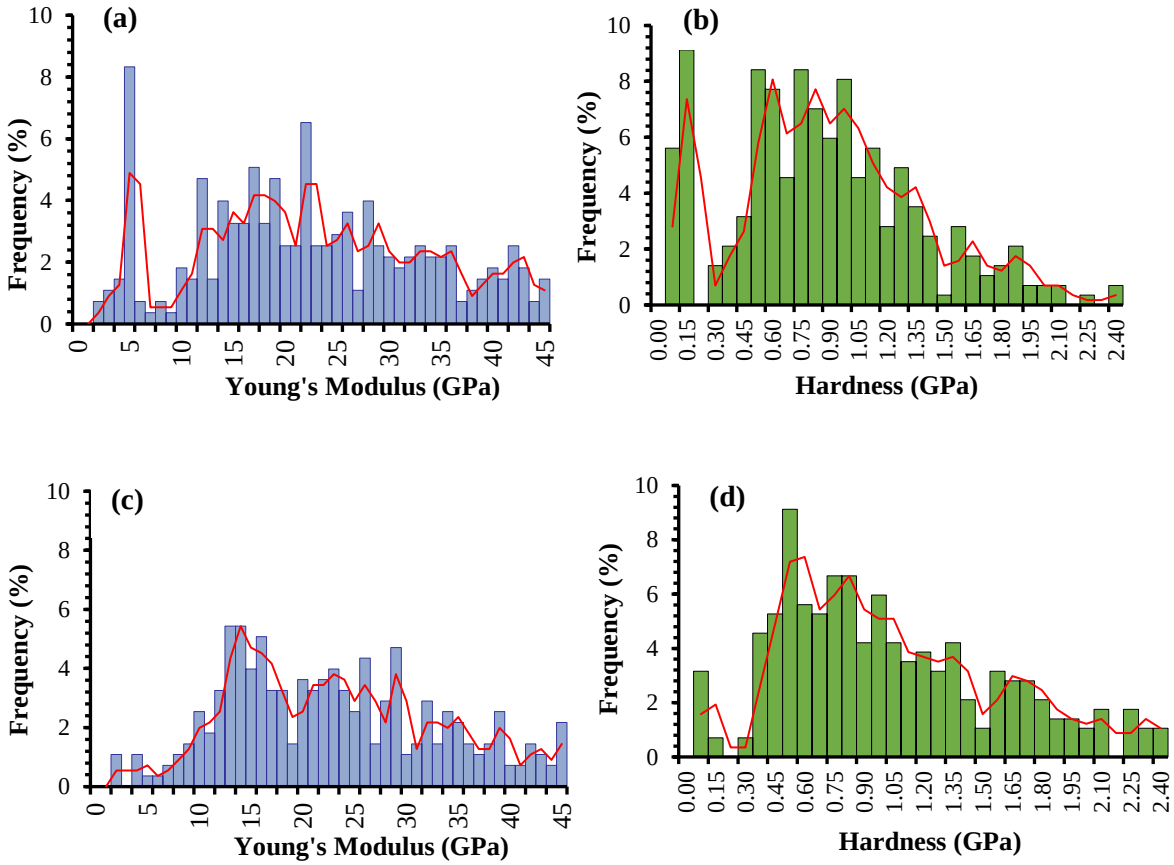

Fig. 7.12 Experimental elastic modulus and hardness frequency of OPC blended fly ash geopolymer: (a) and (b) FA-PC-NS0, and (c) and (d) FA-PC-NS2.

The frequency distributions of the elastic modulus and hardness values of the GGBFS and OPC blended geopolymer specimens with and without 2% nanosilica are presented in Fig. 7.11 and Fig.7.12, respectively. It is observed from Figs. 7.11 and 7.12 that elasticity and hardness values of the studied mixes did not change considerably because of the blending of fly ash with 10% OPC or 15% GGBFS. The intensity of the peaks for elasticity and hardness are almost similar for both the blended mixes. It is noteworthy that despite the differences in the chemical compositions and the amount of calcium oxide in OPC and GGBFS, the rate of polymer network formation and the types of hydrated gel formation are similar in both the mixes (FA-S-NS and FA-PC-NS) [1, 2, 3, 4]. Different peaks with certain range of elasticity

and hardness values were observed which could be assigned as a characteristic of each phase (Figs. 7.11 and 7.12). Similar to the specimen of fly ash-only geopolymer mixture (FA-NS0), elastic modulus of the hydrated gel was found to be within a range of 5.0 to 30.0 GPa. The average hardness values of hydrated gels were observed in a range of H = 0.4 to 1.1 GPa. The second phase intensity, centred at about E > 50.0 GPa and H > 5.5 GPa are attributed to the presence of unhydrated clinker phases which is believed to be the composition of calcite and mullite (Fig. 7.10). The third peaks intensity around E = 30.0 to 50.0 GPa is usually attributed to a mixture of the partial hydrated phase. Finally, the peak intensity of E<5 GPa is consider as a zone dominated by the porous or disintegrated areas.

To investigate the effect of nanosilica in the OPC and GGBFS blended fly ash geopolymer specimens, the volume fractions of different phases were calculated from the nanoindentation data. It can be seen from Table 7.1 that the extent of change in volume fractions of the hydrated phase in both OPC and GGBFS blended geopolymer specimens are very similar. This indicates that the formation of hydrated gels and the rate of microstructure formation are similar and comparable for both calcium reached fly ash based geopolymers with and without nanosilica. Co-existence of C-S-H with sodium aluminosilicate in the hydrated product was found in both OPC and GGBFS blended fly ash based geopolymers [1, 2, 4].

It can be seen from Table 7.1 that the volume fractions of the porous phases in geopolymer mixes with 2% nanosilica (FA-S-NS2 and FA-PC-NS2) are much lower than the values in the corresponding mixes without nanosilica. For example, volume fraction of the porous phase in the specimen of GGBFS blended mix (FA-S-NS) reduced from 12.5% to 9.1% with the inclusion of 2% nanosilica. The volume fraction of hydrated gel phase also increased from 68% (FA-S-NS0) to 81.1% (FA-S-NS2) by nanosilica. The rate of volume fraction changes for other

two phases (unreacted and partially reacted) are not significant with the addition of 2% nanosilica. In mix FA-S-NS2, the unreacted phase showed a minimal decrease than that of mix FA-S-NS0, while partially reacted phase showed a slight decrease from 8.9 % to 6.5%. Unreacted phases such as magnetite, hematite and mullite in OPC and GGBFS blended series were observed in Table 7.2. Calcite [Ca (CO_3)] and hauerite [Ca_3 (SiO_4)O] were also observed in OPC and GGBFS blended fly ash geopolymers.

Similar to the fly ash-only geopolymers, the increased reaction rate by the increase of the Si/Al and Na/Al molar ratios and the nucleation effect of nanosilica has increased the volume fraction of the hydrated product of the OPC and GGBFS blended geopolymers. This reduced the volume fraction of the porous phases and increased compressive strength. As shown in Table 7.2, the compressive strength increased by the inclusion of 2% nanosilica from 26 MPa to 65 MPa in the OPC blended mix and from 25 MPa to 76 MPa in the GGBFS blended mix.

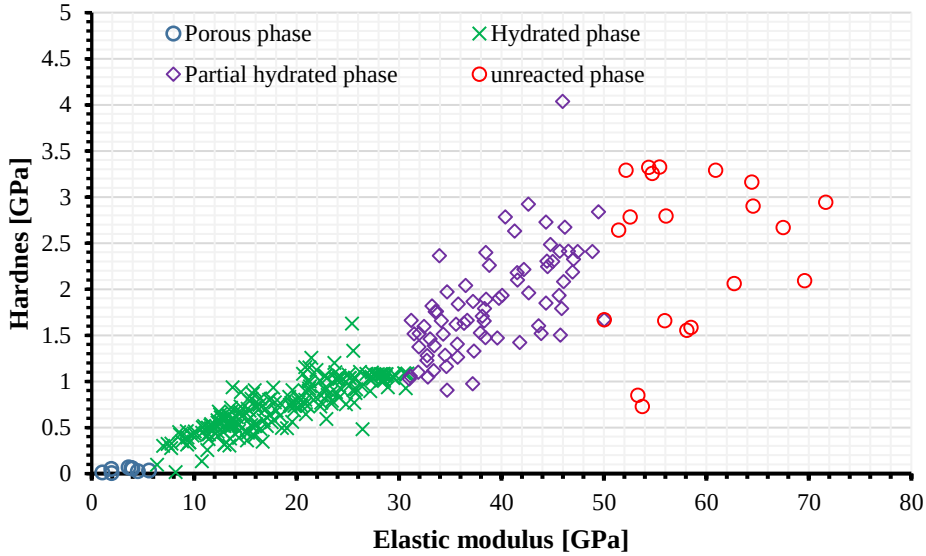

Fig. 7.13 E-modulus and hardness of fly ash only geopolymer mix.

The results of hardness values of hydrated, partially reacted, unreacted and porous phases of the fly ash-only geopolymer specimen (FA-NS0) are plotted against the corresponding elastic modulus values in Fig. 7.13. It can be seen that generally hardness tends to increase with the increase of elastic modulus, though there is a significant scatter in the data. For example in mix FA-NS0, the porous phase characterised by the elastic modulus value of E=0.0 to 5.0 GPa showed the hardness value of H=0.025 to 0.03 GPa. The aluminosilicate gel phase characterised by E=5.0 to 30.0 GPa showed hardness of H=0.3 to 1.1 GPa. Similarly, the partially activated phase characterized by E=30.0 to 50.0 GPa showed hardness of H=1.1 to 2.5 GPa, and the unreacted phase characterized by E> 50.0 GPa showed hardness H> 5.5 GPa. These values are similar to the elastic modulus and hardness values reported by other researchers [23, 24]. Moreover, the elastic modulus and hardness values of fly ash based geopolymer hydrates are similar to those measured on OPC cement hydrates [24, 25].

7.4 Determination of Local Mechanical Properties of ITZ

Nanoindentation test was carried out in the aggregate – geopolymer matrix interfacial areas (varying from 0 to 80 micrometre from the actual interface) at the top of the polished surface specimens. A photograph of a typical test specimen is shown in Fig. 7.14.

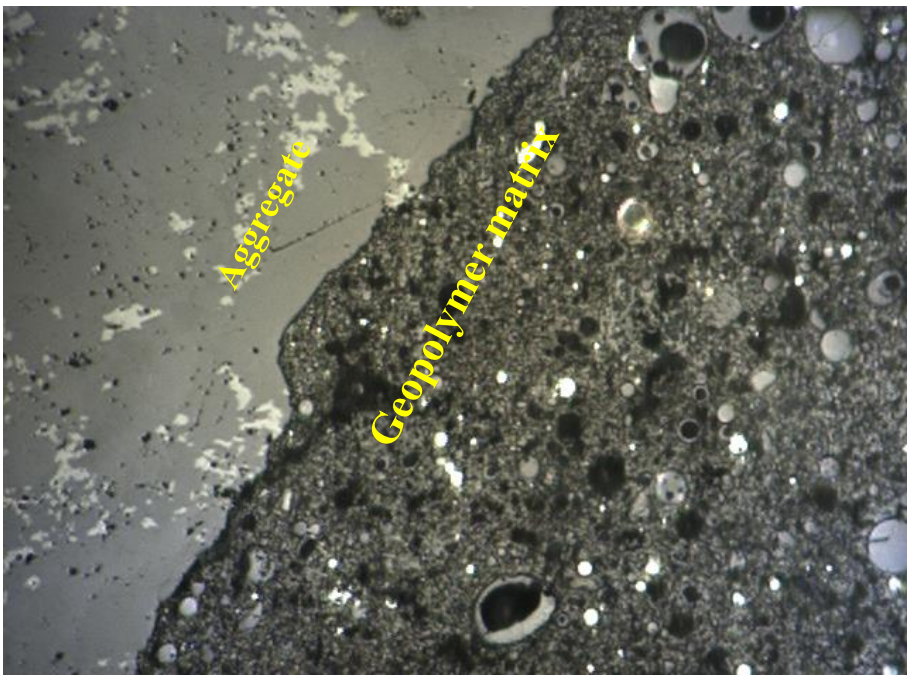

Fig. 7.14 Optical observation of the concrete and aggregate interface in fly ash based geopolymer concrete.

7.4.1 Analysis of the interfacial transition zone by SEM

A series of SEM images (Figs. 7.15 to 7.17) were taken from the flat polished surface of different fly ash based geopolymer concrete mixes to illustrate the interfacial transition zone between the aggregate and hydrated paste with 0 - 2% nanosilica. It is observed from the figures that binder and filler particles, aluminosilicate gel phase and the aggregates of various shades of grey reflected the compositional differences in the composite. A higher magnification was used in this case to examine the microstructure near the indent area to obtain an unbiased representation of the ITZ information with respect to its nanoindentation data.

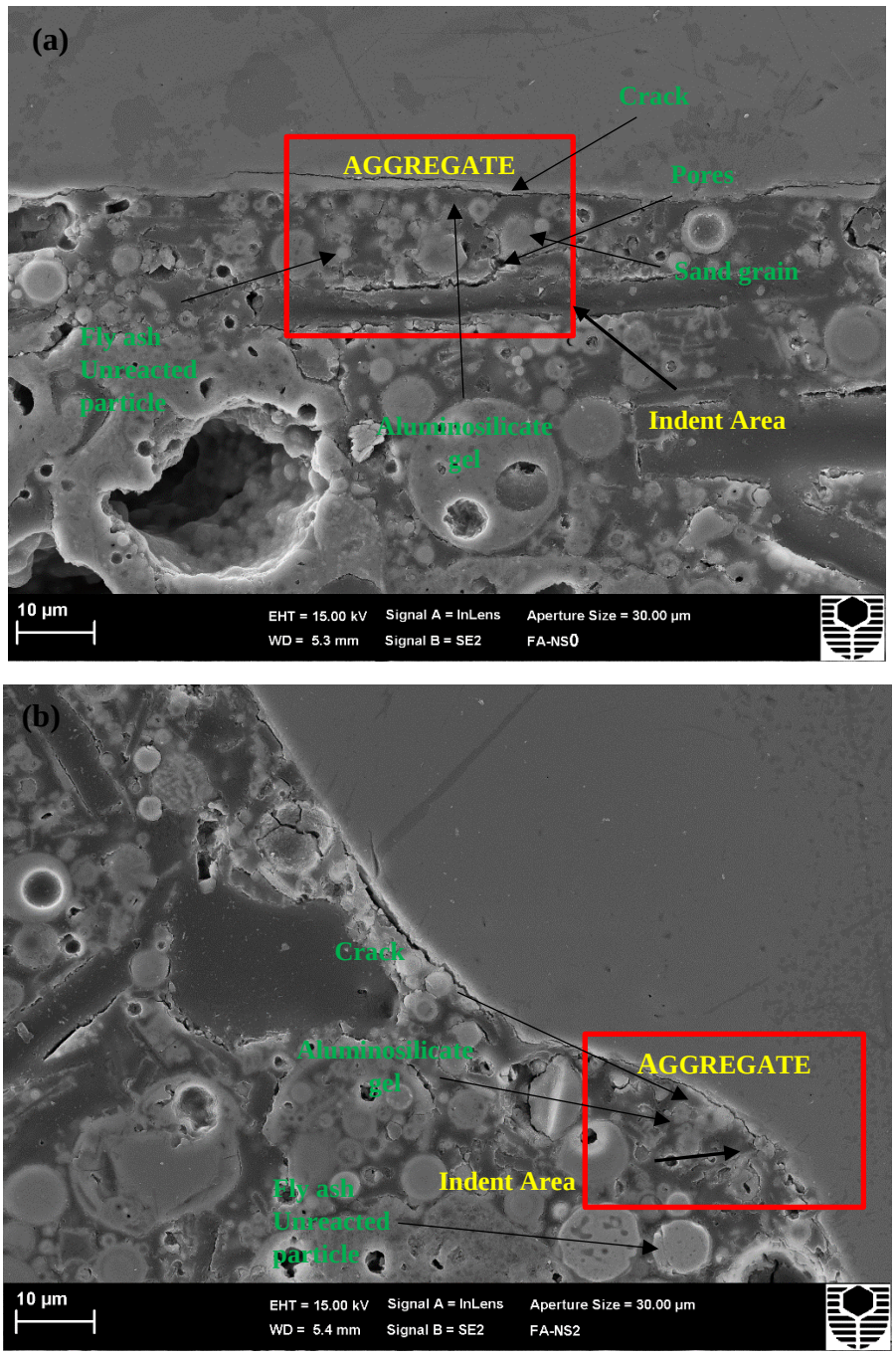

Fig. 7.15 SEM images of fly-ash only geopolymer containing nanosilica: (a) 0 wt. % (FA-NS0), (b) 2 wt. % (FA-NS2).

Different dimensions of small voids with micro cracks were observed near the aggregate and hydrated paste interface of fly ash only geopolymers (Fig. 7.15). A continuous

long crack, larger pore diameter with a significant amounts of untreated particles near the aggregate was observed in FA-NS0 (in the indent area). However, it appears from the Fig. 7.15b that the ITZ characteristic of mix FA-NS2 significantly modified with 2% nanosilica. It is noteworthy that adding of 2% nanosilica in fly ash based geopolymer series, the transition zone of geopolymer concrete has become denser and the size of the voids and crack width were reduced. It seems that the dual effects of nanosilica such as the nucleation effects which eventually increased the amount of aluminosilicate gel along with the filler effects of nanosilica filled the gap between the aggregate and unreacted particles and produced more uniform and denser transition zone. This indicates that a denser microstructure was achieved for fly ash only geopolymer mix with 2% nanosilica and the formation of geopolymer hydrated phase in the ITZ of aggregate was mainly influenced by the wall effect and the degree of geopolymerisation rate.

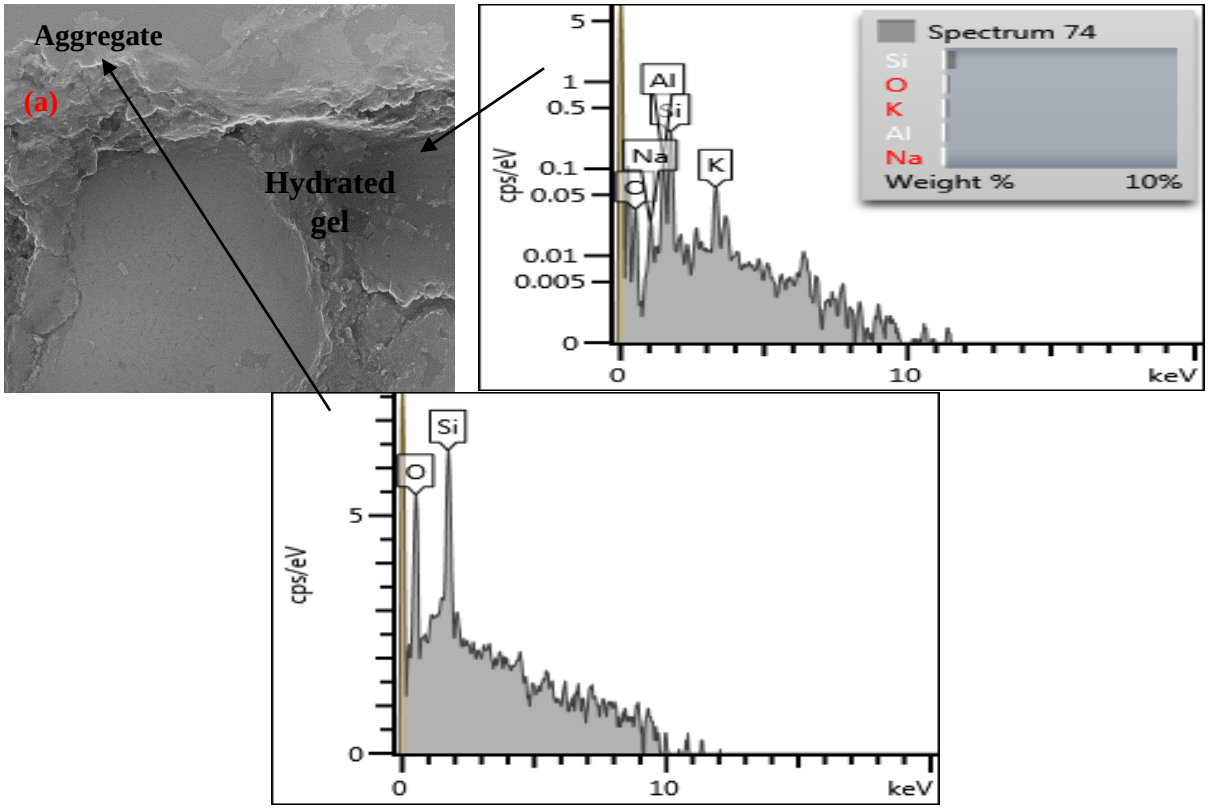

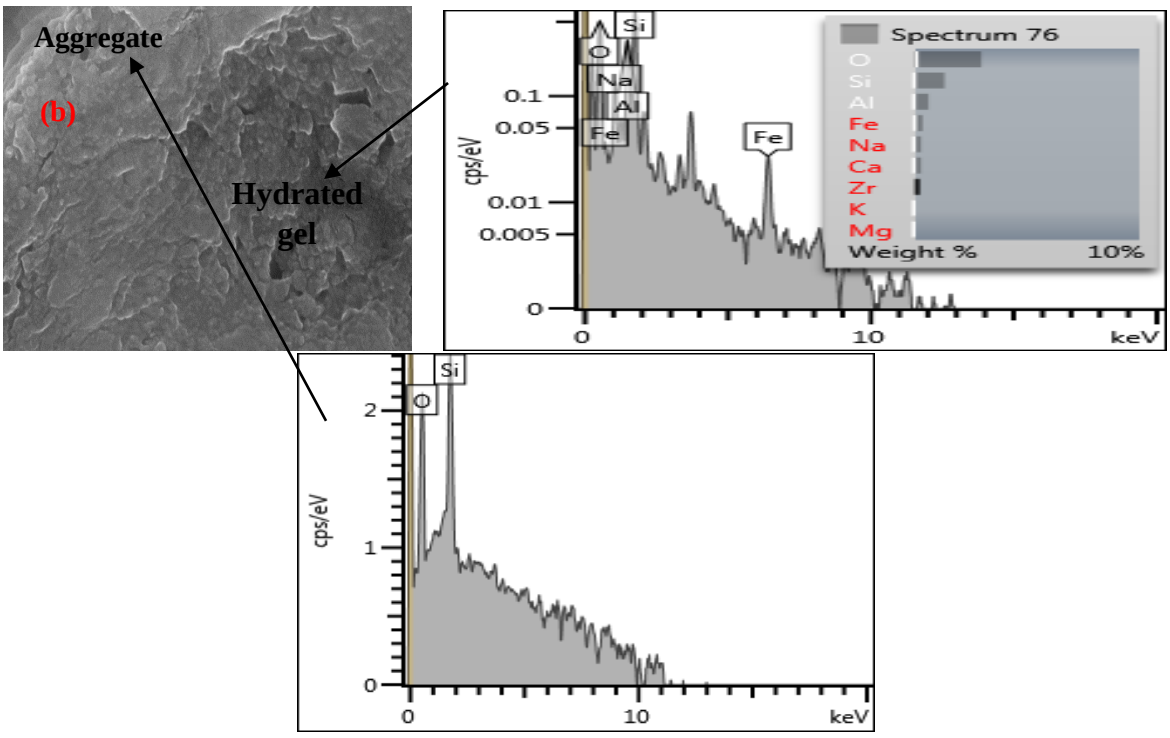

Fig. 7.16 EDX spectra of fly ash only geopolymer containing nanosilica: (a) 0 wt. % (FA-NS0), (b) 2 wt. % (FA-NS2).

EDX spectrum analysis was carried out for fly ash only geopolymer concrete together with the SEM analysis in the indent area. The EDX line analysis was performed at the top of an aggregate and in the hydrated phase area at different locations, as shown in Fig. 7.16. The main element detected at the top of the aggregate is Si. On the other hand, the main elements detected in the hydrated area are Al, Si, Na and Fe. Presence of these elements indicated the formation of sodium aluminosilicate gel in both the mixes.

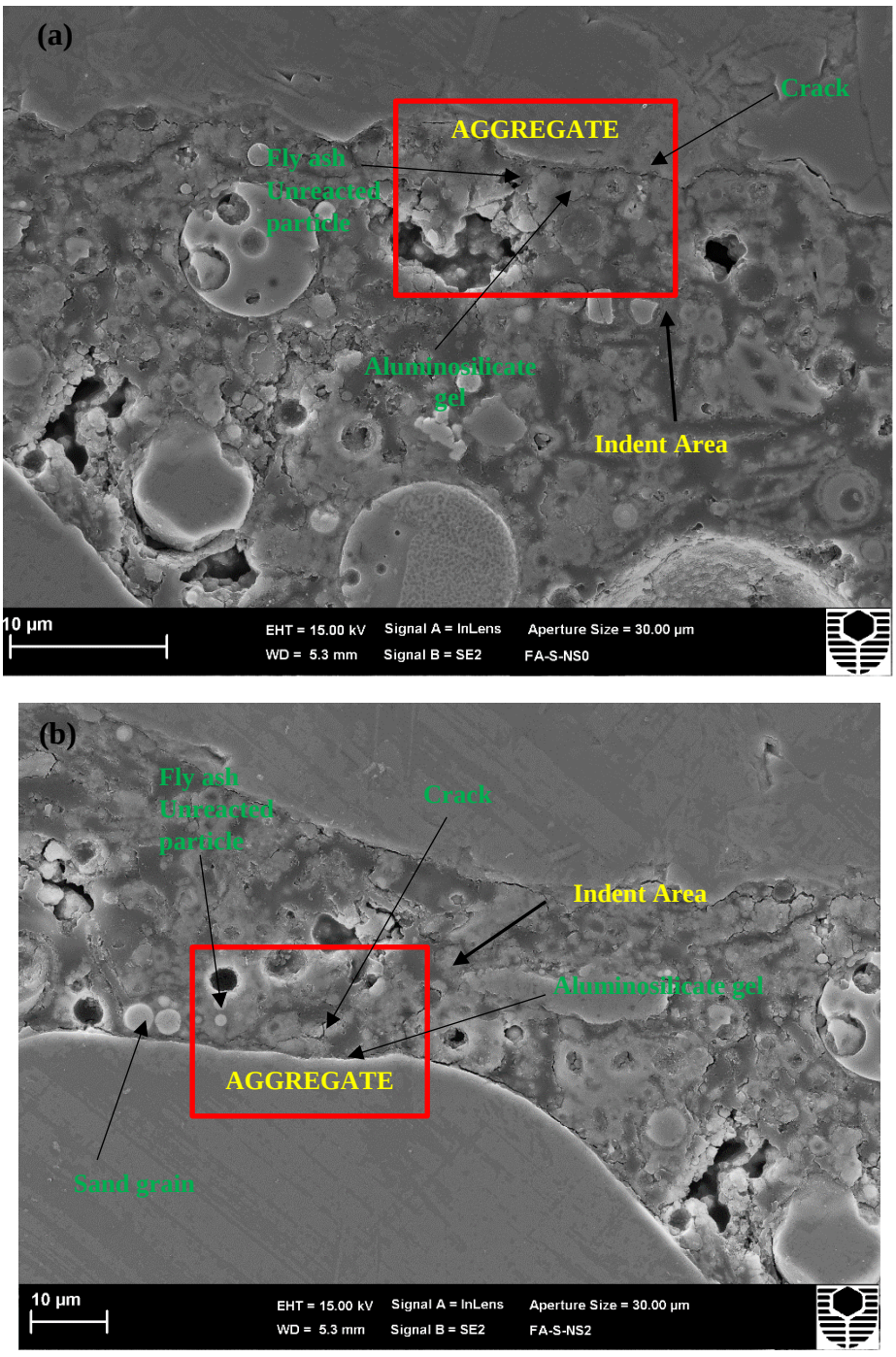

Fig. 7.17 SEM images of GGBFS blended fly ash based geopolymer containing nanosilica: (a) 0 wt. % (FA-NS0), (b) 2 wt. % (FA-NS2).

Figs. 7.17 and 7.18 showed an SEM images together with the EDX analysis on the GGBFS blended fly ash geopolymer concrete with 0% and 2% nanosilica, cured at room

temperature for 28 days. It is noted from Fig. 7.17 (a) that a large amount of porous areas with large visible cracks was observed in the mix FA-S-NS0 without nanosilica. However, it is found that due to the filling and nucleation effects of nanosilica, in mix FA-S-NS2 (Fig.7.17b), the ITZ between the aggregate and hydrated phase are less porous and width of the cracks are smaller than that of Fig. 7.17 (a) (visual inspection). Moreover, it noteworthy that mix FA-S-NS0, the wall effect mechanism where the large amount of unreacted particles from fly ash and GGBFS along with the sand grain are less densely packed in the vicinity of the aggregate as compared to that observed in the mix with 2% nanosilica. This indicates that that lower porosity of the ITZ in FA-S-NS2 with 2% nanosilica pointed out a stronger and more durable interface between the gel matrix and aggregates.

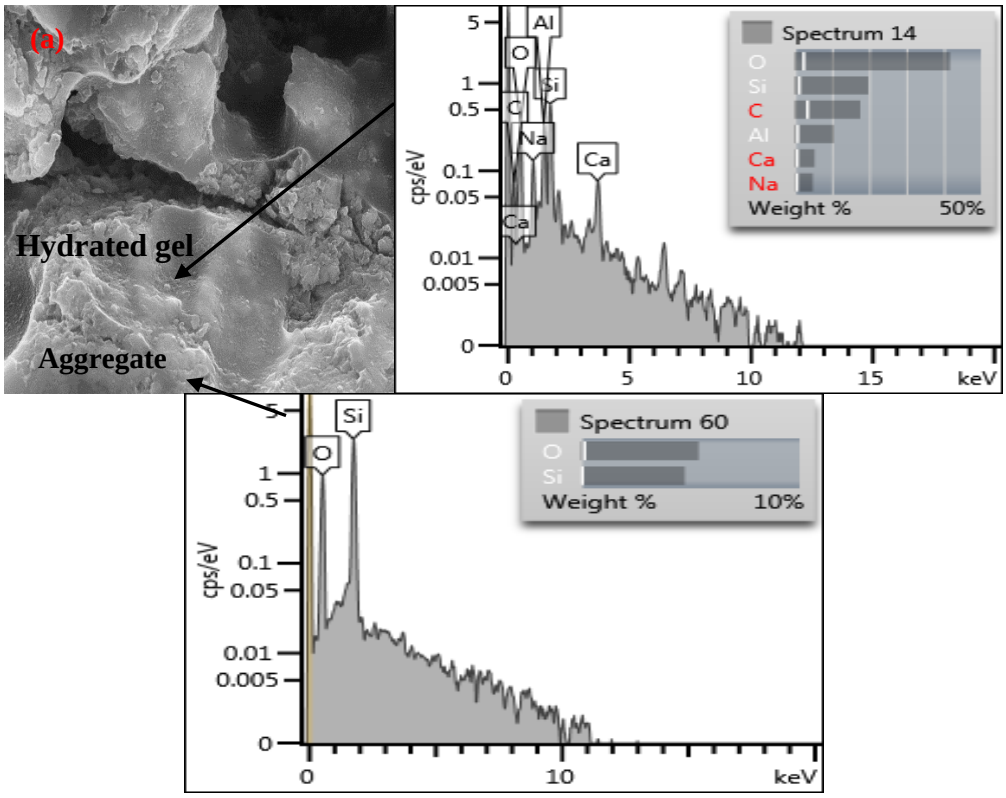

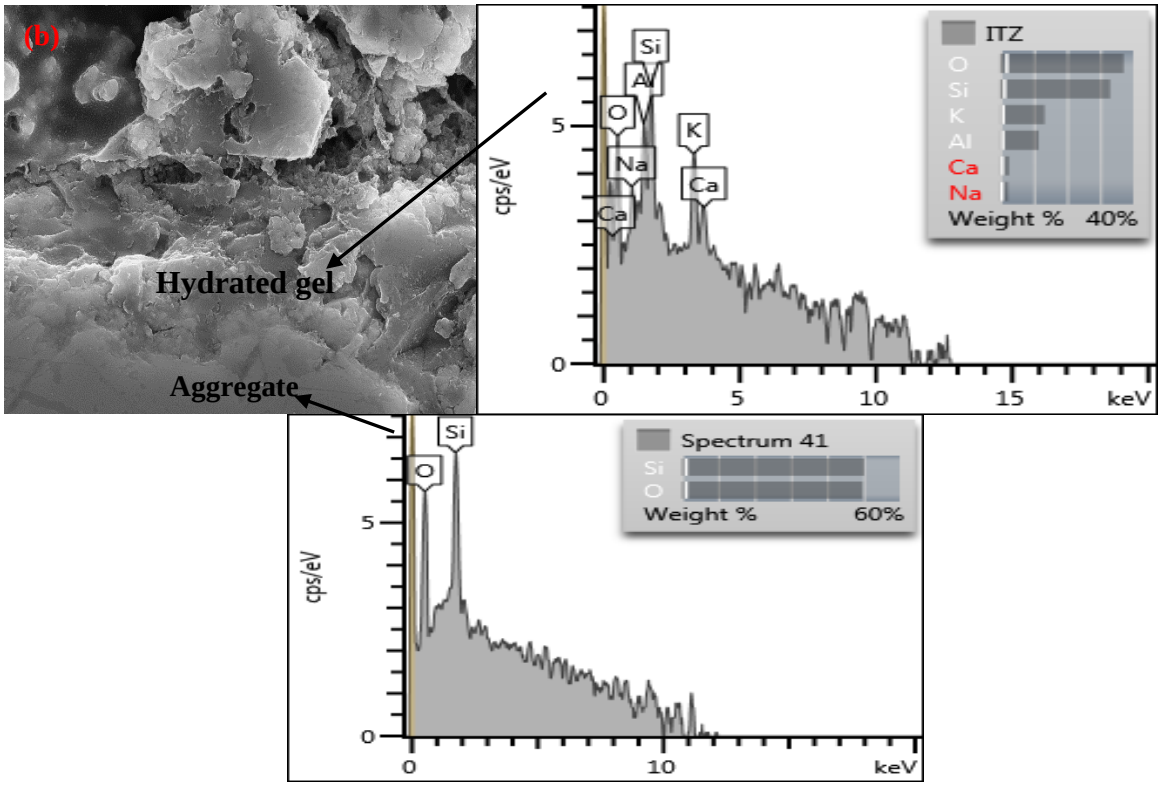

Fig. 7.18 EDX spectra of GGBFS blended fly ash based geopolymer containing nanosilica: (a) 0 wt. % (FA-S-NS0), (b) 2 wt. % (FA-S-NS2).

EDX analysis was also carried out for FA-S-NS0 and FA-S-NS2 mixes in the aggregate and bulk gel matrix to identify the elements. The main elements in the bulk matrix were detected as Na, Al, Si and Ca for both mixes. Whereas in the aggregate phase element was mostly composed of Si.

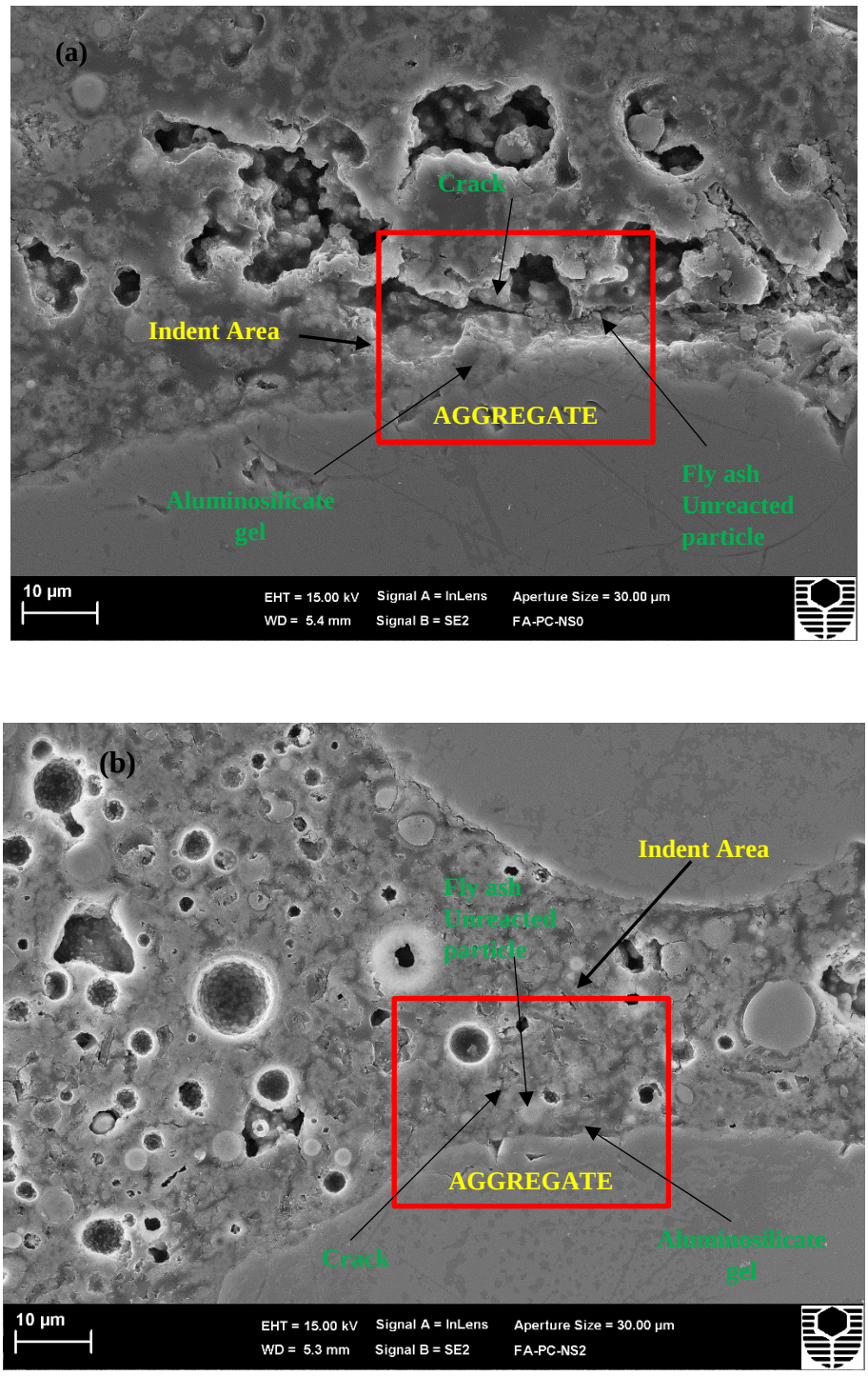

Fig. 7.19 SEM images of OPC blended fly ash based geopolymer containing nanosilica: (a) 0 wt. % (FA-PC-NS0), (b) 2 wt. % (FA-PC-NS2).

Figs. 7.19a and 7.19b show that SEM images of the ITZ for OPC blended fly ash based geopolymer mixes with 0% and 2% nanosilica. It can be seen that mix FA-PC-NS2 with 2%

nanosilica had lower porosity in the ITZ than that with 0% nano silica. It is apparent from Fig. 7.19b that the hydrated paste of mix FA-PC-NS2 adjacent to the aggregate is dense and not particularly porous. On the contrary, a relatively loose bond between the hydrated paste and aggregate can be seen with microcracks intersecting the paste-aggregate contact area for mix FA-PC-NS0 (Fig. 7.19a). This reflects the patchy and irregular distribution of the gel phase and unreacted particles within the ITZ area, which is similar to that was found in the other fly ash-only geopolymer specimens without nanosilica in the previous section.

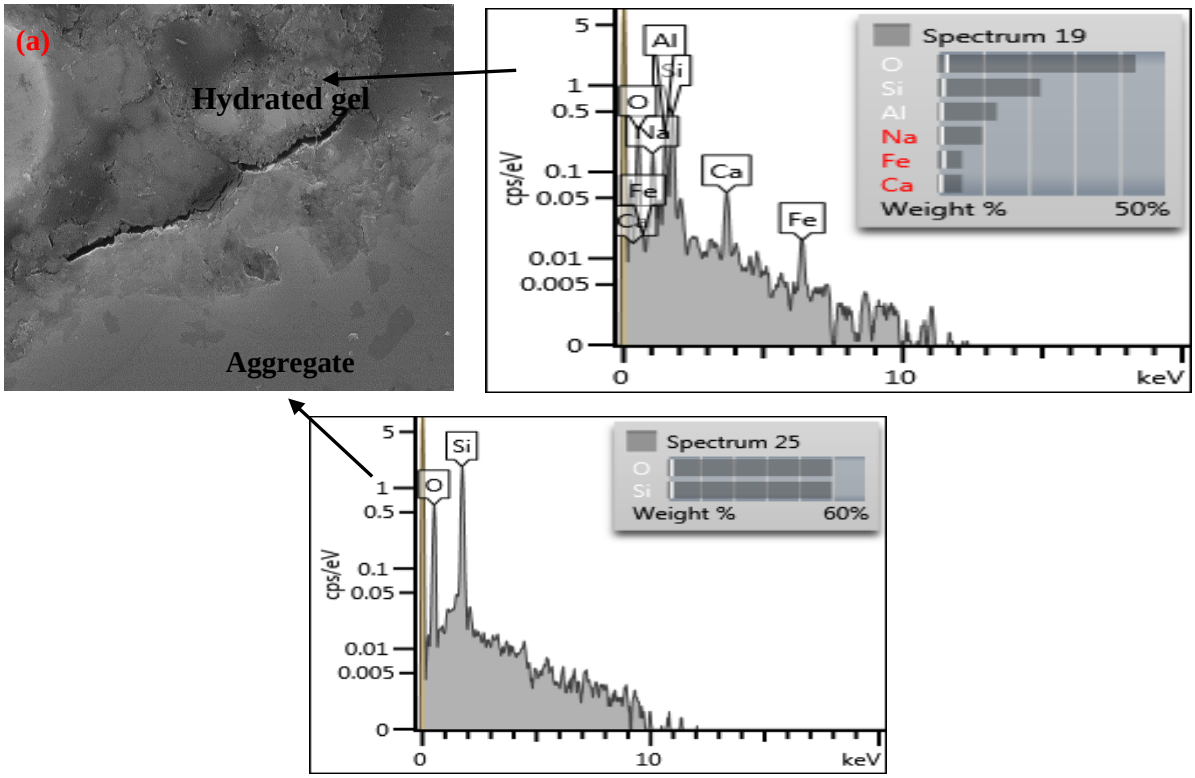

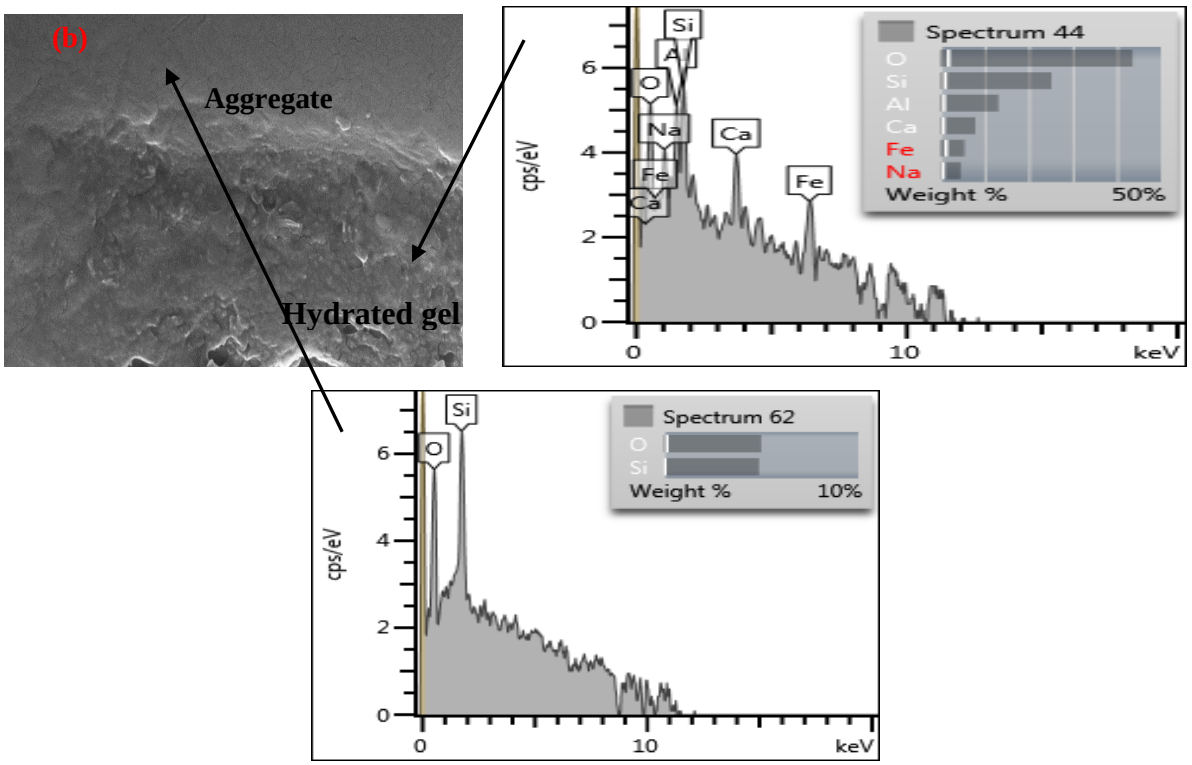

Fig. 7.20 EDX spectra of OPC blended fly ash based geopolymer containing nanosilica: (a) 0 wt. % (FA-NS0), (b) 2 wt. % (FA-NS2).

Fig. 7.20 shows the EDX spectrum of OPC blended fly ash based geopolymer with 0% and 2% nanosilica. It is observed from the figure that both mix contains Na, Al, Si and Ca element. Whereas in the aggregate face element was mostly composed of Si.

7.4.2 Properties of geopolymer ITZ determined by nano indentation

Evaluation of the elastic modulus by nanoindentation along with the SEM images provided a comprehensive insight into the characteristics of ITZ around aggregates in geopolymer concretes of different binder compositions. The typical load-penetration hysteresis curves of nano-indentations in the ITZ area are shown in Fig. 7.21.

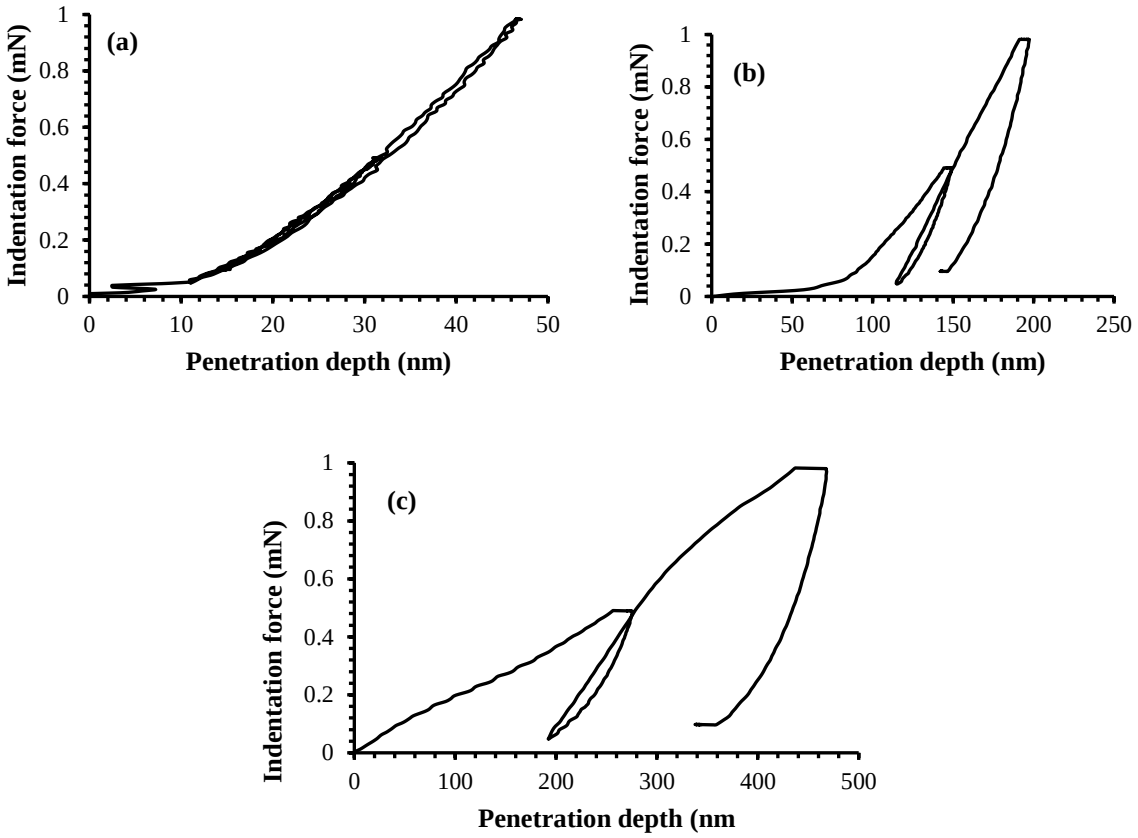

Fig. 7.21 Typical load–indention curves of fly ash geopolymer (a) aggregate (b) aluminosilicate gel and (c) Void or porous phase

The steady P-h curve of Fig. 7.21 (b) shows very clear loading and unloading paths indicating a well-arranged structure of aluminosilicate gel in the vicinity of an aggregate. On the other hand, it is noted from the Figs. 7.21a and 7.21c that the load reached its maximum value at much lower and higher displacements for the aggregate and porous phase, respectively. This eventually resulted in higher and lower elasticity values of the aggregate and porous phase, respectively. It is noteworthy that the weak bonds or the voids in the heterogeneous microstructures exhibited higher amount of displacement for a given load (Fig. 7.21c) than those in the other three different phases.

The elastic modulus values were determined in the regions of -20 µm <L<0 µm, and 0 µm <L<60 µm from the aggregate surface. The region of -20 µm <L<0 µm is in aggregate

phase, whereas the region of 0 µm <L<60 µm distance is in the geopolymer matrix. The results are plotted in Figs. 7.22 to 7.24.

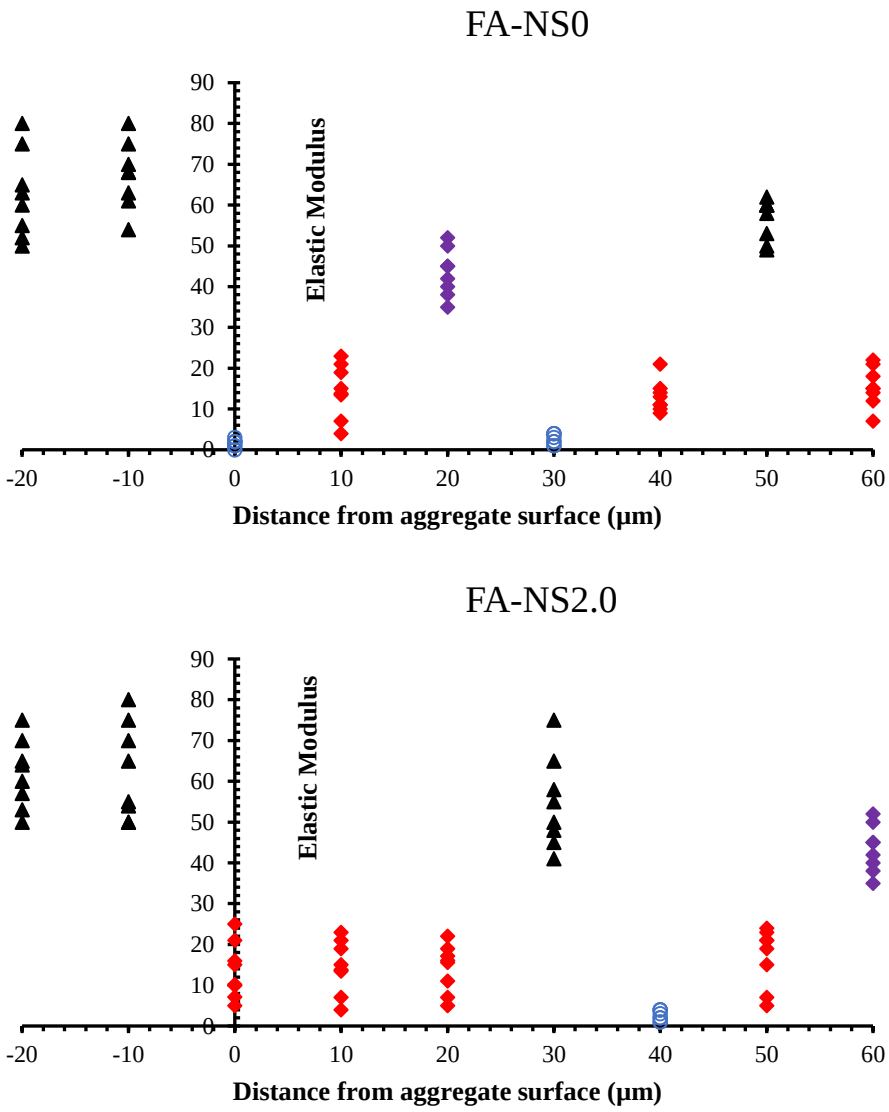

Fig.7.22 Elastic modulus profile in the ITZ of fly ash only geopolymer concrete with 0% and 2% nanosilica

It can be seen from Fig. 7.22 that the elastic modulus for fly ash only geopolymer mixes with 0% and 2% nanosilica varied from 0 GPa (for porous) to 87 GPa (for unreacted). Such large differences in E values were due to the variable nature of the hydrated matrix, present in the aluminosilicate gel. The results in Fig. 7.22 for FA-NS0 (without nanosilica) also revealed

the presence of four distinct phases starting and ending at different distances from the aggregate interface depending on the constituent. It is noted from the figure that the area closest to the aggregate surface (0 μm), the modulus declined to a minimum value that ranged from 0.00 to 5.00 GPa which indicates the presence of high porosity in that area. These values are consistent with the SEM observation in Fig. 7.16a that pointed out hydrated phase dominated by cracks and disintegrated phases in the proximity of aggregates. It is noted from Fig. 7.22 that modulus of elasticity was in the range of 5.00 GPa to 50.00 GPa in the region of 10 to 20 μm from the aggregate surface. The value then decreased to 0.00-5.00 GPa at 30 μm and again picked within range of 5.00 -60.00 GPa in the region of 40-60 μm distance.

The addition of 2% nanosilica in fly ash only geopolymer produced a competing effects: it contributes additional aluminosilicate gel through the geopolymirization process. The E value of the ITZ (Fig. 7.22) was in a range of 5.00 GPa to 25.00 GPa up to 20 μm distance, with porous phase (0.00-5.00 GPa) at 30 μm region. Generally, the ITZ this specimen showed higher E-modulus values than FA-NS0.

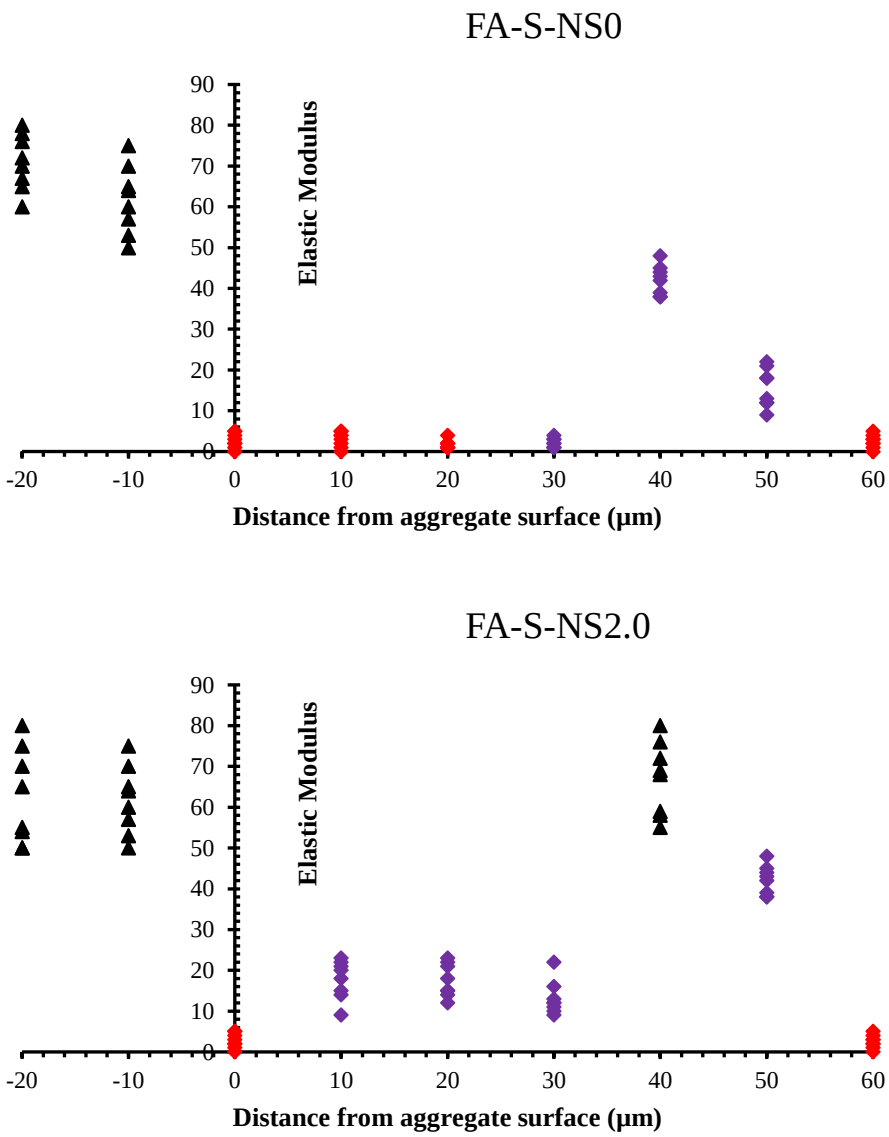

Fig.7.23 Elastic modulus profile in the interfacial transition zones of GGBFS blended fly ash based geopolymer concrete with 0% and 2% nanosilica.

In the specimen of mix FA-S-NS0, elastic modulus was in a range of 0 GPa to 5 GPa at distances up to 30 µm and 60 µm. The elastic modulus then varied from 0.0 to 40 GPa in the region of 40 to 60 µm. For the specimen of mix FA-S-NS2, the corresponding values were in the range of 0.0 to 22 GPa up to 30 µm, and then 0.0 to 80 GPa in the region of 40 to 60 µm.

Thus 2% nanosilica increased the elastic modulus of the ITZ of the GGBFS blended fly ash geopolymer concrete.

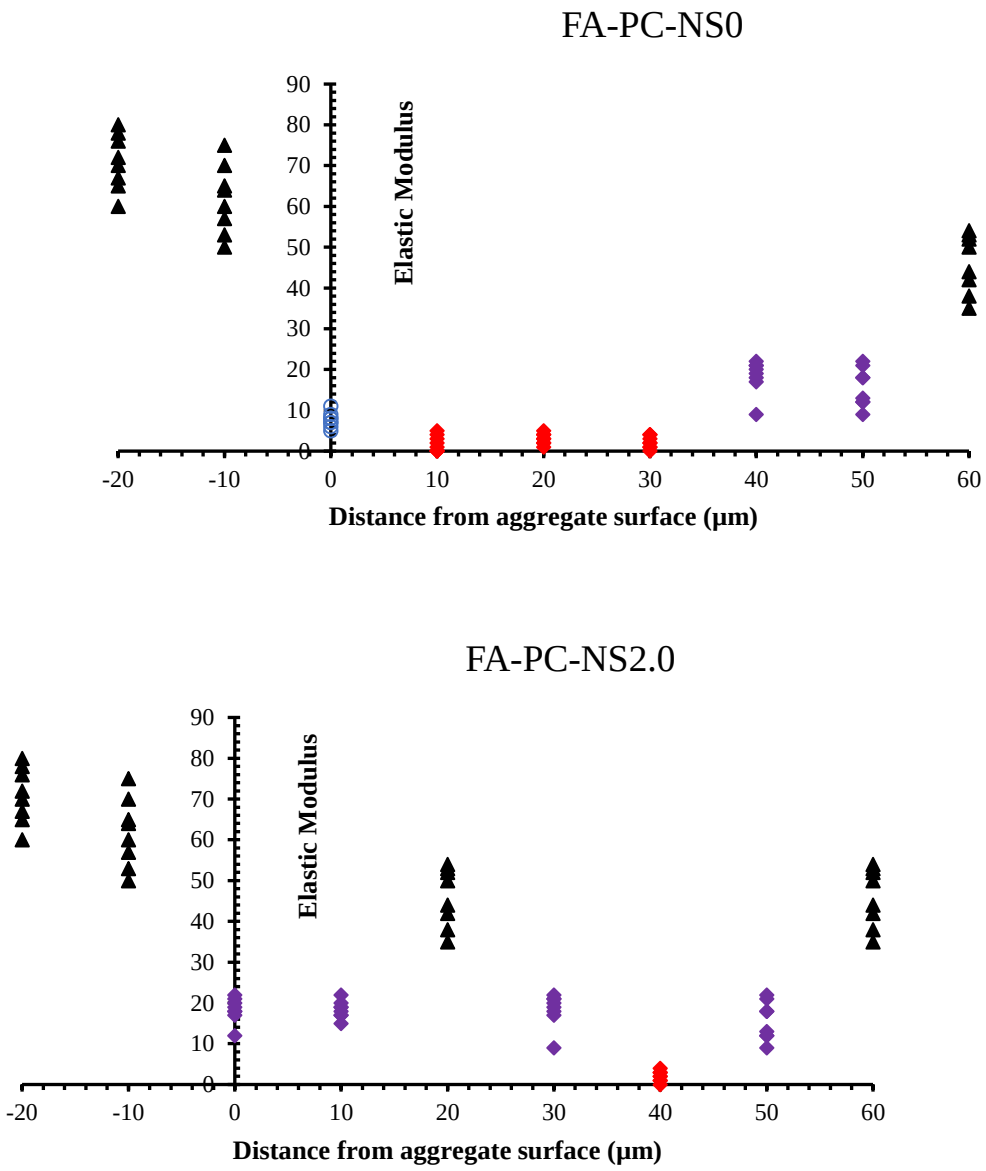

Fig.7.24 Elastic modulus profile in the interfacial transition zones of OPC blended fly ash based geopolymer concrete with 0% and 2% nanosilica, an aggregate and hydrated paste matrix interfacial zone.

A typical result of modulus of elasticity for OPC blended fly ash geopolymer concrete versus distance from the aggregate interface is shown in Fig.7.24. Various E- values in a range

of 0 to 55 GPa were found in the region of 0 to 60 µm from the aggregate surface. For FA-PC-NS0, E values were found in a range of 6-11 GPa at the interface and then 0-5 GPa were noted at distances up to 30 µm. Elastic modulus of 9 GPa to 52 GPa were found in the region of 40 µm to 60 µm.

A different trend was observed in the elastic modulus profile of mix FA-PC-NS2. It was noted from the figure that the results showed a significant variations at the same distance from the interface when the values were compared with the mix FA-PC-NS0. The elastic modulus values were in a range of 11 to 50 GPa up to 30 µm and then 0 to 55 GPa in the region of 40 µm to 60 µm. Thus, nanosilica generally increased the elastic modulus of the ITZ of the OPC blended fly ash geopolymer concrete.

7.5 Summary

Nanoindentation tests were carried out on different fly ash based geopolymer paste samples and in the ITZ of concrete specimens. Hardness and elastic modulus were calculated using Oliver and Pharr method, and statistical techniques were used to analyze the data. Analysis of the test data showed that inclusion of 2% nanosilica reduced the porous phase and increased the aluminosilicate gel phase as compared to the corresponding control mix. The elastic modulus of the ITZ was also found to enhance by the use of nanosilica. This is consistent with the SEM images showing less porous and disintegrated phases in the ITZ of the specimens containing nanosilica.

7.6 Reference

1. J. Nemecek, V. Šmilauer, L. Kopecky, Nanoindentation characteristics of alkali-activated aluminosilicate materials. CemConcr Compos 2011; 33:163–70.

2. P. Deb, P. Nath, P.K. Sarker, The effects of ground granulated blast-furnace slag blending with fly ash and activator content on the workability and strength properties of geopolymer concrete cured at ambient temperature, Mater. Des.62 (2014) 32e39
3. P. Nath, P. K. Sarker, Effect of GGBFS on setting, workability and early strength properties of fly ash geopolymer concrete cured in ambient condition Constr. Build. Mater., 66 (2014) 163–171.
4. P. Nath, P.K. Sarker, Use of OPC to improve setting and early strength properties of low calcium fly ash geopolymer concrete cured at room temperature." Cem. Concr. Comp., 55 (2015) 205–214.
5. W.C.Oliver, G.M.R. Pharr, An improved technique for determining hardness and elastic modulus using load and displacement sensing indentation experiments. J Mater Res 1992; 7:1564–83.
6. A.C. Fisher-Cripps, Nanoindentation, vol. 1. Berlin: Springer; 2002. p. 2–16.
7. S. Timoshenko, J.N. Goodier, Theory of Elasticity, 2nd Ed. McGraw-Hill, N.Y. 1951.
8. E.S. Berkovich, "Three-faceted diamond pyramid for micro-hardness testing," Ind. Diamond Rev. 11 127, 1951, pp. 129–133.
9. G. Constantinides, K. Ravi Chandran, F.-J. Ulm, K. Van Vliet, Grid indentation analysis of composite microstructure and mechanics: principles and validation, Mater. Sci. Eng. A 430 (1) (2006) 189–202.
10. G. Constantinides and F. J. Ulm. The nanogranular nature of C-S-H. Journal of the Mechanics and Physics of Solids, 55(1):64–90, 2007

11. H.Lee, V. Vimonsatit, P. Chindaprasirt, Mechanical and micromechanical properties of alkali activated fly-ash cement based on nanoindentation. Construction and Building Materials 107(2016) 95-102.
12. F. Pelisser, P.J.P Gleize, M.D. Michel, Nanomechanical properties of cement paste, IBRA. de Estruturas e Materiais 4 (2011) 561–74.
13. G. Constantinides, F.J. Ulm, The effect of two types of C–S–H on the elasticity of cement-based materials: results from nanoindentation and micromechanical modelling, Cem Concr Res 34 (2004) 67–80.
14. F.J. Ulm, M. Vandamme, C. Bobko, J.A. Ortega, K. Tai, C. Ortiz, Statistical indentation techniques for hydrated nanocomposites: concrete, bone, and shale, J Amer. Ceram. Soci. 90 (9) (2007) 2677–2692
15. R.F. Feldman, J.J. Beaudoin, Microstructure and strength of hydrated cement, Cem. Concr. Res. 6 (1976) 389–400.
16. L. Sorelli, G. Constantinides, F.J. Ulm, F. Toutlemonde, The nano-mechanical signature of ultra high performance concrete by statistical nanoindentation techniques, Cem Concr Res 38 (2008) 1447–56.
17. P. Trtik, B. B. Münch, P. Lura, A critical examination of nanoindentation on model materials and hardened cement pastes based on virtual experiments, Cem. Concr. Compos. 31 (2009) 705–14.
18. P. Lura, Münch, P. Trtik, Validity of recent approaches for statistical nanoindentation of cement pastes, Cem, Concr, Compos. 2011; 33 (2011) 457–65.
19. F. Pelisser, P.J.P Gleize, M.D. Michel, Nanomechanical properties of cement paste, IBRA. de Estruturas e Materiais 4 (2011) 561–74.

20. G. Constantinides, F.J. Ulm, The effect of two types of C–S–H on the elasticity of cement-based materials: results from nanoindentation and micromechanical modelling, Cem Concr Res 34 (2004) 67–80.
21. A. Fernandez-Jimenez, A. Palomo, Composition and microstructure of alkali activated fly ash mortars. Effect of the activator, Cem. Concr. Res. 35 (2005) 1984–92.
22. M. Rowles, NB.O'Connor,. Chemical optimisation of the compressive strength of aluminosilicate geopolymers synthesised by sodium silicate activation of metakaolinite. J Mater Chem 2003;13:1161
23. J.S.J. Deventer, J.L. Provis, P. Duxon, G.C. Lukey, Reaction mechanisms in the geopolymeric conversion of inorganic waste to useful products, J. Hazard. Mater., 139 (3) (2007) 506-13.
24. A. Palomo, P. Krivenko, L.L. Garcia, E. kavalerova, O. Maltseva, F.A. Jimenez, Review on alkaline activation: new analytical perspectives, Mater. De. Constr., 64(315) (2014) e022.
25. P. Duxson, J.L. Provis, G.C. Lukey, S.W. Mallicoat, W.M. Kriven, J.S.J. Deventer, Understanding the relationship between geopolymer composition, microstructure and mechanical properties, Colloid Surf. A: Physicochem. Eng. Asp., 269 (2005) 47-58.

Every reasonable effort has been made to acknowledge the owners of copyright material. I would be pleased to hear from any copyright owner who has been omitted or incorrectly acknowledged.

CHAPTER 8
SULPHATE RESISTANCE OF FLY-ASH BASED GEOPOLYMER

8.1 Overview

In previous studies [1, 2, 3, 4] fly ash based geopolymer generally demonstrated a high resistance to sulphate attack and therefore, it can be considered as a potential alternative to Portland cement based binders for high sulphate environments. For this reason, the resistance and applicability of fly ash geopolymer binders against sulphate attack were studied in two different stages. In the first stage, effects of the inclusion of nanosilica in geopolymer mortars with different mixture compositions exposed to 5% sodium sulphate and magnesium sulphate solutions were studied at different ages. In the second stage, the possible application of geopolymer as a protective layer on OPC concrete was studied. A 25-mm thick geopolymer mortar or concrete layer was applied around an OPC concrete core and submerged in 5% sodium sulphate solution for 240 days in order to investigate the effectiveness of geopolymer as a protective barrier to OPC concrete in high sulphate environments. The deterioration of the specimens was evaluated by monitoring the visual appearance, mass changes, failure mode and changes in compressive strength. The sulphate solution was replaced weekly and the pH level was monitored regularly to maintain the designated pH of 7.0. The specimens were removed from the sulphate solution after the exposure period and brushed carefully to remove the loose particles from its surface. They were then left for drying under room temperature for 1hr before conducting the measurements.

8.2 Sulphate resistance of fly ash based geopolymer mortar

8.2.1 Visual appearance

Visual appearance of fly ash based geopolymer mortars with and without nanosilica after 120 days of sodium sulphate exposures are presented in Figs. 8.1. Geopolymer mortar specimens were carefully examined at regular intervals to monitor the visible signs of cracking, spalling and delamination under the sulphate attack. The specimens were removed from the sulphate solution after the exposure period and brushed carefully to remove the loose particles from its surface. They were then left for drying under room temperature for 1hr before recording the mass changes.

The extent of deterioration in a sample was classified on a rating scale of 0 to 5, with 0 = no damage, 1 = minor hair line crack, 2 = visible crack, 3 = eroded surface, 4 = clearly disintegrated and distorted and 5 = completely disintegrated and distorted. The appearance of geopolymer specimens without exposure conditions was considered as the reference to create the rating scale. It is noteworthy that sign of deterioration and cracking were observed similar for both sodium and magnesium sulphate exposed geopolymer specimens, hence, figure for only sodium sulphate solution is attached in this section.

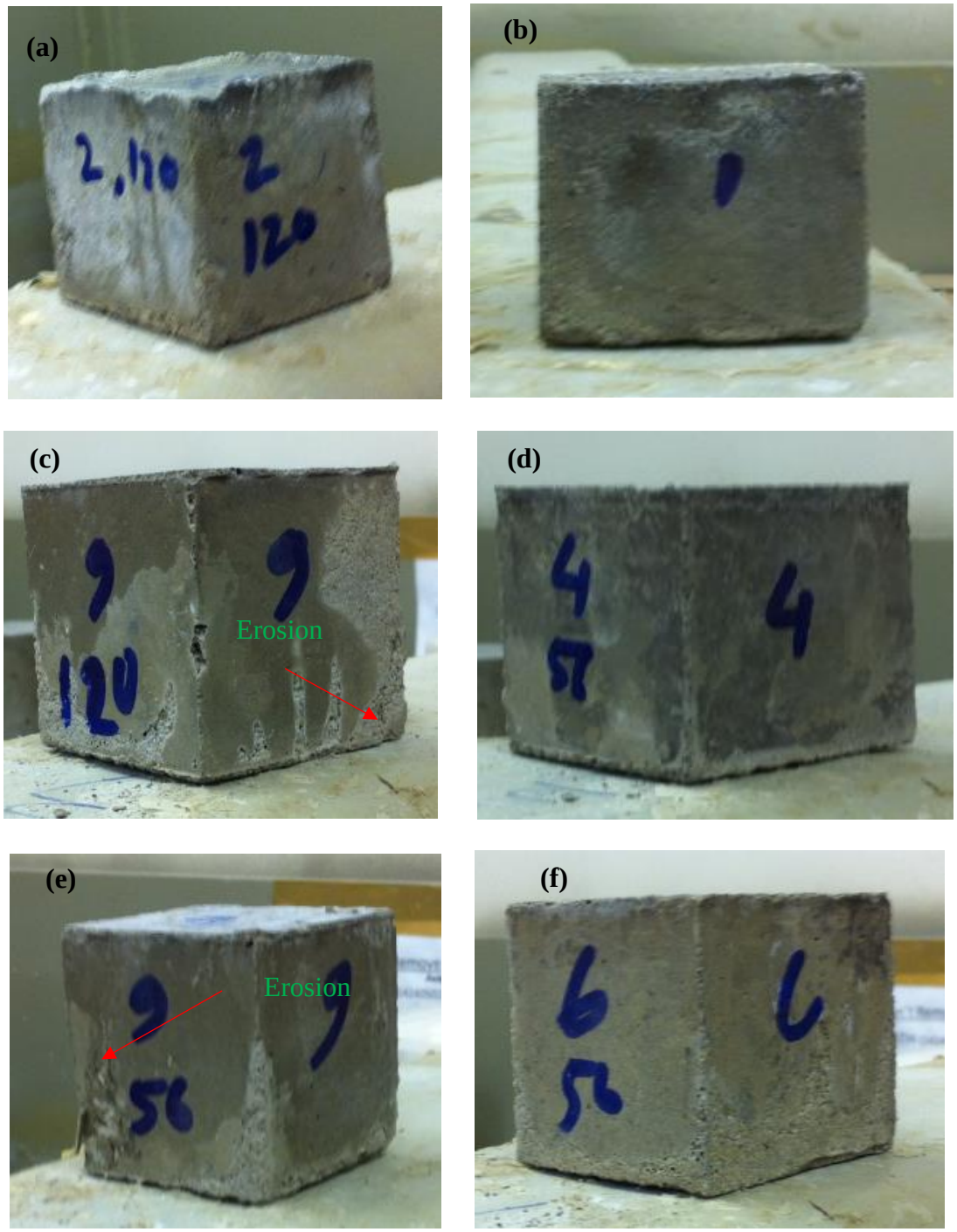

Fig. 8.1 Visual appearance of geopolymer mortar specimens in 5% sodium sulphate solution after 120 days of exposure (a) FA-NS0, (b) FA-NS2 (c) FA-PC-NS0, (d) FA-PC-NS2, (e) FA-S-NS0, (f) FA-S-NS2

It is noted from the Fig. 8.1 that the surface of fly ash only geopolymer specimens didn't show any evidence of deterioration, signs of cracking, disintegration or changes in the external

appearance. However, some minor disintegration was observed for OPC and GGBFS blended mortar specimens without nanosilica. For example, the visual rating of specimen FA-NS0 (Fig. 8.1 a) was observed within the range of 0-1 which indicates no visible sign of cracks or surface distortion after 120 days of exposure both in sodium and magnesium sulphate solutions. Same phenomenon was observed for fly ash only geopolymer mortar specimens with 2% nanosilica (Fig. 8.1b).

GGBFS and OPC blended fly ash based geopolymer mortar without nanosilica soaked in sulphate solutions (sodium and magnesium) started to erode after 75 days of exposure. Some cracks and side spalling were observed in these specimens after 120 days of sulphate exposure (Figs. 8.1c and 8.1e). Rating for both these mixes (FA-PC-NS0 and FA-S-NS0) was observed within a range of 2-3. However, pattern of the surface appearance and erosion behaviour significantly changed with the inclusion of 2% nanosilica in the GGBFS and OPC blended fly ash based geopolymer mortar and rating for these two mixes were in a range of 0-1.

8.2.2 Change in compressive of geopolymer mortar specimens.

The visual observations were very useful to find out the external surface deterioration of sulphate exposed specimens, but the extent of expansion and internal damage can be hardly predicted by visual inspection. For this reason, changes in length and compressive strength of geopolymer mortar were investigated in order to determine the extent of damage in the sulphate solutions.

Table 8.1 Change in compressive strength of geopolymer mortar specimens in sulphate solution

Mix Id	Compressive strength (MPa)						
	28 days	56 days		90 days		120 days	
	Reference	Na_2SO_4	$MgSO_4$	Na_2SO_4	$MgSO_4$	Na_2SO_4	$MgSO_4$
FA-NS0	29	31.8	31.4	35.2	34.8	38.3	37.9
FA-NS2	60	68.2	67.6	70.2	69.4	73.1	72.5
FA-PC-NS0	19	18.8	18	17.6	17	15	14.2
FA-PC-NS2	53	59.2	58.7	61.5	61	67.5	66.9
FA-S-NS0	24	23.3	22.9	22.1	21.5	20.5	19.8
FA-S-NS2	51	58.1	57.6	61.2	60.6	62.6	62

The compressive strengths of the mortar specimens after 120 days of immersion in 5% $MgSO_4$ and Na_2SO_4 solutions and the 28-day compressive strength prior to the sulphate exposure are presented in Table 8.1. It is noted from the table that almost all mixes except FA-PC-NS0 and FA-S-NS0 showed increase in compressive strength after 120 days of sulphate exposures. Mix FA-PC-NS0 showed a decrease in compressive strength by 22% in $MgSO_4$ and 21% in Na_2SO_4, whereas, mix FA-S-NS0 showed strength decrease of 3% and 2% in $MgSO_4$ and Na_2SO_4 respectively. However, the specimens of OPC and GGBFS blended fly ash based geopolymer mixes with 2% nanosilica showed higher strength values after 120 days of sulphate exposures. Mix FA-S-NS2 exhibited 62.0 MPa after 120 days magnesium sulphate exposure as compared to 19.8 MPa by its control mix (FA-S-NS0).

8.2.3 Change in length of geopolymer mortar specimens.

The length changes of the geopolymer mortar specimens with continued immersion in 5% sodium and magnesium sulphate solutions for up to 120 days are shown in Figs. 8.2 and 8.3.

The geopolymer specimens did not show any sign of expansion in the first few weeks of immersion.

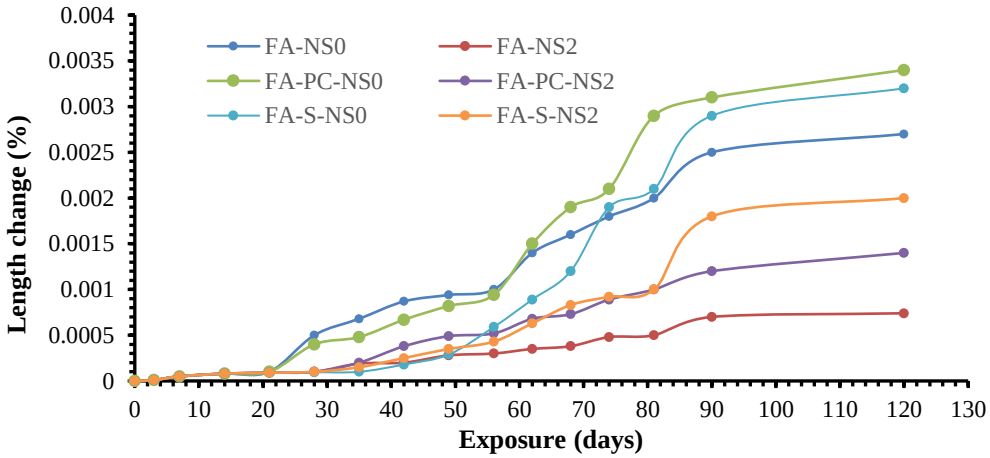

Fig. 8.2 Change in length of fly ash based geopolymer mortar (with and without nanosilica) in 5% sodium sulphate solution.

It is observed from Fig. 8.2 that the influence of 2% nanosilica in fly ash based geopolymer showed less amount of expansion over time than that of its corresponding control mix (FA-NS0). For example, expansion of the specimen FA-NS0 (without nanosilica) after 120 days of sodium sulphate exposure was recorded as 0.0025% whereas, the expansion of specimen FA-NS2 with 2% nanosilica was recorded only 0.0007%. The reduction in expansion can be attributed to the reduction of interconnected capillary pores by the use of 2% nanosilica that eventually reduced the ingress of sulphate ion in the specimen. This observation is also consistent with the difference in damages as shown in Fig. 8.1 and the compressive strengths of Table 8.1. According to previous findings [4] and ACI code [5], the recommended expansion for a cementitious binder having a blend of sulphate resisting cement and pozzolanaic binders must be less than 0.05% after 6 months and should not exceed 0.1% after one year. It is noteworthy from Fig 8.2 that the expansions of all geopolymer mortar specimens were in the range of 0.0007% to 0.0031% which are well below the acceptable limit. Bakharev [6] noted that good performance of fly ash based geopolymer in sulphate solution was attributed to a

more stable cross-linked aluminosilicate polymer structure. In a similar study, Ismail et al. [7] reported the role of sulphate attack in fly ash based geopolymer binder. They stated that Na_2SO_4 does not lead to any apparent degradation of the binder with no conversion of the binder phase. Bascarevic et al. [8] observed that the atomic ratios of Si/Al and Na/Al of the geopolymer samples exposed to Na_2SO_4 solution were lower than in its corresponding reference sample. However, when OPC and GGBFS blended fly ash geopolymer series with 2% nanosilica were exposed in 5% Na_2SO_4 solution, higher amounts of expansion were observed than in the fly ash only geopolymer with 2% nanosilica (FA-NS2). The presence of calcium ion in this case apparently affected the total expansion. Ismail et al. [7] concluded that some Ca^{2+} might be depleted from the gel structure due to ion exchange process and react with the Na_2SO_4 to form gypsum. Puertas et al. [9] also observed the formation of gypsum and ettringite in alkali activated slag specimens.

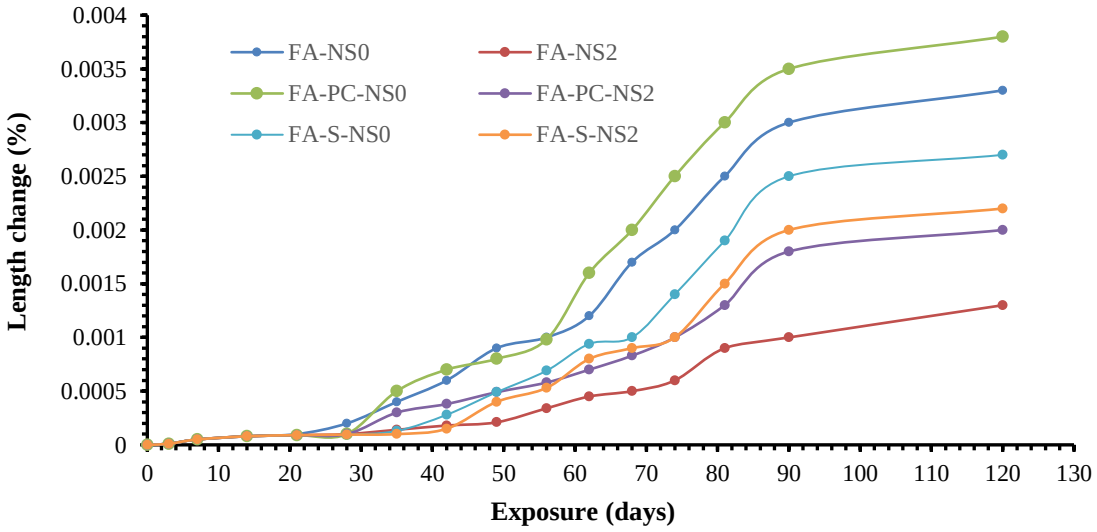

Fig. 8.3 Change in length of fly ash geopolymer mortar (with and nanosilica) in 5% magnesium sulphate solution.

The beneficial effects of 2% nanosilica in fly ash only, OPC and GGBFS blended fly ash geopolymers were also observed in the exposure of magnesium sulphate solution as shown

in Fig. 8.3. For example, in fly ash only geopolymer, after 120 days of magnesium sulphate exposure, the expansion values were noted as 0.003% and 0.001% for FA-NS0 and FA-NS2, respectively. However, the expansion rate of geopolymer samples in magnesium sulphate solution is higher than the similar mix in sodium sulphate solution. Specimens of mix FA-S-NS2 in sodium sulphate solution exhibited about 10% less expansion than in magnesium sulphate solution. Bakharev [6] also noted the exacerbated sulphate deterioration of fly ash based geopolymer when exposed to magnesium sulphate environments.

8.3 Sulphate resistance of OPC concrete core with geopolymer liner as a protective barrier

The mix design for ordinary Portland cement concrete was based on the method recommended by the ACI committee 211 (2009). The composition of OPC mix for the concrete core was a combination of coarse aggregate 1054 kg/m^3, sand 740 kg/m^3, Portland cement 446 kg/m^3 and water 165 kg/m^3. The design calculations for OPC concrete are given in Appendix A. The casted concrete core specimens were cured under lime water up to 28 days. Fig. 8.5 shows the photographs of the test specimen and the cross-section.

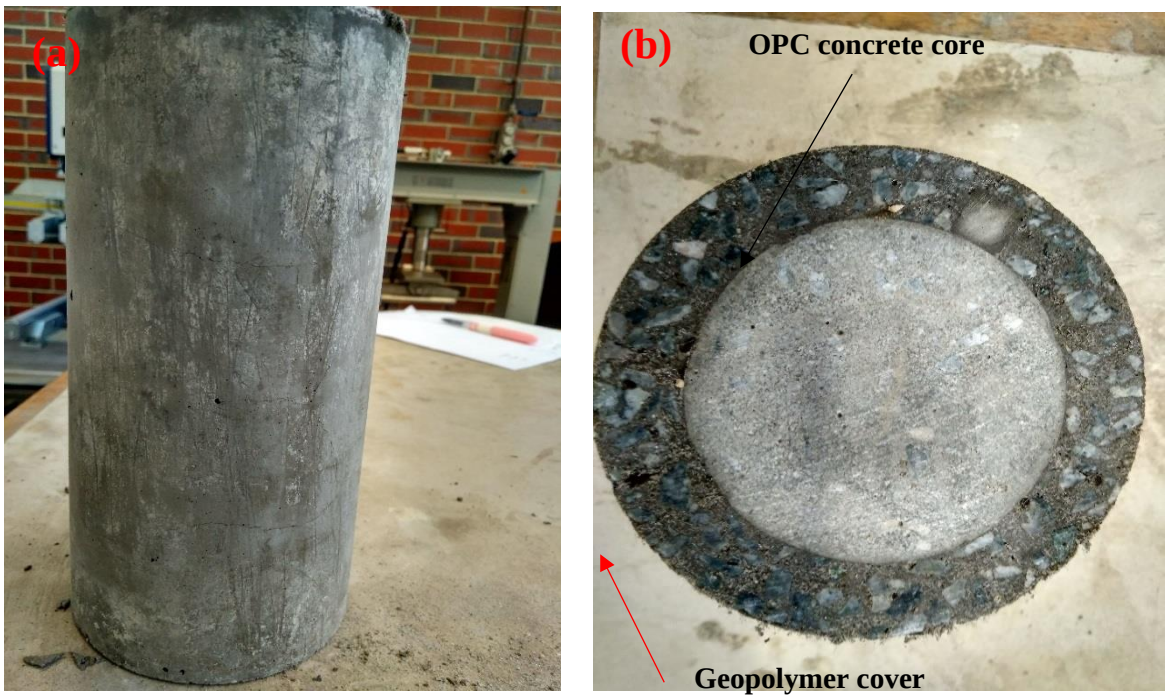

Fig. 8.4. Test specimens (a) Whole cylindrical specimen (b) cross-section.

The specimens were 100 mm × 200 mm cylinders consisting of an OPC concrete core surrounded by a layer of geopolymer mortar or concrete. The hardened OPC concrete core of 50 mm diameter and 100 mm height was placed on a 50 mm PVC chair at bottom in the 100 mm × 200 mm steel mould.

Then the gap between the core and the mould was filled by geopolymer mortar or concrete. The OPC concrete core was roughened by a wire brush in order to help bonding between the OPC concrete core and surrounding geopolymer layer. A number of different combinations of geopolymer mixes as a protective barrier were used to investigate the effectiveness of geopolymer binder composition in the highly sulphate environment. The mix ID and compositions of the geopolymers are given in Table 8.3. Commercial polypropylene fibre as a low dosages (Fig. 8.5) with a tensile strength of 4.0 gef/den was used in the study. The elongation of the polypropylene fibre was observed in a range of 40-100%.

Fig. 8.5. Commercial polypropylene fibre.

Table 8.2 Fibre Properties

Fibre Type	Manufacturer Or Supplier	Length (mm)	Diameter (μm)	Aspect Ratio	Tensile Strength (MPa)	Young's Modulus (GPa	Density (g/cm3)
Polypropylene	Proplex	6	32	188	N/A	N/A	0.91

Table 8.2 Mix proportions of geopolymer mixes (Kg/m^3)

Mix	Fly ash only				GGBFS blended Fly ash			
ID	FA-N	FA-FI	FA-CA-N	FA-FI-C-N	FA-S	FA-S-FI	FA-S-CA-N	FA-S-FI-C-N
Sand	1173	1173	1173	1173	1173	1173	1173	1173
Fly ash	734	730.3	711.33	707.66	623.33	619.66	604.67	604.67
GGBFS	-	-	-	-	110.00	110.00	110.00	110.00
OPC	-	-	-	-	-	-	-	-
SH[a]	97.78	97.78	97.78	97.78	97.78	97.78	97.78	97.78
SS[b]	195.56	195.56	195.56	195.56	195.56	195.56	195.56	195.56
Nano silica	-	-	14.67	14.67	-	-	14.67	14.67
Fiber	-	3.67	-	3.67		3.67	3.67	3.67
CA[c]	-	-	1209	1209	-	-	1209	1209

[a]Sodium hydroxide, [b]Sodium silicate, [c] coarse aggregate

Fly ash based geopolymer specimens (FA only, FA-CA-N and FA-S) without polypropylene fibre and coarse aggregate showed initial visible sign of cracks at different locations because of shrinkage. However, the specimens remained intact though cracks were developed. It is noted that cracking of the geopolymer cover will allow easy access of sulphate solution to reach the OPC concrete core. For this reason, 0.5% polypropylene fibre and 7 mm coarse aggregate were introduced in the geopolymer mixes to prevent the development of initial shrinkage cracks. Finally, geopolymer samples were cured at ambient condition (15-20^{0}C and 60±10% RH) until the test days in the designated laboratory curing room.

8.3.1 Visual appearance

Each specimen exposed to 5% sodium sulphate solution was carefully examined for any visible surface damage. The sulphate solution was replaced weekly and the pH level was monitored regularly to maintain the designated pH of 6.0 to 8.0. All significant changes at the surface of the specimens were marked and compared with its initial appearance before immersion in the sulphate solution. Table 8.4 and Fig. 8.6 present the visually observed changes of the specimens for immersion up to 240 days.

Table 8.4 Summary of visual damage of samples exposed to 5% sodium sulphate solution

Duration (days)	FA	FA-FI	FA-CA-N	FA-FI-CA-N	FA-S	FA-S-FI	FA-S-CA-FI	FA-S-FI-CA-N
	Fly ash	Fly ash + fibre	Fly ash + coarse aggregate + nanosilica	Fly ash+ fibre + coarse aggregate + nanosilica	Fly ash + Slag	Fly ash + slag + fibre	Fly ash + slag + coarse aggregate + fibre	Fly ash + slag + fibre + coarse aggregate + nanosilica
120	− Visible cracks at different locations	−No visible deterioration	−Visible cracks at different locations	−No visible deterioration	−Visible cracks at different locations	−No visible deterioration	−No visible deterioration	−No visible deterioration
180	−Crack locations and pattern same as those noted at 4 months	−No visible deterioration	−Crack locations and pattern same as those noted at 4 months	−No visible deterioration	− Crack locations and pattern same as those noted at 4 months	−No visible deterioration	−No visible deterioration	−No visible deterioration
240	−Crack locations and pattern same that are noted at 6 months	−No cracks − No disintegration – No expansion and spalling	−Crack locations and pattern same as those noted at 6 months	−No cracks − No disintegration – No expansion and spalling	−Crack locations and pattern same as those noted at 6 months	−No cracks − No disintegration – No expansion and spalling	−No cracks − No disintegration – No expansion and spalling	−No cracks − No disintegration – No expansion and spalling

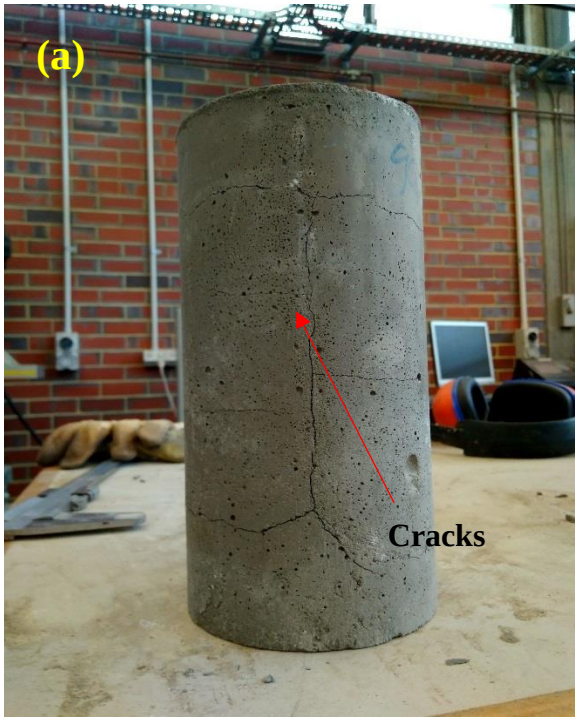

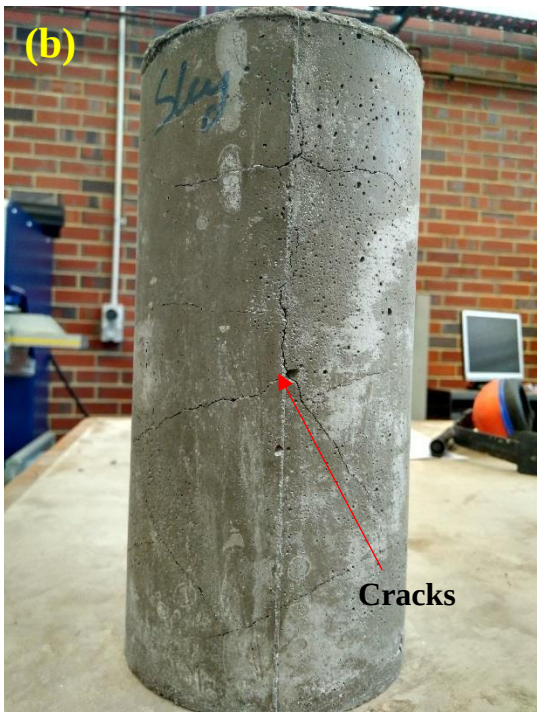

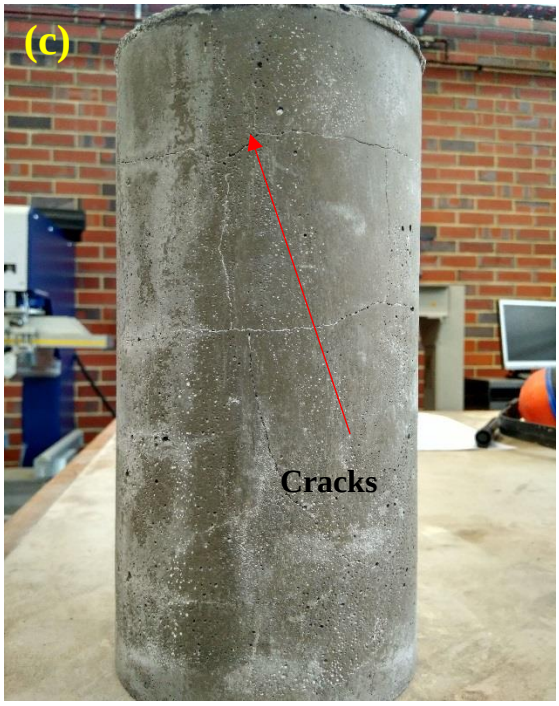
(c)
Cracks


(d)


(e)


(f)
Fits
good

Fig. 8.6 Visual appearance of concrete after 240 days of 5% sulphate exposure (a) FA (b) FA-CA-N (c) FA-S, (d) FA-FI, (e) FA-S-FI, (f) FA-FI-CA-N, (g) FA- S-CA-FI, (h) FA-S-FI-CA-N.

From the periodic visual inspections (Figs. 8.6a-h), no significant disintegration, expansion, spalling and bending of samples were observed for up to 240 days of sulphate exposure. It can be seen from Figs. 8.6a that there was cracks in the geopolymer mortar layer. These cracks were developed because of shrinkage before immersion of the specimens in sulphate solution since there was no fibre in the geopolymer mortar. However, it is noteworthy that after 240 days of sulphate exposure, crack locations and pattern of these specimens did not change from those initially observed before immersion. No spalling or wide cracks were observed in any part of the specimens because of sulphate exposure. Similar phenomena were also displayed by the specimens containing geopolymer outer layer of mixes FA-CA-N (Fig. 8.6b, with coarse aggregate and no fibre) and FA-S (Fig. 8.6c, slag with fly ash and no fibre).

On the other hand, the specimens with 0.5% polypropylene fibre and with or without coarse aggregate in the outer geopolymer layer (Figs. 8.6d-h) did not show any sign of cracks or deterioration before and after 240 days of sulphate exposure. Therefore, the use of polypropylene fibre at a dosage of 0.5% by volume of the geopolymer mortar or concrete was effective to eliminate the occurrence of any shrinkage crack and subsequently protect the OPC concrete core from any damage in 5% sulphate solution for up to 8 months of immersion.

8.3.2 Change in mass of specimens with geopolymer liner

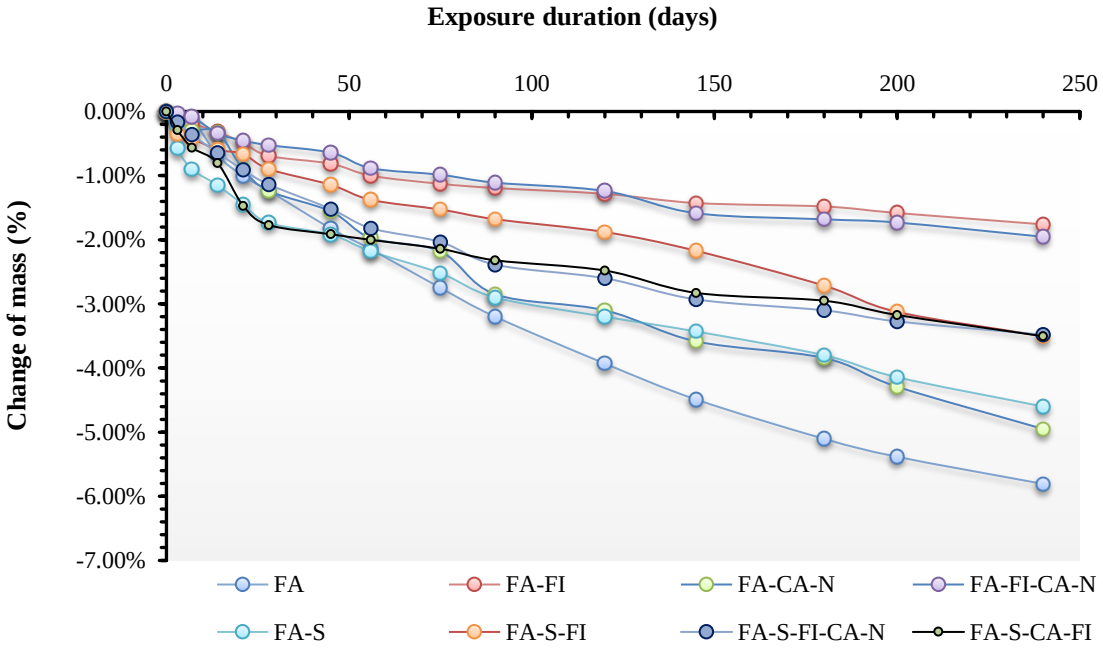

Fig. 8.7 Change in mass of geopolymer specimens submerged in 5% sodium sulphate solution.

The mass change of the specimens immersed in 5% sodium sulphate solution for up to 240 days was monitored as a possible indicator of degradation and the results are presented in Fig. 8.7. The mass of the individual specimen was measured on an electronic scale at different ages and compared to its initial mass value before immersion. It is observed from Fig.8.7 that generally mass loss increased with the increase of the immersion period for all the specimens.

However, the magnitude of mass loss varied for different geopolymer mixtures. It is noteworthy from the figure that the specimens without fibres in the geopolymer (FA, FA-CA-N and FA-S) exhibited higher mass loss than those of the specimens with fibre. This is because of the occurrence of shrinkage cracks in the specimens without fibres prior to the immersion in sulphate solution. For example, among all the mixes, the specimens with fly ash only geopolymer mortar layer showed the highest mass loss (5.8%). The higher value of mass loss for the FA only geopolymer mix can be attributed to the ingress of sulphate solution through the existing cracks in geopolymer layer and possible disintegration of the OPC core to some extent. This observation also matched with the visual appearance (Fig. 8.7a) and the change in compressive strength presented in the following section. However, the geopolymers based on FA only and FA-S with 0.5% fibre and 7 mm aggregate showed less mass losses since use of fibre prevented shrinkage cracks in the specimens before immersion. For example, the specimen with geopolymer mix FA-FI (fly ash only with fibre) exhibited only 1.7% mass loss after 240 days of immersion as compared to 5.8% for the specimen with FA only geopolymer. Similar phenomenon was also observed in the other specimens with fibre (FA-FI-CA-N and FA-S-FI-CA-N) after 240 days of sulphate exposure.

8.3.3 Failure mode of specimens in compression test

The typical failure mode and crack pattern of concrete specimens in compression test are shown in Figs. 8.8 and 8.9.


(a)

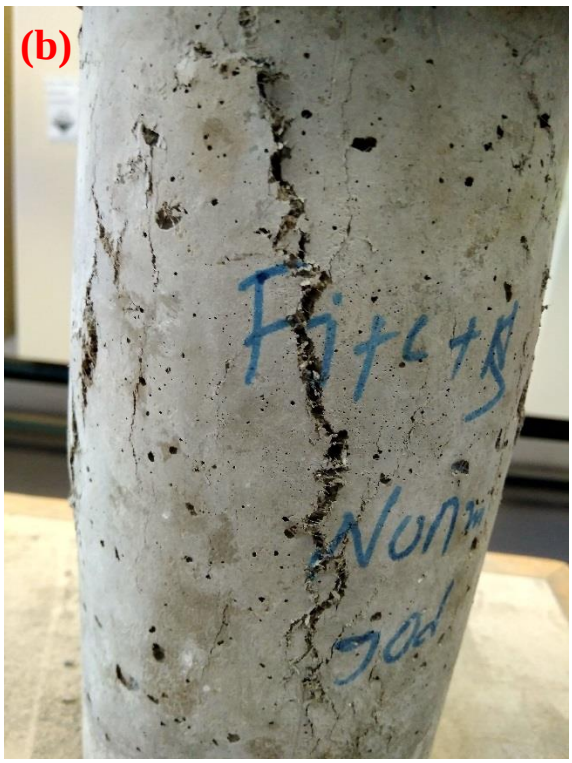
(b)


(c)


(d)

Fig. 8.8. Typical failure modes of geopolymer specimens without polypropylene fibre and 7mm coarse aggregate.

All the specimens sustained under a certain load limits until the first longitudinal crack was initiated. It is observed that the first crack started at the top of the cylinder (Fig. 8.8a) and then propagated downwards to the bottom with an inclined and irregular shape (8.8b and 8.8c). It is noteworthy that the failure of specimens with FA only, FA-CA-N and FA-S geopolymers occurred along the first crack line and the cracks spread mostly in the geopolymer cover region (Fig.8.8 c). The first crack was observed at about 21 MPa and a sudden drop after the peak load was observed especially in the specimens with geopolymers without polypropylene fibre. For example, it can be seen in Fig. 8.8f, that failure of the specimen occurred by separation of the cover geopolymer leaving the OPC core intact. Therefore, the failure of the specimens with no fibre in the geopolymer outer layer occurred by spalling of this layer.


(a)


(b)


(c)


(d)

Fig. 8.9. Typical failure modes of geopolymer specimens with polypropylene fibre and 7mm coarse aggregate.

The failure mode and load-carrying capacity of the specimens with fibre and coarse aggregate in the geopolymer layer were significantly different from those without fibre and

aggregate. It is noted from Fig. 8.9 that the inclusion of 0.5% polypropylene fibre had significant effect on the crack initiation time and cracking pattern. This phenomenon was observed in the specimens of FA-S-CA and FA-CA-N with 0.5% polypropylene fibre, where fibre increased the crack initiation time and increased the load capacity by as much as 90% as compared to those of the corresponding specimens without fibre. It is noted from the figure that formation of the primary crack occurred first in longitudinal direction, then additional cracks appeared surrounding the first one and finally the first crack was widened and passed through the OPC concrete core. Moreover, in some specimens, several cracks appeared simultaneously in which each one occurred near the edge on the opposite sides (Figs. 8.9a, b, c). Longitudinal splitting cracks also appeared in some specimens tested until final crushing of the OPC concrete core (Fig.8.7h).

It can be seen from the Figs. 8.8 and 8.9 that the geopolymer layer was not deteriorated by sulphate attack and it effectively protected the inner OPC concrete core. A direct exposure of the sulphate solution to the OPC concrete cylinder would cause a complete collapse of the specimen with less duration of immersion. It can be concluded that improving integrity of the geopolymer layer by adding 0.5% fibre can effectively enhance the confinement of the cover to make the core and cover work as a composite element. As a result, the failure planes passed through both the geopolymer cover and the OPC core instead of the geopolymer cover only, as observed in the specimens without fibre. Therefore, the fibre reinforced geopolymer layer can be considered as an effective way to enhance the structural integrity and durability of OPC concrete.

8.3.4 Change in compressive strength after immersion in sulphate solution

Compressive strengths of the cylinders containing different types of geopolymer cover after sulphate exposure of up to 240 days are plotted in Fig. 8.8. Compressive strengths of the specimen before immersion was taken as the reference strength for comparison. It is noted from the figure that compressive strength gradually decreased with the increase of immersion time. Fig. 8.8 indicates that the period of sulphate exposure has a considerable effect on the compressive strength of specimens, especially in the specimens with shrinkage cracks in geopolymer layer before immersion. It is noteworthy that the specimens without fibre and aggregate exhibited higher strength loss than those with fibre and aggregates.

The highest strength losses were observed in specimens with geopolymers of FA only and FA-CA-N mixes, where strength decreased by 32% and 22%, respectively, after 240 days of immersion. The compressive strength of of the specimen with FA only geopolymer after 240 days of sulphate exposure was 16.3 MPa as compared to 25 MPa before immersion. The specimens with FA-CA-N and FA-S geopolymers also exhibited similar strength losses after 240 days of sulphate exposure. It is noted from Fig.8.8 that the strength loss was improved with the inclusion of fibre and aggregate in the geopolymer layer. For example, FA only geopolymer with 0.5% polypropylene fibre showed 20.1 MPa after 240 days of sulphate exposure as compared to 22.1MPa before immersion. However, among all the mixes of fly ash series, FA only mix with 0.5% polypropylene fibre, 7mm aggregate and 2% nanosilica showed the highest strength. Compressive strength of this specimen was 68.5 MPa before immersion that decreased to 63.4 MPa after 240 days of sulphate exposure.

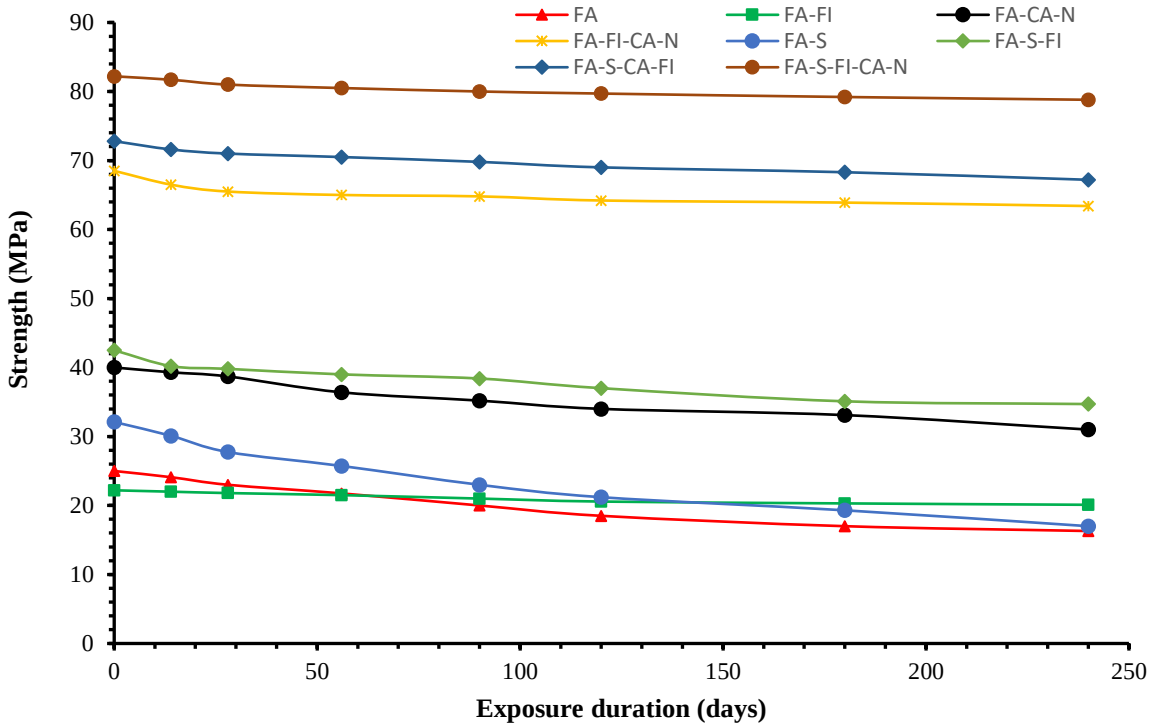

Fig. 8.10 Change in compressive strength of concrete specimens after 240 days of sulphate exposure.

The specimens with GGBFS blended fly ash geopolymer (FA-S) layer exhibited 9% to 53% strength loss by 240 days of sulphate exposure. The highest strength decreases for the FA-S geopolymer layer was from 32.1 MPa to 17 MPa by 240 days of immersion. Compressive strength of the specimen with geopolymer of FA-S-Fi decreased from 42 MPa to 34.7 MPa. However, among all the geopolymers, the GGBFS blended fly ash geopolymer with 0.5% polypropylene fibre, 7mm aggregate and 2% nanosilica showed highest strength of 82.1 MPa before immersion that decreased to 79.2 MPa after 240 days of sulphate exposure.

8.4 Summary

Specimens of geopolymer mortar and OPC concrete cores with the geopolymer cover as a protective barrier were exposed to sulphate solution for 120 and 240 days, respectively. The

evaluation of sulphate resistance of geopolymer mortar was done by determination of visual inspection, and changes in compressive strength and length. A good correlation among the expansion rate, change in compressive strength and surface damages was observed for all specimens. The fly ash based geopolymer mortar showed less expansion after 120 days in sulphate solution as compared to the corresponding OPC and GGBFS blended fly ash based geopolymers without nanosilica. However, the expansion and loss of compressive strength were significantly lower when 2% nanosilica was used in the mixes.

The visual appearance of the OPC concrete core with the geopolymer covers after soaking in 5% sodium sulphate solution up to 240 days revealed that there was no change in the appearance of the specimens. It is also observed that bonding between the geopolymer cover and OPC concrete core increased by the use of 0.5% polypropylene fibre and 7 mm aggregate in the cover geopolymer. This eventually increased compressive strength of the composite specimens. Therefore, applying a fibre reinforced geopolymer cover can be considered as an effective way to increase the sulphate resistance of OPC concrete.

8.5 Reference

1. D.M.J. Sumajouw, D. Hardjito, D. Geopolymer Concrete for a Sustainable Future, Presented: Green Processing Conference, Fremantle, Western Australia., 10-12 May, 2004.
2. 2. P. Duxson, A. Fernandez-Jimenez, Geopolymer Technology: The Current State of the Art, Journal of Materials Science, 2006, DOI 10.10 07/s10853-006-0637-z.
3. 3. B.V. Rangan, Fly Ash-Based Geopolymer Concrete", Research Report GC 4, Engineering Faculty, Curtin University of Technology, Perth, Australia, 2008.

4. 4. J. Clifton, G. J. Frohnsdorff, C.F. Ferraris, Standards for evaluating the susceptibility of cement based materials to external sulphate attack, Maters scie of conc,s ulfate attack mechanisms, (1999) 337-355.
5. American Concrete Institute, "Guide to Durable Concrete", ACI 201.2R-08 (ACI Committee 201), MI, USA, 2008.
6. T. Bakharev, Durability of geopolymer materials in sodium and magnesium sulphate solutions. Cement and Concrete Research 35 (2005) 1233–1246
7. I. Ismail, S.A. Bernal, J.L. Provis, S. Hamdan, J.S.J. van Deventer, Microstructural changes in alkali activated fly ash/slag geopolymers with sulphate exposure, Mater. Struct. 46 (2013) 361–373.
8. Z. Bascarevic, Z. Miladinovic, N. Marjanovic, M. Komljenovic, V. Nikolic, R. Petrovic, Impact of sodium sulphate solution on mechanical properties and structure of fly ash based geopolymers. Mater and Struc 48 (2015) 683–697
9. F. Puertas, D.G. Mejía, J.A. Fernández, S. Delvasto, J. Maldonado, Alkaline cement mortars. Chemical resistance to sulphate and seawater attack. Mater. Constr. 52(2002) 55–71

Every reasonable effort has been made to acknowledge the owners of copyright material. I would be pleased to hear from any copyright owner who has been omitted or incorrectly acknowledged.

CHAPTER 9

CONCLUSION

9.1 Introduction

Use of nanosilica and ultrafine fly ash are gaining wider attention due to their significant effects on the microstructural and mechanical properties of Portland cement-based binders. Effects of the incorporation of these two finer materials in fly ash based geopolymer binders have been investigated in this study. This Chapter presents a summary of the study and a set of conclusions drawn from the study.

A low-calcium fly ash (FA) was used as the principal source of aluminosilicate and it was blended with either 15% blast furnace slag (GGBFS) or 10% Portland cement (OPC) in order to accelerate setting and strength development of geopolymers at room temperature. The geopolymer mixtures are divided into three main series as fly ash-only (FA), OPC blended fly ash (FA-PC) and GGBFS (slag) blended fly ash (FA-S). Effects of nanosilica varying from 1% to 3% and ultrafine fly ash from 5% to 15% on enhancement of the mechanical and durability properties of geopolymers were studied. The blaine's surface areas of the fly ash, ultrafine fly ash, OPC and GGBFS were 340 m2/kg and 523 m2/kg, 370 m2/kg and 450 m2/kg, respectively. The average particle diameter of nanosilica was 15 nm. The binder to alkaline liquid ratio was kept constant at 0.4 with a constant sodium silicate to sodium hydroxide ratio of 2.0 and NaOH molarity of 8M. Local coarse and fine aggregates were used in the mortar and concrete mixtures. Test specimens were demoulded at 24 hours after casting and continued to cure at 15 oC to 20 oC and relative humidity of 70±10% until tested. The investigated properties included workability, setting time, compressive strength, porosity, sorptivity,

microstructural development, micromechanical properties by nano indentation, drying shrinkage, carbonation, and resistances to acid and sulphate attacks.

Workability of fresh concrete mixtures was determined by slump test in accordance with the ASTM standard. Cylinder specimens of 100 mm in diameter and 200 mm in height were used for compressive strength and sorptivity tests. Small cut samples were examined by scanning electron microscopy (SEM) applying a MIRA3 TESCAN using backscattered electron imaging. The samples were coated with carbon before putting the samples for SEM. X-ray diffraction analyses (XRD) were performed using a Siemens D500 Bragg–Brentano diffractometer in a 2h-range of 5–80Θ. Operating conditions for the XRD were set a 40 kV and 30 mA using a Cu ka X-ray source. Porosity test was carried out on samples of 10×10×5 mm size using an Autoscan mercury intrusion porosimeter. The equipment used to determine the porosity can generate a maximum pressure of 60 ksi. The contact angle and surface tension for the tests were 140° and 480 dyn/cm, respectively.

For the nanoindentation, small cube samples (10×10×10 mm) were prepared according to AS 1012.1: 2014 [43]. All cast samples were kept in a temperature-controlled curing room where the temperature was maintained at 23(±1) ^{0}C, further subjected to the demoulding process after 24 hr. Nanoindentation samples were ground and polished using silicon carbide papers with the reduced gradations of 52, 35, 22 and 15 μm to expose the sample surfaces and then samples were put through a final stage of grinding and polishing using reduced carbide papers of 52, 35, 22 and 15μm, as well as diamond suspensions of reduced gradations of 9, 6, 3, 1 and 0.05 μm on a polishing cloth. Samples were then mounted onto sample disks, further placed into samples trays for nanoindentation tests.

Resistance to sulfuric acid was determined by the modified test method B of the ASTM C 267 standard. The geopolymer cube mortar specimens were fully immersed in 3% sulfuric acid solution at the age of 28 days for 12 consecutive weeks. For sulphate resistance tests, the test specimens were immersed in 5% sodium and magnesium sulphate solution for various periods of exposure. Cylinder specimens of dimension 100 mm diameter and 200 mm height were used for changes in compressive strength and mass tests, and prism specimens of 75 mm ×75 mm ×285 mm were used to test the length change for each mixture.

9.2 Conclusions

Based on the test results, the following conclusions are drawn:

- Inclusion of nanosilica and ultrafine fly ash reduced the setting time of fly ash based geopolymer binders. In fly ash-only geopolymers, the setting times were still long after addition of 3% nanosilica and 15% ultrafine fly ash. For the GGBFS blended geopolymers, the initial setting time varied between 80 and 46 minutes, and the final setting time varied between 350 and 200 minutes by the inclusion of the 3% nanosilica and ultrafine fly ash up to 15%. The setting times of the OPC blended geopolymers were shorter than these values. Thus, a range of setting times could be achieved by including small percentages of nanosilica and ultrafine fly ash, GGBFS and OPC in the fly ash based geopolymers.
- Compressive strength of ambient-cured geopolymers was found to increase with the addition of nanosilica at early ages. The 7-day strength increased by blending of low calcium fly ash with OPC or GGBFS and it increased further with the addition of nanosilica. Strength increased with the addition of nanosilica up to a dosage of 2% and then it declined with further addition. The maximum 28-day compressive strength

among all the mixes was 72 MPa which was obtained for the geopolymer paste containing 83% fly ash, 15% GGBFS, and 2% nanosilica. The strengths of this mix were 39 MPa and 53 MPa at 7 and 14 days respectively. The Si/Al ratio of the mixes containing 2% nanosilica resulting in maximum strength varied between 1.33 and 1.40.

- The use of ultrafine fly ash also increased the compressive strength of geopolymers. The percentage of ultrafine fly ash to maximise the strength development was found to be 10% for the fly ash-only geopolymer, and 5% for the GGBFS and OPC blended geopolymers. The compressive strength of the geopolymers containing these percentages of ultrafine fly ash were between 31 MPa and 36 MPa at 7 days and between 48 and 54 MPa at 28 days. These strengths are considered suitable for various in-situ concrete applications.
- Inclusion of nanosilica improved the early-age strength of geopolymer mortars based on fly ash alone or that blended with OPC or GGBFS. Flow of the freshly mixed mortars gradually decreased with the increase of nanosilica due to its high specific surface. Compressive strength of the ambient-cured geopolymer mortars varied from 17 to 19 MPa at 7 days and from 29 to 60 MPa at 28 days. Strength development in ambient condition continued to the age of 90 days, however at slower rates at the ges after 56 days. The optimum dosage of nanosilica for maximum compressive strength was found to be 2% of the binder. Similar to the geopolymer paste and mortar mixtures, use of nanosilica and ultrafine fly ash increased compressive strength of geopolymer concrete.
- The incorporation of nanosilica and ultrafine fly ash in the fly ash based geopolymer concrete increased the strengths. Strength at 28 days increased for the 2% replacement of nanosilica with SS/SH ratio of 2.0.

- The SEM images showed that the addition of nanosilica improved the compactness of the reaction product. The contribution of nanosilica to the formation of a more compact and dense microstructure with better interlocking morphology has resulted in the increase of compressive strength. The EDX spectra showed that additional reaction products such as CSH or CASH and NASH are produced in the mixes containing OPC and GGBFS. Formation of these additional reaction products further improved the microstructure of the geopolymer pastes increasing the compressive strength. Improvement of the density of microstructure by nanosilica was evidenced in SEM images. Eventually it reduced porosity and increased compressive strength of geopolymers.

- The SEM photographs of the geopolymers showed that ultrafine fly ash improved the compactness of the microstructure with better binding of the unreacted or partially reacted particles by the reaction products. The amorphous content of the reaction product increased by ultrafine fly ash. Crystalline phases such as quartz, mullite, hematite and magnetite were present in all the geopolymers with the additional phases of calcite and Hatrurite in the geopolymers containing GGBFS and OPC.

- The elastic modulus and hardness values for different phases of fly ash only based geopolymer with 2% nanosilica are comparable with the values obtained for the mix without nanosilica. The nanoindentation on fly ash-GGBFS based and fly ash-OPC based geopolymer showed the similar trend of indentation depth to elastic modulus relationship as in the case of fly ash only geopolymer. The elastic modulus and hardness values of the studied mixes did not change considerably because of the blending of fly ash with 15% GGBFS or 10% OPC.

- The volume fractions of hydrated aluminosilicate gel in the fly ash only geopolymer increased from 70.0% to 78.9% with the addition of 2% nanosilica. Volume fractions of the hydrated phase in both fly ash-GGBFS based and fly ash-OPC based geopolymer with or without nanosilica are very similar. The volume fractions of porous phases in fly ash-GGBFS based and fly ash-OPC based geopolymer with 2% nanosilica were lower than the values in corresponding mixes without nanosilica. There was not significant change in volume fractions of the unreacted and partially reacted phases with the use of 2% nanosilica.
- The increased reaction rate and nucleation effect of nanosilica increased the hydrated phase and reduced the porous phase of geopolymer. A relationship can also be observed amongst the compressive strength, Si/Al and Na/Al molar ratios and volume fractions of different phases. The increase of volume fractions of hydrated phase and reduction of porous phase by the inclusion of 2% nanosilica, as determined by statistical deconvolution of the nanoindentation data correlated with the porosity measured by MIP tests.
- Sorptivity of the specimens with 2% nanosilica was less than that of the control specimen. All the specimens remained intact after 90 days of immersion in 3% sulfuric acid solutions with some erosion on the surface of the specimens containing OPC. The average mass loss of the specimens of three series decreased from 2.6% to 1.8% after 90 days of immersion. The strength loss of the specimens without nanosilica ranged from 30% to 41% while that of the specimens with 2% nanosilica ranged from 9% to 11% after 90 days of immersion. Therefore, the acid resistance of geopolymer mortars significantly improved with the inclusion of 2% nanosilica.

- After 90 days of immersion in acid solutions, the microstructures of the specimens with nanosilica were found to be more compact as compared to the specimens without nanosilica. The combined effects of the nanosilica as a filler and enhanced reactivity of the aluminosilicate source materials refined the pore structure to develop a more compact microstructure. This reduced the porosity and sorptivity of the binder matrix. As a result there was less damage in the matrix after immersion in acid solution and hence reduced loss of mass and strength in the specimen's containing nanosilica.
- The incorporation of nanosilica and ultrafine fly ash in fly ash based geopolymer mortar cured at room temperature reduces the carbonation effects. Carbonation penetration depth was reduced from 15mm to 5mm with the addition of 2% nanosilica and 15% ultrafine fly ash in fly ash based geopolymer mortar.
- The drying shrinkage of geopolymer concrete decreased with the optimum amount of nanosilica and ultrafine fly ash in the mixes. Incorporation of 2% nanosilica in the binder of fly ash based geopolymer concrete showed less drying shrinkage than the control mix. Moreover, the values of drying shrinkage for all geopolymer concrete mixes at 56 days were well below than 1000 × 10-6 as specified by AS 1379-2007 (Standard Australia, 2007).

9.3 Opportunity of further research on geopolymer concrete

This study canbe extended in the following area

- Extensive Transmission Electron Microscopy need to conduct to evaluate the reaction product, its nature and shape as well as to justify Si/Al ratio of the selected region with degree of reaction at the nanoscale.

- Thermogravimetric analysis analysis can be carried to measure mass loss of specimens with temperature ranges 100-1000°C, which will indicate the bonding strength or bonding formation (Si-O-Si) in the geopolymer structure with nanoparticles and ultrafine fly ash.
- Differential Scanning Calorimeter instrument can be used for nanobased materials in depth to detect the phase transitions of N-A-S-H or C-A-S-H with finer materials.
- It has been found that increase of finer matrials or calcium bearing compond enhance the durabity and mechanical strength with compromising the workability and setting time. Hence, more research is required to invent appropriate retarder and superplasticiser to control the rheology of bf blended mixes.
- Chemical bond in the paste matrix (Si-O-T, T=Si or Al) from the formation of broad band at wavenumber (cm-1) for nanobased material need to investigate extensively.
- This study has been limited to short-time structural and durability properties. The perfoamcnce of the additive-blended mixes in the longer term need to be investigated. For example, chloride exposure can be included in further durability studies as chloride attack is one of the principal mechanisms.

Appendix A Concrete Mix design

Concrete Mix Design (ACI 211.4R-08)

Given Information **OPC1 mixture**

Specified Compressive Strength at 28 days f'_c= 6525 psi (45MPa)

Fine Aggregate Properties

Fine ness Modulus	=	1.97	
Relative density (Oven dry)	=	2.595	
Absorption	=	0.99	%
Bulk density (BD)	=	105.4	lb./ft^3 (1686.76kg/m^3)

Coarse Aggregate Properties

Relative density (Oven dry)	=	2.728	
Absorption	=	0.718	%
Bulk density (BD)	=	99.039	lb./ft^3 (1584.9 kg/m^3)

Cement Property

Relative Density (Sp. Gr.) = 3.15

Step 1 Select Slump and Required Strength

Slump = 4 inch 100mm (Table 6.1)
Required Avg. Strength = (6525+1200) =7725psi =53.27MPa

Step 2 Select Maximum Size of Aggregate

Maximum size of aggregate =0.75 inch =20mm (Table 6.2)

Step 3 Select Optimum Coarse Aggregate Content.

Fractional Volume of OD, CA, VCA =0.66 (Table 6.3)
Mass of Dry CA = (Bulk density of CA * VCA*27)
=1764.87lb/yd^3
= 1046.07kg/m^3

Step 4 Estimate Mixing Water and Air Content

Required Water =279lb/yd^3 =165.36kg/m^3 (Table 6.4)
Air Content = 1.5%
Void content of Fine Aggregate =(1- BD of FA/ (RD of A*62.4))*100
=34.9%

Mixing Water Adjustment = (Void content of FA-35)*8
= -0.72 lb/yd3
Water after Adjustment =278.27 lb/yd3

Step 5 Select w/c ratio

Water to Cementitious Material ratio, w/cm =0.37 (Table 6.5)

Step 6 Calculate Content of Cementitious Materials

Mass of Cementitious Materials = (required water / water cement ratio)

$=754.05 lb/yd^3 = 446.92 kg/m^3$

Step 7 Proportion Basic Mixtures with Cement Only

	ft^3	lb/yd^3	kg/m^3
Cement	3.84	754.05	446.93
CAg	10.37	1764.87	1046.04
FAg	7.92	1282.44	760.10
Water	4.47	279.00	165.36
Air	0.41		

Appendix B Fly ash based geopolymer mix proportions

B1 Fly ash-only based geopolymer mix

Mixtures	Coarse aggregate (kg/m^3)			Sand (kg/m^3)	Fly ash (kg/m^3)	GGBFS (kg/m^3)	Cement (kg/m^3)	NaOH sol (kg/m^3)	Na_2SiO_3 sol (kg/m^3)	Nanosilica (kg/m^3)	Ultrafine (kg/m^3)
	20mm	10mm	7mm								
FA-NS0.0	767.52	168.48	280.8	651	400	-	-	53.33	106.67	-	-
FA-NS0.5	767.52	168.48	280.8	651	398	-	-	53.33	106.67	2	-
FA-NS1.0	767.52	168.48	280.8	651	396	-	-	53.33	106.67	4	-
FA-NS1.5	767.52	168.48	280.8	655.2	394	-	-	53.33	106.67	6	-
FA-NS2.0	767.52	168.48	280.8	655.2	392	-	-	53.33	106.67	8	-
FA-NS2.5	767.52	168.48	280.8	655.2	390	-	-	53.33	106.67	10	-
FA-NS3.0	767.5	168.48	280.8	655.2	388	-	-	53.33	106.67	12	-
FA-S-NS0.0	767.52	168.48	280.8	655.2	340	60	-	53.33	106.67	-	-
FA-S-NS0.5	767.52	168.48	280.8	655.2	338	60	-	53.33	106.67	2	-
FA-S-NS1.0	767.52	168.48	280.8	655.2	336	60	-	53.33	106.67	4	-
FA-S-NS1.5	767.52	168.48	280.8	655.2	334	60	-	53.33	106.67	6	-
FA-S-NS2.0	767.52	168.48	280.8	655.2	332	60	-	53.33	106.67	8	-

B2 GGBFS blended fly ash based geopolymer mix

Mixtures	Coarse aggregate (kg/m^3)			Sand (kg/m^3)	Fly ash (kg/m^3)	GGBFS (kg/m^3)	Cement (kg/m^3)	NaOH sol (kg/m^3)	Na_2SiO_3 sol (kg/m^3)	Nanosilica (kg/m^3)	Ultrafine (kg/m^3)
	20mm	10mm	7mm								
FA-S-NS2.5	767.52	168.48	280.8	651	330	60	-	53.33	106.67	10	-
FA-S-NS3.0	767.52	168.48	280.8	655.2	328	60	-	53.33	106.67	12	-
FA-PC-NS0.0	767.52	168.48	280.8	655.2	360	-	40	53.33	106.67	-	-
FA-PC-NS0.5	767.52	168.48	280.8	655.2	358	-	40	53.33	106.67	2	-
FA-PC-NS1.0	767.52	168.48	280.8	655.2	356	-	40	53.33	106.67	4	-
FA-PC-NS1.5	767.52	168.48	280.8	655.2	354	-	40	53.33	106.67	6	-
FA-PC-NS2.0	767.52	168.48	280.8	655.2	352	-	40	53.33	106.67	8	-
FA-PC-NS2.5	767.52	168.48	280.8	655.2	350	-	40	53.33	106.67	10	-
FA-PC-NS3.0	767.52	168.48	280.8	655.2	348	-	40	53.33	106.67	12	-
FA-UF05	767.52	168.48	280.8	655.2	380	-	-	53.33	106.67	-	20
FA-UF10	767.52	168.48	280.8	655.2	360	-	-	53.33	106.67	-	40
FA-UF15	767.52	168.48	280.8	655.2	340	-	-	53.33	106.67	-	60

B3 OPC blended fly ash based geopolymer mix

Mixtures	Coarse aggregate (kg/m^3)			Sand (kg/m^3)	Fly ash (kg/m^3)	GGBFS (kg/m^3)	Cement (kg/m^3)	NaOH sol (kg/m^3)	Na_2SiO_3 sol (kg/m^3)	Nanosilica (kg/m^3)	Ultrafine (kg/m^3)
	20mm	10mm	7mm								
FA-S-UF00	767.52	168.48	280.8	655.2	340	60	-	53.33	106.67	-	-
FA-S-UF05	767.52	168.48	280.8	655.2	320	60	-	53.33	106.67	-	20
FA-S-UF10	767.52	168.48	280.8	655.2	300	60	-	53.33	106.67	-	40
FA-S-UF15	767.52	168.48	280.8	655.2	280	60	-	53.33	106.67	-	60
FA-PC-UF00	767.52	168.48	280.8	655.2	360	-	40	53.33	106.67	-	-
FA-PC-UF05	767.52	168.48	280.8	655.2	360	-	40	53.33	106.67	-	20
FA-PC-UF10	767.52	168.48	280.8	655.2	360	-	40	53.33	106.67	-	40
FA-PC-UF15	767.52	168.48	280.8	655.2	360	-	40	53.33	106.67	-	60

APPENDIX C: Compressive strength test

Compressive strength test: FLY ASH ONLY

Mix ID SERIES: FA-NS (PASTE)

Mix id (testing date		FA-NS0		FA-NS1.0		FA-NS2.0		FA-NS3.0	
Days	No	Strength (MPa)	Avg. Strength (MPa)	Strength (MPa)	Avg. Strength (MPa)	Strength (MPa)	Avg. Strength (MPa)	Strength (MPa)	Avg. Strength (MPa)
7	1	19.00	17.72	31.4	32.2	41.00	39.5	27.00	29.8
	2	16.44		33.0		38.00		32.60	
14	1	24.00	22.81	39.0	41.84	54.00	53.95	40.00	39.28
	2	21.62		44.68		53.9		38.56	
28	1	31.00	29.12	51.0	54.3	64.00	66.62	35.00	36.03
	2	27.24		57.6		69.24		37.06	
90	1	33.00	32	54.0	56	65.00	68	56.00	59
	2	31.00		58.0		71.00		62.00	

Mix ID SERIES: FA-S-NS (PASTE)

Mix id (testing date		FA-S-NS0		FA-S-NS1.0		FA-S-NS2.0		FAS--NS3	
Days	No	Strength (MPa)	Avg. Strength (MPa)	Strength (MPa)	Avg. Strength (MPa)	Strength (MPa)	Avg. Strength (MPa)	Strength (MPa)	Avg. Strength (MPa)
7	1	22.0	23.16	29.00	28.21	39.00	38.63	35.00	37.5
	2	24.32		27.42		38.63		40.00	
14	1	31	33.42	39.00	38.41	55.00	54	42.3	43
	2	35.84		37.82		53.00		43.7	
28	1	37.00	38.59	57.00	55.99	71.00	72.79	48.1	47.91
	2	40.18		54.98		74.58		51.72	
90	1	39.00	40	57.00	59.0	73.00	74	48.1	50
	2	41.00		61.00		75.00		51.9	

Mix ID SERIES: FA-PC-NS (PASTE)

Mix id (testing date		FA-PC-NS0		FA-PC-NS1.0		FA-PC-NS2.0		FAS--NS3	
Days	No	Strength (MPa)	Avg. Strength (MPa)	Strength (MPa)	Avg. Strength (MPa)	Strength (MPa)	Avg. Strength (MPa)	Strength (MPa)	Avg. Strength (MPa)
7	1	15.0	16.84	22.00	23.55	37.2	39.5	23.1	24.1
	2	18.68		25.1		41.8		25.72	
14	1	23.1	21.77	38.00	37.61	53.00	53.95	29.80	30.16
	2	20.44		37.22		54.9		30.52	
28	1	27.00	28.47	49.00	50.00	62.1	65.19	37.3	38.67
	2	29.94		51.00		68.28		40.04	
90	1	27.00	30	53.00	52.00	68.2	67	39.00	40
	2	33.00		51.00		65.8		41.00	

Mix ID SERIES: FA-NS (MORTAR)

Mix id (testing date		FA-NS0		FA-NS1.0		FA-NS2.0		FA-NS3.0	
Days	No	Strength (MPa)	Avg. Strength (MPa)	Strength (MPa)	Avg. Strength (MPa)	Strength (MPa)	Avg. Strength (MPa)	Strength (MPa)	Avg. Strength (MPa)
7	1	18	19.90	29	26.10	36	34.55	18	17.49
	2	21.9		27		33		17	
28	1	27	29.01	47.9	46.74	60	60.18	40	38.00
	2	29		46		60		36.5	
56	1	33	32.07	60	58.64	69	67.75	44	43.40
	2	31		57.5		66		43	
90	1	35	34.81	59	60.10	68.9	69.10	47.3	45.80
	2	34		61		69.2		46.0	

Mix ID SERIES: FA-S-NS (MORTAR)

Mix id (testing date		FA-S-NS0		FA-S-NS1.0		FA-S-NS2.0		FA-S-NS3.0	
Days	No	Strength (MPa)	Avg. Strength (MPa)	Strength (MPa)	Avg. Strength (MPa)	Strength (MPa)	Avg. Strength (MPa)	Strength (MPa)	Avg. Strength (MPa)
7	1	13.2	13.04	16.2	17.6	28.00	26.32	14.3	15.04
	2	12.88		17.92		24.64		15.78	
28	1	23.2	24	34.5	35	52.00	51.48	36.2	37
	2	24.8		35.5		50.96		37.8	
56	1	29.1	28.47	40.0	41.75	57.1	58.2	43.5	44
	2	27.84		43.5		58.9		44.5	
90	1	29.1	31.9	45.00	44.92	57.7	60.1	46.2	47.44
	2	34.7		44.84		62.5		48.68	
180	1	33.2	34	45.3	46	64.1	63	49.8	50
	2	34.8		46.7		61.9		50.2	

Mix ID SERIES: FA-PC-NS (MORTAR)

Mix id (testing date		FA-NS0		FA-NS1.0		FA-NS2.0		FA-NS3.0	
Days	No	Strength (MPa)	Avg. Strength (MPa)	Strength (MPa)	Avg. Strength (MPa)	Strength (MPa)	Avg. Strength (MPa)	Strength (MPa)	Avg. Strength (MPa)
7	1	10.2	9.61	25.0	24.98	31.1	30.32	17.0	15.91
	2	9.02		24.96		29.54		14.82	
28	1	18.2	19.68	37.2	39.06	52.8	53.6	31.8	33.49
	2	21.16		40.92		54.4		35.18	
56	1	26.1	27.9	42.3	43.92	57.0	59.2	39.2	40.45
	2	29.7		45.54		61.4		41.7	
90	1	30	31.34	42.3	42.27	61.0	61.68	43.0	44.24
	2	32.68		42.24		62.36		45.48	
180	1	33.75	34	49.0	50	64.0	65	46.0	46
	2	34.25		51.0		66.0		46.0	

Mix ID SERIES: FA-NS (CONCRETE)

Mix id (testing date		FA-NS0		FA-NS1.0		FA-NS2.0		FA-NS3.0	
Days	No	Strength (MPa)	Avg. Strength (MPa)	Strength (MPa)	Avg. Strength (MPa)	Strength (MPa)	Avg. Strength (MPa)	Strength (MPa)	Avg. Strength (MPa)
7	1	9.0	9.2	17.5	18.9	24.0	25.2	21.0	22.1
	2	9.4		20.3		26.4		23.2	
28	1	16.8	17.5	31.0	32.1	44.0	45.2	38.0	37.1
	2	18.2		33.2		46.4		36.2	
56	1	20.9	21.2	34.5	36.8	47.2	48.9	43.0	41.8
	2	21.5		39.1		50.6		40.6	
90	1	24.2	23.5	39.2	40.1	51.2	52.1	43	44.2
	2	22.8		41.0		53.0		45.4	

Mix ID SERIES: FA-S-NS (CONCRETE)

Mix id (testing date		FA-S-NS0		FA-S-NS1.0		FA-S-NS2.0		FA-S-NS3.0	
Days	No	Strength (MPa)	Avg. Strength (MPa)	Strength (MPa)	Avg. Strength (MPa)	Strength (MPa)	Avg. Strength (MPa)	Strength (MPa)	Avg. Strength (MPa)
7	1	6.0	7.1	14.9	15.2	23.0	23.8	17.0	16.2
	2	8.2		15.5		24.6		15.4	
28	1	14.9	15.8	23.0	24.2	36.0	37.5	28.0	29.2
	2	16.7		25.4		39.0		30.4	

Mix ID SERIES: FA-PC-NS (CONCRETE)

Mix id (testing date		FA-PC-NS0		FA-PC-NS1.0		FA-PC-NS2.0		FA-PC-NS3.0	
Days	No	Strength (MPa)	Avg. Strength (MPa)	Strength (MPa)	Avg. Strength (MPa)	Strength (MPa)	Avg. Strength (MPa)	Strength (MPa)	Avg. Strength (MPa)
7	1	6.9	7.5	16.2	16.5	22.2	21.5	16.2	17.8
	2	8.1		16.8		20.8		19.4	
28	1	14.2	15.8	23.0	21.5	39.1	38.5	23.0	25.6
	2	17.4		20.0		37.9		28.2	

56	1	19.0	18.2	23.0	25.2	39.1	42.2	27.0	29.2
	2	17.4		27.4		45.3		31.4	
90	1	23.0	21.5	26.8	28.9	46.1	44.5	31.0	33.2
	2	20.0		31.0		42.9		35.0	

Appendix D Nanoindentation

Mix ID SERIES: FA-NS (PASTE)

Test	Modulus At Max Load (GPa)	Hardness At Max Load (GPa)	Drift Correction (nm/s)	Disp at Max Load (nm)	Load At Max Load (mN)	Time At Start Of Approach	Area Coefficient 1	Area Coefficient 2
1	6.372	0.215	-0.089	394.558	0.969	11:43:44 PM	2.54E+01	1.05E+03
2	15.635	1.288	-0.009	161.382	0.96	11:49:59 PM	2.54E+01	1.05E+03
4	16.33	0.805	-0.046	187.407	0.961	11:58:34 PM	2.54E+01	1.05E+03
7	84.384	7.716	0.007	81.65	0.972	12:15:40 AM	2.54E+01	1.05E+03
9	12.774	0.312	-0.092	305.164	0.967	12:25:15 AM	2.54E+01	1.05E+03
10	15.283	1.483	-0.01	157.307	0.962	12:30:56 AM	2.54E+01	1.05E+03
11	18.697	2.631	0.002	136.732	0.971	12:35:43 AM	2.54E+01	1.05E+03
12	15.417	1.938	-0.023	150.534	0.966	12:40:44 AM	2.54E+01	1.05E+03
13	16.323	0.674	-0.083	203.187	0.968	12:44:30 AM	2.54E+01	1.05E+03
14	12.574	0.563	-0.03	229.376	0.968	12:51:36 AM	2.54E+01	1.05E+03
15	15.435	0.411	-0.084	259.258	0.962	12:56:34 AM	2.54E+01	1.05E+03
16	14.969	0.61	-0.028	214.301	0.96	1:03:13 AM	2.54E+01	1.05E+03
17	66.271	21.397	-0.02	97.757	0.967	1:06:59 AM	2.54E+01	1.05E+03
18	7.754	0.269	-0.097	344.916	0.963	1:13:30 AM	2.54E+01	1.05E+03
19	15.646	0.471	-0.086	241.21	0.961	1:19:26 AM	2.54E+01	1.05E+03

20	42.009	4.862	0.013	100.067	0.967	1:25:00 AM	2.54E+01	1.05E+03
21	8.557	0.291	-0.035	329.855	0.97	1:29:12 AM	2.54E+01	1.05E+03
22	194.391	19.022	-0.005	69.11	0.968	1:35:00 AM	2.54E+01	1.05E+03
23	8.354	0.379	-0.102	290.676	0.96	1:39:29 AM	2.54E+01	1.05E+03
24	14.483	1.164	-0.051	169.413	0.961	1:45:17 AM	2.54E+01	1.05E+03
25	41.982	5.208	-0.023	100.118	0.969	1:50:35 AM	2.54E+01	1.05E+03
26	11.911	0.579	-0.089	228.634	0.968	1:55:16 AM	2.54E+01	1.05E+03
27	9.266	0.451	-0.067	265.3	0.965	2:00:29 AM	2.54E+01	1.05E+03
28	22.88	0.652	-0.083	196.937	0.963	2:04:25 AM	2.54E+01	1.05E+03
29	5.904	0.243	-0.117	374.025	0.961	2:10:55 AM	2.54E+01	1.05E+03
30	15.159	0.804	-0.053	190.408	0.963	2:16:19 AM	2.54E+01	1.05E+03
31	115.28	34.705	-0.024	85.442	0.968	2:20:19 AM	2.54E+01	1.05E+03
32	179.123	34.354	-0.006	74.236	0.971	2:26:21 AM	2.54E+01	1.05E+03
33	21.542	0.791	-0.074	181.829	0.97	2:30:56 AM	2.54E+01	1.05E+03
36	47.23	3.437	-0.017	99.474	0.967	2:46:38 AM	2.54E+01	1.05E+03
37	20.085	1.329	-0.061	150.261	0.962	2:52:02 AM	2.54E+01	1.05E+03
38	77.155	3.774	-0.027	88.452	0.964	2:57:34 AM	2.54E+01	1.05E+03
39	18.944	1.403	-0.024	149.991	0.961	3:02:31 AM	2.54E+01	1.05E+03
40	41.088	5.839	-0.01	100.989	0.968	3:08:22 AM	2.54E+01	1.05E+03
42	7.306	0.058	-0.136	759.684	0.961	3:16:36 AM	2.54E+01	1.05E+03
43	59.53	6.131	-0.004	89.795	0.97	3:23:44 AM	2.54E+01	1.05E+03
44	16.47	0.472	-0.081	239.821	0.961	3:28:36 AM	2.54E+01	1.05E+03

Mix ID SERIES: FA-NS2 (PASTE)

Test	Modulus At Max Load (GPa)	Hardness At Max Load (GPa)	Drift Correction (nm/s)	Disp at Max Load (nm)	Load At Max Load (mN)	Time At Start Of Approach	Area Coefficient 1	Area Coefficient 2
1	44.483	5.317	0.618	98.411	0.975	4:17:09 PM	2.54E+01	1.05E+03
2	89.908	10.267	0.57	80.623	0.971	4:23:41 PM	2.54E+01	1.05E+03
4	16.564	0.768	0.432	192.025	0.972	4:32:54 PM	2.54E+01	1.05E+03
5	17.2	0.826	0.415	183.784	0.961	4:38:15 PM	2.54E+01	1.05E+03
6	20.953	0.879	0.427	173.922	0.967	4:43:10 PM	2.54E+01	1.05E+03
8	13.049	0.931	0.355	186.514	0.963	4:52:50 PM	2.54E+01	1.05E+03
9	12.142	0.468	0.348	251.54	0.972	4:57:51 PM	2.54E+01	1.05E+03
10	11.115	0.238	0.304	356.904	0.973	5:03:25 PM	2.54E+01	1.05E+03
11	16.906	0.627	0.33	207.977	0.961	5:08:57 PM	2.54E+01	1.05E+03
12	64.897	6.4	0.33	87.606	0.97	5:12:42 PM	2.54E+01	1.05E+03
13	28.199	3.595	0.304	115.682	0.971	5:19:50 PM	2.54E+01	1.05E+03
16	11.946	0.602	0.179	224.107	0.963	5:34:15 PM	2.54E+01	1.05E+03
17	36.372	2.275	0.263	114.001	0.967	5:41:41 PM	2.54E+01	1.05E+03
18	18.861	0.685	0.141	196.669	0.96	5:46:11 PM	2.54E+01	1.05E+03
21	14.951	0.876	0.149	184.77	0.963	6:01:27 PM	2.54E+01	1.05E+03

23	17.371	0.646	0.085	205.733	0.971	6:11:42 PM	2.54E+01	1.05E+03
25	41.054	2.876	0.104	105.807	0.968	6:21:00 PM	2.54E+01	1.05E+03
26	56.571	6.15	0.144	91.162	0.971	6:26:56 PM	2.54E+01	1.05E+03
28	73.74	5.044	0.136	85.839	0.964	6:36:48 PM	2.54E+01	1.05E+03
29	21.964	0.465	0.017	236.493	0.969	6:41:46 PM	2.54E+01	1.05E+03
32	16.895	1.075	0.073	167.294	0.962	6:55:59 PM	2.54E+01	1.05E+03
33	31.508	1.823	0.046	124.571	0.97	7:00:57 PM	2.54E+01	1.05E+03
37	13.987	0.863	0.032	188.993	0.968	7:21:24 PM	2.54E+01	1.05E+03
38	14.057	0.543	0.003	228.147	0.96	7:26:51 PM	2.54E+01	1.05E+03
39	23.853	1.106	-0.027	155.378	0.971	7:32:53 PM	2.54E+01	1.05E+03
40	27.279	2.371	-0.005	121.726	0.969	7:37:11 PM	2.54E+01	1.05E+03
41	40.136	4.935	0.017	101.648	0.969	7:43:07 PM	2.54E+01	1.05E+03

Mix ID SERIES: FA-PC-NS (PASTE)

Test	Modulus At Max Load (GPa)	Hardness At Max Load (GPa)	Drift Correction (nm/s)	Disp at Max Load (nm)	Load At Max Load (mN)	Time At Start Of Approach	Area Coefficient 1	Area Coefficient 2
2	35.794	0.924	0.009	159.014	0.971	8:45:24 PM	2.54E+01	1.05E+03
3	67.86	5.004	0.043	87.506	0.964	8:50:42 PM	2.54E+01	1.05E+03
4	16.291	1.011	0.016	172.43	0.965	8:56:19 PM	2.54E+01	1.05E+03
6	32.813	1.602	0.045	128.071	0.964	9:05:31 PM	2.54E+01	1.05E+03
7	34.168	0.742	-0.005	177.67	0.966	9:12:27 PM	2.54E+01	1.05E+03
8	14.045	0.385	0.009	271.717	0.969	9:16:29 PM	2.54E+01	1.05E+03
9	33.927	3.564	0.048	108.573	0.966	9:22:05 PM	2.54E+01	1.05E+03
10	17.954	0.472	-0.056	238.047	0.964	9:27:16 PM	2.54E+01	1.05E+03

11	57.104	2.847	0.025	98.614	0.961	9:33:05 PM	2.54E+01	1.05E+03
12	38.45	1.882	-0.002	118.329	0.964	9:39:32 PM	2.54E+01	1.05E+03
13	48.799	3.076	0.039	100.527	0.968	9:43:33 PM	2.54E+01	1.05E+03
14	58.807	5.809	0.034	90.167	0.969	9:48:05 PM	2.54E+01	1.05E+03
15	80.038	6.987	0.031	82.671	0.964	9:52:38 PM	2.54E+01	1.05E+03
16	17.959	0.446	-0.009	244.961	0.963	9:57:45 PM	2.54E+01	1.05E+03
17	21.799	0.826	-0.032	178.011	0.971	10:02:47 PM	2.54E+01	1.05E+03
18	28.92	1.023	0.029	155.745	0.971	10:07:44 PM	2.54E+01	1.05E+03
19	92.13	14.317	0.027	81.811	0.971	10:12:28 PM	2.54E+01	1.05E+03
20	23.669	1.476	0.031	140.934	0.971	10:16:57 PM	2.54E+01	1.05E+03
21	17.562	0.707	-0.02	195.845	0.96	10:22:10 PM	2.54E+01	1.05E+03
22	64.316	4.138	0.025	90.256	0.961	10:26:57 PM	2.54E+01	1.05E+03
25	11.895	0.36	-0.074	286.109	0.97	10:41:59 PM	2.54E+01	1.05E+03
26	17.363	1.113	-0.004	165.035	0.969	10:48:39 PM	2.54E+01	1.05E+03
27	33.418	1.344	-0.037	135.885	0.964	10:52:26 PM	2.54E+01	1.05E+03
28	88.895	8.448	0.035	80.455	0.967	11:00:09 PM	2.54E+01	1.05E+03
29	21.04	0.315	0.003	293.163	0.968	11:03:52 PM	2.54E+01	1.05E+03
30	29.726	1.041	-0.007	154.014	0.971	11:10:42 PM	2.54E+01	1.05E+03
31	42.194	2.212	0.011	111.028	0.962	11:16:11 PM	2.54E+01	1.05E+03
32	398.275	142.123	0.03	74.01	0.97	11:20:44 PM	2.54E+01	1.05E+03
33	84.926	8.912	0.034	81.569	0.972	11:27:07 PM	2.54E+01	1.05E+03
34	9.463	0.464	-0.032	260.58	0.961	11:30:55 PM	2.54E+01	1.05E+03
35	22.642	0.425	-0.043	247.995	0.972	11:37:52 PM	2.54E+01	1.05E+03
36	40.721	1.022	0.021	149.252	0.967	11:42:50 PM	2.54E+01	1.05E+03
37	44.932	3.129	0.014	101.81	0.96	11:48:58 PM	2.54E+01	1.05E+03

38	28.128	0.848	-0.04	170.166	0.971	11:53:06 PM	2.54E+01	1.05E+03
40	107.041	27.13	0.03	84.25	0.967	12:02:34 AM	2.54E+01	1.05E+03
41	28.009	1.177	-0.034	147.142	0.965	12:08:49 AM	2.54E+01	1.05E+03
42	205.23	25.381	0.039	69.634	0.969	12:14:54 AM	2.54E+01	1.05E+03
43	14.206	0.514	-0.129	233.954	0.961	12:18:41 AM	2.54E+01	1.05E+03

Mix ID SERIES: FA-PC-NS2 (PASTE)

Test	Modulus At Max Load (GPa)	Hardness At Max Load (GPa)	Drift Correction (nm/s)	Disp at Max Load (nm)	Load At Max Load (mN)	Time At Start Of Approach	Area Coefficient 1	Area Coefficient 2
1	301.482	38.93	0.484	66.766	0.972	4:27:57 PM	2.54E+01	1.05E+03
2	227.58	67.26	0.458	76.376	0.974	4:34:22 PM	2.54E+01	1.05E+03
3	15.059	0.656	0.319	207.862	0.965	4:38:32 PM	2.54E+01	1.05E+03
4	7.665	0.37	0.333	299.817	0.971	4:46:07 PM	2.54E+01	1.05E+03
5	16.802	0.53	0.275	226.385	0.966	4:50:02 PM	2.54E+01	1.05E+03
6	7.769	0.325	0.279	315.325	0.962	4:56:44 PM	2.54E+01	1.05E+03
7	9.328	0.392	0.245	281.725	0.962	5:03:09 PM	2.54E+01	1.05E+03
8	17.298	0.802	0.239	186.995	0.971	5:07:11 PM	2.54E+01	1.05E+03
9	49.306	8.13	0.269	96.208	0.966	5:13:16 PM	2.54E+01	1.05E+03
10	11.355	0.5	0.166	244.675	0.961	5:17:16 PM	2.54E+01	1.05E+03
11	15.487	0.646	0.19	208.491	0.966	5:24:25 PM	2.54E+01	1.05E+03
12	46.34	5.971	0.198	96.858	0.966	5:28:32 PM	2.54E+01	1.05E+03
13	38.056	2.672	0.159	108.844	0.961	5:34:39 PM	2.54E+01	1.05E+03
14	17.364	1.635	0.189	148.926	0.97	5:41:29 PM	2.54E+01	1.05E+03
15	15.391	0.788	0.129	191.729	0.966	5:45:15 PM	2.54E+01	1.05E+03

16	437.611	173.702	0.178	74.724	0.97	5:52:15 PM	2.54E+01	1.05E+03
17	6.645	0.154	-0.032	462.474	0.966	5:56:21 PM	2.54E+01	1.05E+03
18	18.6	1.995	0.131	140.221	0.963	6:02:55 PM	2.54E+01	1.05E+03
19	9.26	0.367	0.035	291.158	0.964	6:07:48 PM	2.54E+01	1.05E+03
20	10.503	0.171	0.067	422.81	0.96	6:13:26 PM	2.54E+01	1.05E+03
21	66.77	7.532	0.136	86.798	0.966	6:18:07 PM	2.54E+01	1.05E+03
25	82.907	19.591	0.112	87.895	0.964	6:37:49 PM	2.54E+01	1.05E+03
26	21.747	0.416	0.073	249.979	0.96	6:42:57 PM	2.54E+01	1.05E+03
28	52.806	9.856	0.081	95.465	0.967	6:55:18 PM	2.54E+01	1.05E+03
29	13.593	0.405	0.081	266.134	0.972	7:01:36 PM	2.54E+01	1.05E+03
30	168.784	33.911	0.088	75.357	0.972	7:06:24 PM	2.54E+01	1.05E+03
32	19.998	0.713	0.04	192.844	0.972	7:17:06 PM	2.54E+01	1.05E+03
33	9.967	0.436	0.013	265.247	0.959	7:21:54 PM	2.54E+01	1.05E+03
35	26.827	0.91	0.04	165.343	0.968	7:31:45 PM	2.54E+01	1.05E+03
36	59.416	6.86	0.053	89.765	0.968	7:36:56 PM	2.54E+01	1.05E+03
37	57.284	5.991	0.072	90.851	0.971	7:40:55 PM	2.54E+01	1.05E+03
38	14.816	0.638	-0.011	210.948	0.964	7:47:51 PM	2.54E+01	1.05E+03
39	19.962	2.058	0.033	136.602	0.966	7:52:05 PM	2.54E+01	1.05E+03
40	8.801	0.35	-0.025	300.867	0.968	7:59:21 PM	2.54E+01	1.05E+03
41	85.979	8.397	0.023	81.251	0.972	8:03:07 PM	2.54E+01	1.05E+03

Mix ID SERIES: FA-S-NS0 (PASTE)

Test	Modulus At Max Load (GPa)	Hardness At Max Load (GPa)	Drift Correction (nm/s)	Disp at Max Load (nm)	Load At Max Load (mN)	Time At Start Of Approach	Area Coefficient 1	Area Coefficient 2

1	57.515	2.761	0.018	99.317	0.964	11:24:53 PM	2.54E+01	1.05E+03
2	202.195	30.685	0.013	71.111	0.973	11:30:32 PM	2.54E+01	1.05E+03
3	8.875	0.379	-0.102	289.028	0.966	11:35:15 PM	2.54E+01	1.05E+03
4	10.349	0.372	-0.067	286.149	0.97	11:40:29 PM	2.54E+01	1.05E+03
5	15.109	0.571	-0.047	221.824	0.969	11:45:02 PM	2.54E+01	1.05E+03
6	12.344	0.329	-0.083	297.064	0.963	11:50:06 PM	2.54E+01	1.05E+03
7	14.985	0.594	-0.059	217.382	0.964	11:55:18 PM	2.54E+01	1.05E+03
10	22.424	0.646	-0.051	197.875	0.96	12:09:11 AM	2.54E+01	1.05E+03
11	32.638	1.142	-0.038	145.829	0.967	12:14:11 AM	2.54E+01	1.05E+03
12	13.19	0.489	-0.073	241.611	0.96	12:19:14 AM	2.54E+01	1.05E+03
17	37.386	4.15	0.001	104.49	0.969	12:43:28 AM	2.54E+01	1.05E+03
18	37.683	3.449	0.01	105.354	0.963	12:48:31 AM	2.54E+01	1.05E+03
19	71.215	6.896	0.001	85.347	0.97	12:54:06 AM	2.54E+01	1.05E+03
20	16.612	0.46	-0.04	243.595	0.967	12:59:41 AM	2.54E+01	1.05E+03
21	20.921	0.459	-0.06	238.904	0.969	1:04:13 AM	2.54E+01	1.05E+03
22	18.036	0.703	-0.051	196.777	0.971	1:08:11 AM	2.54E+01	1.05E+03
23	10.86	0.361	-0.089	287.87	0.966	1:14:35 AM	2.54E+01	1.05E+03
24	40.715	4.624	0.017	101.246	0.968	1:19:30 AM	2.54E+01	1.05E+03
25	6.721	0.366	-0.082	306.839	0.964	1:24:01 AM	2.54E+01	1.05E+03
26	127.846	39.294	0.015	84.146	0.971	1:30:00 AM	2.54E+01	1.05E+03
27	8.881	0.36	-0.12	296.833	0.97	1:34:07 AM	2.54E+01	1.05E+03
28	18.682	1.567	-0.003	146.54	0.962	1:40:48 AM	2.54E+01	1.05E+03
29	20.327	1.04	-0.015	163.825	0.971	1:46:07 AM	2.54E+01	1.05E+03
30	43.16	0.745	0.002	174.795	0.972	1:51:05 AM	2.54E+01	1.05E+03
32	43.714	2.996	-0.005	103.467	0.966	2:02:03 AM	2.54E+01	1.05E+03
33	25.456	1.968	-0.003	128.563	0.97	2:07:04 AM	2.54E+01	1.05E+03
34	86.887	10.944	0.018	81.493	0.964	2:12:27 AM	2.54E+01	1.05E+03

35	21.63	0.869	-0.039	174.312	0.971	2:17:06 AM	2.54E+01	1.05E+03
36	52.945	5.443	0.022	92.81	0.961	2:22:14 AM	2.54E+01	1.05E+03
37	24.544	0.504	-0.043	223.723	0.964	2:26:33 AM	2.54E+01	1.05E+03
38	12.057	0.563	-0.024	230.327	0.964	2:32:51 AM	2.54E+01	1.05E+03
39	3.726	0.169	-0.139	468.267	0.958	2:37:29 AM	2.54E+01	1.05E+03
41	14.592	0.456	-0.061	247.741	0.964	2:46:52 AM	2.54E+01	1.05E+03
43	10.747	0.549	-0.048	237.946	0.968	2:57:13 AM	2.54E+01	1.05E+03
44	7.869	0.252	-0.097	357.165	0.97	3:02:54 AM	2.54E+01	1.05E+03

Mix ID SERIES: FA-S-NS2 (PASTE)

Test	Modulus At Max Load (GPa)	Hardness At Max Load (GPa)	Drift Correction (nm/s)	Disp at Max Load (nm)	Load At Max Load (mN)	Time At Start Of Approach	Area Coefficient 1	Area Coefficient 2
1	10.272	0.437	-0.039	265.026	0.967	11:29:55 PM	2.54E+01	1.05E+03
2	13.079	0.58	-0.038	224.296	0.963	11:35:18 PM	2.54E+01	1.05E+03
3	68.448	2.099	0.011	105.099	0.973	11:39:13 PM	2.54E+01	1.05E+03
4	57.265	1.439	0.007	123.591	0.968	11:46:02 PM	2.54E+01	1.05E+03
5	21.564	0.573	-0.033	211.99	0.967	11:51:26 PM	2.54E+01	1.05E+03
6	13.145	0.321	-0.119	298.607	0.961	11:56:04 PM	2.54E+01	1.05E+03
7	25.792	3.413	0.035	119.626	0.969	12:02:23 AM	2.54E+01	1.05E+03
9	54.446	3.017	0.025	98.611	0.968	12:12:37 AM	2.54E+01	1.05E+03
10	10.952	0.437	-0.031	262.008	0.963	12:17:55 AM	2.54E+01	1.05E+03
11	109.124	10.125	0.026	76.786	0.972	12:23:19 AM	2.54E+01	1.05E+03
12	18.157	1.428	0.031	151.788	0.971	12:29:08 AM	2.54E+01	1.05E+03
13	13.468	0.618	0.026	217.413	0.966	12:33:36 AM	2.54E+01	1.05E+03
14	12.073	0.464	-0.055	252.461	0.97	12:38:20 AM	2.54E+01	1.05E+03

16	35.217	3.232	0.025	108.36	0.967	12:47:56 AM	2.54E+01	1.05E+03
17	16.687	0.582	-0.028	216.881	0.968	12:53:29 AM	2.54E+01	1.05E+03
19	8.996	0.227	-0.098	369.746	0.962	1:03:10 AM	2.54E+01	1.05E+03
20	29.316	1.272	-0.012	142.067	0.969	1:08:15 AM	2.54E+01	1.05E+03
21	92.218	10.306	0.012	79.981	0.966	1:13:09 AM	2.54E+01	1.05E+03
22	15.647	1.11	-0.023	169.194	0.968	1:18:57 AM	2.54E+01	1.05E+03
24	87.868	13.076	0.023	82.33	0.969	1:29:06 AM	2.54E+01	1.05E+03
25	25.27	0.708	0.008	186.737	0.961	1:34:49 AM	2.54E+01	1.05E+03
26	78.894	10.102	0.02	83.573	0.969	1:38:39 AM	2.54E+01	1.05E+03
27	14.175	0.492	-0.047	239.959	0.967	1:44:56 AM	2.54E+01	1.05E+03
28	13.865	0.492	-0.026	239.593	0.961	1:50:06 AM	2.54E+01	1.05E+03
29	16.124	0.646	-0.026	206.455	0.959	1:55:13 AM	2.54E+01	1.05E+03
30	39.961	2.74	0.025	107.157	0.962	2:00:30 AM	2.54E+01	1.05E+03
31	13.577	0.761	-0.005	198.552	0.961	2:05:06 AM	2.54E+01	1.05E+03
32	224.129	91.389	0.034	80.711	0.964	2:10:36 AM	2.54E+01	1.05E+03
33	36.533	1.07	-0.017	147.446	0.962	2:15:41 AM	2.54E+01	1.05E+03
34	51.505	4.524	0.058	94.616	0.968	2:21:02 AM	2.54E+01	1.05E+03
38	12.512	0.375	-0.043	276.998	0.961	2:40:26 AM	2.54E+01	1.05E+03
39	14.1	0.532	-0.021	230.807	0.964	2:45:47 AM	2.54E+01	1.05E+03
40	13.582	0.398	-0.047	266.489	0.96	2:50:27 AM	2.54E+01	1.05E+03
41	15.962	1.19	0.009	164.507	0.965	2:55:14 AM	2.54E+01	1.05E+03
42	96.663	19.979	0.034	83.46	0.964	2:59:58 AM	2.54E+01	1.05E+03
43	15.608	0.738	-0.037	195.903	0.961	3:04:45 AM	2.54E+01	1.05E+03
44		-5.311	0.043	53.15	0.973	3:09:39 AM	2.54E+01	1.05E+03

Appendix E Binding energy

	Fly ash	Nanosilica	Slag	Sodium silicate
Si	102.55	102.1	101.92	
Al	74.52		74.23	
Na	1072.28		1072.28	1072.28

Geopolymer Mix FA-S-NS0

Total binder content	Unit	400
Fly ash	kg	340
Slag	kg	60
NaOH solution	kg	53.33
Na_2SiO_3 solution	kg	106.67

Binder material chemical composition

Weight of Chemical Component in Fly Ash (XRF data)

SiO_2	46.69%
Na_2O	0.86%
Al_2O_3	29.14%
CaO	3.29%

Amount of fly ash	Unit	340
SiO_2	kg	=340*46.69%= 158.746
SiO_2	B. E	=158.746*102.55= 16279.40
Na_2O	kg	=340*0.86%=2.924
Na_2O	B. E	=2.924*1072.28=3135.34
Al_2O_3	kg	=340*29.14%=99.076
Al_2O_3	B. E	=99.076*74.52=7383.14

Weight of Chemical Component in GGBFS (XRF data)

SiO_2	29.96%
Na_2O	0.31%
Al_2O_3	12.25%
CaO	45.45%

Amount of Slag	Unit	60
SiO_2	kg	=60*29.96=17.976
SiO_2	B. E	=17.976*101.92=1832.11
Na_2O	kg	=60*0.31%=0.186
Na_2O	B. E	=0.186*1072.28=199.44
Al_2O_3	kg	=60*12.25%=7.35
Al_2O_3	B. E	=7.35*74.23=545.59

Alkaline activator chemical composition

Molarity of NaOH sol	8M
Amount of NaOH in solution	26.20%
Amount of H_2O in NaOH in solution	73.80%

Na_2SiO_3 solution	
SiO_2/Na_2O weight ratio in NS solution	2.0000
Amount of Na_2O in NS solution	14.70%
Amount of SiO_2 in NS solution	29.40%
Amount of H_2O in NS solution	55.90%

Weight of Chemical Component in Alkaline Mix	
Sodium Hydroxide (kg)	53.33
Sodium Silicate (kg)	106.67

Sodium Hydroxide	Unit	
Molarity	mol	8M
% NaOH in solution	%	26.20%
Weight of NaOH in solution	kg	=53.33*26.2%=13.97
$2NaOH \rightarrow Na_2O + H_2O$		
Na_2O	B. E	=13.97/2=6.99*1072.8= 7495.296

Sodium Silicate			
SiO_2/Na_2O weight ratio			2.0000
% Na_2O in solution	%	14.70%	
Weight of Na_2O in solution	kg	=106.67*14.7%=15.68	
Na_2O in solution	B. E	=15.68*1072.28=16813.3	

$\%SiO_2$ in solution	%	29.40%
Weight of SiO_2 in solution	kg	=106.67*29.4%=31.36
SiO_2 in solution	B. E	=31.36*101.92=3196.21

Summary (fly ash + GGBFS + NS + NH)		
Total B. E of SiO_2	B. E	=16279.40+1832.11+3196.21=21307.72
Total B. E of Na_2O	B. E	=3135.31+199.44+7495.29+16813.3=27643.34
Total B. E of Al_2O_3	B. E	=7383.14+545.59=7928.73
Total weighted B. E of Na	mol	=27643.34/2=13821.67
Total weighted B. E of Si	mol	=21307.72
Total weighted B. E of Al	mol	=7928.73*2=15857.46

SiO_2/ Al_2O_3 ratio	=21307.72/7928.73 = 2.68
Si/Al ratio	=21278.54/15964.4 = 1.34
Na_2 O/ Al_2O_3 ratio	=27643.34/7928.73=3.48
Na/Al ratio	=3.48

Geopolymer Mix FA-S-NS2

Total binder content	**Unit**	**400**
Fly ash	kg	332
BFSlag	kg	60
Nano $Si0_2$	kg	8
NaOH solution	kg	53.33
Na_2SiO_3 solution	kg	106.67

Binder material chemical composition

Weight of Chemical Component in Fly Ash (XRF data)

SiO_2	46.69%
Na_2O	0.86%
Al_2O_3	29.14%
CaO	3.29%

Amount of fly ash	Unit	332
SiO_2	kg	=332*46.69%= 155.0108
SiO_2	B. E	=155.0108*102.55= 15896.36
Na_2O	kg	=332*0.86%=2.86
Na_2O	B. E	=2.86*1072.28=3061.5
Al_2O_3	kg	=332*29.14%=96.7446
Al_2O_3	B. E	=96.7446*74.52=7209.42

Weight of Chemical Component in GGBFS (XRF data)

SiO_2	29.96%
Na_2O	0.31%
Al_2O_3	12.25%
CaO	45.45%

Amount of Slag		60
SiO_2	kg	=60*29.96=17.976
SiO_2	B. E	=17.976*101.92=1832.11
Na_2O	kg	=60*0.31%=0.186
Na_2O	B. E	=0.186*1072.28=199.44
Al_2O_3	kg	=60*12.25%=7.35
Al_2O_3	B. E	=7.35*74.23=545.59

Weight of Chemical Component in Nanosilica

SiO_2	99.90%

Amount of nanosilica		8
SiO_2	kg	=8*99.90=7.992
SiO_2	B. E	=7.992*102.1=815.98

Alkaline activator chemical composition

Molarity of NaOH sol	8M
Amount of NaOH in solution	26.20%
Amount of H_2O in NaOH in solution	73.80%

Na_2SiO_3 solution	
SiO_2/Na_2O weight ratio in NS solution	2.0000
Amount of Na_2O in NS solution	14.70%
Amount of SiO_2 in NS solution	29.40%
Amount of H_2O in NS solution	55.90%

Weight of Chemical Component in Alkaline Mix		
Sodium Hydroxide	kg	53.33
Sodium Silicate	kg	106.67

Sodium Hydroxide	**Unit**	
Molarity	mol	8M
% NaOH in solution	%	26.20%
Weight of NaOH in solution	kg	=53.33*26.2%=13.97
$2NaOH \rightarrow Na_2O + H_2O$		
Na_2O	B. E	=13.97/2=6.99*1072.28= 7491.66

Sodium Silicate

SiO_2/Na_2O weight ratio		2.0000
% Na_2O in solution	%	14.70%
Weight of Na_2O in solution	kg	=106.67*14.7%=15.68
Na_2O in solution	B. E	=15.68*1072.28=16813.35

%SiO_2 in solution	%	29.40%
Weight of SiO_2 in solution	kg	=106.67*29.4%=31.36
SiO_2 in solution	B. E	=31.36*102.1=3201.856

Summary (fly ash + GGBFS+ NS+ NH)		
Total B. E of SiO_2	B. E	=15902.56+1819.17+3173.63+808.7904=21746.3
Total B. E of Na_2O	B. E	=3063.05+199.54+7495.29+16821.5=27565.95
Total B. E of Al_2O_3	B. E	=7209.42+545.59=7755.01
Total weighted B. E of Na	mol	=27565.95/2=13782.96
Total weighted B. E of Si	mol	=21746.3
Total weighted B. E of Al	mol	=7755.01*2=15510.02

SiO_2/ Al_2O_3 ratio	=21746.3/7755.01 = 2.80
Si/Al ratio	=2.8/2= 1.40
Na_2O/ Al_2O_3 ratio	=27565.95/7755.01=3.55
Na/Al ratio	=3.55